



Crystal Engineering Studies of Squaric Acid Derivatives

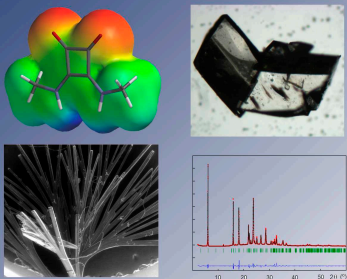
Anna Portell Bueso



Aquesta tesi doctoral està subjecta a la llicència **Reconeixement 3.0. Espanya de Creative Commons.**

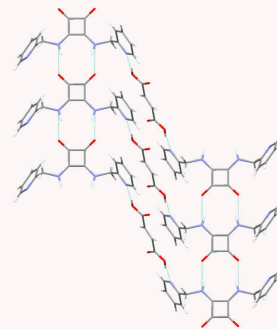
Esta tesis doctoral está sujeta a la licencia **Reconocimiento 3.0. España de Creative Commons.**

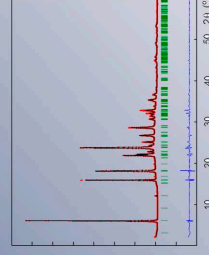
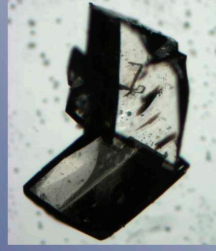
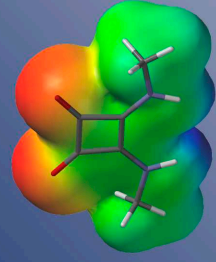
This doctoral thesis is licensed under the **Creative Commons Attribution 3.0. Spain License.**



Estudis d'enginyeria cristal·lina amb compostos derivats de l'àcid esquàric

Anna Portell Bueso

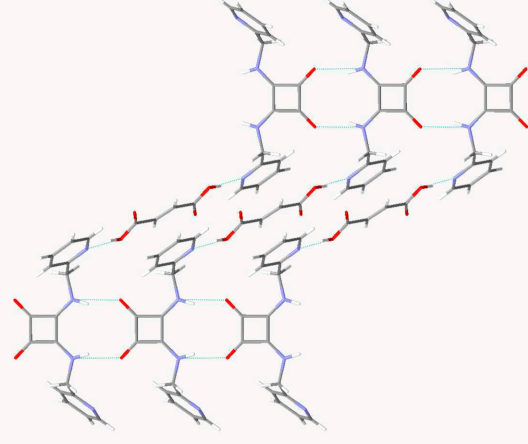




Anna Portell Bueso · Crystal Engineering Studies of Squaric Acid Derivatives

Crystal Engineering Studies of Squaric Acid Derivatives

Anna Portell Bueso



Unitat de Polimorfisme i Calorimetria
Centres Científics i Tecnològics
Universitat de Barcelona
Programa de Doctorat en Química Teòrica i Computacional

Estudis d'enginyeria cristal·lina amb compostos derivats de l'àcid esquàric

Memòria presentada per:
Anna Portell Bueso



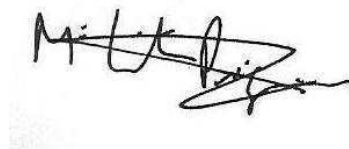
per optar al grau de Doctor per la Universitat de Barcelona.

Dirigida per:

Rafel Prohens López



M^a Cristina Puigjaner Vallet



Tutor:

Juan J. Novoa Vide

Barcelona, Setembre 2014

Unitat de Polimorfisme i Calorimetria
Centres Científics i Tecnològics
Universitat de Barcelona
Programa de Doctorat en Química Teòrica i Computacional

Crystal Engineering Studies of Squaric Acid Derivatives

Memòria presentada per:

Anna Portell Bueso



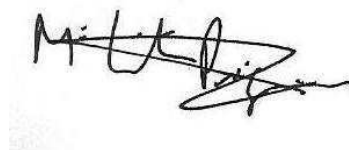
per optar al grau de Doctor per la Universitat de Barcelona.

Dirigida per:

Rafel Prohens López



M^a Cristina Puigjaner Vallet



Tutor:

Juan J. Novoa Vide

Barcelona, Setembre 2014

A la meva família.

Agraïments

Aquesta tesi ha estat un projecte de superació personal. Mirant enrere en el temps quan veia el què implicava fer el doctorat em repetia a mi mateixa que jo no el faria pas. Doncs bé, ja ho diuen que mai no diguis mai...

En primer lloc agraeixo als meus directors de tesi Rafel i Cristina la confiança dipositada en mi per a realitzar tot aquest treball d'investigació. Especialment a en Rafel, per insistir i convèncer-me que una tesi és un procés d'aprenentatge i perseverància, que no naixem ensenyats i que el més important no és el resultat sinó el desenvolupament personal i professional al llarg del doctorat. Gràcies per a despertar-me la curiositat d'empendre aquest camí i pel suport que m'has donat en tot moment, fins i tot en la distància. Cristina, aquesta tesi no seria la mateixa sense la teva visió crítica i rigurosa. M'has transmès els teus coneixements de polimorfisme, anàlisi tèrmica i cocristalls i m'has acompanyat en el camí com una amiga.

Agraeixo també al Rafa, company de laboratori i confessor, gràcies pels teus consells, la teva metòdica i organització. Em vas ensenyar a moure'm pel laboratori com a casa i em vas fer sentir còmode des del primer dia. Sento que aquesta tesi és un projecte dels quatre, perquè sense tu no hauria estat possible portar-ho tot endavant.

Amb aquesta tesi hem après tots quatre sobre el món del polimorfisme i els cocristalls, hem desenvolupat tècniques i eines de treball i ens posicionem amb experiència davant de nous projectes futurs.

Aquesta tesi m'ha portat a conèixer altres àrees de la ciència com la difracció de raigs X. Agraeixo al Xavier la paciència i les moltes hores invertides en mi, per ensenyar-me tots, i remarco, tots els meus coneixements de difracció. Ets un pou de ciència i et dono les gràcies per haver-lo compartit amb mi. També a la Mercè, li agraeixo les classes de difracció de monocristall, les hores de discussió sobre les resolucions i la prioritat dels meus cristalls.

Durant aquests anys d'investigació he tingut ocasions de fer estades curtes a altres universitats amb grans investigadors experts com Dario Braga, Fabrizia Gre-

pioni, Lucia Maini, Radovan Černý i compartir discussions a congressos amb Joel Bernstein, una persona entrenyable. Amb els resultats obtinguts hem escrit articles en col·laboració amb altres grups de recerca i voldria agrair especialment a en Salvador Tomàs per haver calculat les constants de dimerització de la dimetil-squaramida, en Max Latévi, pels càlculs realitzats amb la dibenzilesquaramida, a en Toni Frontera i Antonio Bauzá per haver accedit a desenvolupar l'estudi de les interaccions de π -*stacking* dels derivats d'àcid esquàric i a la Maria Antonia Molins per haver dut a terme els experiments de ressonància magnètica del compost **2**.

Més personalment, també voldria remarcar el meu sincer agraiment als meus amics per donar-me suport i respectar el meu temps en moments de molta feina.

Finalment i el més important, agraeixo molt especialment a la meva família, la meva mare, el meu pare i el meu germà Xavi, perquè sempre estan al meu costat en tota decisió i moment de la meva vida. També al Carles, per acompanyar-me en aquesta darrera etapa del doctorat i animar-me a creure en mi en moments difícils.

Table of Contents

List of Figures	ix
List of Tables	xxi
1 Introduction	1
1.1 Chemistry of the solid state	1
1.1.1 Crystal engineering	1
1.1.2 Solid state forms	1
1.1.2.1 Polymorphs	1
1.1.2.2 Thermodynamics of polymorphs	3
1.1.2.3 Solvates and hydrates	6
1.1.2.4 Amorphous solids	6
1.1.2.5 Salts	6
1.1.2.6 Cocrystals	7
1.1.3 Supramolecular chemistry	8
1.1.3.1 Intermolecular interactions	9
1.1.3.2 Cocrystals design and prediction	11
1.1.3.3 Cocrystals formation	13
1.2 Squaric acid derivatives	14
2 Objectives	19
3 Results and discussion	21
3.1 Polymorphism of disquaramides	21
3.1.1 3,4-Bis-benzylamino-cyclobut-3-ene-1,2-dione (1)	22

3.1.2	3,4-bis-(2-methylaminopyridyl)-1,2-dioxo-3-cyclobutene (2) .	27
3.1.3	3,4-bis-(2-ethylaminopyridyl)-1,2-dioxo-3-cyclobutene (3) . .	31
3.1.4	3,4-bis-(2-dimethylamino-ethylamino)-1,2-dioxo-3- cyclobutene (4)	34
3.2	From solution to the crystal	41
3.2.1	Cooperativity	44
3.2.1.1	Quantifying intermolecular interactions: Hunter’s approach	46
3.3	Crystal engineering: cocrystals design	57
3.3.1	First strategy: preorganization	59
3.3.2	Second strategy: cocrystallization with complementary co- formers via peripheral interactions	66
3.3.2.1	Cocrystals with hydrogen bond donor cofomers . .	66
3.3.2.2	Cocrystals with hydrogen bond acceptor cofomers	71
3.4	Self-assembling and template effect: helical architectures	73
3.5	Charged squaric acid derivatives: the electrostatic compression phe- nomenon	77
3.5.1	Zwitterionic squaramide/squarate compounds	77
3.5.2	Squarate salts	82
4	Screening Techniques	85
4.1	Introduction	85
4.2	Polymorphic Screening	88
4.2.1	Solubility study	88
4.2.2	Crystallization experiments from the solubility study	88
4.2.3	Solvent mediated transformation experiments (slurries) . . .	89
4.2.4	Precipitation experiments under kinetic conditions	89
4.2.4.1	Precipitation experiments by rapid cooling from high temperature to low temperature (PHT)	89
4.2.4.2	Precipitation experiments by antisolvent addition (PAD)	89
4.2.5	Crystallization experiments under thermodynamic conditions	90

4.2.5.1	Crystallization experiments by slow cooling from high temperature to r.t. (CHT)	90
4.2.5.2	Crystallization experiments by solvent evaporation at r.t. (CRT)	90
4.2.5.3	Crystallizations experiments by antisolvent diffusion at r.t.(CAD)	90
4.3	Cocrystal screening	90
4.3.0.4	Grinding/Drop-grinding experiments (G/DG)	91
4.3.0.5	Reaction Crystallizations (RC)	91
4.3.0.6	Precipitation experiments by rapid cooling from high temperature to low temperature (PHT)	91
4.3.1	Crystallization experiments to obtain single crystals	91
4.3.1.1	Crystallizations experiments by slow cooling from high temperature to r.t. (CHT)	91
4.3.1.2	Crystallization experiments by antisolvent diffusion at r.t. (CAD)	92
4.3.1.3	Recrystallization experiments from the reaction crystallization solids (RRC)	92
5	Crystal structure determination from powder X-ray diffraction data	93
6	Experimental Section	103
6.1	Materials and equipment	103
6.2	Synthesis of squaramides	106
6.2.1	Synthesis of compound 1	107
6.2.2	Synthesis of compound 2	108
6.2.3	Synthesis of compound 3	108
6.2.4	Synthesis of compound 4	109
6.2.5	Synthesis of compound 5	109
6.2.6	Synthesis of compound 6	110
6.2.7	Synthesis of compound 7	111
6.2.8	Synthesis of compound 8	112

6.2.9	Synthesis of compound 9	112
6.2.10	Synthesis of compound 10	113
6.2.11	Synthesis of compound 11	113
6.2.12	Synthesis of compound 12	114
6.2.13	Synthesis of compound 13	114
6.2.14	Synthesis of compound 14	115
6.2.15	Synthesis of compound 15	116
6.2.16	Synthesis of compound 16	117
6.3	Synthesis of squarate salts and amidosquaric acid derivatives	117
6.3.1	Synthesis of compound 17	118
6.3.2	Synthesis of compound 18	118
6.3.3	Synthesis of compound 19	119
6.3.4	Synthesis of compound 20	119
6.3.5	Synthesis of compound 21	120
6.3.6	Synthesis of compound 22	120
7	Conclusions	121
	Bibliography	123
A	Experimental polymorph screening	147
A.1	Compound 1	148
A.2	Compound 2	149
A.3	Compound 3	150
A.4	Compound 4	152
A.5	Compound 5	153
A.6	Compound 7	154
A.7	Compound 8	155
A.8	Compound 9	156
A.9	Compound 10	158
A.10	Compound 11	159
A.11	Compound 12	160

A.12 Compound 17	162
B Experimental cocrystal screening	163
B.1 Coformers	164
B.2 Compound 2	165
B.3 Compound 4	166
B.4 Compound 5	169
B.5 Compound 7	169
B.6 Compound 10	170
B.7 Compound 12	173
B.8 Compound 17	175
C Figures	177
C.1 Polymorphs	177
C.1.1 Compound 1 , form I	178
C.1.2 Compound 1 , form II	180
C.1.3 Compound 1 , form III	182
C.1.4 Compound 2 , form I	184
C.1.5 Compound 2 , form II	186
C.1.6 Compound 3 , form I	188
C.1.7 Compound 3 , form II	190
C.1.8 Compound 3 , form III	191
C.1.9 Compound 3 , form IV	192
C.1.10 Compound 4 , form II	194
C.1.11 Compound 4 , form III	196
C.1.12 Compound 5 , form I	198
C.1.13 Compound 6 , form I	200
C.1.14 Compound 7 , form I	202
C.1.15 Compound 8 , form I	204
C.1.16 Compound 9 , form I	206
C.1.17 Compound 10 , form I	208

C.1.18	Compound 10 , form II	210
C.1.19	Compound 10 , form III	212
C.1.20	Compound 11 , form I	214
C.1.21	Compound 12 , form I	216
C.1.22	Compound 12 , form II	218
C.1.23	Compound 12 , form III	220
C.1.24	Compound 12 , form IV	222
C.1.25	Compound 13 , form I	224
C.1.26	Compound 17 , form I	226
C.1.27	Compound 17 , form II	228
C.1.28	Compound 17 , form III	230
C.2	Multicomponent solids	233
C.2.1	Cocrystal of 2 : fumaric acid, form A	234
C.2.2	Cocrystal of 2 : fumaric acid, form B	236
C.2.3	Cocrystal of 2 : <i>p</i> -nitrobenzoic acid	238
C.2.4	Cocrystal of 4 : fumaric acid, form A	240
C.2.5	Cocrystal of 4 : fumaric acid, form B	242
C.2.6	Salt of 4 : squaric acid, form A	244
C.2.7	Salt of 4 : squaric acid, form B	246
C.2.8	Cocrystal of 4 : resorcinol, form A	248
C.2.9	Cocrystal of 4 : resorcinol, form B	250
C.2.10	Cocrystal of 10 : resorcinol, form A	252
C.2.11	Cocrystal of 10 : resorcinol, form B	254
C.2.12	Cocrystal of 10 : hydroquinone, form A	256
C.2.13	Cocrystal of 10 : hydroquinone, form B	258
C.2.14	Salt 18	260
C.2.15	Salt 19	262
C.2.16	Salt 20	264
C.2.17	Salt 21	266
C.2.18	Salt 22	268

C.2.19 Salt of 17 :squaric acid	270
D Resum	273

List of Figures

1.1	Layout of molecular solid forms	2
1.2	Ritonavir's polymorphs	2
1.3	Burger-Ramberger plots	5
1.4	Crystal engineering and supramolecular chemistry	9
1.5	Examples of graph sets in hydrogen bond arrays	10
1.6	Examples of supramolecular synthons	12
1.7	Schematic phase diagrams	14
1.8	Anionic forms of squaric acid	15
1.9	Squaramide scheme	15
1.10	Zwitterionic resonance forms of squaramides	16
1.11	Squaramide anion complex	17
1.12	Squaramide's possible conformations	17
3.1	Squaramide model compounds	22
3.2	PXRD patterns of forms I, II and III of 1	23
3.3	DSC thermograms of forms I, II and III of 1	23
3.4	DSC thermogram of the reversible phase transition of form II	24
3.5	Crystal structures of forms I, II and III of 1	25
3.6	Overlapped conformers in the asymmetric unit of form II of 1	26
3.7	Zig-zag patterns of forms I, II and III of 1	26
3.8	Hirshfeld surfaces and fingerprint plots of both conformers of form II of 1	26
3.9	Different possible combinations of dipole moment alignments	27
3.10	PXRD diagrams of forms I and II of 2	28

3.11	DSC thermograms of forms I and II of 2	28
3.12	DSC of form I of 2	29
3.13	Hot stage photomicrographs of 2	29
3.14	Crystal structures and Hirshfeld surfaces of forms I and II of 2 . .	30
3.15	PXRD diagrams of forms I, II, III and IV of 3	32
3.16	DSC thermograms of forms I, II, III and IV of compound 3	32
3.17	Hot stage photomicrographs of 3	33
3.18	Variable temperature PXRD analysis of form I of 3	33
3.19	Crystal structure of form I of 3	34
3.20	Experimental PXRD diagrams of forms I + α , II and IV, and calculated PXRD diagram of form III of 4	35
3.21	DSC thermogram of forms I (+ α), II and III	36
3.22	DSC thermogram of form I showing a reversible transition to form IV of 4	36
3.23	Hot stage photomicrographs of compound 4	37
3.24	Polymorphic transformations of compound 4	37
3.25	Crystal structures of forms II of 4	38
3.26	Crystal structures of forms III of 4	39
3.27	Summary of the polymorphic systems studied in this chapter	40
3.28	Two diferent conformations of disecndary squaramides	41
3.29	Conformational equilibrium and $^1\text{H-NMR}$ spectrum of 2 in CDCl_3 at 240 K, 260 K and 290 K	42
3.30	2D $^1\text{H-NMR}$ COSY at 240 K of 2 upon dilution	43
3.31	Proposed thermodynamic cycle for dimerization of 2	43
3.32	Cooperativity in water molecules	44
3.33	Cooperativity in Urea and Formamide	45
3.34	Scheme and chain and ribbon interaction motifs for 5	46
3.35	MEP plotted of the squaric acid	47
3.36	Hydrogen bond parameters for the three conformations of 5	49
3.37	Induction effects favouring and disfavouring the second hydrogen bond	49

3.38	MEP surfaces and hydrogen bond parameters after the first interaction of anti/anti and syn/syn conformers	50
3.39	Interaction energies of the terminal monomer	51
3.40	Crystal structure of compound 5	51
3.41	Aggregation scheme of 2 according to Hunter's approach	52
3.42	Scheme, crystal structure and Hirshfeld's surface of 6	52
3.43	Scheme, crystal structure and Hirshfeld's surface of compound 7	53
3.44	Possible supramolecular synthons for compound 8	54
3.45	Dimeric aggregates observed in the crystal structure of 8 together with the Hirshfeld's surfaces	54
3.46	α and β parameters and dimers in the crystal structure of 9	55
3.47	Scheme of possible supramolecular synthons with both donor and acceptor cofomers.	57
3.48	Predicted interaction energies of 5 and 7	58
3.49	Cofomers used in the cocrystal screening of compounds 5 and 7	59
3.50	Scheme of cocrystal design strategies.	59
3.51	Scheme of 10 and 11	60
3.52	Expected supramolecular synthons for 10 together with their corresponding graph sets.	61
3.53	PXRD diagrams of forms I, II and III	62
3.54	Modulated DSC experiment of form I.	62
3.55	Crystal structures of forms I and II of 10	63
3.56	DFT interaction energies for the anti and syn oligomers.	64
3.57	Expected cocrystal of 10 and resorcinol.	65
3.58	Crystal structures of the resorcinol cocrystals.	65
3.59	Scheme of 2 and 4	67
3.60	Crystal structure of the ACN solvate of 2 and fumaric acid cocrystal	68
3.61	Crystal structure of the MeOH/Water solvate of 4 and fumaric acid cocrystal	69
3.62	Head-to-tail motifs of multicomponent forms of 2 and 4	69
3.63	PXRD diagrams of the two anhydrous cocrystals of 4 with resorcinol.	70

3.64	Crystal structure of 4 :resorcinol cocrystal, form I	70
3.65	Hydrate of the salt between 4 and squaric acid.	71
3.66	Scheme of a general disquaramide with peripheral hydrogen bond donor groups and 12	71
3.67	Crystal structures of ethanol and DMSO/water solvates of 12 . . .	72
3.68	Possible cyclic and polymeric aggregates of 13	73
3.69	Crystal structure of 13	74
3.70	Rotation of the two helices in the racemic crystal of 13	75
3.71	Macrocyclic squaramides 14 , 15 and 16	76
3.72	Scheme of the electrostatic compression phenomenon in squarate assemblies	77
3.73	Synthesis of the zwitterionic squaramide 17 and the schematic self-assembling through electrostatic compression	78
3.74	Different assembling motifs for 17	78
3.75	Stacked dimers for anhydrous forms I and II of 17	79
3.76	MEP surface of the crystal structure of form I	79
3.77	Supramolecular synthon observed in forms I and II of 17	80
3.78	Supramolecular synthons of the hydrate form III	81
3.79	Crystal structure of monosquarate/ 17 salt	82
3.80	Squarate and amidosquarate salts 18-22	83
3.81	Crystal structures of the amidosquarate salts 18-22	83
4.1	Thermal phenomena usually observed in a DSC analysis.	86
4.2	Antisolvent diffusion scheme.	90
5.1	SDPD using direct-space methods	94
5.2	Structure determination methods	97
5.3	Global optimization algorithm in SDPD	99
6.1	Scheme of squaramides' synthesis.	107
6.2	Synthesis of Dibenzylsquaramide.	107
6.3	Synthesis of 3,4-Bis(2-methylaminopyridyl)-1,2-dioxo-3-cyclobutene.	108
6.4	Synthesis of 3,4-Bis(2-ethylaminopyridyl)-1,2-dioxo-3-cyclobutene.	108

6.5	Synthesis of 3,4-Bis(2-dimethylamino-ethylamino)-cyclobut-3-ene-1,2-dione.	109
6.6	Synthesis of 3,4-Bis-methylamino-cyclobut-3-ene-1,2-dione.	110
6.7	Synthesis of 2,7-Diaza-bicyclo(6.2.0)dec-1(8)-ene-9,10-dione.	110
6.8	Synthesis of 3,4,9,10-Tetrahydro-3,10-diaza-benzocyclobuta-cyclooctene-1,2-dione.	111
6.9	Synthesis of 3-ethoxy-4-methylamine-cyclobut-3-ene-1,2-dione.	112
6.10	Synthesis of 3-ethoxy-4-(2-pyridin-2-yl-ethylamino)-cyclobut-3-ene-1,2-dione.	112
6.11	Synthesis of 1,4-Bis-(3-aminopropyl)piperazine-bis-monosquaramide ester.	113
6.12	Synthesis of 1,4-Bis-(3-aminopropyl)piperazine-bis-squaramide.	113
6.13	Synthesis of 3,4-Bis-(2-(4-hydroxy-phenyl)-ethylamino)-cyclobut-3-ene-1,2-dione.	114
6.14	Synthesis of 3-(2-Dimethylamino-ethylamino)-4-(2-(4-hydroxy-phenyl)-ethylamino) cyclobut-3-ene-1,2-dione.	115
6.15	Synthesis of 2,7,12,17-Tetraaza-tricyclo(16.2.0.0 ^{8,11})eicosa-1(18),8(11)-diene-9,10,19,20-tetraone.	116
6.16	Synthesis of cycloaminopropylpiperazinesquaramide.	116
6.17	Synthesis of cycloaminopropylpiperazinesquaramide.	117
6.18	Scheme of hydrolized squaramides' synthesis and their salts.	118
6.19	Synthesis of 3-(2-Dimethylamino-ethoxy)-4-hydroxy-cyclobut-3-ene-1,2-dione.	118
6.20	Synthesis of squarate : dibenzylamine salt	119
6.21	Synthesis of squarate : 1,4-bis(3-aminopropyl)piperazine salt	119
6.22	Synthesis of diethylamididosquaric acid : diethylamine salt	120
6.23	Synthesis of squarate : tyramine salt	120
B.1	List of cofomers used in this work	164
C.1	Crystallographic data of form I of 1 obtained by SXRD	178
C.2	Powder X-ray diffractogram of form I of 1	178
C.3	DSC thermogram of form I of 1	179

C.4	TGA thermogram of form I of 1	179
C.5	¹ H-NMR spectrum of form I of 1	179
C.6	Crystallographic data of form II of 1 solved by PXRD	180
C.7	Powder X-ray diffractogram of form II of 1	180
C.8	DSC thermogram of form II of 1	181
C.9	TGA thermogram of form II of 1	181
C.10	Crystallographic data of form III of 1 obtained by SXRD	182
C.11	Powder X-ray diffractogram of form III of 1	182
C.12	DSC thermogram of form III of 1	183
C.13	TGA thermogram of form III of 1	183
C.14	Crystallographic data of form I of 2 obtained by SXRD	184
C.15	Powder X-ray diffractogram of form I of 2	184
C.16	DSC thermogram of form I of 2	185
C.17	TGA thermogram of form I of 2	185
C.18	¹ H-NMR spectrum of form I of 2	185
C.19	Crystallographic data of form II of 2 solved by PXRD	186
C.20	Powder X-ray diffractogram of form II of 2	186
C.21	DSC thermogram of form II of 2	187
C.22	TGA thermogram of form II of 2	187
C.23	¹ H-NMR spectrum of form II of 2	187
C.24	Powder X-ray diffractogram of form I of 3	188
C.25	DSC thermogram of form I of 3	188
C.26	TGA thermogram of form I of 3	189
C.27	¹ H-NMR spectrum of form I of 3	189
C.28	Powder X-ray diffractogram of form II of 3	190
C.29	DSC thermogram of form II of 3	190
C.30	Powder X-ray diffractogram of form III of 3	191
C.31	DSC thermogram of form III of 3	191
C.32	Powder X-ray diffractogram of form IV of 3	192
C.33	DSC thermogram of form IV of 3	192

C.34	Crystallographic data of form II of 4 solved by PXRD	194
C.35	Powder X-ray diffractogram of form II of 4	194
C.36	DSC thermogram of form II of 4	195
C.37	TGA thermogram of form II of 4	195
C.38	¹ H-NMR spectrum of form II of 4	195
C.39	Crystallographic data of form III of 4 obtained by SXRD	196
C.40	Calculated powder X-ray diffractogram of form III of 4	196
C.41	DSC thermogram of form III of 4	197
C.42	TGA thermogram of form III of 4	197
C.43	Crystallographic data of form I of 5 obtained by SXRD	198
C.44	Powder X-ray diffractogram of form I of 5	198
C.45	DSC thermogram of form I of 5	199
C.46	TGA thermogram of form I of 5	199
C.47	¹ H-NMR spectrum of form I of 5	199
C.48	Crystallographic data of form I of 6 obtained by SXRD	200
C.49	Powder X-ray diffractogram of form I of 6	200
C.50	DSC thermogram of form I of 6	201
C.51	TGA thermogram of form I of 6	201
C.52	¹ H-NMR spectrum of form I of 6	201
C.53	Crystallographic data of form I of 7 obtained by SXRD	202
C.54	Powder X-ray diffractogram of form I of 7	202
C.55	DSC thermogram of form I of 7	203
C.56	TGA thermogram of form I of 7	203
C.57	¹ H-NMR spectrum of form I of 7	203
C.58	Crystallographic data of form I of 8 obtained by SXRD	204
C.59	Powder X-ray diffractogram of form I of 8	204
C.60	DSC thermogram of form I of 8	205
C.61	TGA thermogram of form I of 8	205
C.62	Crystallographic data of form I of 9 obtained by SXRD	206
C.63	Powder X-ray diffractogram of form I of 9	206

C.64	DSC thermogram of form I of 9	207
C.65	TGA thermogram of form I of 9	207
C.66	¹ H-NMR spectrum of form I of 9	207
C.67	Crystallographic data of form I of 11 solved by PXRD	208
C.68	Powder X-ray diffractogram of form I of 10	208
C.69	DSC thermogram of form I of 10	209
C.70	TGA thermogram of form I of 10	209
C.71	¹ H-NMR spectrum of form I of 10	209
C.72	Crystallographic data of form II of 10 solved by PXRD	210
C.73	Powder X-ray diffractogram of form II of 10	210
C.74	DSC thermogram of form II of 10	211
C.75	TGA thermogram of form II of 10	211
C.76	¹ H-NMR spectrum of form II of 10	211
C.77	Powder X-ray diffractogram of form III of 10	212
C.78	DSC thermogram of form III of 10	212
C.79	TGA thermogram of form III of 10	213
C.80	¹ H-NMR spectrum of form III of 10	213
C.81	Powder X-ray diffractogram of form I of 11	214
C.82	DSC thermogram of form I of 11	214
C.83	TGA thermogram of form I of 11	215
C.84	¹ H-NMR spectrum of form I of 11	215
C.85	Powder X-ray diffractogram of form I of 12	216
C.86	DSC thermogram of form I of 12	216
C.87	TGA thermogram of form I of 12	217
C.88	¹ H-NMR spectrum of form I of 12	217
C.89	Powder X-ray diffractogram of form II of 12	218
C.90	DSC thermogram of form II of 12	218
C.91	TGA thermogram of form II of 12	219
C.92	¹ H-NMR spectrum of form II of 12	219
C.93	Crystallographic data of form III of 12 obtained by SXRD	220

C.94	Calculated powder X-ray diffractogram of form III of 12	220
C.95	DSC thermogram of form III of 12	221
C.96	TGA thermogram of form III of 12	221
C.97	Crystallographic data of form IV of 12 obtained by SXRD	222
C.98	Calculated powder X-ray diffractogram of form IV of 12	222
C.99	Crystallographic data of form I of 13 solved by PXRD	224
C.100	Powder X-ray diffractogram of form I of 13	224
C.101	DSC thermogram of form I of 13	225
C.102	TGA thermogram of form I of 13	225
C.103	¹ H-NMR spectrum of form I of 13	225
C.104	Crystallographic data of form I of 17 obtained by SXRD	226
C.105	Powder X-ray diffractogram of form I of 17	226
C.106	DSC thermogram of form I of 17	227
C.107	TGA thermogram of form I of 17	227
C.108	¹ H-NMR spectrum of form I of 17	227
C.109	Crystallographic data of form II of 17 obtained by SXRD	228
C.110	Calculated powder X-ray diffractogram of form II of 17	229
C.111	DSC thermogram of form II of 17	229
C.112	Crystallographic data of form III of 17 obtained by SXRD	230
C.113	Calculated powder X-ray diffractogram of form III of 17	231
C.114	DSC thermogram of form III of 17	231
C.115	Powder X-ray diffractogram of form A of 2:fumaric acid cocrystal	234
C.116	DSC thermogram of form A of 2:fumaric acid cocrystal	234
C.117	TGA thermogram of form A of 2:fumaric acid cocrystal	235
C.118	¹ H-NMR spectrum of form A of 2:fumaric acid cocrystal	235
C.119	Crystallographic data of form B of 2:fumaric acid cocrystal obtained by SXRD	236
C.120	Powder X-ray diffractogram of form B of 2:fumaric acid cocrystal	237
C.121	DSC thermogram of form B of 2:fumaric acid cocrystal	237
C.122	Powder X-ray diffractogram of 2:p-nitrobenzoic acid salt	238
C.123	DSC thermogram of 2:p-nitrobenzoic acid salt	238

C.124	TGA thermogram of 2:p-nitrobenzoic acid salt	239
C.125	¹ H-NMR spectrum of 2:p-nitrobenzoic acid salt	239
C.126	Powder X-ray diffractogram of form A of 4:fumaric acid salt	240
C.127	DSC thermogram of form A of 4:fumaric acid salt	240
C.128	DSC thermogram of form A of 4:fumaric acid salt	241
C.129	¹ H-NMR spectrum of form A of 4:fumaric acid salt	241
C.130	Crystallographic data of form B of 4:fumaric acid salt obtained by SXRD	242
C.131	Calculated powder X-ray diffractogram of form B of 4:fumaric acid salt	243
C.132	Powder X-ray diffractogram of form A of 4:squaric acid salt	244
C.133	DSC thermogram of form A of 4:squaric acid salt	244
C.134	TGA thermogram of form A of 4:squaric acid salt	245
C.135	¹³ C-NMR spectrum of form A of 4:squaric acid salt	245
C.136	Crystallographic data of form B of 4:squaric acid salt obtained by SXRD	246
C.137	Calculated powder X-ray diffractogram of form B of 4:squaric acid salt	247
C.138	DSC thermogram of form B of 4:squaric acid salt	247
C.139	¹³ C-NMR spectrum of form B of 4:squaric acid salt	247
C.140	Crystallographic data of form A of 4:resorcinol cocrystal obtained by SXRD	248
C.141	Powder X-ray diffractogram of form A of 4:resorcinol cocrystal	248
C.142	DSC thermogram of form A of 4:resorcinol cocrystal	249
C.143	TGA thermogram of form A of 4:resorcinol cocrystal	249
C.144	Powder X-ray diffractogram of form B of 4:resorcinol cocrystal	250
C.145	DSC thermogram of form B of 4:resorcinol cocrystal	250
C.146	TGA thermogram of form B of 4:resorcinol cocrystal	251
C.147	¹ H-NMR spectrum of form B of 4:resorcinol cocrystal	251
C.148	Crystallographic data of form A of 10:resorcinol cocrystal ob- tained by SXRD	252
C.149	Powder X-ray diffractogram of form A of 10:resorcinol cocrystal	253

C.150	DSC thermogram of form A of 10:resorcinol cocrystal	253
C.151	TGA thermogram of form A of 10:resorcinol cocrystal	253
C.152	Crystallographic data of form B of 10:resorcinol cocrystal obtained by SXRD	254
C.153	Powder X-ray diffractogram of form B of 10:resorcinol cocrystal .	254
C.154	DSC thermogram of form B of 10:resorcinol cocrystal	255
C.155	TGA thermogram of form B of 10:resorcinol cocrystal	255
C.156	¹ H-NMR spectrum of form B of 10:resorcinol cocrystal	255
C.157	Powder X-ray diffractogram of form A of 10:hydroquinone cocrystal	256
C.158	DSC thermogram of form A of 10:hydroquinone cocrystal	256
C.159	TGA thermogram of form A of 10:hydroquinone cocrystal	257
C.160	¹ H-NMR spectrum of form A of 10:hydroquinone cocrystal	257
C.161	Powder X-ray diffractogram of form B of 10:hydroquinone cocrystal	258
C.162	DSC thermogram of form B of 10:hydroquinone cocrystal	258
C.163	TGA thermogram of form B of 10:hydroquinone cocrystal	259
C.164	¹ H-NMR spectrum of form B of 10:hydroquinone cocrystal	259
C.165	Crystallographic data of 18 salt obtained by SXRD	260
C.166	Powder X-ray diffractogram of 18 salt	261
C.167	DSC thermogram of 18 salt	261
C.168	¹³ C-NMR spectrum of 18 salt	261
C.169	Crystallographic data of 19 salt obtained by SXRD	262
C.170	Powder X-ray diffractogram of 19 salt	262
C.171	DSC thermogram of 19 salt	263
C.172	TGA thermogram of 19 salt	263
C.173	¹³ C-NMR spectrum of 19 salt	263
C.174	Crystallographic data of 20 salt obtained by SXRD	264
C.175	Powder X-ray diffractogram of 20 salt	265
C.176	DSC thermogram of 20 salt	265
C.177	Crystallographic data of 21 salt obtained by SXRD	266
C.178	Powder X-ray diffractogram of 21 salt	266
C.179	DSC thermogram of 21 salt	267

C.180	TGA thermogram of 21 salt	267
C.181	¹³ C-NMR spectrum of 21 salt	267
C.182	Crystallographic data of 22 salt obtained by SXRD	268
C.183	Powder X-ray diffractogram of 22 salt	269
C.184	DSC thermogram of 22 salt	269
C.185	Crystallographic data of 17 salt obtained by SXRD	270
C.186	Powder X-ray diffractogram of 17 salt	271
C.187	DSC thermogram of 17 salt	271
C.188	TGA thermogram of 17 salt	271

List of Tables

1.1	Non-covalent intermolecular interactions	11
3.1	Calorimetric data for the different crystal forms of 1	23
3.2	Crystal data for the three polymorphs of 1	25
3.3	Calorimetric data for crystal forms of 2	28
3.4	Crystal data of forms I and II of 2	31
3.5	Calorimetric data for crystal forms of 3	33
3.6	Crystal data for form I of compound 3	34
3.7	Calorimetric data for the crystal forms of 4	37
3.8	Crystal data of 4	38
3.9	Interaction energies for 5	50
3.10	Cocrystallization experiments with 2 and 4	67
3.11	Cocrystal experiments with 12	72
3.12	Helix-packing motifs and CH/ π interaction in 13	75
4.1	Crystallization methods	85
4.2	Solvents classification	87
A.1	Solubility of 1	148
A.2	Slurry experiments of 1 from the solubility study	148
A.3	Precipitation and crystallization experiments of 1	148
A.4	Precipitation and crystallization experiments of 1 by antisolvent addition	148
A.5	Solubility of 2	149
A.6	Slurry experiments of 1 from the solubility study	149

A.7	Precipitation and crystallization experiments of 2	149
A.8	Precipitation and crystallization experiments of 2 by antisolvent addition	150
A.9	Solubility of 3	150
A.10	Slurry experiments of 3 from the solubility study	150
A.11	Precipitation and crystallization experiments of 3	151
A.12	Precipitation and crystallization experiments of 3 by antisolvent addition	151
A.13	Solubility of 4	152
A.14	Slurry experiments of 4 from the solubility study	152
A.15	Crystallization experiments of 4	152
A.16	Crystallization experiments of 4 by antisolvent addition	152
A.17	Solubility of 5	153
A.18	Slurry experiments of 5 from the solubility study	153
A.19	Precipitation and crystallization experiments of 5	153
A.20	Precipitation and crystallization experiments of 5 by antisolvent diffusion	154
A.21	Solubility of 7	154
A.22	Slurry experiments of 7 from the solubility study	154
A.23	Crystallization experiments of 7 by antisolvent diffusion	155
A.24	Solubility of 8	155
A.25	Slurry experiments of 8 from the solubility study	155
A.26	Precipitation and crystallization experiments of 8	155
A.27	Crystallization experiments of 8 by antisolvent diffusion	156
A.28	Solubility of 9	156
A.29	Slurry experiments of 9 from the solubility study	156
A.30	Precipitation and crystallization experiments of 9	157
A.31	Solubility of 10	158
A.32	Slurry experiments of 10 from the solubility study	158
A.33	Precipitation and crystallization experiments of 10	158
A.34	Crystallization experiments of 10 by antisolvent diffusion	159

A.35 Solubility of 11	159
A.36 Slurry experiments of 11 from the solubility study	159
A.37 Precipitation and crystallization experiments of 11	160
A.38 Crystallization experiments of 11 by antisolvent diffusion	160
A.39 Solubility of 12	160
A.40 Slurry experiments of 12 from the solubility study	160
A.41 Crystallization experiments of 12 by antisolvent diffusion	161
A.42 Solubility of 17	162
A.43 Crystallization experiments of 17	162
A.44 Crystallization experiments of 17 by antisolvent diffusion	162
B.1 Drop grinding experiments of 2 and selected cofomers	165
B.2 Reaction crystallization experiments of 2 and selected cofomers . .	165
B.3 Crystallization experiments of 2 and selected cofomers from high temperature to r.t.	165
B.4 Crystallization experiments of 2 and selected cofomers by antisol- vent diffusion at r.t.	165
B.5 Recrystallization experiments from reaction crystallization solids of 2 and selected cofomers from high temperature to r.t.	165
B.6 Drop grinding experiments of 4 and selected cofomers	166
B.7 Reaction crystallization experiments of 4 and selected cofomers . .	166
B.8 Crystallization experiments of 4 and selected cofomers from high temperature to r.t.	167
B.9 Recrystallization experiments of the solids obtained by drop grinding between 4 and resorcinol	167
B.10 Crystallization experiments of 4 and selected cofomers by antisol- vent diffusion at r.t.	167
B.11 Crystallization experiments of the reaction crystallization solids of 4 and selected cofomers by antisolvent diffusion at r.t.	167
B.12 Drop grinding experiments of 7 and selected cofomers in a 1:1 molar ratio	169
B.13 Reaction crystallization experiments of 5 and selected cofomers . .	169
B.14 Drop grinding experiments of 7 and selected cofomers	169

B.15 Reaction crystallization experiments of 7 and selected coformers . . .	169
B.16 Crystallization experiments of 7 and oxalic acid in a 1:1 molar ratio by antisolvent diffusion	169
B.17 Crystallization experiments of 7 and selected coformers in a 1:1 molar ratio from high temperature to r.t.	170
B.18 Crystallization experiments of 7 and phosphoric acid (PHA) in a 1:1 molar ratio by antisolvent diffusion	170
B.19 Drop grinding experiments of 10 and selected coformers	170
B.20 Reaction crystallization experiments of 10 and selected coformers .	171
B.21 Precipitation experiments of 10 and resorcinol by rapid cooling from high temperature to 0°C	171
B.22 Crystallization experiments of 10 and selected coformers from high temperature to r.t.	171
B.23 Crystallization experiments of 10 and selected coformers by solvent evaporation at r.t.	172
B.24 Crystallization experiments of 10 and resorcinol in a 1:2 molar ratio by antisolvent diffusion	172
B.25 Crystallization experiments of 10 and hydroquinone by antisolvent diffusion	172
B.26 Drop grinding experiments of 12 and selected coformers	173
B.27 Reaction crystallization experiments of 12 and selected coformers .	173
B.28 Crystallization experiments of 12 and selected coformers from high temperature to r.t.	173
B.29 Crystallization experiments of 12 and selected coformers in a 1:2 molar ratio in DMSO by antisolvent diffusion	174
B.30 Crystallization experiments of 17 and selected coformers by antisol- vent diffusion	175

List of abbreviations

ACN	Acetonitrile
API	Active pharmaceutical ingredient
b.p.	Boiling point
BY	Bipyridine
CA	Citric acid
CAD	Crystallization experiments by antisolvent diffusion at r.t.
CHT	Crystallization experiments by slow cooling from high temperature to r.t.
COSY	Correlation spectroscopy
CRT	Crystallization experiments by slow cooling from high temperature to r.t.
CSD	Cambridge Structural Database
CSE	Crystallization experiments by seeding at r.t.
CSS	Crystallization experiments of the dissolutions obtained from the solubility study
NMR	Nuclear magnetic resonance spectroscopy
DBS	Dibenzylsulfoxide
DCM	Dichloromethane
DHBA	3,5-dihydrobenzoic acid
DMF	<i>N,N</i> -dimethylformamide
DMSO	Dimethylsulfoxide
DMSO- <i>d</i> ₆	Deuterated dimethylsulfoxide
DMU	Dimethylurea
DSC	Differential scanning calorimetry
EAFUS	Everything added to food in the United States
ETG	Ethylene glycol
EtOH	Ethanol
Et ₂ O	Diethyl ether
EtOAc	Ethyl acetate

FA	Fumaric acid
FDA	Food and drug administration
FRA	Formic acid
g	Gram
GLA	Gluconic acid
GMA	Glutamic acid
GRA	Glutaric acid
GRASS	Generally regarded as safe
HY	Hydroquinone
I	Insoluble
IA	Isethyonic acid
IPA	Isopropyl alcohol
ISNA	Isonicotinamide
LA	Lactic acid
m	Multiplet
MEK	Methyl ethyl ketone
MeOH	Methanol
mg	Milligrams
m/z	Mass-to-charge ratio
MHz	Megahertz
MIBK	Methyl isobutyl ketone
mL	Milliliters
m.p.	Melting point
MS	Mass spectrometry
NA	Nicotinamide
OA	Oxalic acid
PA	Propionic acid
PAA	Precipitation experiments by rapid addition of antisolvent at r.t.
PHA	Phosphoric acid
PHT	Precipitation experiments by rapid cooling from high to low temperature
PNBA	<i>p</i> -nitrobenzoic acid
ppm	Parts per million
PS	Partially soluble
PSD	Phase solubility diagram
PXRD	Powder X-ray diffraction
PY	Pyridine
RE	Resorcinol

r.t.	Room temperature
s	Singlet
S	Soluble
SQA	Squaric acid
SXRD	Single X-ray diffraction
t	Triplet
T	Temperature
T_g	Glass transition temperature
T_{tr}	Transition temperature
TFE	Tetrafluoroethanol
TGA	Thermal gravimetric analysis
THF	Tetrahydrofuran
TPD	Ternary phase diagram
TPPO	Triphenylphosphine oxide
UR	Urea
V	Volume
Z	Number of molecules in the crystallographic cell
Z'	Number of molecules in the asymmetric unit

Chapter 1

Introduction

1.1 Chemistry of the solid state

1.1.1 Crystal engineering

The term of crystal engineering was first introduced by Pepinsky in 1955 [1] and later developed by Schmidt. [2] Crystal engineering is defined as the design of crystal architectures starting from molecular building blocks and it studies the different crystal forms of compounds such as solvates, salts, cocrystals and polymorphs as possible routes for new functional materials (Fig. 1.1). It has become a key topic in the last few years, in both academic and industrial research, due to the impact that new crystalline materials have in different areas such as supramolecular chemistry, [3, 4] non-linear optical materials, [5, 6] coordination polymers [7] and pharmaceutical sciences, [8] usually with the aim of improving the physicochemical properties and also generating intellectual property. [9, 10] Crystal engineering permits a rational approach to the investigation of solid forms. [11]

1.1.2 Solid state forms

1.1.2.1 Polymorphs

Over the last decades polymorphism has been an intense area of research in solid-state chemistry. [12, 13] Polymorphism is defined as "the ability of an element or compound to exist in different crystal forms; with a different space disposition of the molecules which form the crystal". [14] Such differences in crystal packing and inter/intramolecular interactions can lead to considerable different physical and chemical properties, such as particle size, shape, hardness, melting point, density,

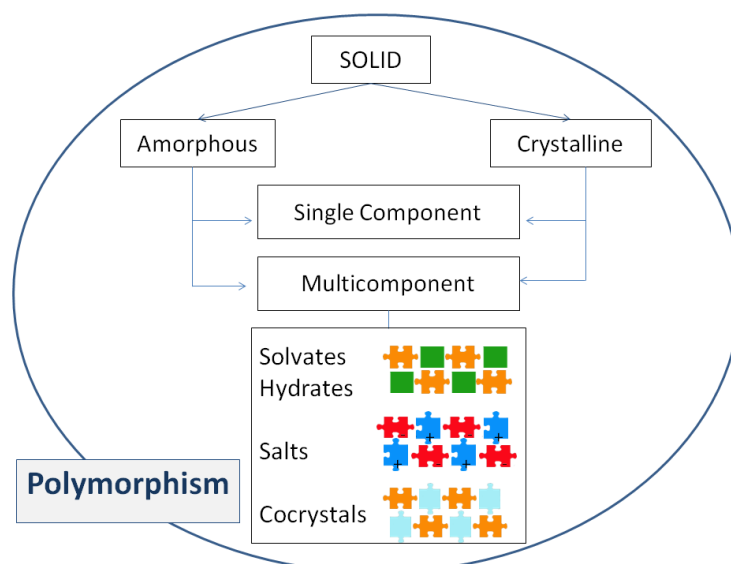


Fig. 1.1: Layout of molecular solid forms

solubility, dissolution rate, hygroscopicity, reactivity, heat capacity and stability, [15–18] which affect drug manufacturing processes [19, 20] and bioavailability, [21] mainly concerning the pharmaceutical industry. Other areas such as agrochemicals, pigments, dyes and explosives are also affected by polymorphism. [12, 22–25]

The first reported example of polymorphism of molecular compounds was benzamide in 1832 [26] and later on the ritonavir's phase transformation [27] alarmed the pharmaceutical industry (Fig. 1.2). Another similar case has been reported more recently for rotigotine, a Parkinson's disease drug. [28]

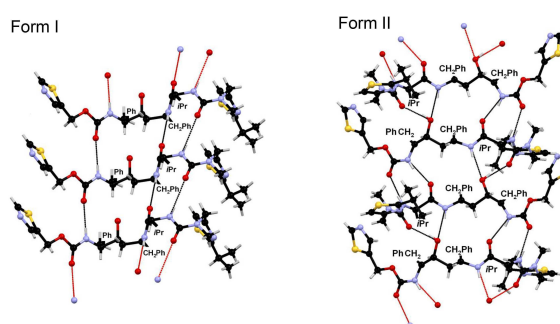


Fig. 1.2: Ritonavir's polymorphs [29]

Polymorphism and crystallization have become essential for research and the pharmaceutical industry with special importance on generic drugs over the last decade. About 80 per cent of pharmaceutical API's (Active Pharmaceutical Ingredient) show polymorphism and it has become a constant concern to the patent system, since a crystalline modification of a substance represents the existence of a new solid form with potentially different properties, converting it to a competitor

of a patented compound. [14, 16, 30, 31] Although today polymorphism is a well known phenomenon, predicting the occurrence and the properties of a particular polymorph of a given compound, as well as obtaining the desired polymorph are still a challenge to researchers. [32–38]

1.1.2.2 Thermodynamics of polymorphs

In a polymorphic system it is of great interest to determine the relative stability of the different forms. The ability of a polymorph to crystallize is determined by thermodynamic and kinetic factors. [39] As a consequence of the different disposition of the molecules in the crystal lattice and the non-covalent interactions, the energies of the polymorphs are also different and in extension the physicochemical properties of each solid form. Only one of the forms is the thermodynamically stable at a specific temperature and the rest of the forms may transform into the stable one. [14] However, it is possible that this transformation needs high activation energy and consequently the existence of metastable forms which do not transform during long periods of time is allowed. In the pharmaceutical industry, usually metastable forms are of special interest since they have advantageous properties such as high solubility, major bioavailability, and better behaviour in grinding or milling and compression processes. However, mechanical stress processes and high humidity conditions can accelerate polymorphic transformations from metastable to the stable forms, because of the tendency to reduce their free energy. [14, 16]

The knowledge of the thermodynamic and kinetic landscape of a polymorphic system is crucial to understand the formation of the different phases and their interrelations. The relation among different phases of a substance is governed by the rule of phases established by Gibbs:

$$P + F = C + 2 . \quad (1.1)$$

Being C the number of components, P the number of phases in equilibrium and F the number of degrees of freedom of the system. In case of a pure substance ($C = 1$) exhibiting two forms, two phases are in equilibrium ($P = 2$) and the system presents one degree of freedom. The conclusion drawn from the rule of phases is that only one form exists in a determined temperature and pressure, except in the transition temperature (T_{tr}), where the two phases coexist in equilibrium. According to this rule, the process of transformation of one polymorph into another (a phase transition) takes place at a specific temperature and pressure.

Relative stability between polymorphs

In the late nineteenth century, Lehmann classified the polymorphic systems into monotropic and enantiotropic systems, whereas Ostwald discovered the principles of thermodynamic and kinetic relationships between polymorphs (Ostwald's Rule of Stages). [12] If the system is reversible, the two forms are related enantiotropically and a transition temperature exists, in which the relative stability of the two polymorphs is inverted. The low melting form is the most stable below the transition temperature, and the high melting form is stable over that value. The transition on heating is always endothermic, whereas on cooling it is exothermic. On the contrary, if the transition between phases is irreversible, the two forms are related monotropically and the highest melting form is the most stable at all temperatures until the melting. In that case, the only possible spontaneous transformation is from the lowest melting point form to the highest melting point form, and such transformation is necessarily exothermic. [16, 40, 41]

Determining the relative stability between polymorphs is of great importance, since in the case of monotropy it will be impossible to obtain a metastable form starting from the stable one in the solid state. On the other hand, in the case of enantiotropy it is possible to obtain any of the forms depending on the temperature. In general, the thermodynamic relationship between two polymorphs is represented by the Gibbs free energy versus temperature plot. Burger and Ramberger, [42] proposed alternative plots called energy diagrams, in which free Gibbs energy and enthalpy of both polymorphs versus temperature are represented. (Fig. 1.3) [12, 14, 34, 40]

Rules for the prediction of the thermodynamic relationship between polymorphs

Thermodynamic relationships between polymorphs can be deduced experimentally by solubility measurements, solution-mediated polymorphic transformation studies, calorimetric analyses, density data and spectroscopy analysis. Tamman in 1926 was the first to develop some rules for predicting the thermodynamic relative stability between two or more polymorphs. Later, Burger and Ramberger in 1979, Yu in 1995 and Grunenber *et al.* in 1996 made extensive their applications. [12, 14, 40, 42, 43] The following empirical rules were extracted:

Heat of transition rule: two polymorphs are enantiotropically related if an endothermic phase transition between both forms exists at a temperature below the lower melting point. [14, 40, 41]

Heat of melting rule: two polymorphs are enantiotropically related if the higher melting point form presents the lowest enthalpy of melting, otherwise they are

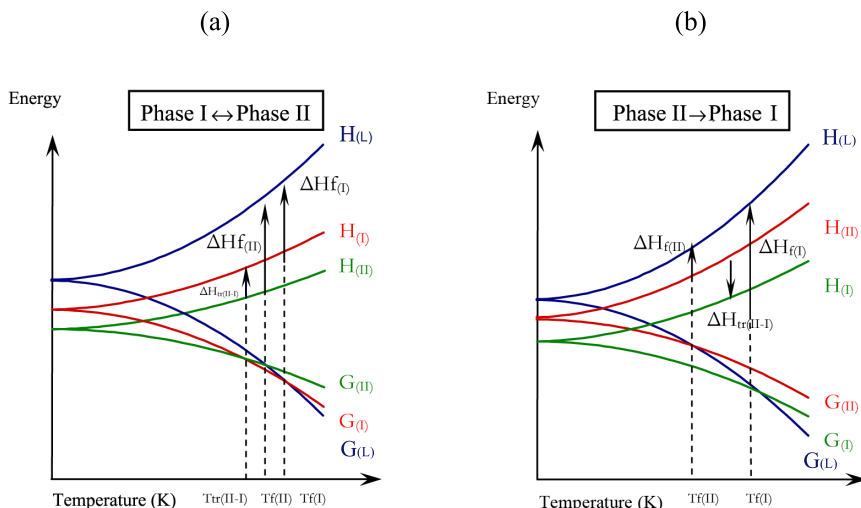


Fig. 1.3: Burger-Ramberger plots; (a) Enantiotropy and (b) Monotropy

monotropically related. [14, 40, 41]

Entropy melting rule: two polymorphs are enantiotropically related if the higher melting point form presents the lowest entropy of melting. On the contrary, they are monotropically related. [14, 43] However, this rule has several exceptions.

Heat capacity rule: two polymorphs are enantiotropically related if the higher melting point form has the bigger heat capacity, at a specific temperature. This rule has a limited application since similar heat capacities are difficult to be measured accurately. [14, 40]

Density rule: it is based on the principle established by Kitaigorodskii, taking into account the compact packing of the molecular crystals. [44] The most stable form of a system without hydrogen bonds in the absolute zero temperature has the highest density, since Van der Waals intermolecular interactions are stronger. Therefore, the crystal structure with the most efficient packing will have also the lowest free energy. However, this rule presents exceptions since energetically favorable hydrogen bonds can compensate the loss of energy of Van der Waals interactions and they can stabilize the polymorph with lower density. [12, 14, 44]

Other rules exist, but they are not widely applicable because of their error percentage.

1.1.2.3 Solvates and hydrates

Molecular compounds can also exist as solvates, which are solid phases containing solvent molecules that occupy regular positions in a stoichiometric or non-stoichiometric ratio in the crystalline structure. [14, 45, 46] Solvates are generally more soluble and dissolve faster than the pure substance. When the solvent is water they are called hydrates and, although they are usually less soluble than the anhydrous form, [47] they have much more interest in the pharmaceutical industry, because of its non toxicity and its high stability due to the capacity of the water molecules to form hydrogen bonds. [16] Moreover, these solid forms are of relevance in polymorphism since desolvation may lead to new polymorphs.

1.1.2.4 Amorphous solids

Amorphous solids consist of disordered arrangements, lacking a long-range order of molecules in the solid phase. Since they are metaestable forms, with a strong tendency to crystallize even more in contact with moisture, it is difficult to commercialize them in the pharmaceutical industry. However, they present a high interest in terms of solubility and bioavailability. Processes such as liophilisation and spray-drying are broadly used to produce amorphous solids. [16] An amorphous phase is named vitreous below a temperature called glass transition temperature (T_g) and it tends to behave like a crystalline solid having similar properties such as the plastic deformation and little order of the molecular disposition. Over this temperature, the substance is called rubber and it behaves more like a liquid phase, having similar molecular mobility, which may facilitate its spontaneous crystallization with a low exothermic heat variation associated and its subsequent melting at higher temperature. [40]

1.1.2.5 Salts

There are specific cases when the target compound is ionizable and it is possible to form a salt with a basic or acidic cofomer. [48] Salts are highly soluble in water and they show higher bioavailability than their corresponding neutral species. For this reason, they are, in many cases, preferably chosen over the free acid or base in the formulation of pharmaceutical compounds. Additionally, salt formation can improve crystallinity and stability. Approximately half of the APIs in the pharmaceutical market are salts. [14, 18, 49]

1.1.2.6 Cocrystals

Cocrystals have been known since the late 19th century. Quinhydrone was the first reported cocrystal by F. Wöhler in 1844. [50] They are an alternative to salts when these do not have the appropriate solid state properties or cannot be formed due to the absence of ionizable sites in a chemical compound. The definition of a cocrystal has brought considerable debate regarding them as multicomponent crystals: "complexes of two or more neutral molecules, each one existing as a solid at room temperature, interacting in the crystal lattice via non-covalent interactions: mainly hydrogen bonds, Van der Waals or π - π interactions". [14, 17, 51, 52] Recently, the Center for Drug Evaluation and Research of the Food and Drug Administration (FDA) has released the latest regulatory classification of pharmaceutical cocrystals: a cocrystal is a dissociable API-excipient complex classified as a drug product intermediate that can improve drug performance. [53]

Whether a compound is a salt or a cocrystal has been an issue of discussion among solid state chemists. [54, 55] Cocrystals and salts may be distinguished by the absence or not of a proton transfer between components. [56, 57] A pKa difference between two reactants (typically $\Delta \text{pka} > 3$) is used as a criterion for selecting counterions of salt formation. When the $\Delta \text{pka} < 1$ the resulting compound will almost exclusively be a cocrystal. However, there is a range between 0 and 3 in which no accurate prediction is possible to make. The difference between a salt and a cocrystal is the proton location in the crystal. Nevertheless, there is no sharp borderline between the two types of multicomponent crystals but a continuum, [54, 55, 58–60] since a molecular cocrystal can transform into a salt on variations in temperature or pressure. [61–63]

Cocrystals have recently gained the interest of different research areas such as nonlinear optics, solvent free organic synthesis, host-guest chemistry and photographic film formulation and they have become an additional tool in the pharmaceutical field. [60] In crystal engineering of pharmaceutical interest, a major goal is achieved when an API is induced to form a cocrystal by suitable complexation with another molecule known as a coformer, which is selected on the basis of molecular recognition through complementary sites with the API [64] from the GRAS (Generally Regarded as Safe) [65, 66] and EAFUS (Everything Added to Food in the United States) [67] lists published by the FDA. Cocrystallization of pharmaceuticals can improve some of the solid-state properties of the drugs, such as bioavailability, [68] dissolution rate, [69] physical stability, [70], flowability, chemical stability, [71] compressibility [72], hygroscopicity, [73] and the new solid forms can offer the possibility of patenting a protected API without infringing the originator's patent. [70, 74, 75] Cocrystals and salts can also present polymorphism, suggesting additional options

to modify properties, increase patent protection and improve marketed formulations. [10, 76–85] Opposite to what was previously thought, [86] cocrystal polymorphism is highly frequent and several examples of pharmaceutical cocrystals that show polymorphism have been reported to date. [77, 84, 87–89] Investigating the polymorphic behaviour of a compound is crucial for determining the solid state properties of a system and it is equally important when regarding cocrystal forms. Of several methods, cocrystallization from solution and mechanochemical methods are the mainly used for cocrystal formation and a combination is needed to identify as much polymorphic forms as possible. [90] Although several examples of pharmaceutical cocrystals are reported in the literature, none has been approved for use by the FDA yet, therefore much effort needs to be directed to the pharmaceutical cocrystal research.

A particular class of cocrystals formed by a neutral molecule and an inorganic salt are named ionic cocrystals and they have recently also received much attention in the pharmaceutical field. [91, 92]

1.1.3 Supramolecular chemistry

The term supramolecular chemistry has been defined by the Nobel laureate Jean-Marie Lehn as "the chemistry of molecular assemblies and of the intermolecular bond". [93] The principles of self-assembly and molecular recognition are intimately associated paradigms of supramolecular chemistry. The original research on supramolecular chemistry remains on synthetic receptors capable of "host-guest" type behavior in molecular recognition processes in which molecules select each other via favorable intermolecular interaction to yield a well-defined complex in solution in a coherent and cooperative manner, without the need to break or form covalent bonds. [94, 95] Pedersen, [96] Lehn [97] and Cram [98] developed the concepts of molecular recognition and self-assembly as an area of scientific research. Nowadays, supramolecular chemistry has evolved into an interdisciplinary field that bridges biology, chemistry and physics. Crystal engineering has been applied under the concept of supramolecular chemistry to design cocrystals by means of energy or structure based rational approaches on the paradigm of intermolecular interactions and molecular recognition to obtain new functional materials with specific properties. [52] A cocrystal is the consequence of a molecular recognition event between different molecular species. The subsequent crystal self-assembly is a non-equilibrium process via intermolecular interactions subject to the crystallization conditions and processes such as association and nucleation take place before crystal formation. (Fig. 1.4)

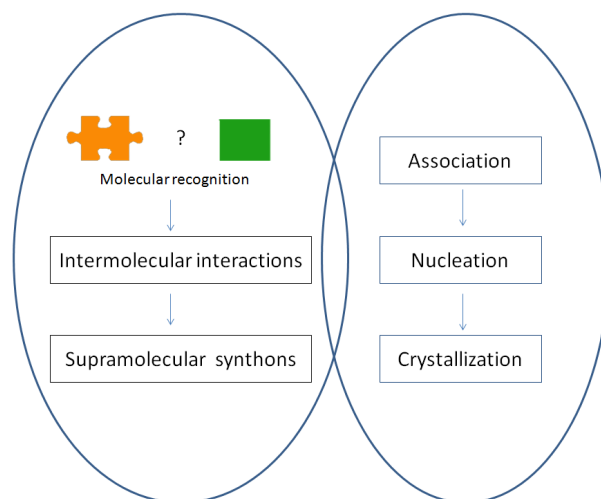


Fig. 1.4: Crystal engineering and supramolecular chemistry

1.1.3.1 Intermolecular interactions

Intermolecular interactions can be characterized by their ability to participate in directional or non-directional forces. Crystals of supramolecular systems are an example of structures that arise from both kind of interactions. On the first group, hydrogen bonding, halogen bonding, ion pair, ion-dipole [99] and dipole-dipole [100–102] interactions are largely electrostatic interactions. The anisotropic nature of dipoles provide a degree of directionality, as well as hydrogen and halogen bonding and also CH- π interactions. [103, 104]. On the other hand, induced-dipole interactions such as ion-induced-dipole and Van der Waals or London dispersion forces are weaker than permanent dipole interactions and they are the most commonly encountered non-directional interactions. Although not useful in cocrystal design, they are important in crystal packing. [105, 106]

The most notable interaction is hydrogen bond. Ubiquitous in science, hydrogen bonds are of relevance in assembling processes due to their directionality and strength. [107] It was in 1931, in a paper describing the nature of the chemical bond, when Pauling first used the descriptor "hydrogen bond". [108] A hydrogen bond may be formed when the electronegativity of A relative to hydrogen in an A-H covalent bond is sufficient to cause deshielding of the hydrogen. [109, 110] The hydrogen bond then forms with an acceptor atom B that comprises lone-pair electrons or polarizable π -electrons resulting in an A-H \cdots B arrangement. Hydrogen bonds have the flexibility to exist between varieties of functionalities with different lengths and geometries. [111] For pharmaceutical cocrystals, hydrogen bond plays a significant role and a graph set notation system introduced by Etter *et al.* in

1990 [107, 112] has been used widely to describe and label hydrogen bond motifs. For principal motifs: chains C, dimers D, rings R and intramolecular hydrogen bonds S as descriptors of hydrogen-bonded molecular solids are defined (Fig. 1.5).

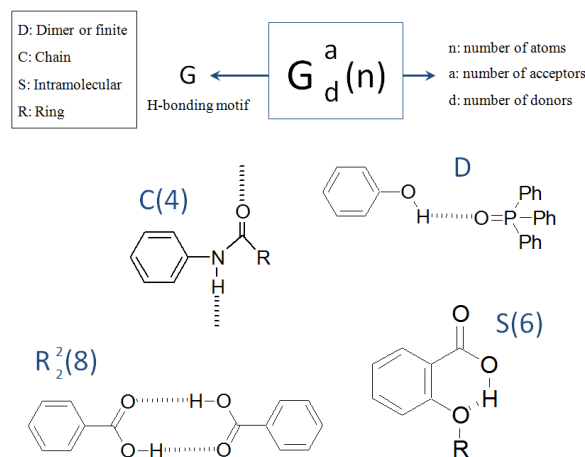


Fig. 1.5: Examples of graph sets in hydrogen bond arrays

In parallelism to hydrogen bonding, halogen bonding is a relatively strong and directional non covalent interaction of the type B–XY where B represents a Lewis base, commonly nitrogen, oxygen, sulphur or selenium with a non bonding electron pair, and X a halogen atom. Another reported type of halogen bonds is X···N. [113–116]

Electrostatic interactions such as ion pair are defined to exist when a cation and an anion are close enough in space that the energy associated with their electrostatic attraction is larger than the available energy to separate them. Ion-dipole and dipole-dipole is another type of electrostatic interactions in which the positive charge ends of a dipole interact with the negatively charge ends or ion. The latter forces are responsible for holding solvent molecules together and raising boiling points.

Other interactions which play a role in supramolecular chemistry and critical biological processes are those between π -surfaces (π - π stacking), cation- π , anion- π and polar- π . [117, 118] π - π interactions, can exist in different conformations: parallel displaced, T-shaped or edge-to-face, and tilted-T, [119–121] and all of them have been reported as part of the complexation of aromatic compounds within structurally diverse hosts in which complementary electrostatic interactions also play a role. Cation- π interactions have been reported to be comparable in nature and strength to the strongest intermolecular interactions. [122, 123] Theoretical studies of anion- π interactions support the concept of electron deficient aromatic surfaces

exhibiting favorable interactions towards anions with binding energies comparable to hydrogen bonds [124] Weaker than cation and anion- π interactions, polar- π interactions take part when a polar molecule interacts with the quadrupole moment of a π system. Any hydrogen bond donor will experience a favorable electrostatic interaction with the face of a benzene ring. These interactions are observed in protein structures and contribute to solid state packing forces.

On the other side of electrostatics, the hydrophobic effect is the single most important component in biological molecular recognition processes such as protein folding, membrane formation, small molecule binding by receptors in water. [118]

A comparison of the main intermolecular interactions is shown in table 1.1.

Tab. 1.1: Non-covalent intermolecular interactions.²

Interaction	Bond Energies (kJ/mol)	Building blocks	Products
Covalent	200–400	Atoms	Molecules
Hydrogen Bond	4–120		
Dipole–Dipole	5–50		
$\pi - \pi$ stacking	< 50	Molecules	Supermolecules
Van der Waals	< 5		

1.1.3.2 Cocrystals design and prediction

A detailed understanding of the supramolecular chemistry of the present functional groups is a prerequisite for designing a cocrystal, since it facilitates the appropriate selection of cocrystal formers. Structure based cocrystal design consists in locating which functional groups can interact with a cofomer using as a reference an empirical resource such as the Cambridge Structure Database (CSD), [125] which facilitates statistical analysis of packing motifs and many empirical information concerning common functional groups and how they engage in molecular association and form supramolecular synthons. [126]

A supramolecular synthon is a probabilistic event that represents directionality, and it is deeply embedded into the theory and practice of crystal engineering, since it is the structural unit that conveys the essential features of a crystal structure. Supramolecular synthons can be classified in two groups: homosynthons and heterosynthons. [127] Homosynthons occur between identical and complementary

²Data compiled from [94]

functional groups and some examples are: carboxylic acids, amide dimers and catemer synthons. On the other hand, heterosynthons occur between two different but complementary functional groups and some examples are: carboxylic–amide and carboxylic acid–pyridine synthons. [128] (Fig. 1.6)

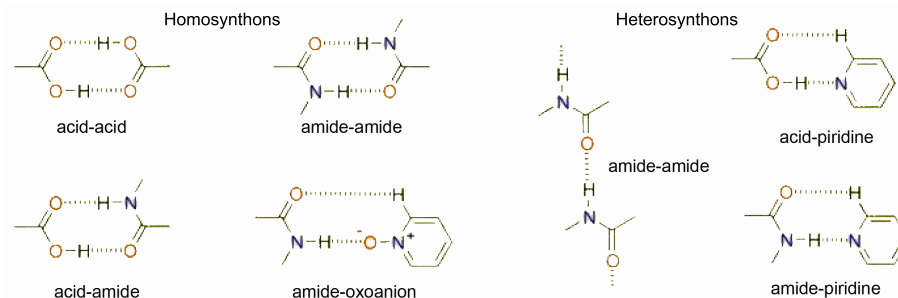


Fig. 1.6: Examples of supramolecular synthons

The supramolecular synthon approach [60] has its origins in 1894, when Emil Fischer postulated that an enzyme interacts with its substrate as a key does with its lock. [129] Later, the term of supramolecular synthon has been defined by Desiraju [64,126,130] as "structural units within supermolecules which can be formed and/or assembled by known or conceivable synthetic operations involving intermolecular interactions".

Cocrystallization is the result of competing molecular associations between different molecules and hydrogen bonds are mainly the basis of molecular recognition phenomena and responsible for the generation of a huge variety of molecular networks in the crystalline state. Thus, the crystal construction might be seen as a kinetically sequential event, in which initially the most robust synthon is formed with strong and directional interactions followed by other synthons involving slightly weaker and less directional interactions. Although competition between synthons makes it complicated, [64,85] empirical conclusions over the hierarchy of supramolecular synthons and in particular concerning hydrogen bonds are useful guidelines for cocrystal design. [52,131,132] The identification of reliable supramolecular synthons is the preliminary step in the design and analysis of multicomponent crystal structures. The main empirical guidelines described by Etter can be summarized as follows: [107]

- All good proton donors and acceptors are used in hydrogen bonding
- A six-membered ring with intramolecular hydrogen bonds is formed in preference to intermolecular hydrogen bonds
- The best proton donors and acceptors remaining after intramolecular hydrogen bond formation form intermolecular hydrogen bonds to one another.

A cocrystal is only expected to form if it is thermodynamically more stable than its free components. Understanding the relationship between the structure of a molecule and the preferred pattern of packing during the assembly of a multicomponent crystalline solid would provide insight into the design of solids with properties that depend on the relative alignment of the constituent molecules. Thus, understanding the nature and energetic orderings of non covalent interactions is essential for predicting the structures and properties of complex molecular systems. Apart from structure based methods for designing cocrystals, computational attempts have been recently exploited to predict cocrystal formation on the basis of various parameters: lattice energy calculations by Sally Price and coworkers, [133, 134] Hansen solubility parameters (HSPs), [135] enthalpies as implemented in COSMOtherm software. [136] More recently, a new predictive methodology has been developed by Chris Hunter, based on surface site interaction points calculated from the *ab initio* molecular electrostatic potential surface of the molecule in the gas phase. [137–139]

Unfortunately, cocrystal stoichiometry and additional components, such as solvent or water, which may become incorporated into the structure during synthesis, are other complications that hinder structure prediction. Therefore, reliable predictions of which structures will actually crystallize remains a challenging area of ongoing research and cocrystal synthesis is still limited within the real mode of trial-and-error experimentation for the foreseeable future. [140–143]

Rationalizing and predicting patterns of packing in molecular solids has proven to be difficult and different experimental strategies for engineering the design of molecular aggregates have been developed. [144–146] However, it still remains a scientific challenge to understand the nature of crystal packing forces and their impact upon physicochemical properties of different crystal forms.

1.1.3.3 Cocrystals formation

Various experimental methods can be performed to cocrystallize two entities: grinding, drop-grinding, cocrystallization from solution, reaction crystallization and co-melting are mainly used, and experimental conditions such as temperature, solvent, solute concentration, additives, vessel design, time heating, cooling rates, pH and mixing ratios are possible variables to be modified. [10, 74, 147] A first step of cocrystal formation is to study the existing equilibrium between the two solid phases and the solvent.

To depict the phase behavior of cocrystallizing systems, solubility diagrams are useful: binary phase diagram (BPD) [148] of A and B shows the thermal stability of

the cocrystal system and the eutectics, phase solubility diagram (PSD) [149] shows the solubility curves of solid phases as a function of solution concentration of A and B and ternary phase diagrams (TPD) [150,151] shows the thermodynamic outcome of a crystallization of cocrystal components (A and B) in a solvent (S) at a given temperature (Fig. 1.7). Solubilities of the two components are of special interest, since the difference in solubility alters the location and the shape of the region in which a cocrystal is thermodynamically stable.

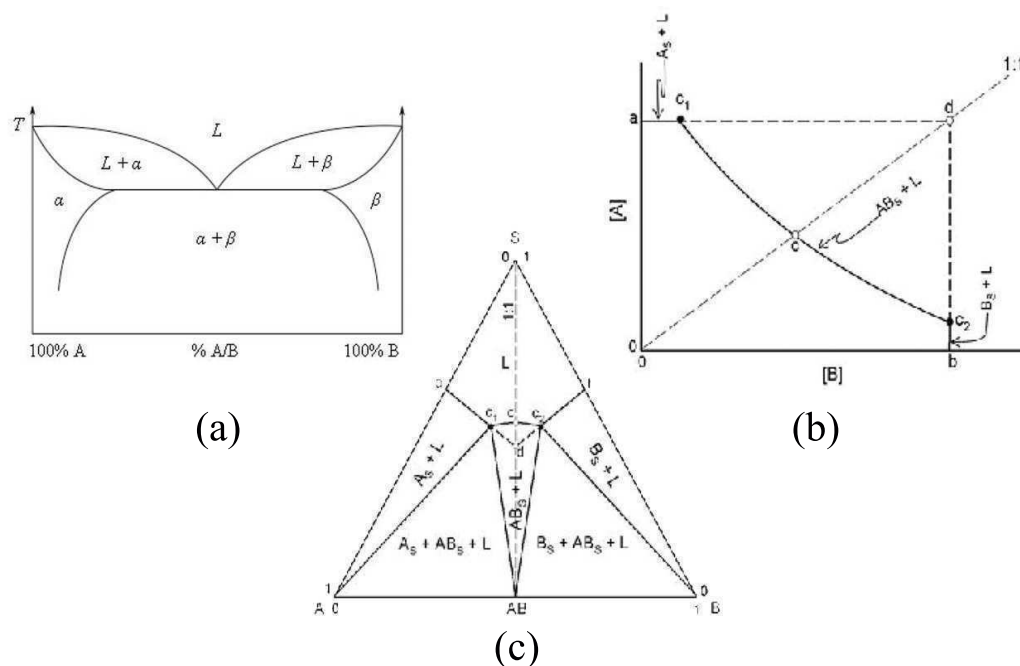


Fig. 1.7: Schematic (a) BPD, (b) PSD and (c) TPD diagrams [152,153]

After choosing the proper coformers, an experimental cocrystal screening is conducted in order to identify the solid forms obtained and verify if the previous prediction has been true. Since it is difficult to automate and labor intensive, high throughput methods have become of relevance. [154,155] The final step of cocrystal preparation is the performance of tests of newly formed compounds which includes both *in vitro* and *in vivo* tests for pharmaceutical cocrystals.

1.2 Squaric acid derivatives

In this PhD thesis, the solid state knowledge is applied to different squaric acid derivatives. Squaric acid (3,4-dihydroxy-3-cyclobutene-1,2-dione, (1)) was first synthesized by Cohen [156] and it is a colorless cyclobutene derivative of unusually high chemical and thermal stability. It is a strong diprotic acid, which can form mono- and dianions on deprotonation by amines (Fig. 1.8). [157–159] All the neutral

and ionic species possess a certain degree of electron delocalization, but it is most pronounced in (3), which is considered to be aromatic.

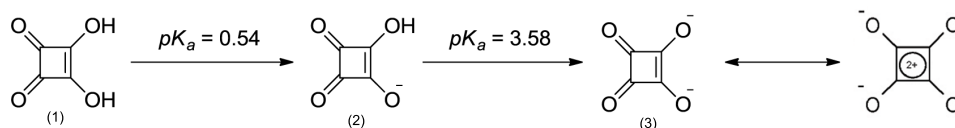


Fig. 1.8: Anionic forms of squaric acid

After the discovery of moniliformin, a semisquaric acid salt isolated from maize molds *Fusarium moniliforme* and *Gibberella Fujikuroi*, [160] numerous analogues derivatives of squaric acid have been synthesized and showed interesting physiological properties. [161] For all these abovementioned characteristics and its nature of small, flat and rigid molecule which can self-assemble by strong hydrogen bonds, squaric acid is a versatile potential molecule frequently used in crystal engineering to build up multicomponent systems with metals or organic bases to give specific two- or threedimensional aggregates. [162–166] In bioorganic chemistry, squaric acid can be used in enzymatic reactions, since its different resonance forms can mimic acidic functions. [167, 168] In other fields, squaric acid has been applied to the design of photoreceptors, organic solar cells and optical recording. [169]

A family of compound derivatives from squaric acid are cyclobutenediones and, in particular, squaramides (Fig. 1.9), which exhibit interesting and useful properties as supramolecular synthons. The presence of two donor and two acceptor hydrogen bonding groups in a rigid squaric ring have attracted in the past the attention of researchers in different areas such as medicinal chemistry, enantioselective catalysis, supramolecular chemistry and biochemical processes. [170–172]

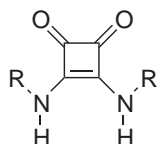


Fig. 1.9: Squaramide scheme

Squaramides have been widely studied in dissolution and various applications of these compounds have been recently reported. Unsymmetrical squaramides have been used as pharmaceutically active compounds into the treatment of various inflammatory diseases [173] and they have been also patented for their application in the treatment of asthma, multiple sclerosis, and rheumatoid arthritis. [174]

Still in medicine, other squaramides have been used as carboxylates, sulfonates and phosphates isosteric groups to enhance biological activity. [175] In biochemistry, squaramide-type nucleotide analogues have been studied as potential biologically active compounds such as antiviral and anticancer agents [157, 176–178] and as transmembrane anion transporters and ion channels for the treatment of a broad spectrum of disease types, with better properties than analogous ureas and thioureas. [179] In molecular recognition systems, squaramides are complementary to cations and anions, such as quaternary ammonium salts, [180, 181] carboxylates, [171] anion sulfates [182] and phospholipids. [171] These properties have been applied into the design of sensing devices [180, 183, 184] and nanoparticles. [185] Besides the abovementioned physiological properties of cyclobutenediones, these compounds have been also proved as powerful synthetic building blocks [170] and as chiral auxiliaries for asymmetric catalysis [186, 187] and different reactions such as Michael addition, [188] Friedel-Crafts reaction, [189] α -amination, [190] dynamic kinetic resolution [191] and Morita–Baylis–Hillman reaction. [189]

From a structural point of view, squaramides are analogous to squaric acid and they can be described as viniligous amides. The rigid and planar structure of the cyclobutenedione ring ($C_4N_2O_2$), containing two coplanar carbonyls and two N-H almost coplanar, induces a definite orientation of N-H groups, which enhances the linear hydrogen bonding specificity for some substrates. [192] The hydrogen bond capabilities are strengthened by the delocalization of the nitrogen lone pair electrons into the four-member ring to form zwitterionic resonance forms (Fig. 1.10) [193] and theoretical calculations have demonstrated that its partial aromaticity increments with the formation of complexes with anions and cations. [194–196]

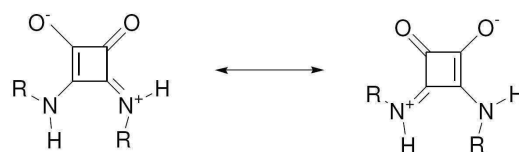


Fig. 1.10: Zwitterionic resonance forms of squaramides

For all these characteristics, squaramides have been studied in supramolecular chemistry as an efficient alternative to ureas and thioureas in the design of neutral multisite receptors, since they present advantages in duality binding, rigidity, hydrogen bonding, acidity and chemical stability. [197–199] Computational studies have illustrated the enhanced hydrogen bond donor ability and acidity of squaramides in comparison to ureas and thioureas. [200] The squaramido functionality shows duality and participates readily in ditopic or polytopic binding (anions and cations) (Fig. 1.11) even in competitive solvents, more than their counterparts' ureas and

thioureas. [185,197,198,201] Squaramides have been also proven good substitutes to thioureas in asymmetric catalysis. [171]

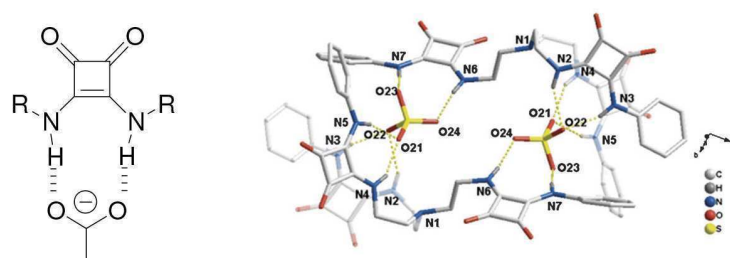


Fig. 1.11: Squaramide anion complex [202]

Previous studies of secondary squaramides in solution demonstrate that these compounds can exist in several conformations due to the partially restricted rotation of the C-N bond (anti/anti and anti/syn conformers) (Fig. 1.12). [192,197,203]

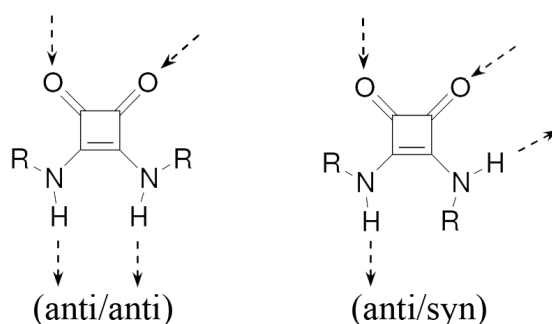


Fig. 1.12: Squaramide's possible conformations

The low energy barrier of rotation enables squaramides to exist in different conformations, which are geometrically capable to form self-assembling aggregates, stabilized through intra or intermolecular hydrogen bonds, even in highly competitive polar solvents. [181,192,204]

Although the properties of squaramides in solution are well known, to the best of our knowledge no information has been previously reported about their conformational preferences in the solid state. Only a few crystal structures of disubstituted squaramides have been described. [205,206]

In this PhD thesis, the solid state properties of squaramides will be investigated, as well as their applicability into the design of new multicomponent crystals.

Chapter 2

Objectives

This thesis is a multidisciplinary study of the solid state of squaric acid derivatives by combining approaches from areas such as crystal engineering, organic synthesis, supramolecular chemistry and crystallography.

The main objectives of this thesis are:

- To analyze the structural preferences in the solid state of the abovementioned family of compounds, which have been poorly studied in the past.
- To design new crystalline materials derived from squaric acid in order to study new supramolecular synthons.
- To explore relevant chemical phenomena such as template effect, preorganization, cooperativity and electrostatic compression.

In order to accomplish these objectives, a series of squaric acid derivatives has been synthesized and their crystal forms have been analyzed by means of several experimental techniques. In this sense, a crystal structure solution method based on powder X-ray diffraction has been optimized.

Chapter 3

Results and discussion

It is well known that squaramides exhibit a dual donor–acceptor hydrogen bonding ability in solution which make them interesting targets in areas such as supramolecular chemistry or medicinal chemistry. However, the lack of information about the solid state properties of squaramides encouraged us initially to conduct a polymorph screening of several model compounds with the objective to learn more about the structural features and conformational preferences of this family of compounds. On a second stage, this information was used to design new supramolecular architectures through crystal engineering strategies. Finally, the analysis of their crystal structures, in combination with important associated chemical phenomena such as cooperativity, preorganization and electrostatic compression, helped us to establish crystallographic and chemical relations among these compounds.

3.1 Polymorphism of disquaramides

In this chapter the polymorphism of several model compounds are separately discussed (Fig. 3.1). Each model compound has been carefully designed with its particular interest: dibenzylsquaramide (**1**) has no additional hydrogen bond donors/acceptors apart from the squaramide moiety and it is geometrically restricted compared to other models, the two dipyrindyl squaramides (**2** and **3**) have different aliphatic chain lengths and the pyridine groups enhance the hydrogen bond acceptor character of the whole compound, as well as the two dimethylamino groups of dimethylethylenediaminosquaramide (**4**) which in addition is highly flexible.

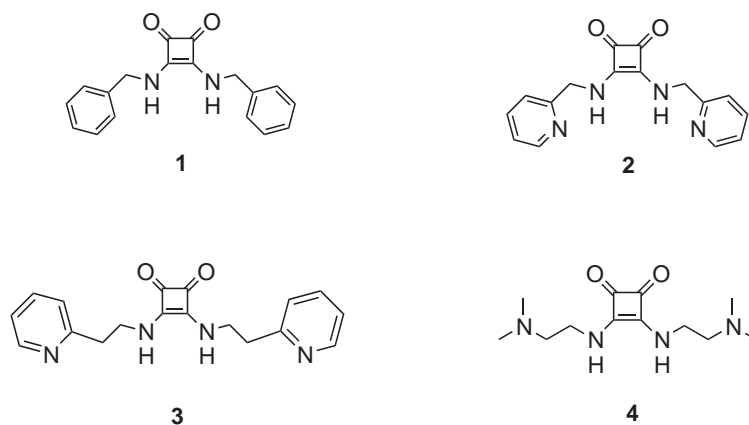


Fig. 3.1: Squaramide model compounds: (1) Dibenzylsquaramide, (2) 3,4-bis-(2-methylaminopyridyl)-1,2-dioxo-3-cyclobutene, (3) 3,4-bis-(2-ethylaminopyridyl)-1,2-dioxo-3-cyclobutene, (4) 3,4-bis-(2-dimethylamino-ethylamino)-1,2-dioxo-3-cyclobutene

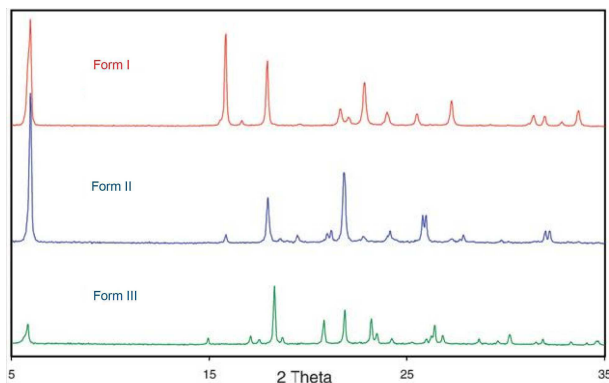
An experimental polymorph screening under different thermodynamic and kinetic crystallization conditions was conducted with all compounds in order to obtain as many crystal forms as possible (Chapter 6.3.6). The different crystal modifications observed were fully characterized by the combination of calorimetric techniques (DSC, TGA), powder X-ray diffraction (PXRD) and hot-stage microscopy. When possible, the crystal structures were determined either by single X-ray diffraction (SXRD) or from PXRD.

3.1.1 3,4-Bis-benzylamino-cyclobut-3-ene-1,2-dione (1)

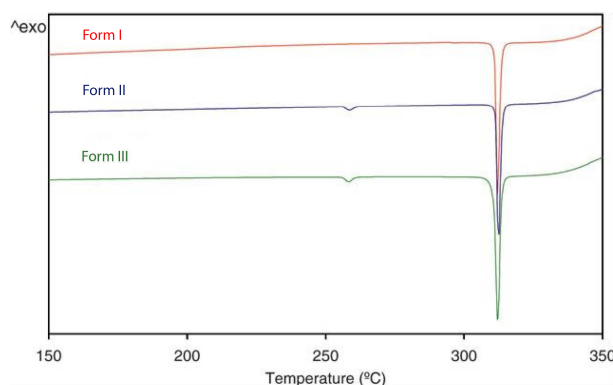
Compound **1** (Dibenzylsquaramide) was obtained according to the literature from diethylsquarate and benzylamine in ethanol as a white solid (Chapter 6.3.6). Since it was highly insoluble in all organic solvents, it could only be recrystallized in polar media such as DMF and DMSO and different combinations of those solvents with polar and non polar antisolvents. The solids obtained revealed a multipolymorphic system consisting of three forms according to their different X-ray diffraction patterns (Fig. 3.2). Experimental screening results are summarized in appendix A.12.

Form I was obtained by slow cooling of a DMF saturated solution of **1** from 70 °C to r.t. Forms II and III could be obtained by slow diffusion of diethyl ether or dioxane, respectively, into a DMSO saturated solution at r.t. (See appendix A.12).

DSC analyses of forms I, II and III reveal the melting of the anhydrous form I at 311 °C (Fig. 3.3). In addition, DSC analyses of forms II and III show a solid-solid transition at 256 °C into form I, which was confirmed by both variable heating rate DSC (the endothermic phenomenon is displaced when changing the heating rate) and variable temperature PXRD analyses. Interestingly, the transition temperature

Fig. 3.2: PXRD patterns of forms I, II and III of **1**

is observed at almost the same value in both cases. Although several polymorphs can present the same melting point, [207] to the best of our knowledge this is the first time that two forms share the same transition temperature.

Fig. 3.3: DSC thermograms of forms I, II and III of **1**

Taking into account the prediction rules (see 1.1.2.2) and some calorimetric experiments, the relative stability of the polymorphs of **1** was deduced. Their DSC analyses revealed that the two polymorphic forms II and III transform through a solid-solid transition into form I at the same temperature (Tab. 3.1).

Tab. 3.1: Calorimetric data for the different crystal forms of **1**

Forms	Transition		Melting	
	Onset (°C)	ΔH (J/g)	Onset (°C)	ΔH (J/g)
I	-	-	311	165
II	257	2	-	-
III	256	3	-	-

Since the transition is endothermic, according to the Burger and Ramberger's

heat of transition rule (section 1.1.2.2), II and III are enantiotropically related to form I. In an enantiotropic system the phase transition must be reversible so it might be detectable in a heating-cooling DSC analyses. Figure 3.4 shows a DSC thermogram of form II in which the reversible phase transition is observed endothermic while heating and exothermic on cooling.

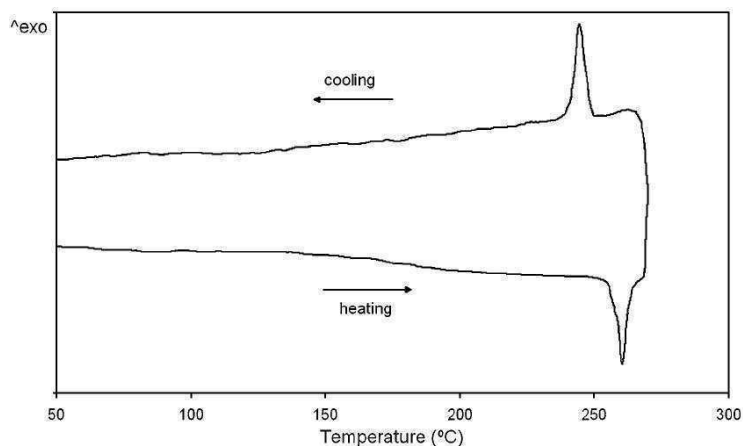


Fig. 3.4: DSC thermogram of the reversible phase transition of form II on heating and cooling

Single crystals of forms I¹ and III², suitable for X-ray structure determination (Fig. 6.2), were grown by slow cooling of a saturated solution of **1** in DMF at 70°C and by slow diffusion of dioxane into a saturated solution of **1** in DMSO at r.t., respectively.

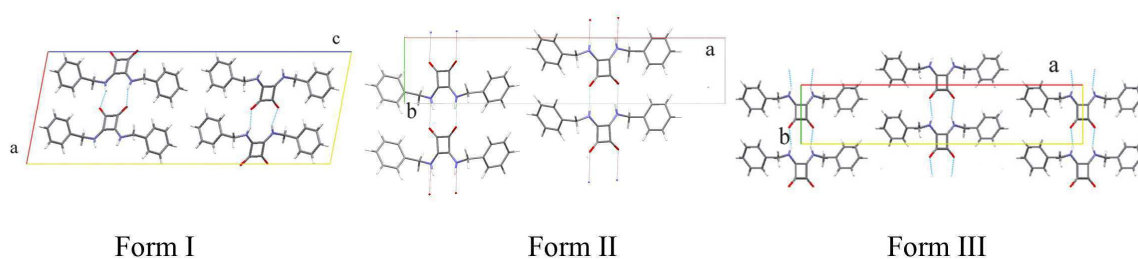
Since no suitable single crystals were obtained for form II³, its crystal structure was determined by means of direct-space methods. Despite the facts of having a tiny amount of sample and of preferred orientation problems caused by the usual needle shape crystals, the use of high quality glass capillary, good resolution and high statistics laboratory powder XRD data lead to a successful structure solution. The results enabled the following discussion of relevant crystallographic features of the three polymorphs (Fig. 6.2).

Forms I, II and III crystallize in monoclinic non-centrosymmetric space groups C2, Pc and C2/c, respectively. All three forms reveal a well defined head-to-tail hydrogen bonding motif among the squaramide units through two amide hydrogens and two carbonyl oxygens (N-H/O) with similar intermolecular distances (Tab. 3.2). Secondary $\pi - \pi$ stacking of the benzene rings in edge-to-face and offset stacked geometries [121] are also observed in the direction of *b* axis for form I and *c* axis

¹CCDC 676071 contains the crystallographic data.

²CCDC 686074 contains the crystallographic data.

³CCDC 914675 contains the crystallographic data.

Fig. 3.5: Crystal structures of forms I, II and III of **1**

for forms II and III. CH- π interactions are also present in the three forms and the offset stacked molecules form a zig-zag pattern (Fig. 3.7).

Tab. 3.2: Crystal data for the three polymorphs of **1**, being M1 and M2 the two conformers in the asymmetric unit (*Standard deviations have not been calculated since distances are obtained from Rietveld refinement).

Forms	Space Group	Z (Z')	d NH \cdots O (Å) M1/M2	$d_{centroids}$ (Å) M1/M2	$d_{CH-\pi}$ (Å)
I	<i>C</i> 2	4(1)	2.834(6) 2.838(6)	4.410	3.895
II	<i>P</i> <i>c</i>	4 (2)	2.844 2.900 / 2.837 2.839*	5.271 / 5.181	3.501 2.989
III	<i>C</i> 2/ <i>c</i>	4 (1)	2.779(3) 2.779(3)	3.263	5.242

The main difference among them is that the asymmetric unit of form II contains more than one molecule ($Z'=2$). Polymorphs, and crystal structures in general, where the number of molecules in the asymmetric unit is greater than 1 ($Z' > 1$) are relatively rare and their occurrence is still the subject of debate, mostly regarding their thermodynamic stability. [208–211] The two molecules in the asymmetric unit show two different conformations as a result of the aromatic ring rotation (Fig. 3.6). Since the asymmetric unit contains two different conformers, there are two types of stacking arrangements. On the one hand, for the first array of molecules, the centroid-centroid distance is 5.27 Å, the lateral displacement distance is 4.86 Å and the interplanar distance is 2.05 Å, with an angle between rings of 37.77°. On the other hand, for the second array of molecules, the centroid to centroid distance is 5.18 Å, the perpendicular distance between the offset stacked rings is 4.63 Å with a displacement angle of 43.80° and lateral displacement of 2.3 Å (Fig. 3.7).

Calculation of Hirshfeld surfaces [212–214] and fingerprint plots [215] is a useful way to analyze the intermolecular interactions in molecular crystals. The fingerprint

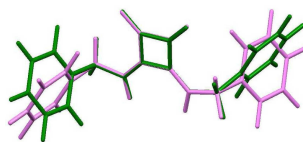


Fig. 3.6: Overlapped conformers in the asymmetric unit of form II of **1**

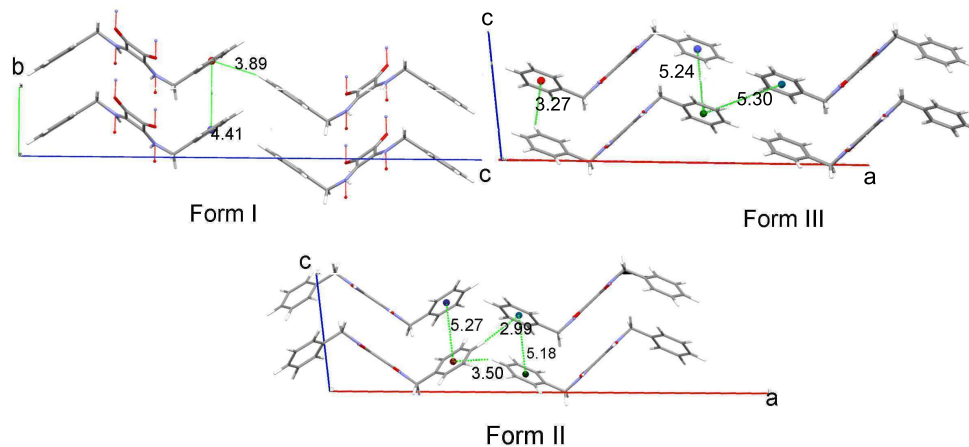


Fig. 3.7: Zig-zag patterns of forms I, II and III of **1**

plots of the two different conformers in the asymmetric unit show the same hydrogen bonding motif (red circles) but subtle differences of packing, denoting a similar crystallographic environment for the two conformers (Fig. 3.8).

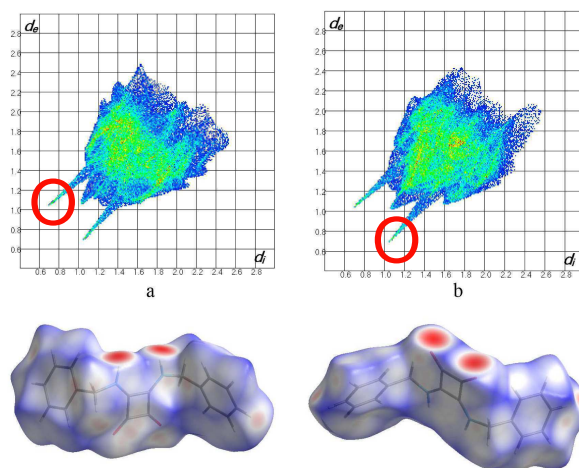


Fig. 3.8: Hirshfeld surfaces (below) and fingerprint plots (above) of both conformers of form II of **1**, with d_e (left) and d_i (right) mapped in colour (in both cases red represents the closest contacts, and blue the most distant contacts)

It is important to notice the different packing direction of the squaramide columns when comparing the three polymorphs. Self-assembled chains of disecundary squaramides can be oriented in three different manners: parallel, antipa-

parallel, and unparallel alignments with implications in the crystal polarity, which can produce Non-Linear Optical (NLO) materials, [216–219] interesting for the development of technological devices. Since the molecular dipole moment of **1** is high (8.15 Debbyes)⁴, the most likely alignment expected is the antiparallel one, which minimizes the net dipole moment in the crystal. [220–222] Whereas forms II and III show an antiparallel alignment in the direction of the head-to-tail alignment, form I exhibits an unparallel configuration, with an angle of 144° between the dipole moment vectors (Fig 3.9) which could present NLO properties. Electronic microscopy experiments were performed to confirm NLO properties of form I, but no significant conclusions could be extracted.

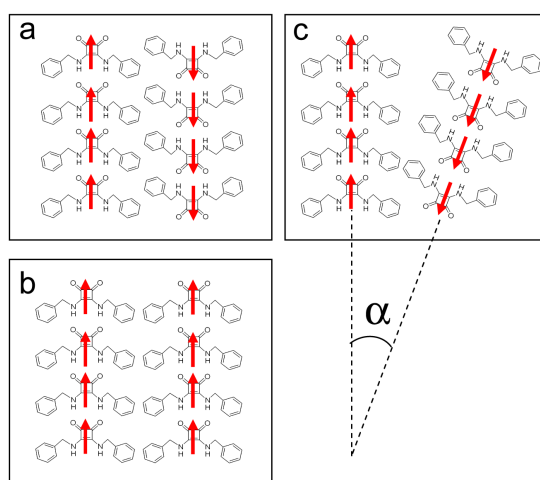


Fig. 3.9: Different possible combinations of dipole moment alignments; (a) antiparallel, (b) parallel and (c) unparallel, showing the angle between dipole moment vectors

In conclusion, three forms of dibenzylsquaramide are reported, two of them sharing a solid-solid transition at the same temperature towards the highest melting polymorph, which is a rare observation. The same hydrogen bonding head-to-tail motif is observed in their crystal structures and further insight investigations are directed to other compounds with additional donor-acceptor functional groups to reveal their crystal preferences.

3.1.2 3,4-bis-(2-methylaminopyridyl)-1,2-dioxo-3-cyclobutene (2)

Compound **2** was prepared from diethylsquarate and 2-methylaminopyridine in ethanol with high yield. An intensive polymorph screening resulted in two polymorphs I and II confirmed by PXRD analyses (Fig. 3.10).

⁴Calculated with Spartan'10 using a DFT B3LYP/6-31G* functional

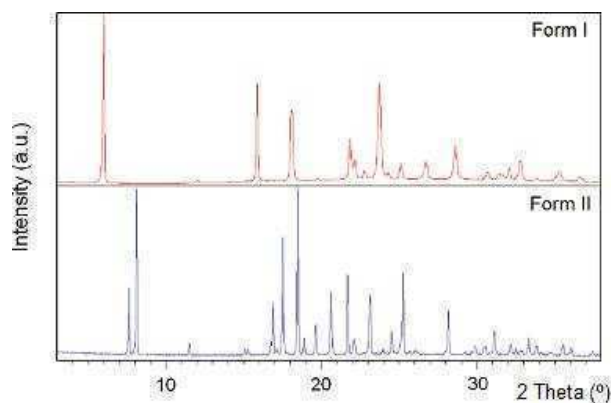


Fig. 3.10: PXRD diagrams of forms I and II of **2**

DSC analysis of form I shows its melting at 166 °C together with a simultaneous crystallization of form II. Finally, the subsequent melting of form II is observed at 186 °C followed by its decomposition (Fig. 3.11).

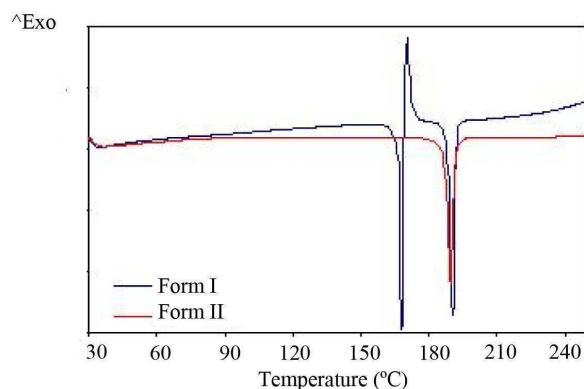


Fig. 3.11: DSC thermograms of forms I and II of **2**

Calorimetric data for crystal forms of **2** are summarized in table 3.3.

Tab. 3.3: Calorimetric data for crystal forms of **2** (*enthalpies are not precise due to overlapped thermal phenomena)

Forms	Melting		Crystallization	
	Onset (°C)	ΔH (J/g)	Onset (°C)	ΔH (J/g)
I	166	>68*	-	-
II	186	90	$\tilde{169}$	>37*

Form I was obtained during the experimental polymorph screening as plate shaped crystals from crystallizations under different conditions. However, form II could only be obtained by crystallization from the melt. Form I was heated at

175 °C (10 °C/min) in the DSC crucible under nitrogen atmosphere to obtain form II, which remained stable when cooling to r.t. Therefore, it could be characterized by powder X-ray diffraction (See appendix A.12).

Occasionally, an endothermic solid-solid transition was observed by DSC (Fig. 3.12), starting from form I at low heating rate (1 °C/min), revealing an enantiotropic relationship between the two polymorphs, being form I the stable polymorph below the transition temperature (ca. 160 °C).

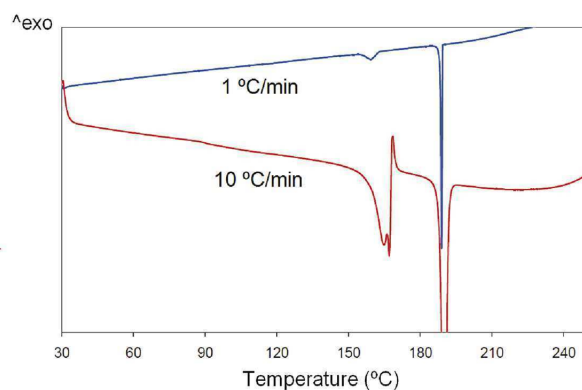


Fig. 3.12: DSC of form I of **2** showing the melting/crystallization phenomena (red) and the occasionally observed solid–solid transition from form I to II (blue)

This thermal behaviour was corroborated qualitatively by thermomicroscopy. When heating form I, a partial solid-solid transition to form II was observed around 168–169 °C. Simultaneously, the remaining form I melted and form II crystallized from the melt also at 169 °C. Finally, form II melted with decomposition at 190 °C (Fig. 3.13).

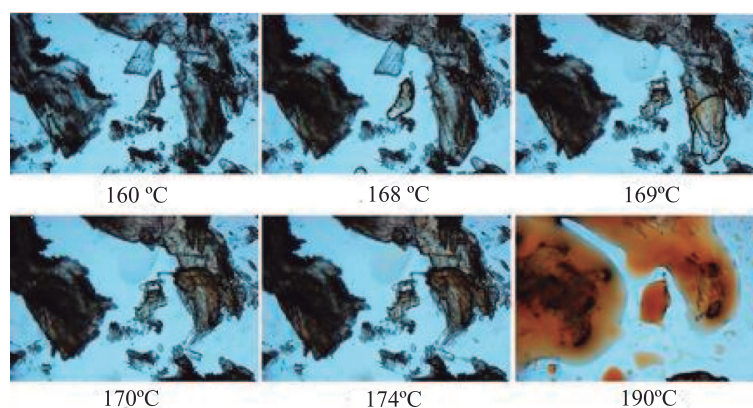


Fig. 3.13: Hot stage photomicrographs of **2**, showing the solid-state phase transition from form I to form II together with melting and crystallization phenomena upon heating at 10 °C/min

The crystal structure of form I⁵ was determined by single crystal XRD using a crystal grown by slow diffusion of toluene into a solution of **2** in DMF at r.t. Since single crystals of form II suitable for single-crystal XRD could not be grown, its crystal structure determination was instead carried out directly from PXRD data, exploiting the direct-space strategy for structure solution using EAGER software.⁶

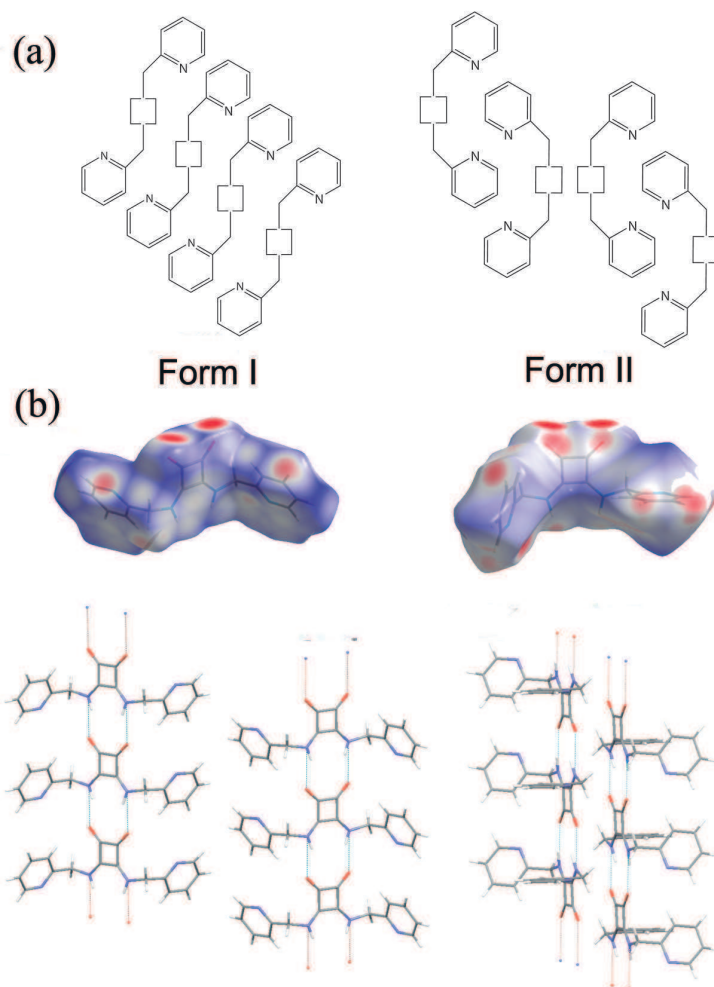


Fig. 3.14: Crystal structures and Hirshfeld surfaces of forms I and II of **2**

The crystal structures of both forms (Fig. 3.14) present a well-defined head-to-tail hydrogen bonding motif between squaramide units together with secondary $\pi-\pi$ stacking as for **1**. Aryl $\text{CH}\cdots\text{N}$ pyridine interactions are also observed. Crystal data are shown in table 3.4.

The dominant $\text{NH}\cdots\text{O}$ hydrogen bonding interactions that give rise to catemeric assemblies are seen in the Hirshfeld surface plots for both polymorphs (brightest red areas in figure 3.14 (b)). However, the head-to-tail motif of form II is arranged

⁵CCDC 805689 contains the crystallographic data.

⁶CCDC 826650 contains the crystallographic data.

Tab. 3.4: Crystal data of forms I and II of **2** (*Standard deviations have not been calculated since distances are obtained from Rietveld refinement)

Forms	Space Group	Z (Z')	d NH \cdots O (Å)	$d_{centroids}$ (Å)	d CH-N _{pyridine} (Å)
I	Pc	2 (1)	2.834(8) 2.848(6)	3.851	2.578(5)
II	P-1	2 (1)	2.804 2.836*	-	2.916*

in antiparallel rows of self-associated squaramide molecules whereas form I presents parallel orientated head-to-tail rows. Different secondary interactions are established in each case, corresponding to the structural particularities between the two polymorphs. $\pi-\pi$ stacking interactions in form I are replaced by edge-to-face CH- π interactions in form II. Furthermore, while the aromatic groups are located on the same side of the squaric ring in form II, they are arranged in a zig-zag manner in form I (Fig. 3.14(a)).

3.1.3 3,4-bis-(2-ethylaminopyridyl)-1,2-dioxo-3-cyclobutene (3)

Compound **3** was prepared from diethylsquarate and 2-ethylaminopyridine in ethanol with high yield. An intensive polymorph screening resulted in four polymorphs (Fig. 3.15).

Form I was obtained during the experimental polymorph screening in different conditions as a white powder or needle shaped crystals, suitable for single X-ray diffraction analysis. Form II could only be obtained by crystallization from the melt and forms III and IV were obtained from rapid cooling precipitation of **3** in ethanol and water, respectively (See appendix A.12).

DSC analysis of form I shows two endothermic phenomena apparently corresponding to the melting of different polymorphs (Fig. 3.16). However, various alternative hot stage microscopy analyses show a solid-solid transition at the same temperature as the first endothermic phenomenon registered by DSC (Fig. 3.17). Complementary low heating rate and heating-cooling DSC experiments cannot confirm the nature of the first endothermic phenomenon, since no presence of any transition is detected and no separation of a possible overlapped melting/crystallization processes is observed. In a variable temperature PXRD experiment of form I (Fig. 3.18), peaks of form II are detected at 198 °C and the subsequent melting of form II is observed at 224 °C together with its decomposition at 250°C. The DSC analysis of

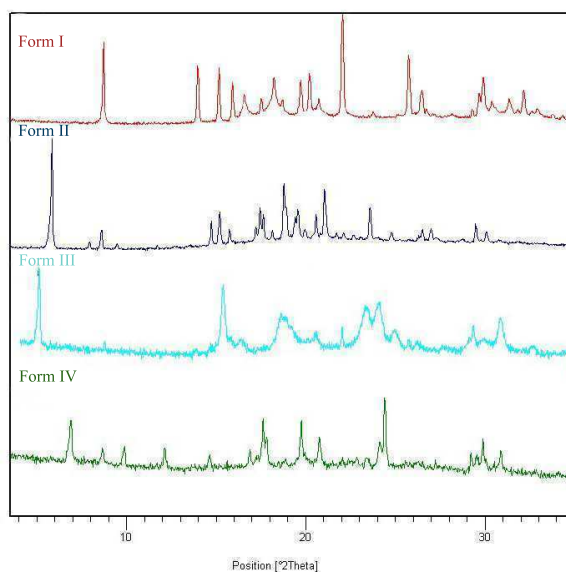


Fig. 3.15: PXRD diagrams of forms I, II, III and IV of **3**

form III shows a melting and crystallization phenomenon at 168 °C and form IV melts at 180 °C.

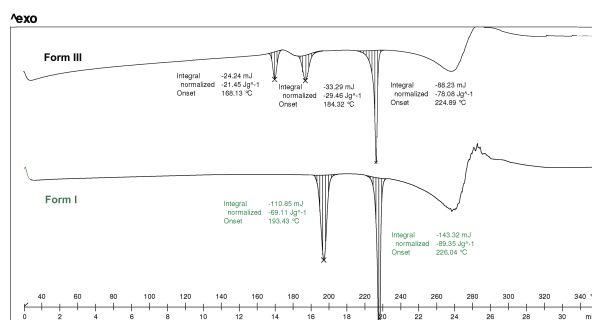
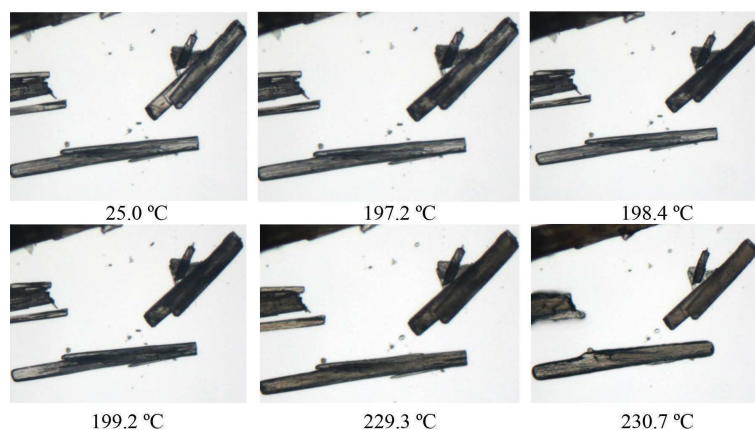
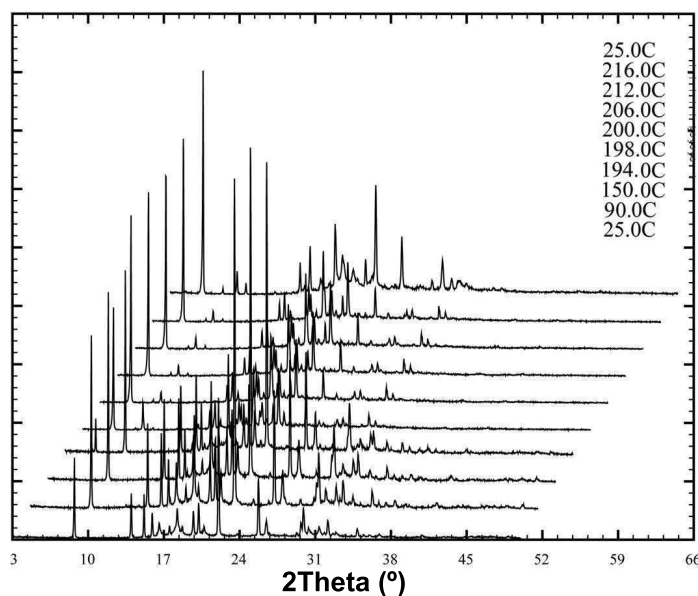


Fig. 3.16: DSC thermogram of form I, II, III, IV of compound **3**

Calorimetric data for crystal forms of compound **3** are summarized in table 3.5.

Tab. 3.5: Calorimetric data for crystal forms of **3**

Forms	Thermal phenomena	
	Onset (°C)	ΔH (J/g)
I	198	69
II	224	92
III	168	22
IV	180	39

Fig. 3.17: Hot stage photomicrographs of **3**, showing the solid-state phase transition from form I to form II and the subsequent melting phenomenon upon heating at 10 °C/minFig. 3.18: Variable temperature PXRD analysis of form I showing the transformation into form II of **3**

The crystal structure of form I is reported in the CCDC (refcode NIZXOK). Forms III and IV are metastable and no single crystals could be obtained. Broad powder diffraction peaks and low crystallinity hindered the cell indexing attempts. Form II, however, could only be obtained by hot treatment of form I and it presents a good quality powder diffractogram. Although several attempts of indexing its powder diffractogram were done, no reasonable solution was achieved.

The crystal structure of form I (Fig. 3.19) presents a well defined head-to-tail hydrogen bonding motif between squaramide units arranged in opposite directions, together with secondary edge-to-face CH- π interactions similar to those described for form I of **2**. Pyridine rings adopt a zig-zag conformation and aryl CH \cdots N pyridine interactions are also observed. Crystal data are shown in table 3.6.

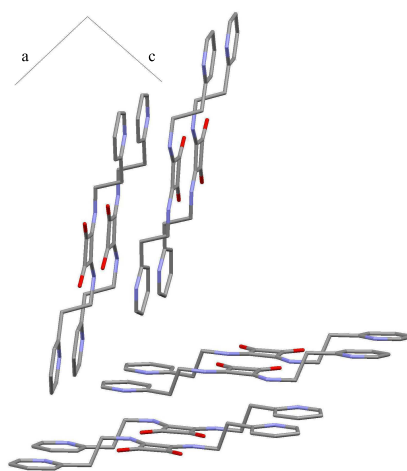


Fig. 3.19: Crystal structure of form I of **3** (hydrogens not shown)

Tab. 3.6: Crystal data for form I of compound **3**

Form	Space Group	Z (Z')	d NH \cdots O (\AA)	d CH-N _{pyridine} (\AA)
I	Pna ₂ ₁	4 (1)	1.795(4) 1.883(2)	2.701(5)

3.1.4 3,4-bis-(2-dimethylamino-ethylamino)-1,2-dioxo-3-cyclobutene (**4**)

Compound **4** was readily prepared from diethylsquarate and dimethylethylenediamine in ethanol with high yield. An intensive polymorph screening resulted in several polymorphs, not all obtained in pure form (Fig. 3.20).

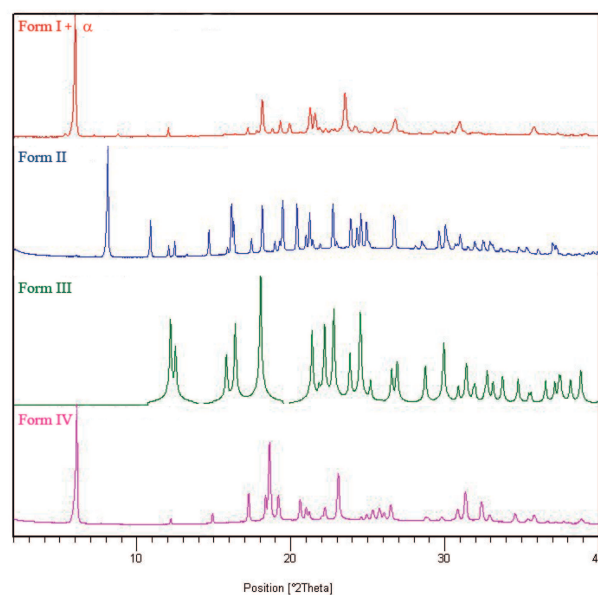


Fig. 3.20: Experimental PXRD diagrams of forms I + α , II and IV, and calculated PXRD diagram of form III of **4**

Form I was obtained directly from synthesis and other crystallizations with different solvents. Some efforts to index its diffractogram were unsuccessful, probably due to either the contamination with an unknown phase (α) or to a poor resolution diffractogram. Although further efforts to purify the sample by recrystallization were done, no success was achieved and no identification of this unknown phase could be done.

Form II was obtained pure from an experiment of cocrystallization of **4** with glutamic acid, in particular, a recrystallization in ethanol. Apart from studying the polymorphism of squaramides, in this work, special attention has been made on designing cocrystals and analyzing their supramolecular synthons using squaramides as scaffolds (See chapter 3.4). Several cases of new polymorphs obtained by induced crystallization with additives or using cocrystals as key intermediates are reported in the literature. [223, 224] Other attempts of cocrystallization of **4** with urea and nicotinamide in ethanol at r.t through reaction crystallization technique have resulted in form II impurified by the cofomer.

Form III could only be obtained from slow cooling recrystallization in acetonitrile as yellowish needles suitable for SXRD analysis. Finally, form IV has been only detected by DSC analysis from a solid-solid transition of forms I (+ α) and II (Fig. 3.21).

DSC analysis of form I (+ α , which is hypothesized), shows an endothermic transition to form IV (m.p.=227 °C) on heating (confirmed by variable temperature PXRD analysis), starting at about 45 °C with an enthalpy of 4 J/g. When

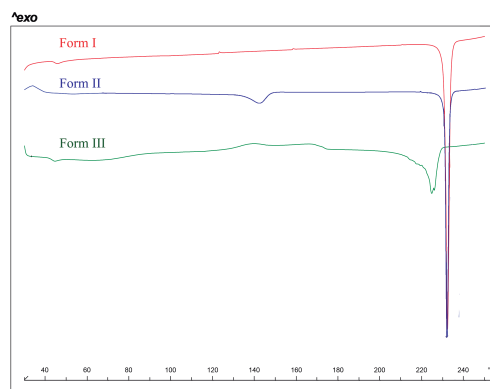


Fig. 3.21: DSC thermogram of forms I (+ α), II and III

a cooling-heating DSC analysis is performed, the transition appears at the same temperature with a lower enthalpy (1.5 J/g), which suggests the possibility of an incomplete reversible transition (Fig. 3.22) confirmed also by complementary thermomicroscopy analyses (Fig. 3.23). Form II presents an endothermic solid-solid phase transition into form IV, at 150°C with an enthalpy of 20 J/g, confirmed by variable temperature PXRD analysis. The DSC analysis of form III shows a solid-solid transition at 44 °C with an enthalpy of 3 J/g.

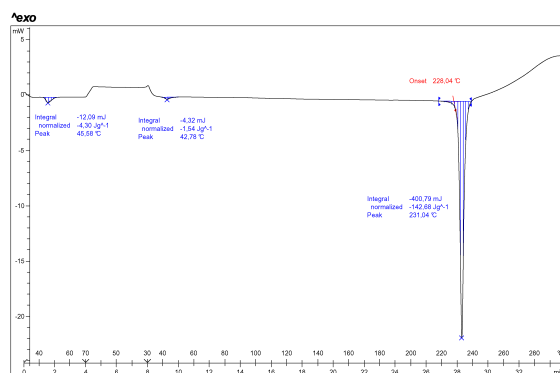


Fig. 3.22: DSC thermogram of form I showing a reversible transition into form IV of **4** on a heating-cooling experiment

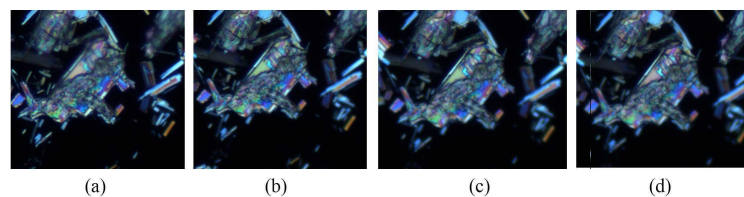


Fig. 3.23: Hot stage photomicrographs of **4**, showing the reversible solid-solid phase transition from form I to IV upon heating at 10 °C/min. (a) T=37°C on heating, (b) T=46°C on heating, (c) T=34°C on cooling, (d) T=28°C on cooling

Calorimetric data for crystal forms of compound **4** are summarized in table 3.7.

Tab. 3.7: Calorimetric data for the crystal forms of **4**

Form	Solid state transition		Melting	
	Onset (°C)	ΔH (J/g)	Onset (°C)	ΔH (J/g)
I	45	4	-	-
II	128	20	-	-
III	44	3	-	-
IV	-	-	227	137

In terms of this multipolymorphic system's thermodynamic relationship, form I (+ α) would be enantiotropically related to form IV. Solid samples of form III kept at r.t. tend to transform irreversibly into form I (+ α). Form II is enantiotropically related to form IV, since an endothermic solid-solid transition is observed by DSC. A scheme of the polymorph transformations among the different forms is shown in figure 3.24.

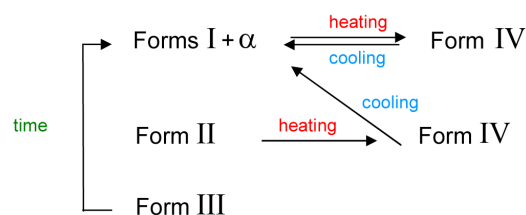


Fig. 3.24: Polymorphic transformations of compound **4**

Several crystallization attempts of form II did not result in a crystal with suitable quality for SXRD analysis, thus, its crystal structure was solved by means of direct space strategies. The crystal structure of form III⁷ was determined by SXRD using

⁷CCDC 1015652 contains the crystallographic data.

needles grown by slow evaporation of an acetonitrile solution of **4** at r.t. The crystal structures of both forms (Fig. 3.25 and Fig. 3.26) present the typical head-to-tail hydrogen bonding motif between squaramide units. The main difference between both structures is the orientation of the parallel squaramide alignments. Crystal data are shown in table 3.8. Two cell indexing attempts of form IV obtained by variable temperature PXRD analysis from form I (+ α) and form II, respectively, suggested Cc or $C2/c$ space groups. Unfortunately no crystal structure determination has been possible in spite of big efforts on obtaining high quality diffractograms of form IV. The differences between cell parameters obtained, as well as the different position of the peaks on the powder diffractogram, can be attributed to the anisotropic dilatation caused by the temperature difference. The use of synchrotron radiation together with further purification efforts may be considered in order to get deeper insight in this multipolymorphic system.

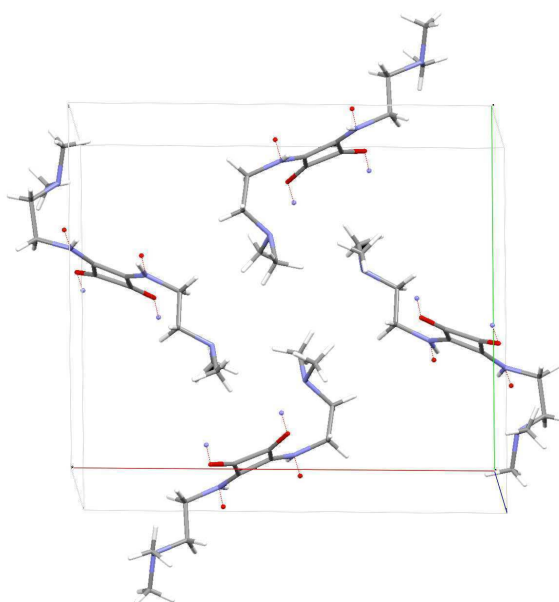


Fig. 3.25: Crystal structures of forms II of **4**

Tab. 3.8: Crystal data of **4** (*Standard deviations have not been calculated since distances are obtained from Rietveld refinement)

Form	Space Group	Z (Z')	distance NH...O (Å)
II	$P2_1/c$	4 (1)	1.975 1.988*
III	$Fdd2$	8 (1)	1.963(13) 1.963(13)

After studying four model dissecondary squaramides in the solid state, the existence of a robust self associating head-to-tail supramolecular synthon is observed in eight crystal structures solved of the thirteen forms identified in total. They present

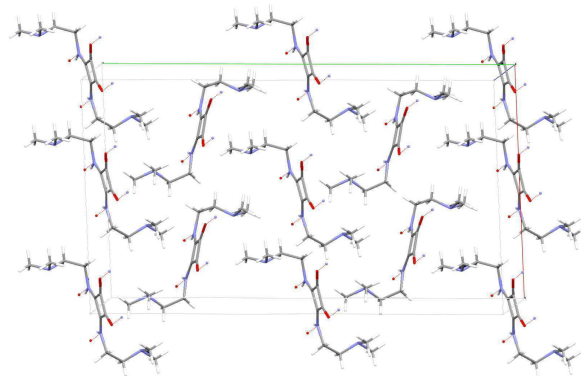


Fig. 3.26: Crystal structures of forms II III of **4**

an identical catemer motif in which assemblies of squaramide units interact through hydrogen bonding and it appears to be unbreakable. The following scheme summarizes the main polymorphic information of the four studied compounds (Fig. 3.27).

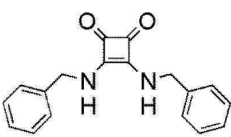
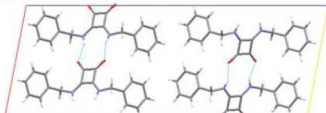
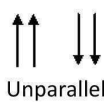
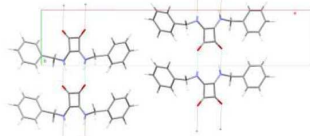
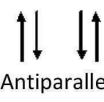
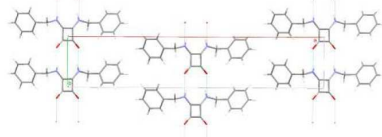
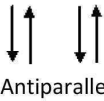
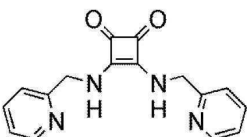
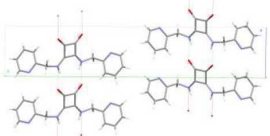
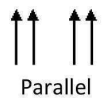
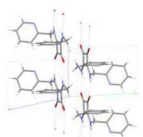
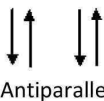
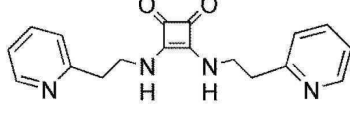
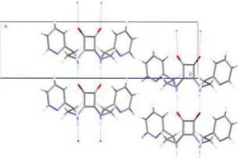
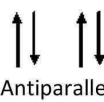
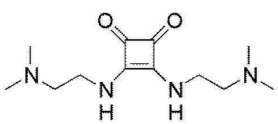
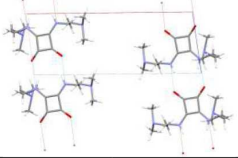
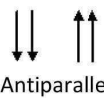
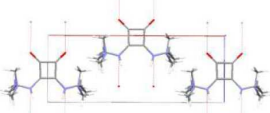
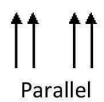
Compound (n° of forms)	Forms	Space group	Z (Z')	Crystal Structure	Catemic head-to- tail
1 (3) 	I	C2	4 (1)		 Unparallel
	II	Pc	4 (2)		 Antiparallel
	III	C2/c	4 (1)		 Antiparallel
2 (2) 	I	Pc	2 (1)		 Parallel
	II	P-1	2 (1)		 Antiparallel
3 (4) 	I	Pna21	4 (1)		 Antiparallel
4 (4 or 5) 	II	P21/a	4 (1)		 Antiparallel
	III	Fdd2	8 (1)		 Parallel

Fig. 3.27: Summary of the polymorphic systems studied in this chapter

3.2 From solution to the crystal

It is well known that the preferred structure of molecular clusters in supersaturated solutions can sometimes resemble the mode of aggregation in the crystal structure, suggesting a possible link between self-aggregation in solution and crystallization processes. [225, 226] In this section, the structural preferences of a specific dissecondary squaramide model compound are analyzed in order to understand the relationship between the structures of aggregates in solution and in the solid state.

Secondary squaramides present two different hydrogen bonding conformations in solution that can act as double donor-acceptor groups: the anti/anti and the anti/syn, both suitable to produce a $R_2^2(n)$ synthon with appropriate donor or acceptor groups. (Fig. 3.28). [227]

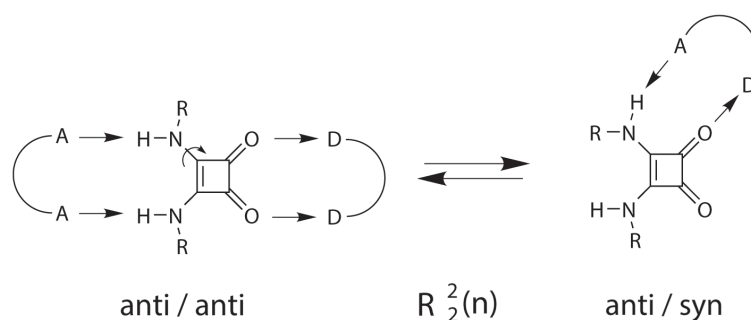


Fig. 3.28: Two different conformations of dissecondary squaramides

Since dibenzylsquaramide (**1**) and, in general, dissecondary squaramides are insoluble in apolar organic solvents due to a strong self association, 3,4-bis-(2-methylaminopyridyl)-1,2-dioxo-3-cyclobutene (**2**) was chosen as a model compound, because it is soluble in organic solvents of low polarity, with the objective to study the interactions of squaramides in solution prior to crystallization. The fact that **2** is soluble in chloroform and other organic solvents allows a broad range of crystallization conditions to be studied.

Initially, **2** was analyzed by $^1\text{H-NMR}$ and its spectrum in CDCl_3 at low temperature presents three sets of N-H signals, suggesting that **2** is present as a mixture of two different conformers, one symmetric and one asymmetric, since the $\text{C-N}_{\text{amidic}}$ bond rotation is frozen (Fig. 3.29). [228]

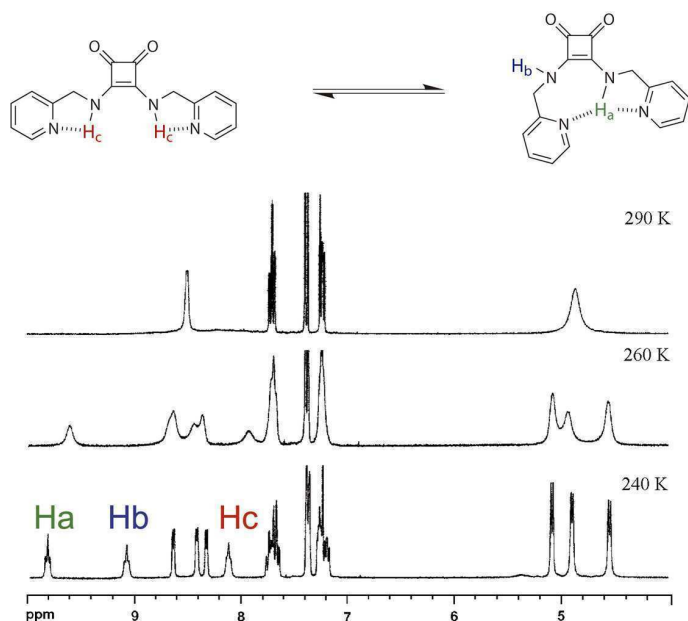


Fig. 3.29: Conformational equilibrium and ^1H -NMR spectrum of **2** in CDCl_3 at 240 K, 260 K and 290 K

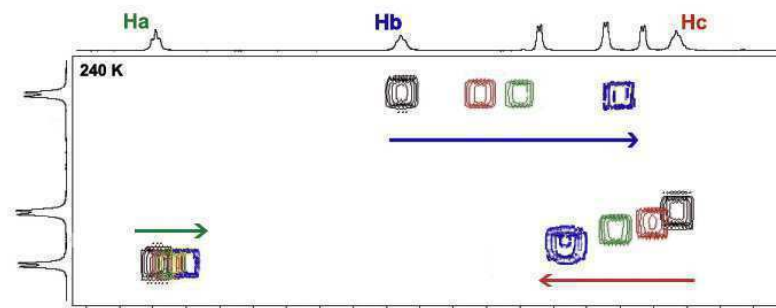
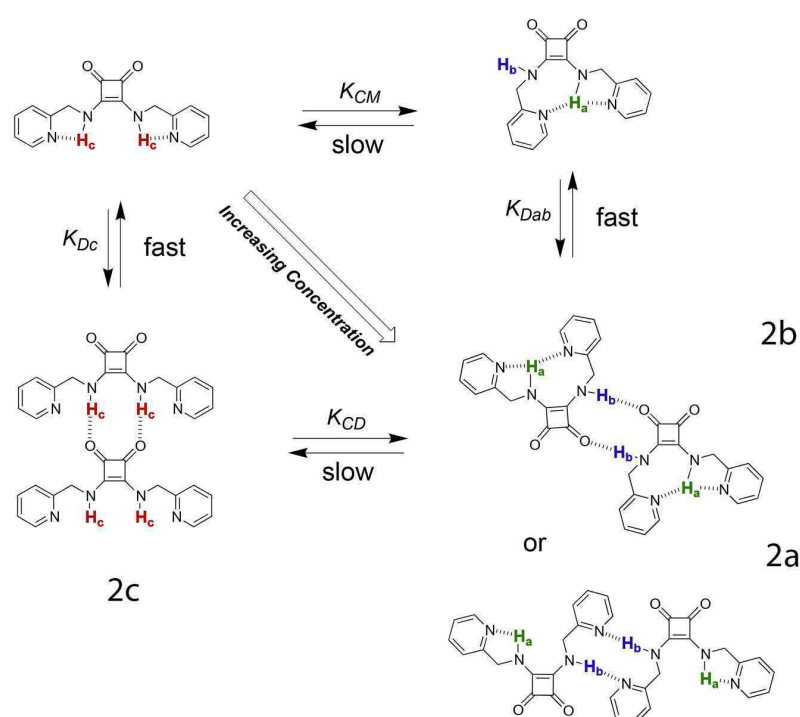
The three sets of signals (H_a , H_b , H_c), corresponding to three different environments of the amidic hydrogens, are assigned to the anti/anti (Fig. 3.31, **2c**) and anti/syn (Fig. 3.31, **2a** or **2b**) dimers on the basis of 2D ^1H -NMR COSY dilution experiments (Fig. 3.30).⁸ The shift observed for the amide protons H_a and H_b (invariability of H_a and large upfield shift of H_b) upon dilution (dimer destruction) gives a strong indication that **2b** is the preferred dimer for the asymmetric conformation (Fig. 3.30). All possible forms of **2** in solution are related through this proposed thermodynamic cycle (Fig. 3.31).

The observed ^1H -NMR shifts for H_a , H_b and H_c together with the concentration and integration values allow the equilibrium constants to be estimated ($K_{CM} = 2.5$, $K_{CD} = 0.56$, $K_{Dab} = 8600\text{ M}^{-1}$, $K_{Dc} = 790\text{ M}^{-1}$).⁹

The results indicate that, on increasing concentration at 240 K, the preferred self-associated form of **2** is **2b**. Thus, under circumstances in which the mode of solution-state aggregation is translated into the crystal structure, it is deducible that crystals obtained from a supersaturated solution of **2** would contain the **2b**

⁸Experiments were run on a Bruker DMX500 instrument equipped with an indirect ^1H - ^{13}C detection probe with gradients along the z axis. A standard sequence from Bruker software was used for COSY experiments (cosygpqf); a total of 128 increments, 4 scans each, were collected.

⁹The conformational equilibrium constant of the monomer K_{CM} was calculated as the ratio of the relevant integrals at the lowest concentration, for which > 95% of **2** is monomeric. Dimerization constants were calculated from the variation in chemical shifts with concentration using the program *NMRDil_Dimer*. [229] The conformational equilibrium constant of the dimer K_{CD} was calculated from the other three constants: $K_{CD} = (K_{CM})^2 K_{Dc} / K_{Dab}$.

Fig. 3.30: 2D ^1H -NMR COSY at 240 K of **2** upon dilutionFig. 3.31: Proposed thermodynamic cycle for dimerization of **2**

motif. In contrast with the polymorph screening carried out, under a broad set of experimental crystallization conditions, catemeric clusters of **2** crystallize into two different polymorphs with the same head-to-tail motif (based on **2c**), with no evidence for any other polymorph with the dimeric motif (**2b** or **2a**) (Chapter 3.1.4). This observation suggests that, although both dimeric and catemeric modes of interaction are significant in low polarity solvents such as chloroform, the formation of clusters with the catemeric motif is only favored due to a possible hydrogen bonding cooperativity. [230] According to the polymorph screening conducted with

compounds **1**, **2**, **3** and **4**, these current results may be extrapolated to all dis-econdary squaramides (on the assumption that other factors do not significantly influence the crystal structure, such as the presence of more strongly competitive hydrogen bonding groups). Taking into account these findings in solution, the cooperativity phenomenon and its relation to the head-to-tail conformation preference of these compounds in the solid state was further studied taking dimethylsquaramide (**5**) as the simplest model compound.

3.2.1 Cooperativity

Cooperativity of weak interactions plays a crucial role in molecular recognition and self-assembly events. A good understanding of cooperativity is therefore essential for obtaining insights into the behavior of both biomolecular systems and synthetic materials. However, while it is often easy to identify cooperativity at work, it is more difficult to predict how it may influence the behavior of a particular system. [230, 231] In the simplest case, when a hydrogen bond is formed between two molecules of water, the redistribution of electron density changes the ability for further hydrogen bonding. The molecule of water donating the hydrogen atom has increased electron density on its 'lone pair' region, [232] which encourages hydrogen bond acceptance, whereas the accepting water molecule has reduced electron density centered on its hydrogen atoms and its remaining 'lone pair' region, which encourages further donation, on the one hand, and discourages further acceptance of hydrogen bonds, on the other hand (Fig. 3.32).

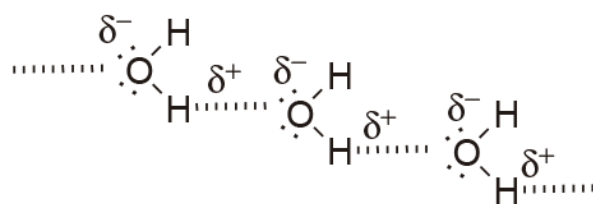


Fig. 3.32: Cooperativity in water molecules

This electron density redistribution, thus, results in cooperativity. In cases for which hydrogen bonding is the primary intermolecular interaction in the solid state, cooperativity in the form of mutual hydrogen bond reinforcement within a hydrogen bonded chain can play a major role in the supramolecular synthon observed in the crystal. Price has demonstrated [233] that the induction energy contribution to the lattice energy of organic compounds is significant, particularly for molecules containing hydrogen bonding groups such as carbamazepine; moreover, there is

evidence that such induction effects are important even in crystals of nonpolar compounds. It has also been shown *in silico* that hydrogen bonded amide chains exhibit a high degree of cooperativity, [234] which arises from the reinforcement of individual hydrogen bonds through the mutual polarization of acceptors and donors along the assembly. Such cooperative interactions are significant in the solid state but are secondary in the liquid or gas phases because the molecules are separated too far to interact in a cooperative way and the dynamics of the molecules also limit the effect. [235] Cooperativity is important when self-complementary molecules assemble into one-dimensional structures by non covalent interactions due to polarization (induction) of interacting groups. [230] This phenomenon has been previously HF, DFT and MP2 studied by Dannenberg *et al.* with urea and formamide (Fig. 3.33). [234, 236]

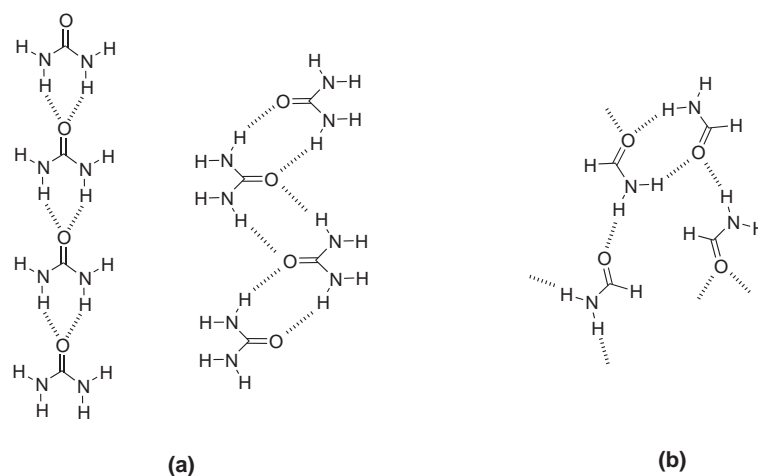


Fig. 3.33: Cooperativity in (a) Urea and (b) Formamide hydrogen bonding patterns [235]

In this chapter we explore cooperativity as the driving force in disquaramides, which produces chains in an anti/anti strong self-associating head-to-tail motif in the solid state, in spite of the fact that other conformations are observed in solution. First, this finding is theoretically rationalized and then experimentally confirmed. Thus, dimethylsquaramide (**5**) (Fig. 3.34 (a)) was chosen as the simplest model to study the conformational preference in the solid state, because of the fact that no relevant secondary interactions with other groups are possible. Due to the partial rotation of the C-N_{amidic} squaramide bond, two different polymeric structures can *a priori* crystallize: chains or ribbons (Fig. 3.34 (b)). In order to predict which synthon is the most stable, the approach proposed by Hunter [138] to the analysis of hydrogen bonding interactions was applied.

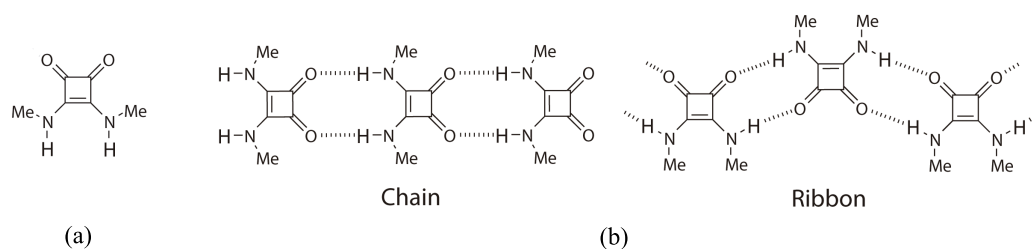


Fig. 3.34: (a) Scheme of **5** (b) Chain and ribbon interaction motifs for **5**

3.2.1.1 Quantifying intermolecular interactions: Hunter's approach

Different approaches have been historically used to understand and predict the core entity that defines the structure of a particular molecular crystal: Gavezzotti proposed a model based on space group information which reduces the structure to small molecular clusters and calculates lattice energies, [237] the pioneering model by Etter is based on strong hydrogen bonding as the driving force in the formation of a molecular crystal, [107] and the supramolecular synthons model is based on functional groups complementarity (already described in the introduction of this thesis). [126] More recently, Hunter proposed a method to quantify intermolecular interactions through the estimation of relative hydrogen bond donor/acceptor parameters of most typical functional groups. [138, 238–242]

Hunter's approach is based on the analysis of experimental data on the thermodynamics of hydrogen bonding interactions in carbon tetrachloride and its correlation to the MEP of a wide range of functional groups. It allows estimation of the free energy of formation of a single hydrogen bond contact based on the calculated gas phase molecular electrostatic potential (MEP) surfaces of any functional group. There have been significant success in using this approach for predicting binding free energies of molecular complexes and formation of cocrystals. [137, 139, 243, 244]

This theoretical model considers only the electrostatic interactions between the permanent charge distributions of two molecules that interact in the gas phase to describe the complex formation. Other components of intermolecular interactions such as repulsion between the electron densities at close distances, induction and dispersion interactions between induced dipoles are considered negligible or constant.

Pioneering Abraham's work on experimental binding constants in carbon tetrachloride allowed the deduction of hydrogen bonding parameters (α_2^H and β_2^H) for many functional groups. Their relation to the binding constant is established from the following equation: [245]

$$\log K = c_1 \cdot \alpha_2^H \cdot \beta_2^H + c_2 \quad (3.1)$$

where c_1 and c_2 are constants that depend on the solvent and α_2^H and β_2^H are functional group constants related to the hydrogen bond donor and acceptor properties of the molecules, respectively.

Hunter demonstrated that these experimental hydrogen bonding parameters strongly correlate with the maximum and minimum of the MEPs and, thus, any intermolecular interaction can be analysed like a form of hydrogen bonding, with some exceptions such as aromatic stacking. [245] Intermolecular interaction between two molecules will take place between the maximum in the electrostatic potential on the Van der Waals surface, which is usually located near a hydrogen atom, and the minimum, usually located over a lone pair or an area of π -electron density (Fig. 3.35).

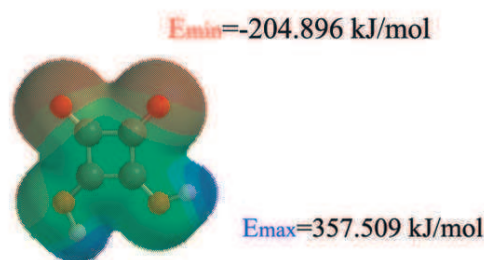


Fig. 3.35: MEP plotted on the Van der Waals surface of the squaric acid calculated by using DFT method and a positive point charge. Positive regions are blue, negative regions red and neutral regions green. [138]

However, there are specific compounds, like carbon tetrachloride, which have no hydrogen bond donors and their MEP surfaces are strongly positive due to withdrawing electron effects of neighbouring atoms and the diffusion of these electrons.

A linear correlation between maxima and minima in the MEP surfaces and the experimentally determined values of α_2^H and β_2^H parameters of various functional groups [245] have been found in carbon tetrachloride and a mathematic rescaling is applied to extrapolate the values to any solvent or the solid state. Thus, α and β parameters can be calculated from the resulting equations 3.2 and 3.3, using the second equivalence of the equations when experimental values of α_2^H and β_2^H are available, or using the first equivalence when experimental data are not available but calculated AM1 molecular electrostatic potential surface (MEPS) is needed.

$$\alpha = E_{max}/52kJmol^{-1} = 4.1(\alpha_2^H + 0.33) \quad (3.2)$$

$$\beta = E_{min}/52kJmol^{-1} = 10.3(\beta_2^H + 0.06) \quad (3.3)$$

An improvement of the hydrogen bonding parameters has been recently reported by Hunter based on the use of DFT calculations. [238]

In this approach, only neutral molecules have been studied since experimental values of α and β of salts have not been determined due to the low solubility of these substances in carbon tetrachloride and other factors such as counterion association. [246]

In this study, the MEPS of compound **5**, was obtained in the gas phase using *ab initio* calculations and converted into the corresponding hydrogen bond donor/acceptor parameters α and β .¹⁰

In principle, **5** can exist in three conformations as a result of the rotation of both C-N bonds: anti/anti, anti/syn and syn/syn. However, only anti/anti and syn/syn conformations would yield catemeric structures due to cooperativity effects so the existence of crystals with the anti/syn conformation can be considered unlikely. The hydrogen bond parameters obtained for the three possible conformers show that the anti/anti conformation would produce the strongest intermolecular interaction (Fig. 3.36). Assuming that dispersion and packing effects could be similar for all the possible polymorphs, crystal structures of disquaramides should prefer this synthon, as it has been experimentally proven with the results of the previous polymorph screenings.

The individual interaction of each particular synthon can be estimated as the sum over both NH...OC contacts with equation (3.6), [225] where α_i are the hydrogen bond donor parameters, β_i are the hydrogen bond acceptor parameters and the sum represents the sum over both interactions.

$$\Delta E = - \sum_i^n \alpha_i \beta_i \quad (3.6)$$

Density functional theory (DFT) calculations were also performed on hydrogen bonded anti/anti and syn/syn dimers in order to compare with the interaction pair-

¹⁰ α and β parameters have been calculated by using the following equations extracted from reference: [137,247]

$$\alpha = 0.0000162 \times E_{max} \times E_{max} + E_{max} \times 0.00962 \quad (3.4)$$

$$\beta = 0.0000146 \times E_{min} \times E_{min} - E_{min} \times 0.00930 \quad (3.5)$$

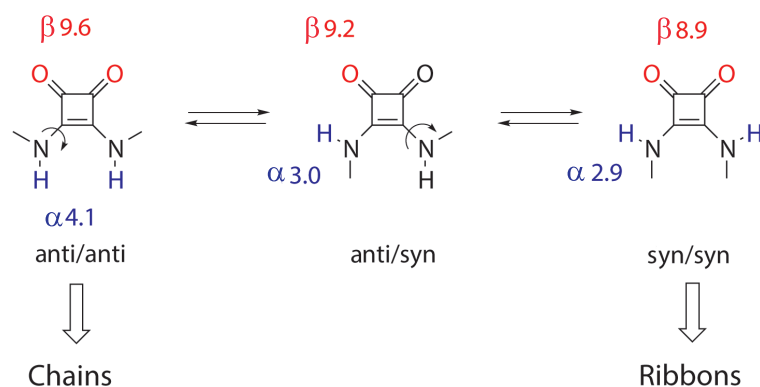


Fig. 3.36: Hydrogen bond parameters for the three conformations of **5**

ing energy¹¹ and counterpoise corrections for basis set superposition error (BSSE) were used for the calculation of the interaction energy (Tab. 3.9 (a)). [248] Interestingly, the relative DFT interaction energies (56 kJ/mol for the anti/anti *versus* 73 kJ/mol for the syn/syn) are opposite to those estimated through equation 3.6 (79 kJ/mol for the anti/anti *versus* 52 kJ/mol for the syn/syn). However, this can be explained in terms of a mutual induction effect that makes the second hydrogen bond stronger in the syn/syn dimer and weaker in the anti/anti dimer (Fig. 3.37).

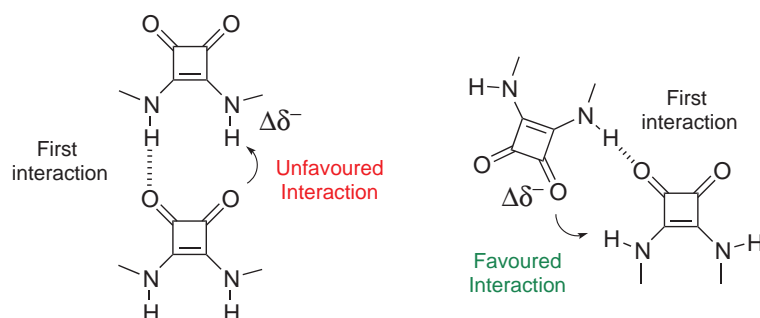


Fig. 3.37: Induction effects favouring and disfavoring the second hydrogen bond

This effect was roughly simulated by calculating the hydrogen bond parameters of dimers with only one hydrogen bonding interaction. Geometries of the monomers were minimized independently and then positioned in such a way that only one interaction is possible and with a distance between the NH proton and the carbonylic oxygen fixed at 2.0 Å. In this simulation, once the first interaction is established, the remaining free NH and CO groups can interact and then a rough estimation of the interaction energy can be done using equation (3.6) (Fig. 3.38). Thus, the interaction energies for the anti/anti and the syn/syn dimers are -59.2 and -80.2 kJ/mol respectively (Tab. 3.9 c). These values are closer to those from DFT calculations

¹¹Geometries were optimized at the B3LYP 6-31G* level of calculation. The interaction energies were calculated at the B3LYP 6-31+G* level of theory.

and strongly support our hypothesis (Tab. 3.9).

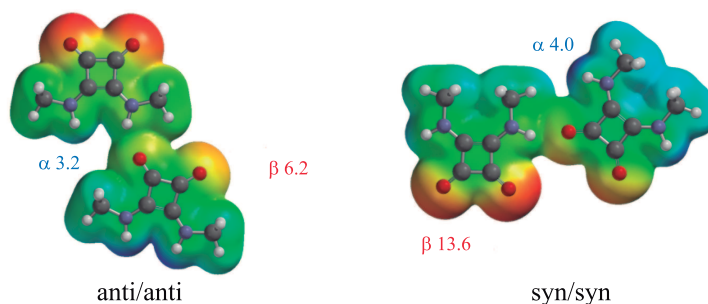


Fig. 3.38: MEP surfaces and hydrogen bond parameters after the first interaction of anti/anti and syn/syn conformers

Tab. 3.9: Interaction energies calculated by (a) DFT, (b) using equation 3.6 and hydrogen bond parameters for non cooperative dimers and (c) for cooperative dimers of **5**

Synthon	Interaction Energy (kJ/mol)		
	a	b	c
anti/anti	-56.0	-78.7	-59.2
syn/syn	-73.1	-51.6	-80.2

This effect, however, is compensated as monomers are added to the chain. Interaction energies of the terminal monomer are represented in figure 3.39 as a function of the number of molecules in the chain/ribbon aggregate for **5**.¹² As the aggregate grows, the interaction energy increases in the anti conformation while it remains practically constant in the syn conformation. Again a cooperative induction effect explains this phenomenon: once the monomer is linked to the anti/anti aggregate an electronic polarization takes place, which reinforces the interaction with subsequent monomers. Hydrogen bonds increase in strength due to this redistribution of the electron density along the chain. [249] Dipolar moment reflects this effect: it increases as monomers are added to the anti/anti aggregate but it is constant or zero in odd or even number of units respectively in the syn/syn aggregate. However, in the syn/syn aggregate there is neither polarization nor increased interaction as monomers are added. This suggests an explanation for why dialkyl squaramides, in absence of potential additional interacting functional groups, exhibit only the anti/anti supramolecular synthon.

¹²Geometries for the syn/syn aggregates were optimized by DFT (6-31G*) methods while those for the anti/anti aggregates were taken directly from the crystal structure of **5**.

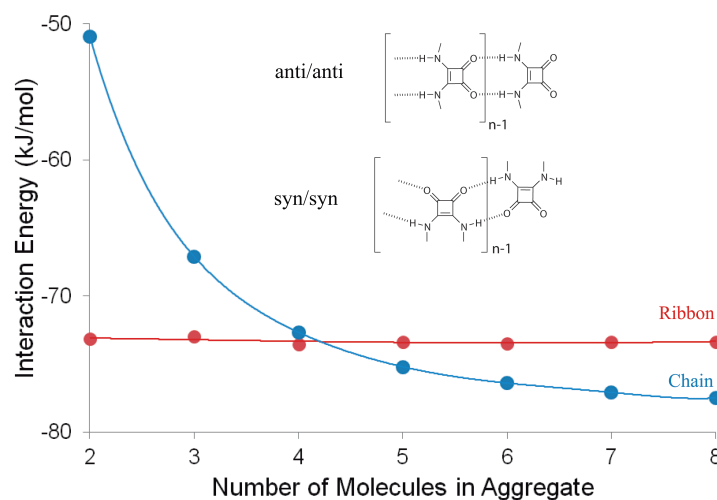


Fig. 3.39: Interaction energies of the terminal monomer (anti/anti: blue; syn/syn: red) calculated at the DFT B3LYP 6-31+G* level of theory using Spartan'10 software [247]

In order to validate this hypothesis, a polymorph screening was run with **5** (see appendix A.12), yielding in all cases the same polymorph with the predicted anti/anti catemeric structure (Fig. 3.40).

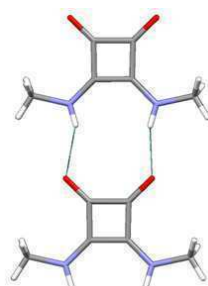


Fig. 3.40: Crystal structure of compound **5**

Once dimethylsquaramide was studied as the simplest model, Hunter's approach was applied to compound **2** the previously studied in solution. Calculated α and β parameters for **2** suggest that **2b** and **2c** are preferred over **2a** in agreement with the NMR results, and that **2c** appears to be slightly more favorable than **2b** (Fig. 3.41). This result is in agreement with the crystal structure grown at r.t. while at 240 K the NMR experiments show **2b** is preferred over **2c**. This difference in behaviour is attributed to the more important contribution of the intramolecular hydrogen bonds at 240 K, which tips the balance in favour of **2b** at low temperature.

Since no syn/syn conformation was observed in any of the mentioned compounds, a covalently forced cyclic disquaramide **6** was designed to study the geometrical

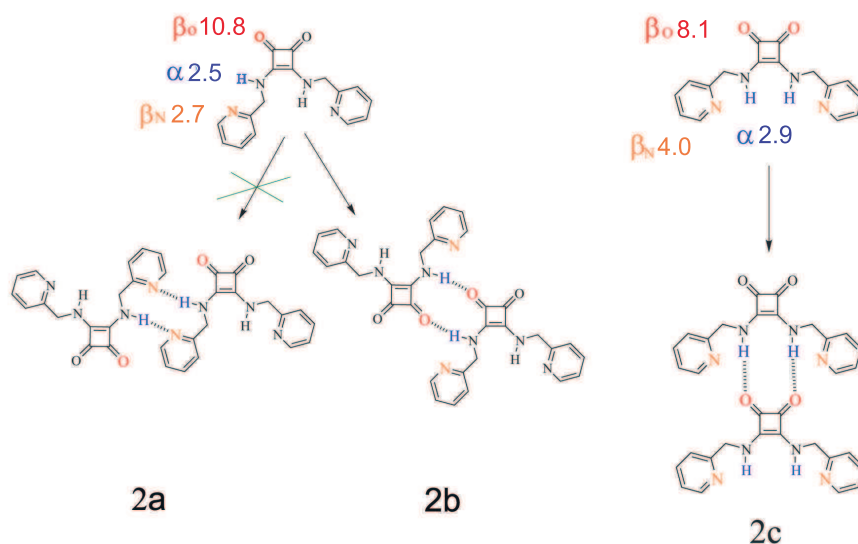


Fig. 3.41: Aggregation scheme of **2** according to Hunter's approach

features of the catemeric structures with such configuration (Fig. 3.42, (a)). It was obtained from diethyl squarate and 1,2-diaminoethane in ethanol. In its crystal structure, the expected $\text{NH}\cdots\text{OC}$ hydrogen bonding is established between two adjacent molecules forming ribbons with the squaramide rings practically in the same plane (Fig. 3.42, (b)).

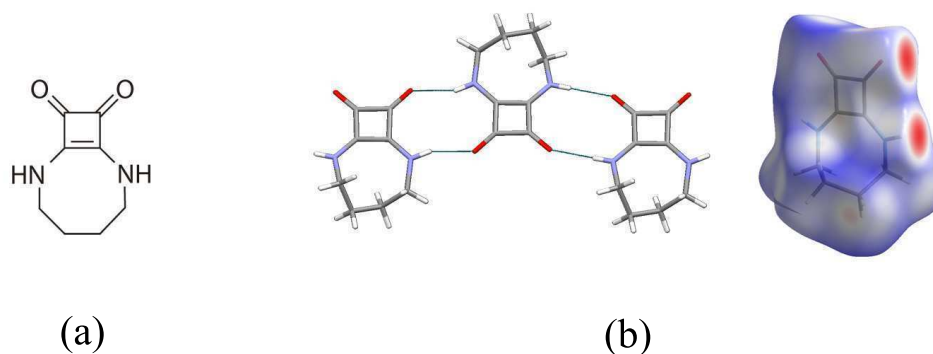


Fig. 3.42: (a) Scheme of **6** (b) Crystal structure and Hirshfeld's surface of **6** in which side interactions in red are shown

Competitive interactions such as $\pi - \pi$ stacking do not affect the anti/anti conformation observed in previous disquaramides (**1**, **2** and **3**). In order to check their influence over the *a priori* less strong syn/syn motif, another macrocyclic compound containing an aromatic group was designed (**7**, Fig. 3.43, (a)). It was obtained in a three-step synthetic route from a condensation of 2-aminomethylbenzylamine with diethyl squarate in ethanol. Needles were grown in the reaction crude and **7** was

solved by single crystal XRD. Again, the expected $\text{NH}\cdots\text{OC}$ hydrogen bonding is established between two adjacent molecules forming ribbons, which are connected through additional $\text{CO}\cdots\text{H}_{\text{aromatic}}$ and $\pi - \pi$ stacking interactions (Fig. 3.43, (b)).

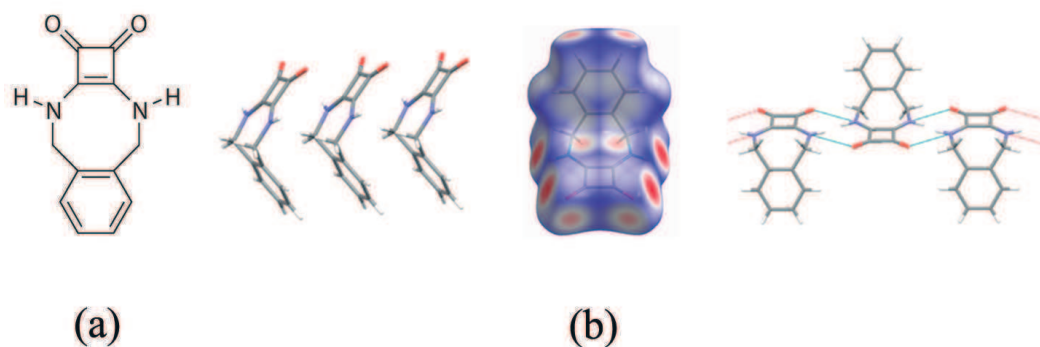


Fig. 3.43: (a) Scheme of **7** (b) Crystal structure and Hirshfeld's surface of compound **7** in which side interactions in red are shown

The observed lateral offset stack is parallelly orientated with a centroid to centroid distance $d(\pi - \pi)$ of 4.31 Å, interplanar distance of 3.55 Å and a lateral displacement of 2.44 Å. However, squaramide rings are not coplanar as in the case of compound **6** (interplane distance of 1.16 Å), but they form a zig-zag arrangement which suggests that the competitive $\pi - \pi$ aromatic interactions can disrupt the formation of an optimal planar hydrogen bond. This phenomenon, which has not been observed in any of the polymorphs of dibenzylsquaramide (**1**), suggests that the cooperativity stabilization in the anti/anti aggregates overcomes possible disrupting secondary interactions while the non cooperative syn/syn synthon is less resistant to their presence.

Once the syn/syn conformation was observed in covalently forced disquaramides we aimed to explore if it could be observed in monosquaramide esters in the solid state through the design of a simple compound able to form strong dimers (Fig. 3.44). Thus, the monosquaramide **8** was prepared from diethylsquarate and methylamine in diethyl ether. Only one polymorph was obtained from a polymorph screening (appendix A.12), and its crystal structure reveals dimeric aggregates of syn conformers. The strong self-complementary squaramide/squaramide dimer is linked to the following one in the crystal through weaker $\text{CO}\cdots\text{H}_{\text{ethyl}}$ interactions (Fig. 3.45).

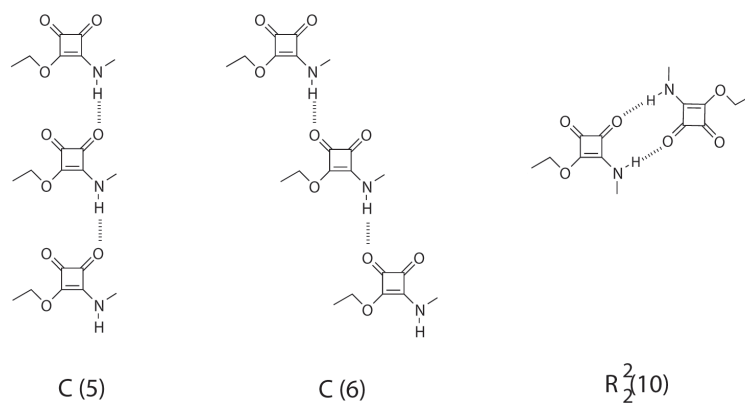


Fig. 3.44: Possible supramolecular synthons for compound **8**

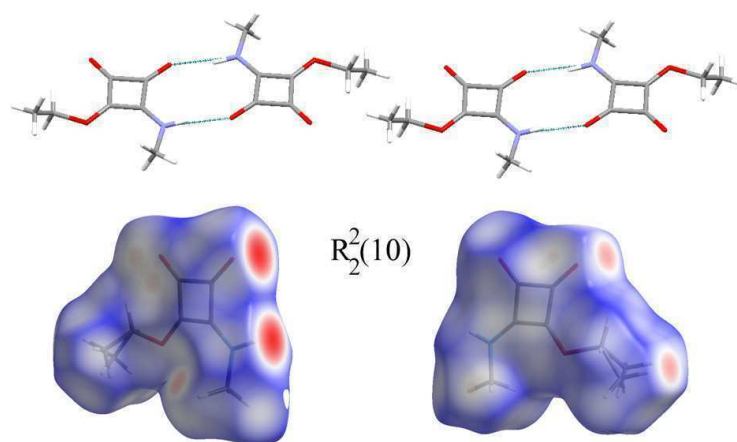


Fig. 3.45: Dimeric aggregates observed in the crystal structure of **8** together with the Hirshfeld's surfaces

This suggests that, in absence of competitive donor/acceptor groups, dimers might be more stable than chains in monosquaramide esters probably due to the difficulty to align efficiently monomers in a head-to-tail manner without losing the advantage of linear cooperativity. In this sense, another model compound (**9**) was designed containing an additional pyridine group in order to explore how competitive groups could affect the $R_2^2(10)$ synthon observed for the very first time in this family of compounds.¹³ For this reason, α and β parameters were calculated in this case, in order to compare them with the experimental results (Fig. 3.46, (a)). The presence of a good hydrogen bond acceptor $N_{pyridinic}$ might favor the formation of a dimeric syn motif different from the synthon observed for compound **8**.

Experimentally, compound **9** was prepared from diethylsquarate and 2-(aminoethyl)pyridine in diethyl ether. A non comprehensive polymorph screening was

¹³A survey at the CCDC shows different supramolecular synthons: ACULEP, ACULIT, ACULIT01, CAQRUH, ETIVIM, IXUVAY, JINRAA, MEGNAO, NEMMEX, SIXFIP.

conducted and only one solid form was obtained (Appendix A.12). The single crystal structure was solved by SXR D and it confirms the prediction that the presence of a good competitive functional group such as pyridine alters the supramolecular synthon, but the conformer syn remains. (Fig. 3.46, (b)). The presence of an ethoxy moiety reduces the electron density around the carbonyl oxygen, and as a result it favors the formation of the dimer through the hydrogen bonding between the pyridil nitrogen and the amidic hydrogen.

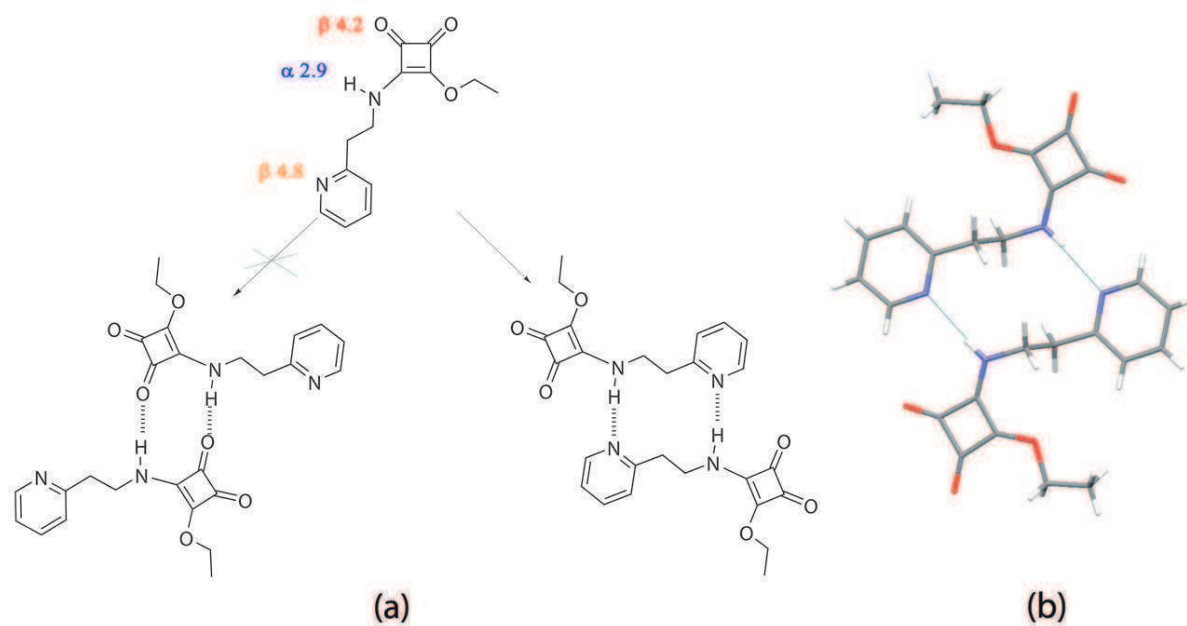


Fig. 3.46: (a) α and β parameters of **9** (b) Dimers in the crystal structure of **9**

3.3 Crystal engineering: cocrystals design

Next step of this work was to design new materials on the basis of the acquired solid state knowledge of squaric acid derivatives. As it has been shown in the previous sections, all attempts to crystallize different forms of disquaramides resulted into the existence of only a robust anti/anti conformational head-to-tail structural mode, unless being the molecule itself covalently modified. Thus, a first attempt was to design cocrystals between disquaramides and strong donor/acceptor complementary functional groups, such as phenols and carboxylic acids, appropriate for the anti/anti and syn/syn conformers, respectively (Fig. 3.47).

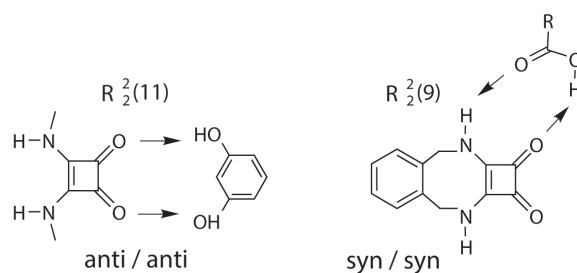


Fig. 3.47: Scheme of possible supramolecular synthons with both donor and acceptor conformers

Although resorcinol and carboxylic acids looked optimal from a geometrical point of view, calculations suggested that cocrystals were not expected to be obtained in the case of simple compounds such as **5** and **7**, because the predicted interaction energies (from equation (3.6)) of these heterosynthons were lower than that of the squaramidic homosynthon (Fig. 3.48).

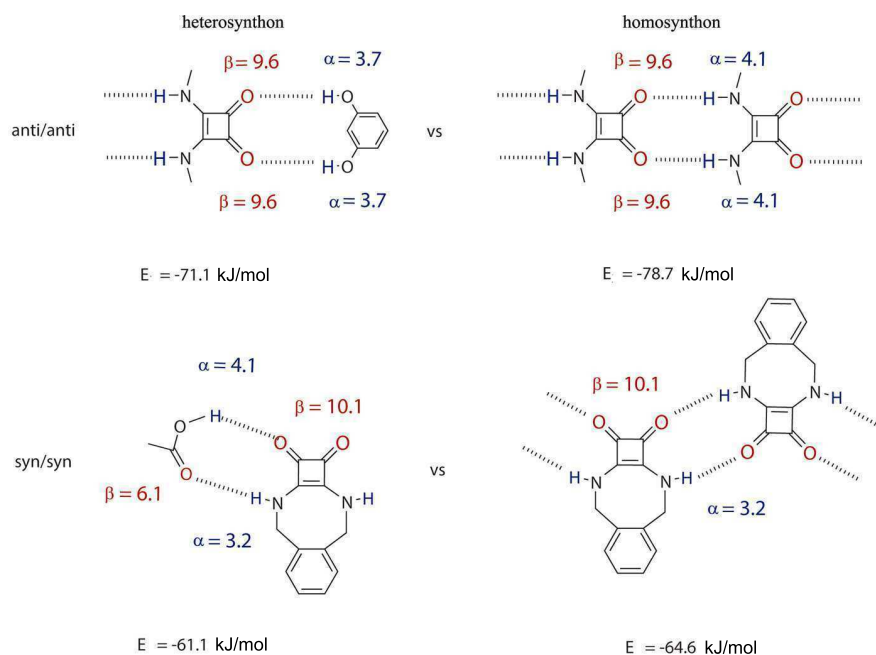


Fig. 3.48: Predicted interaction energies of heterosynthons and homosynthons for anti/anti and syn/syn conformations of **5** and **7**, respectively.

To corroborate this prediction with carboxylic acids and resorcinol, and to extend it to other good donor or acceptor groups, an experimental cocrystal screening with **5** and **7** and a set of different coformers was conducted (See appendix B.8) and did not produce any new cocrystal phase (Fig. 3.49).¹⁴

These findings demonstrate again that the self assembly of squaramide rings is a very strong binding motif, difficult to be perturbed by other competing functional groups in the solid state.

For this reason, two new crystal engineering strategies were designed. The first strategy was to impede the head-to-tail motif via intramolecular interactions and choose complementary coformers taking into account the Hunter's approach (Fig. 3.50 (a)). [250] The second strategy consisted in taking advantage of such a robust synthon by designing new crystalline materials with complementary coformers through the squaramide functionalized secondary chains via peripheral interactions (Fig. 3.50 (b) and (c)). [251]

¹⁴Evidences of a new phase were identified from a cocrystallization experiment with **7** and phosphoric acid. However not enough characterization analyses could be done to confirm the presence of a cocrystal phase.

¹⁶ α and β values extracted from [138].

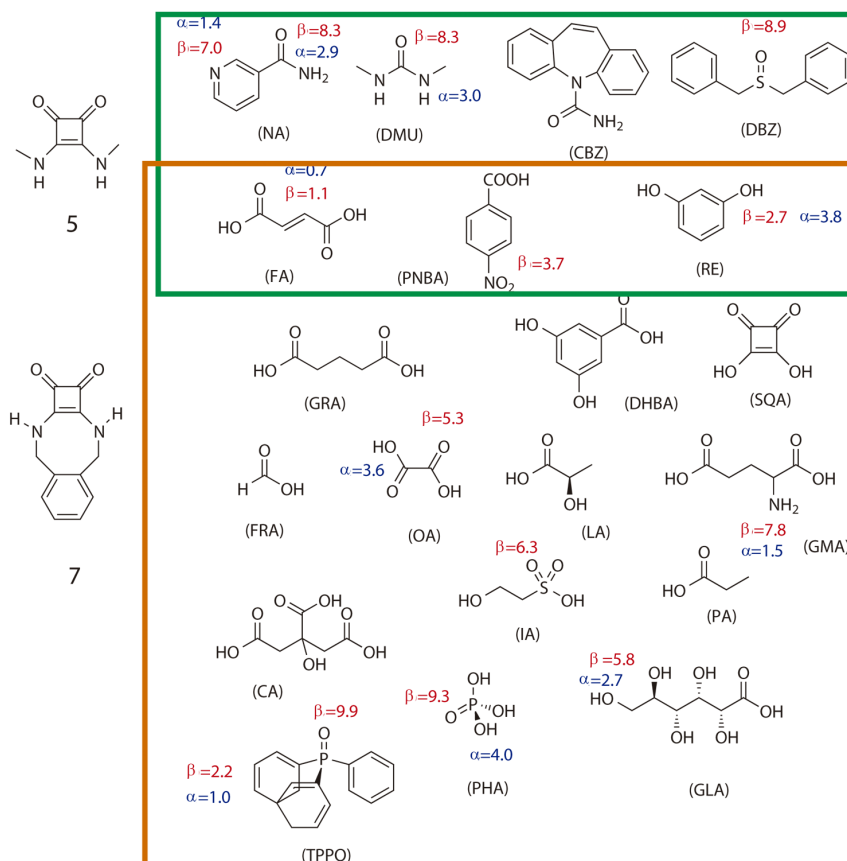


Fig. 3.49: Coformers used in the cocrystal screening of compounds **5** and **7**¹⁶

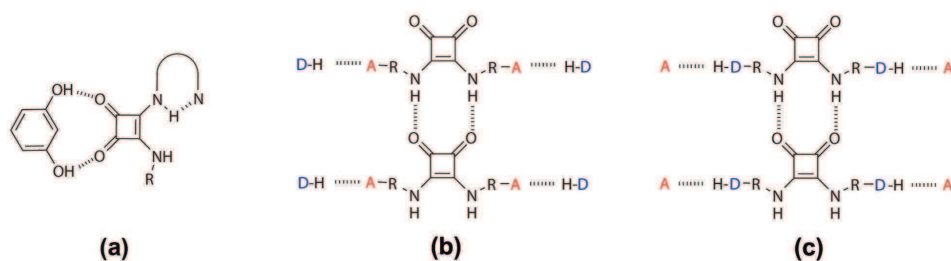


Fig. 3.50: Scheme of cocrystal design: (a) via intramolecular hydrogen-bonding and (b, c) via peripheral interactions

3.3.1 First strategy: preorganization

It is well known that the presence of competing hydrogen bond donor/acceptors in the same molecule can affect the resulting synthons in the crystal. However, in the case of the disquaramides studied in this work (**2**, **3** and **4**) the head-to-tail motif remains invariable. For this reason, we decided to study the effect of

an intramolecular interaction by introducing an extra hydrogen bond acceptor in a squaramide derivative model compound with the objective to modify the preferred cooperative self-associating interaction and to generate new synthons. To achieve this goal two new target compounds (**10** and **11**) were designed (Fig. 3.51).

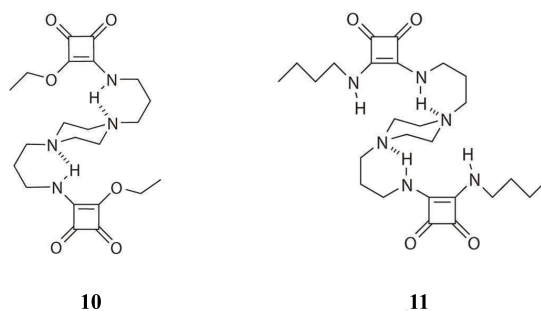


Fig. 3.51: Scheme of **10** and **11**

The bis squaramide-ester model compound **10** was prepared from diethylsquarate and 1,4-bis(3-aminopropyl)piperazine in diethyl ether. This amine has been previously used as a spacer in ditopic thioureas. Piperazine nitrogen establishes intramolecular interactions with thiourea NH protons in the solid state, inducing the formation of "spiral galaxy" motifs with syn/syn polymerization synthons. [250] On the other hand, compound **11** was obtained from the addition of butylamine to a solution of **10** in ethanol, as a very insoluble white solid. A limited polymorph screening was conducted since only DMF, DMSO (at very high temperature), trifluoroethanol and acetic acid could be used for recrystallization and only one form was obtained (see appendix A.12). Unfortunately, although several efforts were made to determine its crystal structure from PXRD by direct space methods, no satisfactory results were obtained. The presence of four amidic NH protons might be responsible for a strong self-assembling difficult to be perturbed, similar to the previously one seen during this work for other squaramides.

Although squaramides are strong hydrogen bonding donor/acceptors, mono-squaramide esters are not so previsible and other synthons have been observed (3.2.1.1). In principle, four different supramolecular synthons for **11** in the solid state were expected: the anti/anti configuration can produce two synthons, the head-to-tail polymer and the intramolecular monomer (Fig. 6.11 (a) and (b)), while the syn/syn configuration can produce the ribbon synthon and another intramolecular monomer (Fig. 6.11 (d) and (c)).

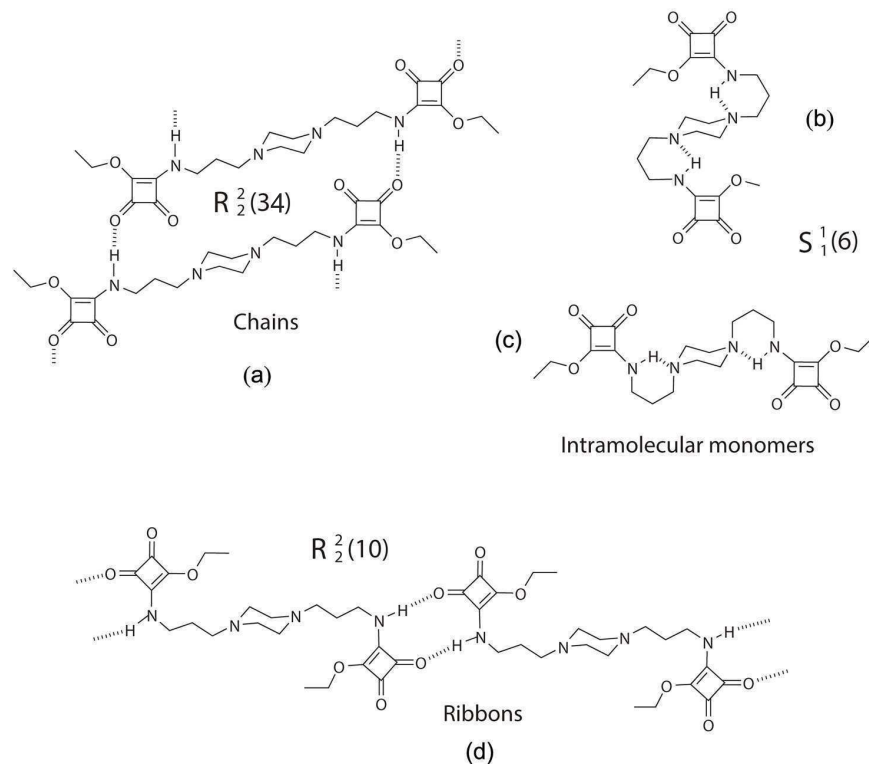


Fig. 3.52: Expected supramolecular synthons for **10** together with their corresponding graph sets

In order to study which synthons are formed, a polymorphism screening was conducted and three forms were obtained: two anhydrous forms and one hydrate.

Form I was obtained pure by precipitation from the synthesis process of **10** and form II could only be obtained pure by heating polymorph I until 160°C and then cooling down to r.t. (Fig. 3.53). Solvent mediated transformation experiments at different temperatures, in which a mixture of forms I and II evolved to pure form II at all temperatures below the melting point of form I, confirmed that both forms are monotropically related, being form II the most stable. The hydrate form (form III) was obtained from the solubility study by slow cooling crystallization in water from 90 °C to r.t.

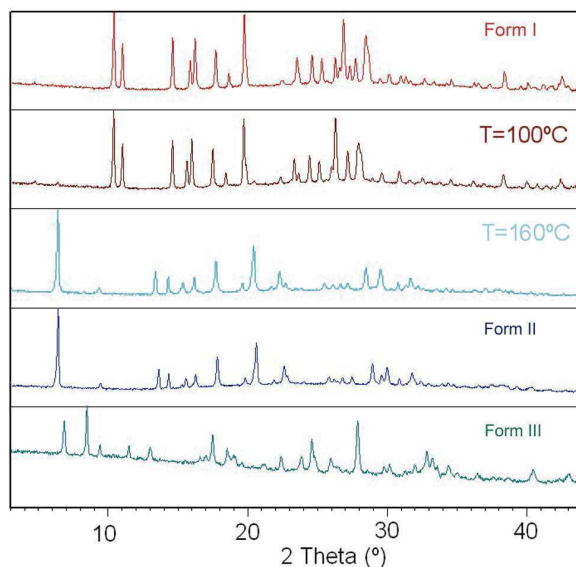


Fig. 3.53: PXRD diagrams of forms I, II and III. Form II was obtained from variable temperature experiments starting from form I (also shown in this figure)

The thermogram of polymorph I, registered at $10^{\circ}\text{C}/\text{min}$, shows an exothermic phenomenon at 135°C which was initially assigned to a solid-solid transition (Fig. 3.54), but a more accurate analysis with modulated DSC revealed overlapped melting and crystallization processes. Finally, the melting of form II is registered at 180°C . The thermogram of form III shows a wide endothermic double peak corresponding to water loss and overlapped melting-crystallization phenomena at 160°C (see appendix C.2.19).

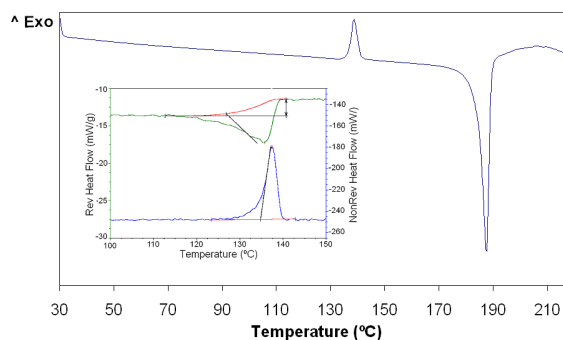


Fig. 3.54: Modulated DSC experiment of form I heating from 30°C to 220°C at $0.5^{\circ}\text{C}/\text{min}$ under nitrogen atmosphere

Since no good quality single crystals of any of the forms could be obtained, their crystal structures were determined from X-ray powder diffraction data by means of direct space methods (Fig. 3.55). However, no crystal structure could be

determined for the hydrate form. According to the thermogravimetric analysis, in which a weight loss of 18% was registered, the hydrate would contain six molecules of water in its structure (see appendix C.2.19).

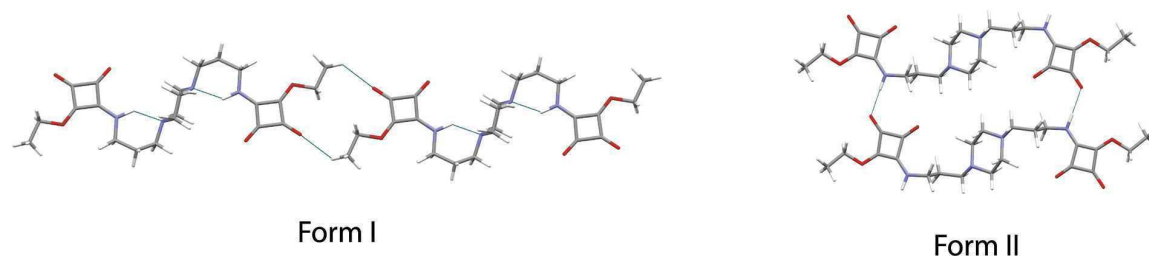


Fig. 3.55: Crystal structures of forms I and II showing intermolecular and intramolecular hydrogen bonding

Form I¹⁷ presents a six-membered ring formed through intramolecular hydrogen bonds, roughly perpendicular to the plane defined by the piperazine ring. Strong hydrogen bonds between the amidic NH and the piperazine nitrogen [$\text{N}-\text{H} \cdots \text{N}$ 2.843(8) Å] make the molecule shrink in a symmetric way. The parallel layers of molecules are stabilized through $\pi - \pi$ stacking interactions ($d_{\text{centroids}}$ 3.851 Å) of the cyclobutene rings and weak hydrogen bonds between the carbonyl oxygens and the piperazine hydrogens. A similar hydrogen bonding pattern has been reported in the "spiral galaxy" bis-thiourea derivatives from N,N'-bis(3-aminopropyl)-piperazine which proved to be very strong. [250] However, in the present case, this synthon corresponds to the metastable form. Form II¹⁸, instead, appears relatively strain-free, showing a head-to-tail hydrogen bonding motif similar to those already described in some other ester amides of squaric acid. [252] The cyclobutene rings interact via $\pi - \pi$ stacking, where the interplanar and centroid to centroid distances are 3.844 and 3.554 Å, respectively. In both cases, the piperazine rings adopt a chair conformation.

Interaction energy calculations of the aggregates resulting from the addition of different monomers for the head-to-tail synthon were performed at the DFT level of theory and compared with the syn/syn ribbon synthon. A model corresponding to the hydrogen bonding unit for each oligomer was extracted from the crystal structure, and the interaction energy was calculated (without further geometry optimization) using the counterpoise correction for basis set superposition error (BSSE). The extrapolation to a high number of monomers gives roughly an interaction energy of 33 kJ/mol per hydrogen bond, very similar to the 35 kJ/mol for the

¹⁷CCDC 883949 contains the crystallographic data.

¹⁸CCDC 883948 contains the crystallographic data.

syn/syn dimer (69 kJ/mol for two hydrogen bonds) (Fig. 3.56). The cooperativity of hydrogen bonding in the catemeric monosquaramide ester is again responsible for the stabilization of this conformer. In this sense, an experimental polymorph screening was conducted and, although finding evidences of polymorphism, no solid forms showing the syn/syn ribbon synthon were obtained despite the fact that it was expected from both geometrically and energetically points of view. Only the predicted (a) and (c) supramolecular synthons (Fig. 6.11) were experimentally obtained.

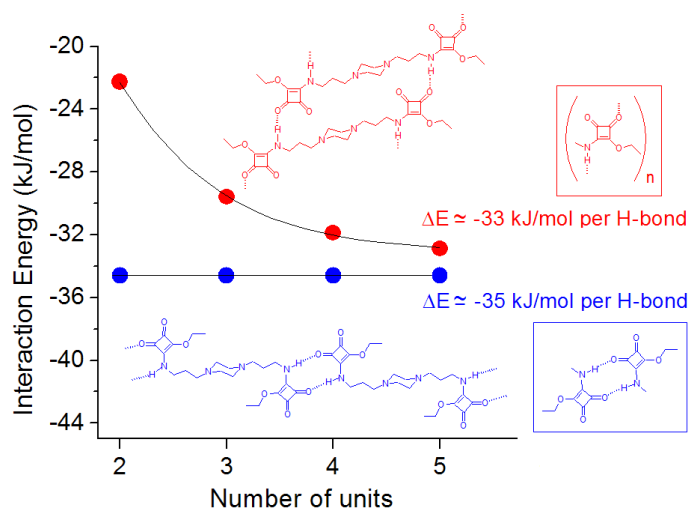


Fig. 3.56: DFT interaction energies for the anti and syn oligomers

Once it was confirmed that the intramolecular hydrogen bond is established in one of the polymorphs, we decided to use this preorganization effect to drive the formation of cocrystals with double hydrogen bond donor cofomers. In order to study this possibility, a cocrystal screening was performed between **10** and resorcinol. The hydrogen bonding donor abilities of resorcinol and **10** are quite similar (α parameters of 3.7 and 3.5, respectively); thus, a qualitative prediction of the likeliness of cocrystallization by using the Hunter's approach is particularly difficult in this case. However, resorcinol was chosen due to its geometrical and hydrogen bonding complementarity (Fig. 3.57), and a cocrystal screening was conducted (see appendix B.8).¹⁹ Two new crystalline phases were obtained (one anhydrous and one hydrate), whose crystal structures could also be determined by means of direct space methods from PXRD.

¹⁹A survey of the November 2011 Cambridge Structural Database has identified over 55 instances of the synthon R₂²(11)

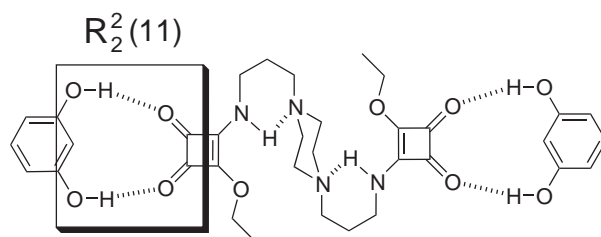


Fig. 3.57: Donor–acceptor complementarity between the expected cocrystal of **10** and resorcinol

An anhydrous cocrystal, with a 1:2 (**10**:resorcinol) stoichiometry, was obtained from the dehydration of the hydrate cocrystal at 120°C in an aluminum DSC crucible under nitrogen atmosphere, whereas the hydrate cocrystal, with a 1:2:2 (**10**:resorcinol:water) stoichiometry, was obtained by crystallization with different solvents during the cocrystal screening. Good quality crystalline structures could be achieved after Rietveld refinement demonstrating the formation of both cocrystals, although not with the expected synthon. In the anhydrous cocrystal, the most remarkable feature of the structure is that, besides the fact that the expected carbonyl–phenol interaction does not take place, each molecule of **10** interacts with another one via the syn/syn ribbon supramolecular synthon which, although being expected, had not been previously observed in any of its two polymorphs (Fig. 6.11, (d)). Moreover, two molecules of resorcinol interact through strong hydrogen bonds with both piperazine nitrogens and the free carbonyl groups of the squaramidic ring (Fig. 3.58).

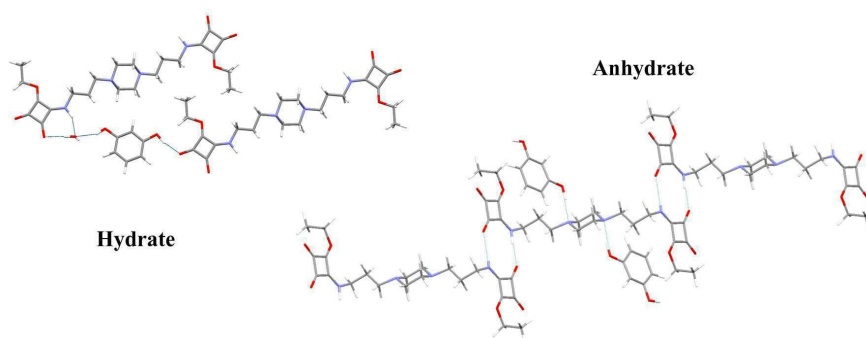


Fig. 3.58: Crystal structures of the resorcinol cocrystals

On the other side, in the hydrate cocrystal, the presence of water produces a dramatic change in the supramolecular synthons present in the structure. In this cocrystal, squaramide molecules do not interact with each other; instead, all its acceptor and donor groups establish hydrogen bonds with water and resorcinol molecules: carbonylic oxygens bond to water and phenol hydrogens while the amidic hydrogen bonds to the water oxygen. The other phenolic resorcinol's hydrogen also

bonds the water oxygen. The structure is completed with piperazine nitrogen–water interactions.

During the experimental cocrystal screening, evidences of polymorphism in these multicomponent solids have been observed, but no further studied, therefore, other supramolecular synthons, including the predicted $R_2^2(10)$, cannot be discarded.

In order to compare the supramolecular synthons observed with resorcinol, another similar coformer was tested: hydroquinone. Although not being geometrically complementary for the expected $R_2^2(10)$ synthon, it is a good double hydrogen bond donor coformer which might influence in crystallizing a new supramolecular architecture. After an experimental screening, three new polymorphic cocrystals were identified but unfortunately no crystal structure could be determined (see appendices B.8 and C.2.19). Research in this direction is still being conducted.

In summary, we have studied how the formation of an intramolecular hydrogen bond affects the polymorphism of a bis-squaramide ester compound. However, this preorganization has been revealed not to be sufficient to drive the formation of a cocrystal with the double donor-double acceptor supramolecular synthon that we expected. On the other hand, three out of the four a priori possible supramolecular synthons predicted for **10** have been observed in its two polymorphs and its anhydrate cocrystal with resorcinol structures.

3.3.2 Second strategy: cocrystallization with complementary coformers via peripheral interactions

All the difficulties in impeding the head-to-tail synthon of the dissecondary squaramides reveal that they can be very attractive to be exploited as molecular scaffolds in the design of new multicomponent crystalline structures because, with a suitable functionalization of the secondary squaramide substituents, complementary coformers could establish strong peripheral interactions with them. [251] In this sense, further insight was given to cocrystallization experiments of disquaramides with functionalized secondary chains with both donor and acceptor groups.

3.3.2.1 Cocrystals with hydrogen bond donor coformers

Two model compounds (**2** and **4**, Fig. 3.59), which have pyridil and dimethylamino functional groups, respectively, were selected for performing an intense experimental cocrystal screening with a set of hydrogen bond donor coformers such as carboxylic acids, phenols and amides (table 3.10). Three and six multicomponent solid forms

of **2** and **4** were identified from 56 and 162 cocrystallization experiments performed, respectively. Evidences of other new phases were detected during the screening.

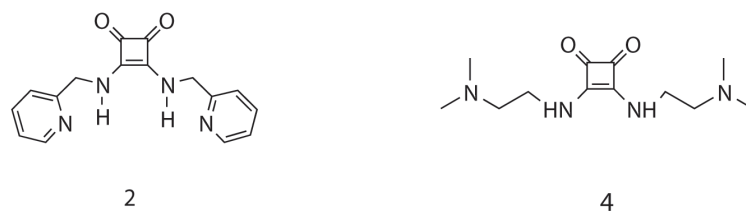


Fig. 3.59: Scheme of **2** and **4**

Tab. 3.10: Cocrystallization experiments with **2** and **4**. -: no solid obtained, 0: no cocrystal, 1: evidences of new phases, 2: cocrystal confirmed by SXRD or PXRD and $^1\text{H-NMR}$

Coformer	Compound 2	Compound 4
Fumaric acid	2	2
<i>p</i> -nitrobenzoic acid	2	1
Glutaric acid	0	1
Glutamic acid	0	1
Oxalic acid	1	1
Citric acid	0	1
Squaric acid	1	2
Resorcinol	0	2
Urea	-	1
Nicotinamide	0	1

One crystal structure of **2** with fumaric acid and three crystal structures of **4** with fumaric acid, resorcinol and squaric acid could be determined by means of direct space methods or SXRD and they are separately discussed as follows.

• Cocrystal of **2** : fumaric acid : ACN

The crystal structure of **2** with fumaric acid²⁰ shows the catemeric head-to-tail motif, as expected, together with hydrogen bonds between the pyridil nitrogen and the carboxylic acid moiety of fumaric acid ($\text{N}\cdots\text{HO}$). A cocrystal is formed according to the carboxylate distances obtained from the crystal structure solved by SXRD as we expected from a difference of pKas ($\Delta \text{pKa} < 3$, $\text{pKa}_{\text{pyridine}}=5.25$; $\text{pKa}_{\text{fumaricacid}}=3.03$) (see chapter 1.2). Moreover, acetonitrile molecules occupy available voids in the crystal structure (not shown) (Fig. 3.60).

²⁰CCDC 1015650 contains the crystallographic data.

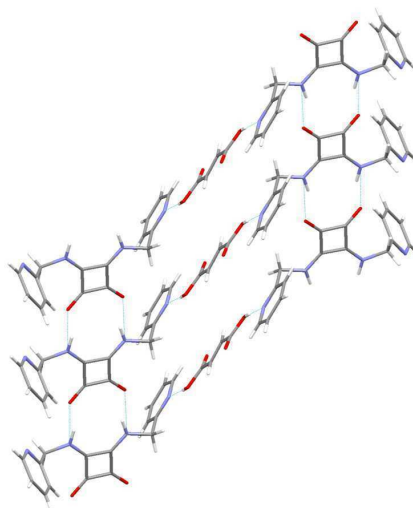


Fig. 3.60: Crystal structure of the ACN solvate of **2** and fumaric acid cocrystal, 1:1:2 (ACN molecules not shown)

- **Salt of 4 : fumaric acid : MeOH : water**

The crystal structure of this solvate,²¹ presents a displaced head-to-tail motif different from the previously described. Methanol and water molecules occupy the empty channels formed by squaramide units and fumaric acid columns. Water molecules connect fumaric acid molecules via hydrogen bonds and methanol molecules interact with the dimethylamino nitrogen atoms. According to the difference of pKas between the dimethylamine (pKa: 10.7) and fumaric acid (pKa: 3.03), this multicomponent solid form was expected to be a salt, however, surprisingly a cocrystal is confirmed by the carboxylic distances (d_{C-O} : 1.20 Å, 1.29 Å and 1.23 Å, 1.28 Å) from the crystal structure solved by SXRD (Fig. 3.61).

²¹CCDC 1015651 contains the crystallographic data.

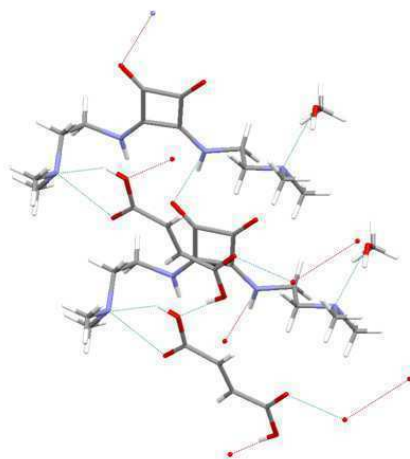


Fig. 3.61: Crystal structure of the MeOH/Water solvate of **4** and fumaric acid 2:2:1:3 cocrystal (water molecules not shown)

Interestingly the crystal structures of **2** and **4** with fumaric acid present a different type of head-to-tail synthon. Both scaffolds are catemeric, but the cocrystal of **2** presents a ring motif ($R_2^2(10)$) formed by ten atoms, in which two hydrogen bond donors and two hydrogen bond acceptors participate. On the other hand, the cocrystal of **4** crystallizes through a displaced head-to-tail motif, due to fumaric acid interactions, forming a chain ($C(6)$), in which one hydrogen bond donor and one hydrogen bond acceptor participate (Fig. 3.62).

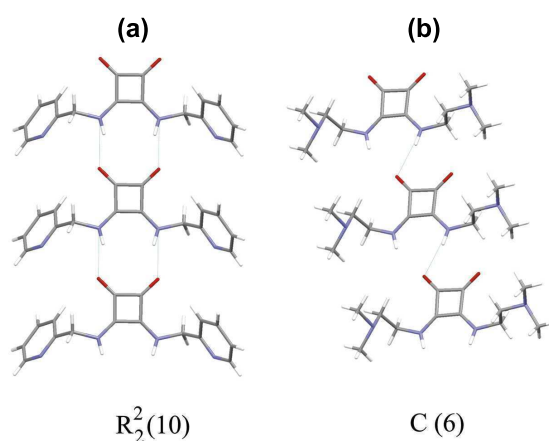


Fig. 3.62: Head-to-tail motifs of multicomponent forms of (a) **2** and (b) **4** (Cofomers not shown)

- **Cocrystal of 4 : resorcinol**

In this case, two polymorphic anhydrous cocrystal forms were identified (Fig. 3.63). Crystal structure of form I, solved by direct space methods, reveals the previously seen head-to-tail squaramide motif ($R_2^2(10)$) through hydrogen bond

interactions while resorcinol molecules interact with peripheral dimethylamino groups of **4** via hydrogen bonding ($N \cdots HO$) linking squaramide columns (Fig. 3.64).

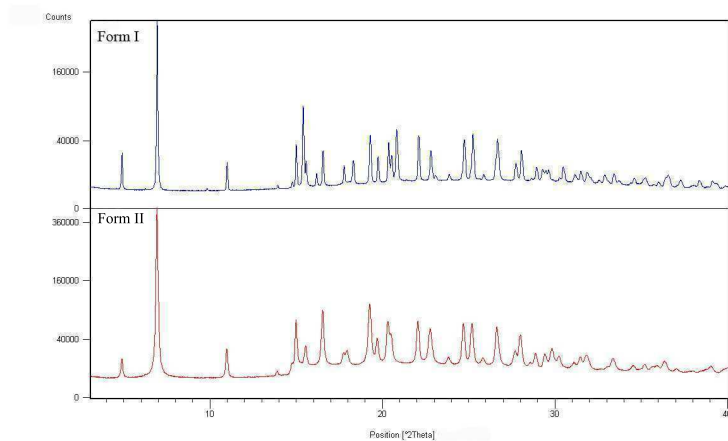


Fig. 3.63: PXRD diagrams of the two polymorphic anhydrous cocrystals of **4** with resorcinol (1:1)

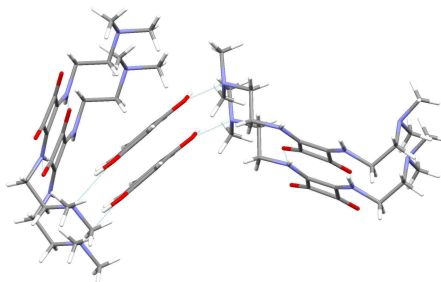


Fig. 3.64: Crystal structure of **4**:resorcinol cocrystal, form I

Although tetragonal cell parameters were determined ($a = 25.48 \text{ \AA}$, $c = 6.07 \text{ \AA}$, $V = 3943 \text{ \AA}^3$) by means of direct-space methods, no acceptable crystal solution for form II could be deduced, from the two different possible space groups I4 and I-4. Probably, a better definition of the diffractogram is needed for an acceptable crystal structure solution. Synchrotron radiation source experiments are planned to overcome this problem.

- **Salt of **4** : squaric acid : water**

The formation of a salt was again expected since squaric acid is a very strong acid ($pK_a = 1.5, 3.4$) which was confirmed according to the squarate distances from the crystal structure solved by SRXD. In this case, the head-to-tail is not observed because of the interaction with the squarate anion (Fig. 3.65). Water

molecules connect squaramide rings and monosquarate groups via hydrogen bonding.

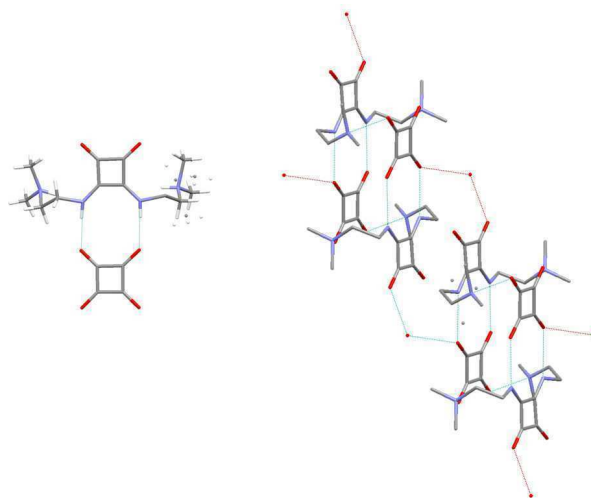


Fig. 3.65: Hydrate of the salt between **4** and squaric acid

3.3.2.2 Cocrystals with hydrogen bond acceptor cofomers

Since the strategy of using secondary squaramides containing peripheral hydrogen bond acceptor functional groups (pyridine and dimethylamine) was successful, we decided to extend this approach by attaching donor functional groups to the squaramide peripheral chains (Fig. 3.66). Compound **12** was synthesized from diethylsquarate and tyramine in ethanol.

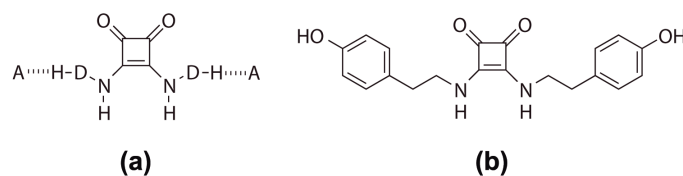


Fig. 3.66: Scheme of (a) a general disquaramide with peripheral hydrogen bond donor groups and (b) **12**

An experimental cocrystal screening was conducted between **12** and a set of different hydrogen bond acceptor compounds (see appendix B.8). Table 3.11 summarizes the cocrystal screening results.

Tab. 3.11: Cocrystal experiments with **12**. -: no solid obtained, 0: no cocrystal, 1: evidences of new phases, 2: cocrystal confirmed by SXRD or PXRD and $^1\text{H-NMR}$

Coformer	Compound 12
oxalic acid	1
resorcinol	0
nicotinamide	1
isonicotinamide	1
bipyridine	1
pyridine	1

As it is shown in table 3.11, some crystallization results suggested the existence of cocrystals with oxalic acid, nicotinamide, isonicotinamide, bipyridine and pyridine but only two crystal structures of solvate of **12** in ethanol and in DMSO/water could be determined by single X-ray diffraction (Fig. 6.13).²²

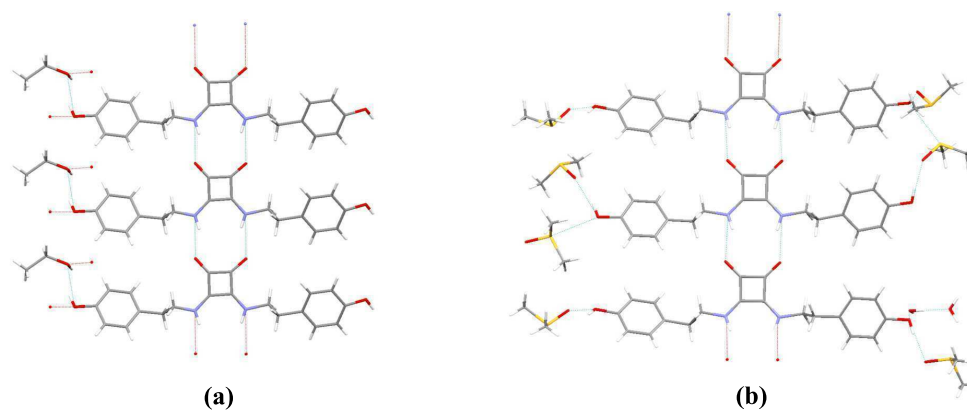


Fig. 3.67: Crystal structures of (a) ethanol and (b) DMSO/water solvates of **12**

Although the solvents ethanol, DMSO and water, were not intended to be used as coformers, the two crystal structures depict the general scheme of our strategy: a head-to-tail motif is again formed between squaramide units while ethanol and DMSO molecules interact via intermolecular hydrogen bonds with the phenol groups. These crystal structures suggest that our strategy of functionalizing the peripheral dissecondary squaramide chains with hydrogen bond donor functional groups in order to design new cocrystals could be successful. However, although many evidences of new crystal forms have been registered through the cocrystal screening conducted, further insight is required to elucidate the crystal structures of the multicomponent solids obtained in order to confirm the success of the design.

²²CCDC 1015653 contains the crystallographic data.

3.4 Self-assembling and template effect: helical architectures

Considering that the robust head-to-tail motif can be used as scaffold, we designed the non symmetrical squaramide (**13**) functionalized with donor and acceptor groups in the same skeleton, with the objective to produce new hydrogen bonded self-assembled architectures with new topological features. Thus, compound **13** was synthesized through a two-step selective condensation of *N,N*-dimethylethylenediamine and tyramine with diethylsquarate in mild conditions. Assuming that the head-to-tail interaction can act as a template, in principle two types of interactions are possible: (a) cyclic and (b) polymeric, which could give raise to helical assemblies (Fig. 3.68).

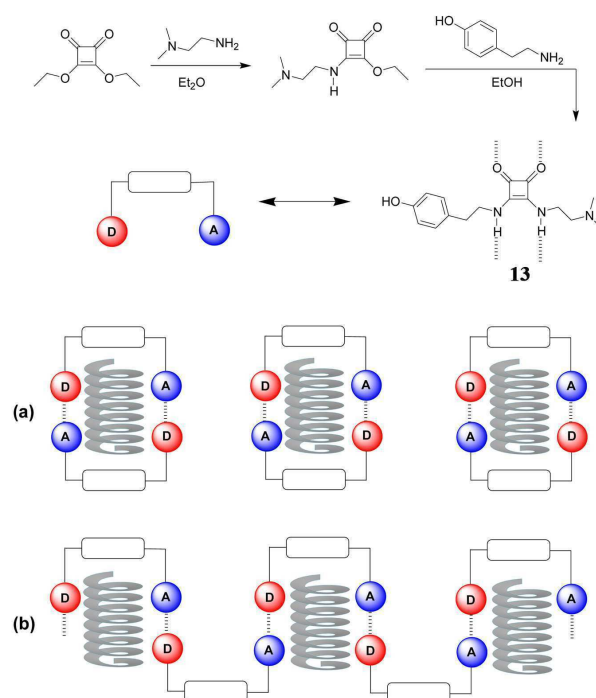


Fig. 3.68: Possible (a) Cyclic and (b) Polymeric aggregates of **13**

The helix is one of the most important structural motifs in nature due to its ubiquitous presence, from the molecular level to the astronomical scale. [253, 254] Helicity shows relevant properties such as chirality and other geometric features which have attracted the attention of the scientific community. [255–257] Examples of helicity include the double-stranded DNA and the assembly of linear proteins into multistranded complexes which are responsible for the genetic information and diverse biological functions. [258] This fascinating natural motif has inspired the design and synthesis from unnatural backbones of a broad variety of artificial he-

lices in the fields of supramolecular chemistry, asymmetric catalysis, biomimetics, etc. [259–261] Thus, the use of synthetic building blocks for the supramolecular assembling into helical polymers [262] has been successfully exploited in the past with metal coordinated helical complexes [255, 263] or self-assembled spiral nanoarchitectures from barbituric acid, [264] among many others. [265–267] In this sense, hydrogen-bonding is a key interaction due to its great directionality and strength which can be used to design highly stable and selective building blocks able to cooperatively drive the formation of polymeric assemblies. [268–270]

Since no crystals of **13** suitable for structure determination by SXRD could be obtained, its crystal structure was solved from laboratory X-ray powder diffraction data by means of direct space methods (Fig. 6.14).²³

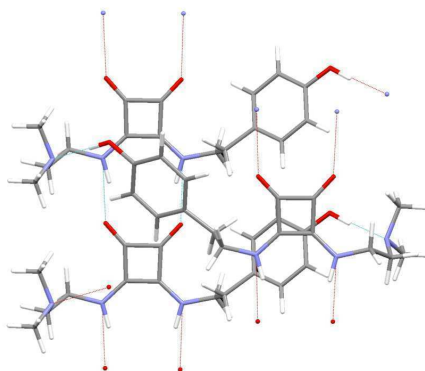
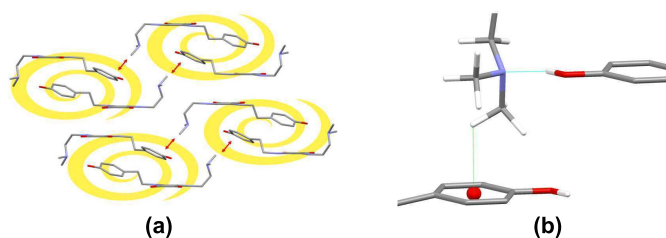


Fig. 3.69: Crystal structure of **13**

The analysis of the crystal structure reveals that the catemeric head-to-tail arrangement remains and helices are individually packed (following model (a) in figure 3.68), connected to others through weak CH– π interactions between the methylamino group and the aromatic ring, [271, 272] with centroid distance of 3.05 Å and C-H centroid angle of 109° (Fig. 3.12, (a)). This nitrogen atom is particularly electronegative due to the strong hydrogen bond with the phenol group which drives the methyl groups to interact efficiently with the face of the aromatic ring (Fig. 3.12, (b)).

²³CCDC 953732 contains the crystallographic data.



Tab. 3.12: (a) Helix-packing motifs via $\text{CH}\cdots\pi$ interactions and (b) $\text{CH}\cdots\pi$ interaction between the methylamino group and the aromatic ring in **13**

Although helical assemblies from an achiral compound such as **13** can a priori form chiral crystals, a racemic mixture of alternating clock and anticlockwise spinning helices has been found (Fig. 3.70).

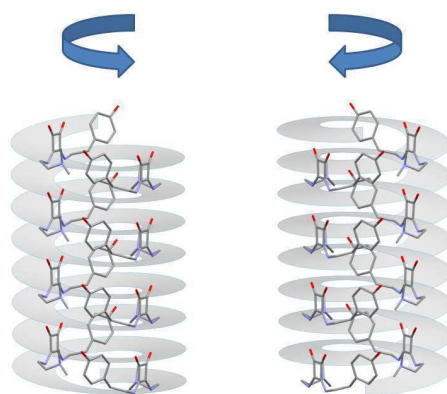


Fig. 3.70: Clock and anticlockwise rotation of the two different helices in the racemic crystal of **13**

This unprecedented helix in a squaramide is driven by a combination of two different head-to-tail interactions and, according to the literature, this example can be considered remarkable in the field of crystal engineering and supramolecular chemistry. The good geometry and donor/acceptor complementarity produces an optimal packing which excludes the possibility to form cavities.

Once the formation of hydrogen-bonded helical structures in a nanotube fashion was observed with compound **13**, another strategy of nanotube formation was considered through the design of cyclic compounds containing two squaramide units covalently linked. In this sense, the formation of nanotubes by macrocyclic squaramides was initially studied and new compounds were synthesized to explore this possibility (Fig. 3.71), (Chapter 6.3.6). However, this research line has been abandoned due to experimental difficulties in crystallizing such compounds. They are very insoluble in most of the solvents and their powder diffraction patterns show

broad bands, suggesting low crystallinity or likely microcrystalline structures. This is supported by DSC analysis which shows profiles with no defined melting point. Further research on this issue could be developed in the future.

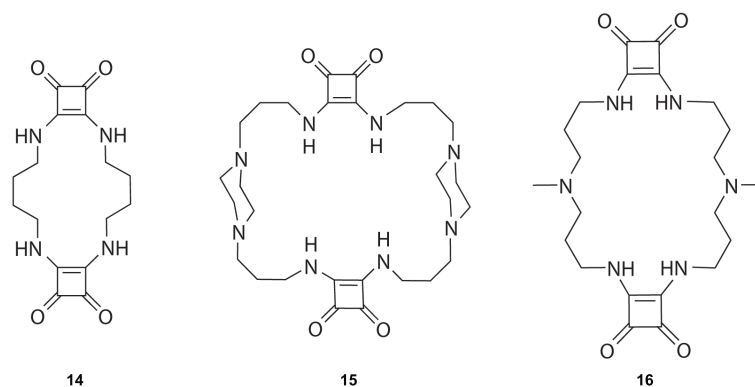


Fig. 3.71: Macrocyclic squaramides **14**, **15** and **16**

3.5 Charged squaric acid derivatives: the electrostatic compression phenomenon

Hydrogen bonding, which combines directionality with strength, π -stacking and their mutual combinations play a key role and have been long and successfully used in supramolecular chemistry. [119,120,273–275] In particular, charge-assisted hydrogen bonds have been exploited to build periodical supramolecular structures. [276–278] The electrostatic nature of this type of hydrogen bond usually strengthens the interaction because of the presence of ionic charges on the hydrogen bonding donor/acceptor interacting groups. [279] This charge assistance preserves the hydrogen bonding directionality while reinforcing the interaction with the help of coulombic forces. [280] In squarate salts, an inverse relation between length and strength of charged rings has been observed which is explained by an electrostatic compression phenomenon. [281] Interionic interactions between anions in the solid state may not correspond to stable intermolecular bonds, in spite of being the donor-acceptor groups distances shorter than the equivalent neutral groups distances. [282,283] In fact, it is a consequence of a stronger attractive interaction of a next-neighbour anion-cation compared to the repulsive effect of anion-anion and cation-cation (Fig.3.72). [284] The balance of attractive and repulsive ionic interactions determines the crystal cohesion. Since electrostatically compressed interactions retain directionality, they are usefull tools in crystal engineering of materials, in relation to conductive and magnetic properties, [285,286] supramolecular chemistry [287] and biochemistry. [288]

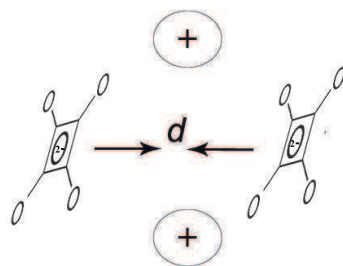


Fig. 3.72: Scheme of the electrostatic compression phenomenon in squarate assemblies

3.5.1 Zwitterionic squaramide/squarate compounds

Taking into account the abovementioned phenomena recently reported in squarate salts, [277,281,286] we decided to exploit charge assisted hydrogen bonding interactions in zwitterionic squaric acid derivatives in combination with electrostatically

driven dimerization to design new supramolecular assemblies in the solid state. With this objective, the zwitterionic squaramide/squarate compound **17** was designed as the building block of a new family of supramolecular assemblies and it was synthesized in one single step from squaric acid and N,N-dimethylethyldiamine in water. [184] The strong acidity of the squaric acid moiety ensures the zwitterionic character of **17**, which in combination with a geometrical complementarity produces the optimal conditions to form self-assembling dimers (Fig. 3.73).

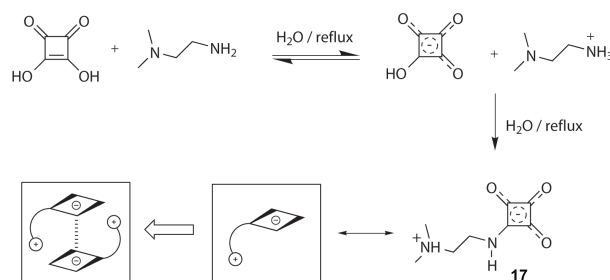


Fig. 3.73: Synthesis of the zwitterionic squaramide **17** and the schematic self-assembling through electrostatic compression

In principle, two different supramolecular synthons are geometrically possible through charge assisted hydrogen-bond interactions if the electrostatically compressed assemblies are formed in the solid state: an $R_2^2(10)$ motif (in a self-assembling manner) (Fig. 3.74 (a)) and a head-to-tail C(5) or C(6) motif (Fig. 3.74 (b)).

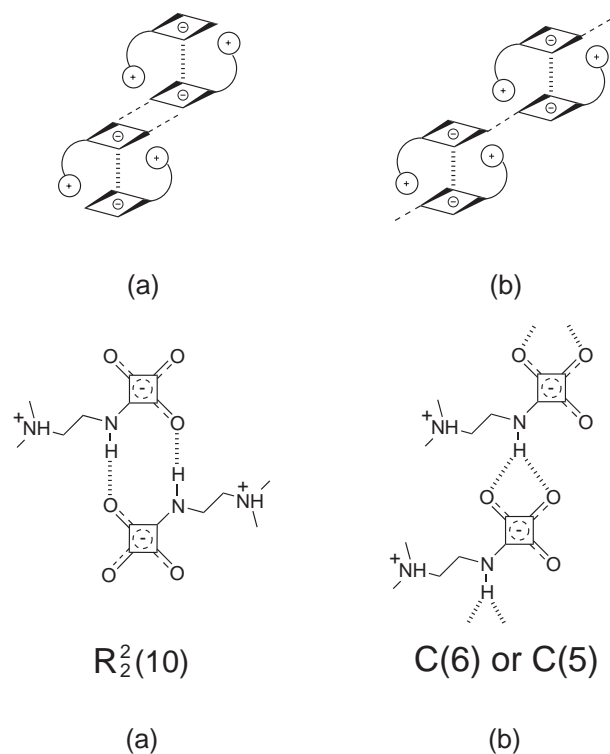


Fig. 3.74: Different assembling motifs for **17**, expected through charge assisted hydrogen bonding

In order to study this hypothesis a polymorph screening was conducted. Crystals of three different phases were obtained through crystallization of **17** by slow diffusion of dioxane in dimethylsulfoxide (form I), of methyltertbutylether in dimethylsulfoxide (form II) and of dichloromethane in water (form III). The structures of two anhydrate polymorphs (forms I and II)²⁴ and a hydrate²⁵ (form III) were solved by SXRD. Form II crystallized concomitantly with form I in all the experiments, however, we were able to isolate flat needles of form II from the crystallization mixture.

In the two anhydrous crystal structures, similar electrostatically compressed dimers establish complementary N-H \cdots O interactions with adjacent dimers. However, squaramide rings in form I are closer to each other than in form II with centroids distances of 3.47 Å and 3.70 Å respectively (Fig. 3.75).

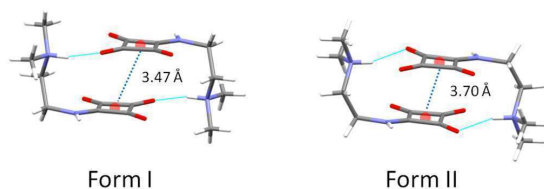


Fig. 3.75: Stacked dimers showing $d_{\text{centroid-centroid}}$ for anhydrous forms I and II of **17**

The most important difference lies on the carbonylic oxygen which is involved in the intermolecular hydrogen bond. While in form I the carbonylic oxygen in anti with respect to the NH is forming the hydrogen bond, in form II this interaction is established by the oxygen in syn. This is the consequence of two geometrically possible hydrogen bond donor/acceptor combinations, since hydrogen bond acceptor ability of the two available carbonyl oxygen atoms are similar (molecular electrostatic potential minima²⁶ of -330 and -349 kJ/mol, figure 3.76).

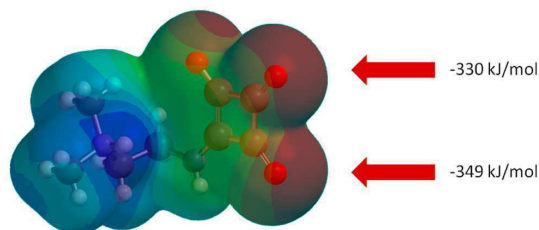


Fig. 3.76: MEP surface at the DFT level of computation of the isolated geometry from the crystal structure of form I

²⁴CCDC 938373 and CCDC 951985 contain the crystallographic data.

²⁵CCDC 938372 contains the crystallographic data.

²⁶MEP surface was computed with Spartan '10 using DFT B3LYP/6-31+G* *ab initio* calculations. The molecule was imported from the crystal structure of form I and was not energy minimized.

This particularity has important consequences on the connexion of the electrostatically compressed dimers in the crystal, producing completely different supramolecular synthons for both polymorphs: $R_2^2(10)$ rings in form I and $C(5)$ chains in form II (Fig. 3.77).

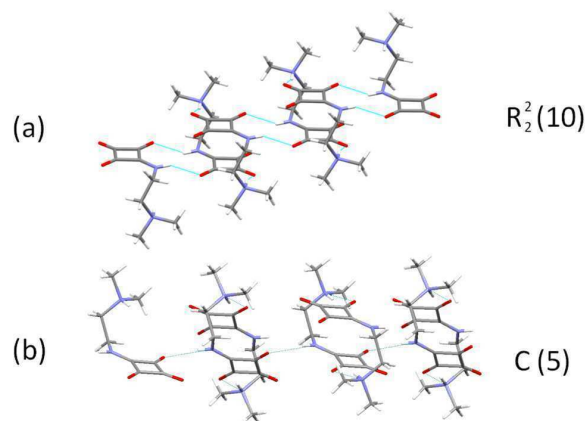


Fig. 3.77: Supramolecular synthon observed in form I (a) and form II (b) connecting the electrostatically compressed dimers in the crystal

On the other hand, in the hydrate form III a different supramolecular synthon is observed. Each compressed dimer interacts with the neighbouring dimer in a C(6) motif with water molecules stabilizing the structure through hydrogen bonding interactions with the free carbonyls. The electrostatically compressed dimer that is formed is very similar to the one in form I, with centroid-centroid distance of 3.52 Å (Fig. 3.78).

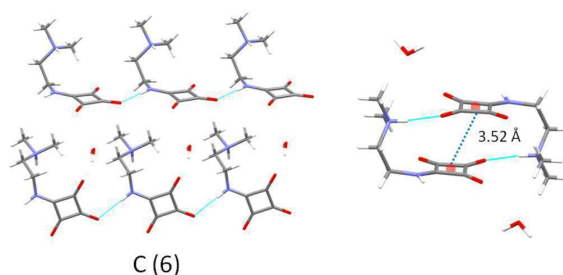


Fig. 3.78: Supramolecular synthons observed together with the stacked dimer in the hydrate form III

Since the condensation reaction between squaric acid and the *N,N*-dimethylethylenediamine is not complete, mixtures of non reacted squaric acid and **17** were present in the synthesis crude and, unexpectedly, crystals of a different phase were isolated from the reaction mass in one of the crystallization experiments conducted (see appendix B.8). The solved crystal structure²⁷ revealed that a new monosquarate/**17** salt was obtained. Interestingly, the structure shows another electrostatically compressed motif which is formed through a combination of a monosquarate anion and two different moieties of **17** in a similar stacked way as in the anhydrous and hydrate forms of **17**, with centroid-centroid distance of 3.51 Å (Fig. 3.79). The most remarkable feature of this structure is that peripheral hydrogen bonding squaric/squaric interactions are established with the same $R_2^2(10)$ motif previously reported by Mathew *et al.*, [159] suggesting that self-assembled zwitterionic squaramides could be used as efficient cofomers for cocrystallization of a variety of donor/acceptor compounds such as carboxylic acids, ureas, amides, etc.

²⁷CCDC 938374 contains the supplementary crystallographic data.

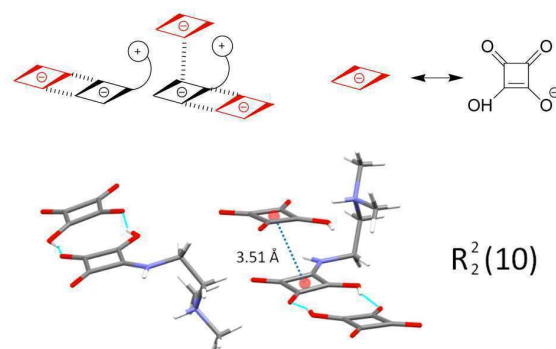


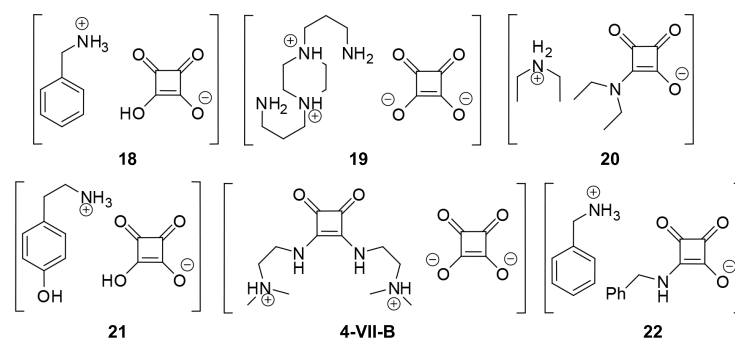
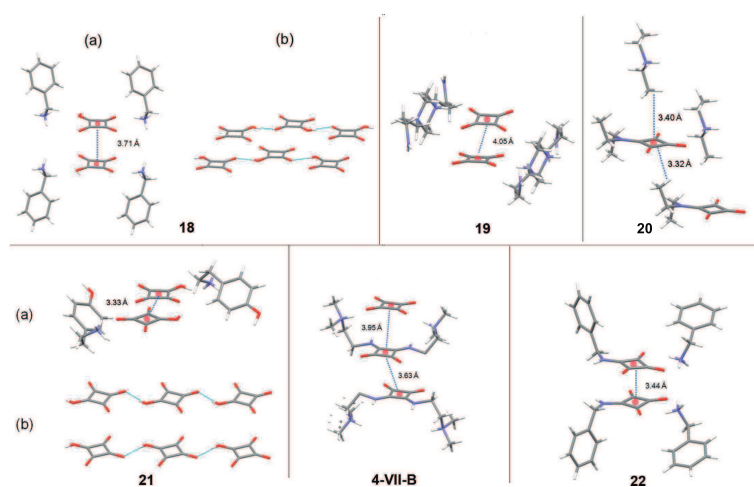
Fig. 3.79: Crystal structure of monosquarate/17 salt

3.5.2 Squarate salts

Squarate salts have been extensively studied in the solid state [159,169,289] and a π -stacking is observed as a consequence of the electrostatic compression phenomenon. As it has been reported, aromaticity and hydrogen bonds are the most important forces driving the interactions in the solid structures of squarate ions, [290] thus we decided to examine the propensity of squaramide, hydrogen squarate and squarate salts in the solid state to establish interactions that are typical of aromatic compounds [291] (stacking interactions, [119,292,293] ion- π , [294–296] C-H/ π , [271,297] etc.). In this sense, a collaborative research with the group of Prof. Frontera was conducted with the aim to extend the knowledge about the forces that govern these specific π -stacked assemblies by combining X-ray characterization and computational analysis of several squarate and amidosquarate salts (Fig. 3.80),²⁸ which were synthesized from squaric acid and the corresponding amine in water (See chapter 6.3.6). In particular, we focused our attention in the analysis of the influence of the four-membered ring aromatic character on the solid state architecture of these mono and di-anion salts directing the type of noncovalent interactions. [298] Moreover, a relation was found between the ability of the squaric acid and its derivatives to establish hydrogen bonds, $\pi - \pi$ stacking and other π -interactions (anion- π , lone pair- π and C-H/ π), which has not been previously analyzed in detail, and the increase in the aromaticity of the ring.²⁹

²⁸CCDC: 987591, 987592, 987593, 987594, 987595 and 987596 contain the crystallographic data.

²⁹The computational details and further experimental information can be found in the published article (Prohens, R. *et al.* *Crystal Growth & Design*, **2014**, *5*, 2578-2587.). They are not included in this Thesis since this research has not been conducted by myself but it is a collaborative work.

Fig. 3.80: Squarate and amidosquarate salts **18-22** studied in this workFig. 3.81: Crystal structures of the amidosquarate salts **18-22** studied in this collaborative research

In summary, we have studied the electrostatic compression phenomenon in zwitterionic squaramides and squarate salts, which is responsible for the formation of new supramolecular synthons confirming the ability of the squaric acid derivatives to establish combined hydrogen bond and π -stacking interactions in the solid state. Their potential for the synthesis of new multicomponent solids with both hydrogen bond donor and acceptor cofomers has been tentatively explored.

Chapter 4

Screening Techniques

4.1 Introduction

There are several methods used for screening of solid forms (table 4.1) described in the literature, either in the solid state or from solution, the latter preferred for the pharmaceutical industry, in which crystallization conditions can be modified by using different solvents, antisolvents, temperatures, heating and cooling rates, additives, concentrations, pH, pressure, saturations, etc. [36, 299]

The characterization of the solid forms obtained from the screening is mainly performed by X-ray diffraction techniques in combination with thermal analysis such as differential scanning calorimetry (DSC, Fig. 4.1), which is also a powerful tool for obtaining useful information of the polymorphic system properties, and thermogravimetry (TGA). Other complementary techniques widely used are solid-state NMR spectroscopy, vibration spectroscopy (IR and Raman), thermomicroscopy,

Tab. 4.1: Crystallization methods

Crystallization from solution methods	Solid state methods
evaporation	cooling from the melt
slurrying	expose to solvent vapour
cooling crystallization	expose to high or low humidity
antisolvent diffusion	sublimation
antisolvent addition	grinding
reverse antisolvent addition	

moisture sorption analysis and surface energy analysis. [14, 23, 40] In case of cocrystals characterization, the use of ^1H -NMR and ^{13}C -NMR spectroscopy is essential.

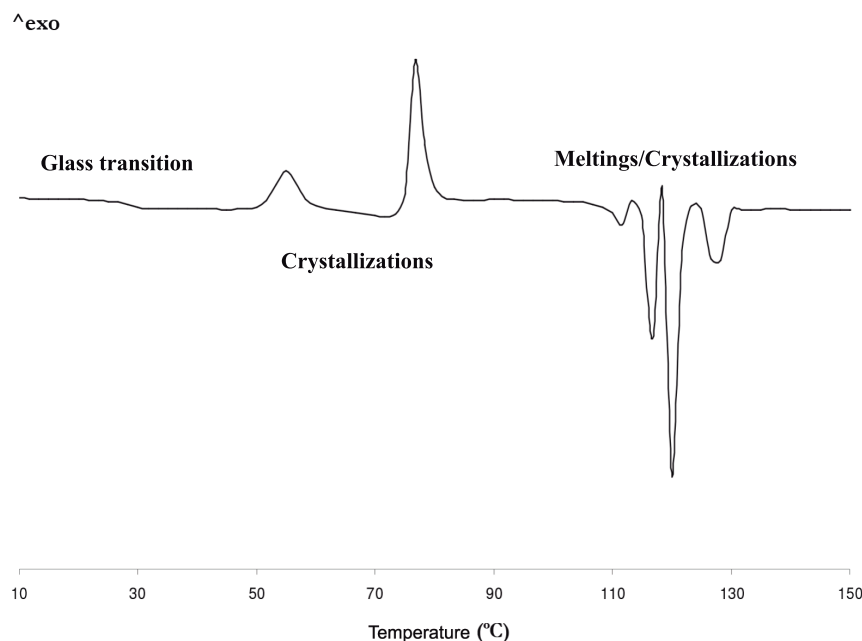


Fig. 4.1: Thermal phenomena usually observed in a DSC analysis [300]

The preference for a polymorph to crystallize in a specific solvent at a given temperature and pressure is influenced by solvent-solute interaction phenomena in the nucleation process, crystal growth, polymorphic transformation and by the intrinsic solvent properties, such as, viscosity, hydrogen bonding ability, dielectric constant and surface tension, which affect the crystallization kinetics of polymorphs. [301,302] Therefore, using solvents with diverse properties increases the probability to find new polymorphs. Previous studies have established solvents classification without including parameters such as acceptor/donor hydrogen bond capacity and viscosity. [303,304] In the present study, a classification according to the clusters method, in particular the average linkage method, has been followed. [305,306] This method classifies 96 solvents in 15 groups by taking into account 8 parameters: acceptor/donor hydrogen bond capacity, polarity/dipolarity, dipolar moment, dielectric constant, viscosity, surface tension and cohesive energy density. A parallel classification is performed, which takes into account just 5 parameters of the aforementioned (discarding viscosity, cohesive energy density and surface tension, which just affect solvent-solvent interactions). [307] Finally, a last classification was done with one or more solvents selected from the coincident solvents from both classifications as main representatives of each group and new groups were created with the non-coincident solvents, discarding acids, bases and potential toxic solvents. With these general criteria 13 groups were obtained and 14 solvents have been used to work experimen-

Tab. 4.2: Solvents classification

Group	Solvent	b.p. ^a	π ^b	μ ^c	δ ^d	d ^e	V ^f	γ ^g	α ^h	β ⁱ	Toxicity
1	Heptane	99	-0.08	0.00	1.91	200	0.39	28.28	0.00	0.00	Low
2	Dioxane	101	0.51	0.00	2.21	372	1.18	47.14	0.00	0.64	Medium
3	Toluene	111	0.54	0.38	2.37	289	0.56	40.20	0.00	0.14	Medium
4	Et ₂ O	34	0.27	1.15	4.24	231	0.22	23.96	0.00	0.41	Low
5	THF	66	0.58	1.75	7.43	337	0.46	39.44	0.00	0.48	Low
6	CH ₂ Cl ₂	39	0.82	1.60	8.93	400	0.41	39.15	0.10	0.05	Medium
7	Acetone	56	0.71	2.88	20.49	362	0.31	33.77	0.04	0.49	Low
8	EtOH	78	0.54	1.69	24.85	619	1.07	31.62	0.37	0.48	Low
9	MeOH	64	0.60	1.70	32.61	808	0.54	31.77	0.43	0.47	Medium
10	ACN	81	0.75	3.92	35.69	523	0.37	41.25	0.07	0.32	Medium
11	DMF	153	0.88	3.82	37.22	464	0.79	49.56	0.00	0.74	Medium
	DMSO	189	1.00	3.96	46.83	573	1.99	61.78	0.00	0.88	Low
12	ETG	85	0.92	2.28	41.40	858	16.10	69.07	0.90	0.52	Medium
13	Water	100	1.09	1.87	78.36	2096	0.89	105.0	1.17	0.47	Low

^aBoiling point (°C)

^bPolarity/dipolarity of the solvent [308]

^cDipole moment (debye) [309]

^dDielectric constant [309]

^eCohesive energy density (Jmol/mL) was calculated from the equation, $(H_{\text{vap}} - RT)/V$, where H_{vap} is the enthalpy of vaporization, R is the gas constant, T is temperature of interest and 298.15 K was used in the calculation, and V is the molar volume at 298.15 K. The value of H_{vap} and V was collected from the reference [309]

^fViscosity of the solvent at 25°C (mPas) [309]

^gSurface tension of the solvent at 25°C (cal/(mol·Å²)) [309, 310]

^hSummation of the hydrogen bond donor propensities of the solvent [310, 311]

ⁱSummation of the hydrogen bond acceptor propensities of the solvent [310, 311]

tally during the screenings. In particular, dimethylsulfoxide and dimethylformamide belong to the same group, but we considered working with both solvents since they are extremely good in dissolving compounds, such as squaramides. Table 4.2 shows a list of the solvents used in this work for the polymorphic and cocrystal screenings. Solvents have been used as purchased, without further purification. This classification has been taken into account with the first four disquaramides. Additional solvents have been used in the whole work due to insolubility of the compounds and other experimental considerations.

4.2 Polymorphic Screening

In the present work, the polymorphic properties of several reported compounds have been experimentally investigated through a general procedure for screening [307] based on previous studies from the literature [12,14,22,312] and our work experience in the Unit of Polimorphism and Calorimetry of the University of Barcelona. Thus, for each compound the following general protocol has been followed:

- Initial solid state characterization of the compounds by PXRD, TGA and DSC.
- Solvent selection and solubility study.
- Samples generation: crystallizations under kinetic and thermodynamic conditions.
- Analysis and characterization of the solids obtained by PXRD, TGA and DSC.
- Crystal structure determination from powder X-ray diffraction or by single crystal X-ray diffraction when possible.
- Study of the relative thermodynamic stability of the polymorphs obtained for each compound.

4.2.1 Solubility study

10 mg of the compound were dissolved in the minimum required volum of the selected solvent (up to 1 mL) at r.t. When the solid did not dissolve, the temperature was raised up to the solvent boiling point. The solubility data of the model compounds in the current study are summarized in appendix A.12)

4.2.2 Crystallization experiments from the solubility study

The vials containing the solutions obtained from the solubility study are kept closed overnight at r.t. and if a solid still does not crystallize the tubs are opened for the solvent to evaporate.

4.2.3 Solvent mediated transformation experiments (slurries)

The same amount of two polymorphs (10-30 mg of each form) were suspended in the selected solvent into a sealed vial under stirring at the tested temperature. At higher temperatures than r.t., the suspension was purged under nitrogen or argon. In case the solvent was too volatile, small amounts of the solvent were added periodically to avoid dryness. Aliquots of the suspended solid were analyzed periodically by PXRD and the diffractograms were compared to the starting material until the transformation was complete. In the present work, this technique has been applied to the solids of the solubility study which are insoluble and they have been slurried overnight.

4.2.4 Precipitation experiments under kinetic conditions

4.2.4.1 Precipitation experiments by rapid cooling from high temperature to low temperature (PHT)

10 mg of the compound were dissolved in the minimum required volume of the solvent at high temperature and the solution was cooled rapidly to 0 °C or at a temperature above the solvent freezing point. All the solids obtained were filtered and air-dried.

4.2.4.2 Precipitation experiments by antisolvent addition (PAD)

10 mg of the compound were dissolved in the minimum required volume of the selected solvent at r.t. If the compound was insoluble at r.t., the suspension was heated until it dissolved. Antisolvents¹ at a 1:2 ratio (solvent:antisolvent) were rapidly added to the solutions at r.t. and if no solid precipitated more antisolvent was added up to a 1:4 ratio (solvent:antisolvent). Finally, in cases in which no solid appeared, solutions were cooled down to 0 °C or at a temperature above the freezing point of the solvent. All the solids obtained were filtered and air-dried.

¹solvents in which the compound is insoluble

4.2.5 Crystallization experiments under thermodynamic conditions

4.2.5.1 Crystallization experiments by slow cooling from high temperature to r.t. (CHT)

10 mg of the compound were dissolved in the minimum volume of the solvent at high temperature. Once the solid was completely dissolved, the stirring and heating were switched off and the solution was allowed to slowly cool down to r.t. The solids obtained were filtered and air-dried.

4.2.5.2 Crystallization experiments by solvent evaporation at r.t. (CRT)

10 mg of the compound were dissolved in the minimum required volume of the solvent at r.t. and, once the solid was completely dissolved, the stirring was stopped and the vial containing the solution was opened to air until a solid crystallized. The solids obtained were filtered and air-dried.

4.2.5.3 Crystallization experiments by antisolvent diffusion at r.t.(CAD)

10 mg of the compound were dissolved in the minimum required volume of the solvent at r.t. into a thin vial, which was sealed with a septum and a needle, through which the antisolvent is allowed to evaporate. The vial was introduced into a bigger vial containing the selected antisolvent, and the system was sealed. The solution was maintained at r.t. until a solid crystallized (Fig.4.2).

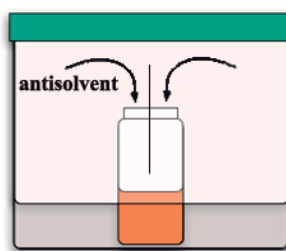


Fig. 4.2: Antisolvent diffusion scheme

4.3 Cocrystal screening

In this section the general procedure of the experimental cocrystal screening techniques used in the present work is described, based on previous studies from the

literature and our work experience. [52,60,74,313,314] However, no extensive cocrystal screening has been performed for each compound, but specific methods for some particular compounds in order to study their crystal structures. All the resulting solids were analyzed by PXRD and new multicomponent phases were confirmed by $^1\text{H-NMR}$.

4.3.0.4 Grinding/Drop-grinding experiments (G/DG)

20-50 mg of a mixture of the compound and the selected coformer in a 1:1, 1:2 or 2:1 molar ratio were introduced together with two steel balls of 3 mm of diameter into a miller. A drop of a selected solvent (5-10 μL), in case of the drop-grinding, was added together with two metallic balls and the miller was programmed at 30Hz for 30 minutes.

4.3.0.5 Reaction Crystallizations (RC)

A saturated solution of the more soluble component was prepared under stirring in a sealed vial. Small amounts of the other component were added until a suspension was obtained. The suspension was kept stirring for a week at room temperature, avoiding the complete evaporation of the solvent by adding little amounts of solvent, if necessary. Finally, the solid was filtered and air-dried.

4.3.0.6 Precipitation experiments by rapid cooling from high temperature to low temperature (PHT)

20-50 mg of a mixture of the compound and the selected coformer in a 1:1, 1:2 or 2:1 molar ratio were introduced into a sealed vial with the minimum required volume of a specific solvent to dissolve the mixture at high temperature. Once the solid was dissolved, the solution was cooled rapidly to 0 °C or at a temperature above the solvent freezing point.

4.3.1 Crystallization experiments to obtain single crystals

4.3.1.1 Crystallizations experiments by slow cooling from high temperature to r.t. (CHT)

20-50 mg of a mixture of the compound and the selected coformer in a 1:1, 1:2 or 2:1 molar ratio were introduced into a sealed vial with the minimum required volume of a specific solvent to dissolve the mixture at high temperature. Once the

solid was dissolved, the heating was switched off allowing the solution to cool down slowly to r.t.

4.3.1.2 Crystallization experiments by antisolvent diffusion at r.t. (CAD)

An aliquot of a solution containing the compound and the cofomer in a 1:1, 1:2 or 2:1 molar ratio at r.t. was introduced into a thin tub sealed with a septum and a needle, through which the antisolvent was allowed to diffuse. It was kept without stirring into a bigger tub containing the selected antisolvent until a solid crystallized.

4.3.1.3 Recrystallization experiments from the reaction crystallization solids (RRC)

A saturated solution of the more soluble component was prepared in the selected solvent at r.t. and the less soluble component was added until a suspension was observed. The temperature was raised and additional solvent was added until a complete dissolution of the solid. Finally, the solutions were slowly cooled down to r.t.

Chapter 5

Crystal structure determination from powder X-ray diffraction data

Powder X-ray diffraction (PXRD) is now one of the most widely used techniques available to materials scientists for studying the structure and microstructure of crystalline solids, specially in cases where suitable single crystals are not available. [315] In recent years, significant progress has been made in all aspects of *ab initio* crystal structure solution from powder diffraction data, [316–320] since organic compounds named Cimetidine [321] and Fluorescein diacetate, [322] were first determined by direct space methods using synchrotron X-ray powder diffraction data. Various methods for the structure determination from powder diffraction data (SDPD) have been used since then and numerous examples of reliable three-dimensional structures [323–329] have been obtained, of comparable quality to those from single crystal experiments.

The challenges encountered in crystal structure solution from PXRD data in the case of molecular crystals are greater compared to non-molecular and framework crystal structures. Molecular crystals tend to have low symmetry, leading to substantial overlap of peaks in their powder diffractograms [330] and specially for organic molecular crystals, the majority of the atoms in the structure are weak X-ray scatterers, resulting in little significant intensity at high diffraction angles. [331] All these issues have been overcome by improving technology, global optimization algorithms and by using novel strategies, [332–334] which allow high rate of success even by using conventional laboratory powder diffraction data, collected under non ideal conditions. [335–338]

During the development of this PhD thesis, various crystal structures have been

solved by means of direct space methods from PXRD data following a methodology which has been optimized in the Polymorphism and Calorimetry Unit in collaboration with the X-ray Diffraction Unit of the Scientific and Technological Centers (CCiT-UB). The procedure is based on a sequential process [316,339] which mainly consists in: (I) indexing and space group determination, (II) structure solution and (III) structure refinement. Each step will be separately presented next. (Fig. 5.1)

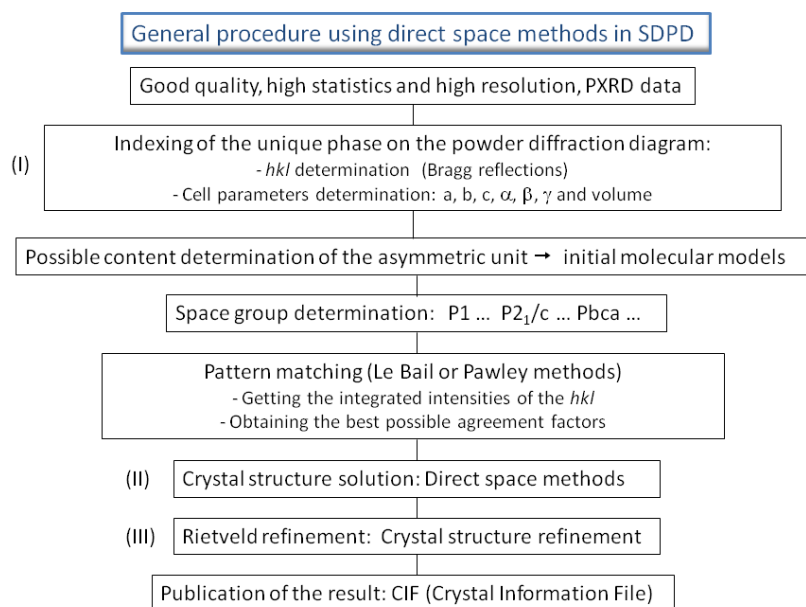


Fig. 5.1: SDPD using direct-space methods

(I) Indexing and space group determination

The first and crucial step in a structure determination from powder diffraction data is indexing, *i.e.* to find the unit cell dimensions (a , b , c , α , β and γ) of the material under investigation. This stage is the key of the whole procedure because a wrong unit cell leads to unsatisfactory structures and in some cases the unit cell cannot be found due to low intensity peaks, peak shoulders, textured samples, extra peaks from unknown impurities or peak overlapping. In the indexing process, low-angle peaks are critical, since peak overlap at high diffraction angles is usually very extensive and consequently high-angle region of X-ray diffraction laboratory data cannot be used reliably.

The most widely used programs for indexing are ITO, [340] TREOR [341] and DICVOL [342,343], which typically consider the maximum peak position of about 20 selected peaks at low diffraction angles of all available diffraction lines. In particular, DICVOL is explained next as it is the program used in this work.

Through automatic peak search and then through careful manual inspection, the diffraction patterns of the crystal structures reported in this work were indexed by using DICVOL04, a trial and error method based on the variation of parameters by successive dichotomy. The impurity tolerance 'imp' is related only to the 20 lines used for searching the solution (additional unindexed lines can be found among the extra input lines in the reviewing process). However, spurious lines increase the risk to miss the correct solution. DICVOL04 offers also the possibility to analyze the presence of a zero-point error and it can suggest more than one solution, due to uncertainty in searching harmonic diffraction lines. Solutions are searched for the smallest cell volumes and they have to be evaluated according to their figures of merit M20 and F20. [344] As a result, the set of d-spacings (d's) and intensities (I's) of peaks can be derived from the pattern and used further in the identification of the space group, according to systematic extinctions in the intensity data, which are shown as a lack of diffraction peaks with certain conditions in its Miller indices. To help in this process, density (ρ) considerations and space group multiplicities are used to check whether the obtained cell parameters correspond to an integer number of a chemical formula in the cell (Z) (Eq. 5.1),

$$\rho = \frac{M \cdot Z}{N_A \cdot V_c} \quad (5.1)$$

where M is the molecular weight, N_A is the Avogadro number and V_c the volume cell.

If the space group cannot be uniquely assigned, structure solution calculations should be carried out separately for each of the possible space groups and the correct structure will be decided at the end of the process.

After indexing and space group assignment, the intensity data are prepared for structure solution by using the profile matching technique, through Le Bail [318] or Pawley [345] fitting methods. Thus, the unit cell parameters obtained from the indexing step are used in the refinement without any structural model; in this step, the intensities are refined as mathematic variables only to give optimal fit to the experimental powder diffraction pattern. In this work, the pattern matching process was followed as developed by Le Bail. The calculated intensities of every 2θ point of the powder diffraction diagram are initially taken equal to an arbitrary value and successively refined to minimize by least squares the χ^2 function through the following equation:

$$\chi^2 = \sum_{i=1}^N \omega_i (y_i^{obs} - y_i^{calc})^2 \quad (5.2)$$

where y_i^{obs} and y_i^{calc} are, respectively, the intensities of the i^{th} point in the digitalized experimental and calculated powder diffraction patterns, and ω_i is a weighting factor for the i^{th} point ($1/y_i$ in our case).

The aim of this process is to obtain reliable values of the variables that describe (a) the peak positions (unit cell parameters and zero-point shift), (b) the background intensity distribution, (c) the peak widths, (d) the peak shape (typically described by a pseudo-Voigt function *i.e.*, a mixture of Gaussian and Lorentzian functions) [346,347] and (e) the peak intensities. All aforementioned refined parameters will be used as input information in a subsequent stage of the structure determination process.

Following a Le Bail multi-step procedure, the integrated intensities, lattice parameters and zero-point shift parameters of the crystal structures determined in this work were refined. The quality of the Le Bail fit is established from the comparison of the simulated and the experimental powder diffraction patterns and it is quantified by the weighted powder profile R-factor (R_{wp}) and χ^2 that considers the entire powder diffraction profile point by point, taking peak overlap implicitly under consideration (Eq 5.3).

$$R_{wp} = 100 \times \sqrt{\frac{\sum_i \omega_i (y_i^{obs} - y_i^{calc})^2}{\sum_i \omega_i y_i^{obs^2}}} \quad (5.3)$$

(II) Structure solution

The aim of structure solution is to obtain the best initial approximation of the crystal structure by using the unit cell, the space group, the background and the profile variables determined in the first step, but without previous knowledge of the actual position of the molecules within the unit cell.

Ab initio structure determination from powder diffraction data methods can be divided into two groups depending on the powder pattern treatment: *reciprocal space methods*, (the most commonly used are the so called direct methods)¹ [315,350,351] and *direct-space methods*. [331,352–356] The first methods consider the observed individual peaks, whereas the latter ones are based on modelling the observed pattern as a whole. [353] (Fig. 5.2)

A. *Reciprocal space methods*: They require the extraction of structure factor amplitudes from individual reflection intensities in the powder pattern, analogously to single-crystal methods, and they are successfully applied to single crystal

¹Other procedures are also used like Patterson synthesis [348] or charge flipping. [349].

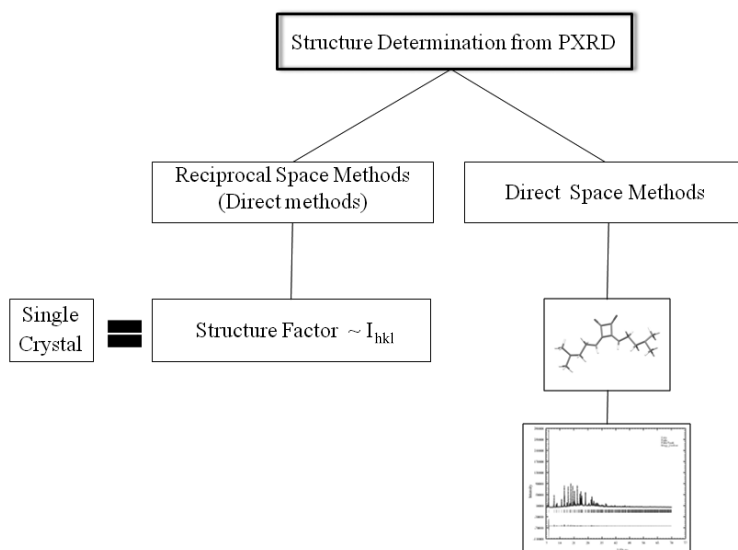


Fig. 5.2: Structure determination methods

data, however, this methodology is much more limited in SDPD. A preliminary decomposition of the experimental profile into the single peaks is required to obtain the integrated intensity (area under each peak) for each reflection. In this sense, various experimental limitations make difficult to apply direct methods: strong overlap of the diffraction peaks generated by the problem of projecting the 3D reciprocal space on a single dimension, which is particularly severe in molecular solids because of their large and low symmetry unit cells; the fact that organic compounds do not usually have dominant strong scattering atoms; the need for a background estimation; the preferred orientation, crystal defects which cause broadening peaks, etc. Significant improvement in overcoming the aforementioned limitations has been achieved using synchrotron-based powder diffractometers to enhance resolution and intensity together with advanced mathematical approaches. [355, 357–359] However, insufficient resolution in powder patterns or limiting crystal size and quality, twinning and other intrinsic structural features still make direct space methods an indispensable technique to solve crystal structures from PXRD data.

- B. *Direct-space methods:* The method is based on the location of building blocks in the cell and the comparison of the calculated and observed diffraction patterns as a whole. Its greatest advantage is that they do not deal with the "phase problem" since the extraction of structure factors is not required. In general terms, it is a global optimization problem of a great complexity in which the

agreement between the observed and calculated diffraction patterns is maximized by a continuous movement of the molecular model around the unit cell, constantly adjusting its conformation, position and orientation. Starting from a random configuration, the free parameters in the structure are varied randomly. In general, the global optimization process in direct space consists of (i) *parametrization*, (ii) *ergodic algorithm* and (iii) *cost function*. [353]

- (i) *Parametrization*: Any direct space search requires the definition of the degree of freedom (DoF) which describes the structure. Structures are described by continuous or discrete parameters; comprising a list of atoms related to each other by bond distances and bond angles and their respective restraints, [360,361] or by using the Z-matrix approach. [362] In order to accelerate the structure solution process, it is necessary to reduce the number of space parameters that describe the molecular model by grouping atoms with prior knowledge of chemical information such as the identity of the molecule and the atomic connectivity. Thus, molecular models can be treated as rigid bodies in which bond lengths and bond angles are fixed at the standard values during the direct-space structure solution calculation and the torsion angles that define the molecular conformation are left as the unique variables to be determined.
- (ii) *Ergodic algorithm*: parameters vary to eventually explore the entire configuration space and the algorithm evaluates if the global minimum path to the true structure is correct. Several optimization algorithms commonly used are Grid Search, [320,363,364] Monte Carlo (MC), [365] MC with Simulated Annealing (SA), [366–369] MC with Parallel Tempering (PT), [370] Genetic Algorithm (GA) [371,372] and Differential Evolution (DE). [373] MC, SA and PT are based on the evaluation of the probability of a given configuration by a Boltzman type distribution known as Metropolis algorithm [374] depending on temperature, which decreases during the optimization to make MC process converge, since lower temperature favors better configurations. In SA, the temperature is slowly decreased after each trial configuration, whereas in PT a single chain of configurations is used with a decreasing temperature. A small number of parallel optimizations is made, each with a different temperature and periodically the algorithm tests an exchange of configurations. PT algorithm is invariant with the number of trials and at all times during the optimization there is the possibility to reach any configuration. PT or multiple SA have been proven to better succeed in overcoming the main drawback of SA, which is to be trapped in a local minimum due to a possible premature decrease of temperature. All the abovementioned algorithms evaluate individ-

ual trials whereas with GA a population of configurations is tested as a group. TOPAS, [375] DASH, [376] FOX (Free objects for crystallography) [360,361] and EAGER [377] among others [378] are the main computer programs of direct space methods using MC algorithm with SA or PT.

- (iii) *Cost function (CF)*: it is the penalty or fitness associated with each trial structure and it is evaluated by several criteria (χ^2 or R_{wp} , [379] crystal energy, atomic coordination, etc). [353] Configurations are compared using a cost function, which is characteristic of how good the structure is (the smaller value the better configuration). However, other validation of structural models can be applied in addition, such as quantum-chemical stability calculations, [380] combined with local or global energy minimization [381–383] or the application of crystallographic rules derived from crystal chemistry of known structures. [384]

The following figure summarizes the procedure of the global optimization algorithm in structure solution using direct space methods.

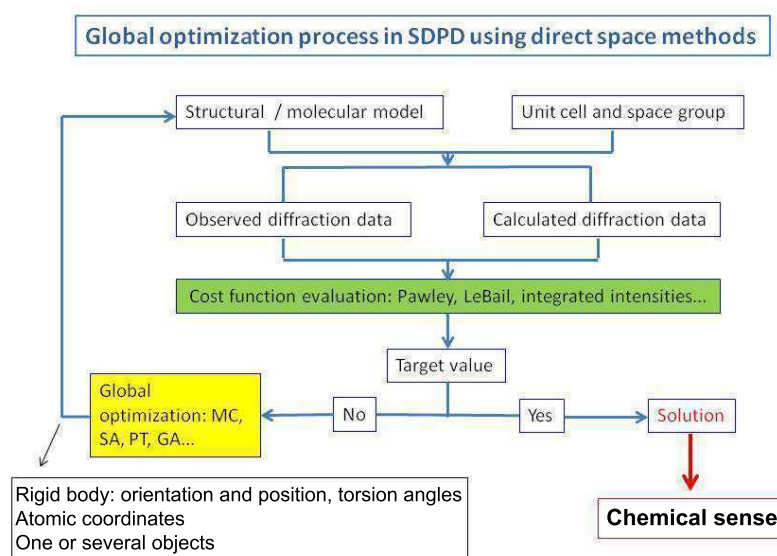


Fig. 5.3: Global optimization algorithm in SDPD

In this work, structure solution has been conducted by means of direct space methods with a reverse Monte-Carlo approach [385] implemented in FOX. Although this program has been in principle designed to solve non-molecular structures better than molecular ones, its use has expanded to small, discrete organic compounds with satisfactory results. [353,386–389] FOX has its own advantages, which are presented

next. The crystal structure can be described using any combination of isolated atoms, molecules or polyhedra. The molecular model can be encoded in two ways: as a molecule, comprising a list of atoms related to each other by bond distances and bond angles and their respective restraints, or as a Z-matrix. The use of a flexible parametrization [361] improves optimization speed and it allows the use of several optimization algorithms (SA or PT). A cost function is defined by each optimized object and any combination of CFs can be used as a particular criterion, moreover, maximum likelihood principles for a correct evaluation of the approximate models have been recently implemented. It is also possible to use jointly all available data sets from different radiation sources and dynamical occupancy correction (DOC) simplifies the problem with special positions when solving non-molecular crystals. Extending the program structure algorithms criterion for validating the structure is easy. It has its own algorithms of indexing and a very intuitive user-friendly graphical interface. [360, 361] In order to obtain the starting structural models of the different phases determined during this work, Monte Carlo calculations were performed with the parallel tempering algorithm implemented in the program FOX and the initial starting molecular models were introduced by Z-matrices approach using the molecular modeling software package Spartan. [247] Optimized structural models at molecular mechanics level of calculation were converted from protein data bank format (.pdb) to a Fenske hall Z-matrix format (.fh) using an open-source OpenBabel program. [390] During the calculations, the observed and calculated intensities were compared generally only in the 2θ range between 2 and 70deg and the molecules were allowed to translate and rotate randomly.

(III) Structure refinement: Rietveld

The final step on SDPD is the structure refinement carried out by the Rietveld method [347, 391], which considers every point in the powder diffraction diagram as an individual intensity measurement, instead of using the integrated intensities $I(hkl)$. During Rietveld refinement the variables defining the structural model (atomic positions and atomic displacement parameters) and the powder diffraction profile (unit cell, zero shift error and shape parameters) are adjusted by least-squares methods (Eq. 5.2) so that an optimal fit between the experimental and calculated powder diffraction patterns is achieved. The calculated powder pattern is obtained based on the crystalline structures, instrumental characteristics, optic parameters related with diffraction phenomenon and other sample features able to be modeled such as microstructure of the considered phases.

Each diffraction peak is characterized by its angular 2θ position, by the medium high width function (FWHM or H) and by its gaussian and lorentzian contributions of the pseudo Voigt function, which best describes the shape of the diffraction

pattern. Texture is usually taken into account through the March-Dollase function. [392] It is generally necessary to use geometric restraints based on standard molecular geometries to avoid problems of instability during Rietveld refinement and to achieve stable convergence of least-squares calculations. The evaluation of the fit is performed according to the Rietveld graphics and mathematic residual indices: the Rietveld graphics represent both diagrams observed and calculated together with the differences diagram, and the mathematic residual indices allow a subsequent following of the adjustment during the refinement (χ^2 and R_{wp} are the most considered factors). The most common programs to perform Rietveld refinement are GSAS [318] and FULLPROF, [393] the latter being used to refine the crystal structures presented in this work.

The Finger's treatment of the axial divergence [394] was taken into account to model the asymmetry of the peak profile. The background was linearly interpolated between a set of selected 2θ points. During Rietveld refinement, the scale factor, zero shift error, cell parameters, peak shape, background points, isotropic temperature factors (refined by types of atoms: C, N, O, H, etc.) and, at last, atomic coordinates of the atoms considered not restricted for moving were adjusted. Planar molecular fragments and hydrogen atoms coordinates were maintained fixed.

Chapter 6

Experimental Section

6.1 Materials and equipment

The characterization of the synthesized compounds during the development of this thesis has been performed using technical instrumentation from the *Centres Científics i Tecnològics* of the *Universitat de Barcelona (CCiT-UB)*.

- **Nuclear magnetic resonance (NMR).** Proton nuclear magnetic resonance (^1H -NMR) spectra and carbon nuclear magnetic resonance (^{13}C -NMR) spectra have been recorded on a Varian Mercury 400 (400 MHz). Variable-Temperature NMR studies have been performed on a Bruker DMX500 (500 MHz) instrument equipped with an indirect ^1H - ^{13}C detection probe with gradients along the z axis. A standard sequence from Bruker software has been used for COSY experiments (cosygpqf): a total of 128 increments, 4 scans each, have been collected. Chemical shifts for proton are reported in parts per million (ppm) downfield from tetramethylsilane and are referenced to residual protium in the NMR solvent (CDCl_3 : δ 7.26, DMSO: δ 2.50). Chemical shifts for carbon are reported in parts per million downfield from tetramethylsilane and are referenced to the carbon resonances of the solvent (CDCl_3 : δ 77.0, DMSO: δ 39.43). Data are represented as follows: chemical shift, multiplicity (br = broad, s = singlet, d = doublet, t = triplet, q = quartet, m = multiplet), coupling constants in Hertz (Hz) and integration.
- **Mass spectrometry (MS).** Mass spectra have been obtained on different spectrometers: API 365 and API 150 from PE SCIEX, and LTQ Orbitrap Velos from Thermo Scientific fitted with an electron spray ionization (ESI) source via Flow Injection Analysis (FIA) in (+) and (-) polarity ionization mode depending on the sample.

- **Powder X-ray diffraction (PXRD).** Laboratory X-ray powder diffraction data have been collected in different instruments and configurations depending on the required type of information:

A) Panalytical X'Pert PRO MPD θ/θ of 240 mm of radius powder diffractometer transmission configuration, using $\text{CuK}\alpha_{1+2}$ radiation ($\lambda = 1.5418 \text{ \AA}$) with a focalizing elliptic mirror, defining a beam height of 0.4 mm, a PIXcel detector working at a maximum detector's active length of 3.347 deg 2θ and 0.01 or 0.02 radians Soller slits. The instrument has worked at 45 kV and 40 mA. Capillary geometry has been used with the samples placed in 0.5 or 0.7 mm of diameter Lindemman capillaries measuring 2θ scans from 2 to 70 deg 2θ , with a step size of 0.013 deg 2θ and a measuring data collection time of 16 hrs (when using 0.02 soller slit) or 60 hrs (when using 0.01 soller slit). When temperature dependent analyses have been performed, an Oxford Cryosystems 700 series Cryostream liquid nitrogen criostat, enabling temperature control of the analysed capillary sample from 90 to 500 K has been used.

B) Panalytical X'Pert PRO MPD θ/θ of 240 mm of radius powder diffractometer transmission configuration, using $\text{CuK}\alpha_{1+2}$ radiation ($\lambda = 1.5418 \text{ \AA}$) with a focalizing elliptic mirror, defining a beam height of 0.4 mm, a PIXcel detector working at a maximum detector's active length of 3.347 deg 2θ and 0.02 radians Soller slits. The instrument has worked at 45 kV and 40 mA. Flat geometry has been used with the samples sandwiched between low absorbing films (poliester films of 3.6 micrometers of thickness) measuring $2\theta/\theta$ scans from 2 to 40 deg 2θ with a step size of 0.026 deg 2θ and a measuring time of 80 seconds per step.

C) Debye-Scherrer INEL CPS-120 powder diffractometer with capillary configuration and curved position sensitive detector of 120 deg with horizontal goniometer of 250 mm of radius in transmission geometry has been used. $\text{CuK}\alpha_1$ radiation ($\lambda = 1.54056 \text{ \AA}$) by means of Ge (111) primary monochromator has been selected. A parabolic multilayer mirror 'OSMIC Gutman optics 13B-413' was placed between the tube and the monochromator. The instrument has worked at 40 kV and 30 mA. Samples were placed in 0.5 mm. diameter glass Lindemann capillaries. Each sample was measured from 2 to 115 deg 2θ , with a step size of 0.029 deg 2θ and a measuring time of 3600 seconds per step. When temperature dependent analyses have been performed, a FURCAP device from INEL that enables to heat capillary samples from r.t. to 523 K has been used. Data acquisition was carried out at several temperatures in a range of r.t. to melting temperature.

- **Single crystal X-ray diffraction (SCXRD).** Laboratory single crystal X-ray diffraction data have been collected in two different instruments depending on the quality of the crystal:

A) MAR345 diffractometer with an image plate detector has been used. Intensities have been collected with graphite monochromatized MoK α radiation using ϕ –scan technique. Oxford cryosystems 700 series cryostream (80 to 500 K) has been required to record low temperature diffraction data. After data collection the crystal structure solution has been attempted by direct methods, using SHELXS97 computer program for determination and refined by full-matrix least-squares method with SHELX97 computer program. [395] Reflections have been assumed as observed applying the condition $I > 2\sigma(I)$. When H atoms have been computed and refined, a riding model with an isotropic temperature factor equal to 1.2 time the equivalent temperature factor of the atom which are linked has been applied.

B) D8 Venture air-cooled system equipped with a multilayer monochromator and a Mo ($\lambda = 0.71073 \text{ \AA}$) or Cu ($\lambda = 1.5418 \text{ \AA}$) microfocus has been used. A 2D area detector PHOTON 100: active area 10x10 cm² and CMOS technology with 1024x1024 pixels, 4 circle goniometer, Kappa geometry with pinhole collimators of 0.8 millimetres, motorized diffracted beam arm with distances sample-detector from 30 to 240 mm and cryogenic system (nitrogen liquid jet) Bruker Cryoflex working in a temperature range of 80 to 400 K has been used. Frames have been integrated with the Bruker SAINT software package using a SAINT algorithm. Data have been corrected for absorption effects using the multi-scan method (SADABS). The structures have been solved and refined using the Bruker SHELXTL Software Package, [396] a computer program for automatic solution of crystal structure and refined by full-matrix least-squares method with SHELXLe Version 4.8.0: a Qt graphical user interface for SHELXL computer program, [397] a program for crystal structure refinement. Reflections have been assumed as observed applying the condition $I > 2\sigma(I)$. When H atoms have been computed and refined, a riding model with an isotropic temperature factor equal to 1.2 time the equivalent temperature factor of the atom which are linked has been applied.

- **Differential scanning calorimetry (DSC).** Experiments have been performed in three different calorimeters: Mettler-Toledo DSC-822e, Mettler Toledo DSC-30 and Perkin Elmer Diamond equipped with a model ULSP90 intracooler. The samples have been placed in aluminum crucibles of 40 μL volume and they have been analyzed under atmosphere of dry nitrogen with 50 mL/min flow rate. The calorimeters has been calibrated with standards

of indium, n-decane and benzene of 99.99% purity. Standard heating rates of 10 °C/min have been used on the range of 30 to 350°C. Occasionally, other special experimental conditions have been required, such as aluminum crucibles of 20 or 100 μL volume, helium or air atmosphere and variable heating rates on the range of 1 to 120 °C/min.

- **Modulated differential scanning calorimetry (MDSC).** Experiments have been performed in a TA Instruments MDSC Q2000 calorimeter. The samples have been placed in aluminum crucibles of 40 μL volume and they have been analyzed under atmosphere of dry nitrogen with 50 mL/min flow rate at 0.5 °C/min on the range of 30 to 200°C. Periods of 60 seconds and amplitude of 0.08°C to satisfy Only Heat conditions.
- **Thermogravimetry (TGA).** Thermogravimetric experiments have been performed in two different instruments.
 - A thermo balance Mettler-Toledo TGA-851e. The samples have been placed in alumina crucibles of 70 μL volume and they have been analyzed under atmosphere of dry nitrogen with 50 mL/min flow rate. The microbalance has been calibrated with indium and aluminum of 99.99% purity. A standard heating rate of 10 °C/min has been used in all experiments.
 - A Perkin Elmer TGA7. The samples have been placed in alumina crucibles of 70 μL volume and they have been analyzed under atmosphere of dry nitrogen with 50 mL/min flow rate. A standard heating rate of 10 °C/min has been used in all experiments.
- **Thermomicroscopy (Hot-stage).** A Nikon polarization microscope (Nikon Eclipse 50i) equipped with a Linkam LTS350 hot stage which can operate in the temperature range of -196-600 °C and digital video recorder facilities have been used. Different experimental heating and cooling rates have been required in order to record the particularities of each polymorphic system's thermal events.
- **Milling:** Retsch ball mill MM2000 equipped with two metal vessels, each one having four 2 mL cavities is used. Two tungsten balls (diameter 3mm) are used in each experiment which is performed at 30Hz for 15 or 30 minutes.

6.2 Synthesis of squaramides

Commercial reagents were purchased from Sigma Aldrich and used as received. Synthesis grade quality solvents were used.

Substituted squaramides can be accessed via modular synthesis under relatively mild conditions. In this work, a modular synthesis via condensation [172, 398, 399] has been used to prepare a wide variety of symmetrical and unsymmetrical squaramides and monosquaramides, enabling the exploration of diverse structures. Ester derivatives of squaric acid, especially diethyl esters (*i*), undergo a condensation with 1 equivalent of a primary amine in a solvent such as diethyl ether to generate a monosquaramide product: squaramide-ester (*ii*). This is possible due to the difference of solubility among the products of the reaction. The squaramide ester has a low solubility in diethyl ether so it precipitates avoiding a second condensation, which has slower kinetics than the first one. This is a case of kinetic regioselectivity and different solubility of squaramide-ester in the media. Since diethylsquarate reactivity is higher than a conventional ester it does not require previous activation. [398] In other cases, when the product to be obtained is a symmetric disquaramide (*iv*), diethylsquarate undergo a condensation with 2 equivalents of a primary amine in ethanol. Since the product of condensation is soluble in the media, it can further react until the disquaramide is formed and precipitates in ethanol. If an asymmetric disquaramide is required, a two-step synthesis is performed: the product of the first condensation with 1 equivalent of amine in ether is isolated and it reacts through a second condensation with 1 equivalent of a different amine in ethanol. The products are obtained by *insitu* crystallization and they can be isolated and purified by filtration and subsequent washes with ethanol or diethylether. Their purity was confirmed by NMR comparing with data from the literature when possible. A scheme summarizing the synthesis is shown in figure 6.1.

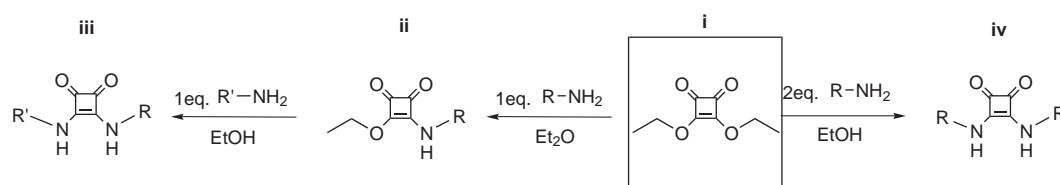


Fig. 6.1: Scheme of squaramides' synthesis

6.2.1 Synthesis of compound 1

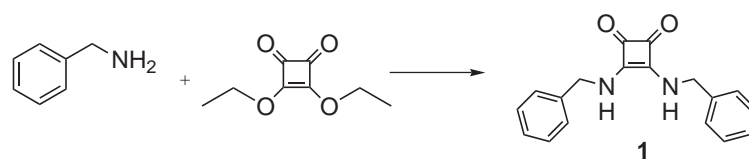


Fig. 6.2: Synthesis of Dibenzylsquaramide

Benzylamine (3.09 mL, 28.0 mmol) was added to a solution of diethylsquarate (1.60 g, 9.43 mmol) in absolute ethanol (66 mL) at r.t. under vigorous stirring and argon atmosphere. After 24 hours, the resulting white solid was filtered and it was washed with absolute ethanol (2 x 10 mL). The solid was dried under vacuum to yield 99 % (2.72 g).

Characterization of 1:

$^1\text{H-NMR}$ ($\text{DMSO-}d_6$, 400 MHz) δ : 7.70 (s, 2H); 7.24 (m, 10 H), 4.02 (d, $J = 7$ Hz, 4H) ppm. $^{13}\text{C-NMR}$ ($\text{DMSO-}d_6$, 100 MHz) δ : 186.6; 171.5; 142.9; 132.6; 131.5; 131.4 ; 50.8 ppm. MS: (ESI) m/z (%): 293.13 ($\text{M}+\text{H}^+$, 100).

6.2.2 Synthesis of compound 2

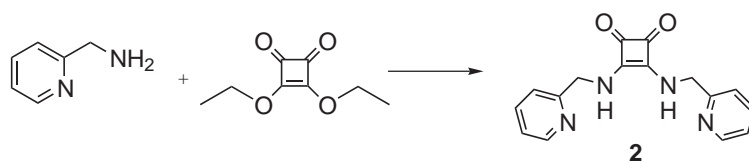


Fig. 6.3: Synthesis of 3,4-Bis(2-methylaminopyridyl)-1,2-dioxo-3-cyclobutene

2-methylaminopyridine (2.92 mL, 28 mmol) was added to a solution of diethylsquarate (1.60 g, 9.43 mmol) in absolute ethanol (66 mL) at r.t. under vigorous stirring and argon atmosphere. After 24 hours the resulting yellowish solid was filtered and washed with absolute ethanol (2 x 10 mL). The solid was dried under vacuum to yield 83% (2.30 g).

Characterization of 2:

$^1\text{H-NMR}$ (CDCl_3 , 400 MHz) δ : 8.49 (d, $J = 4$ Hz, 2H); 7.70 (m, 2H); 7.38 (d, $J = 10$ Hz, 2H); 7.22 (m, 2H); 4.87 (br s, 4H) ppm. $^{13}\text{C-NMR}$ (CDCl_3 , 100 MHz) δ : 184.3; 169.3; 157.4; 149.9; 138.2; 123.6 ; 49.9 ppm. MS: (ESI) m/z (%): 295.12 ($\text{M}+\text{H}^+$, 100).

6.2.3 Synthesis of compound 3

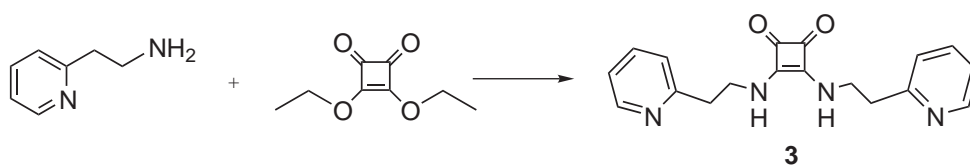


Fig. 6.4: Synthesis of 3,4-Bis(2-ethylaminopyridyl)-1,2-dioxo-3-cyclobutene

2-ethylaminopyridine (2.14 mL, 17.6 mmol) was added to a solution of diethylsquarate (1.02 g, 6.0 mmol) in absolute ethanol (42 mL) at r.t. under vigorous stirring and argon atmosphere. After 24 hours, the resulting white solid was filtered and washed with absolute ethanol (2 x 5 mL). The solid was dried under vacuum to yield 90% (1.76 g).

Characterization of 3:

$^1\text{H-NMR}$ (CDCl_3 , 400 MHz) δ : 8.45 (d, $J = 4$ Hz, 2H); 7.70 (m, 2H); 7.24 (br s, 4H); 4.02 (d, $J = 5$ Hz, 4H); 3.14 (t, $J = 6,4$ Hz, 4H) ppm. $^{13}\text{C-NMR}$ (CDCl_3 , 100 MHz) δ : 183.9; 168.3; 122.6; 124.5; 44.0; 38.1 ppm. MS: (ESI) m/z (%): 323.15 ($\text{M}+\text{H}^+$, 100).

6.2.4 Synthesis of compound 4

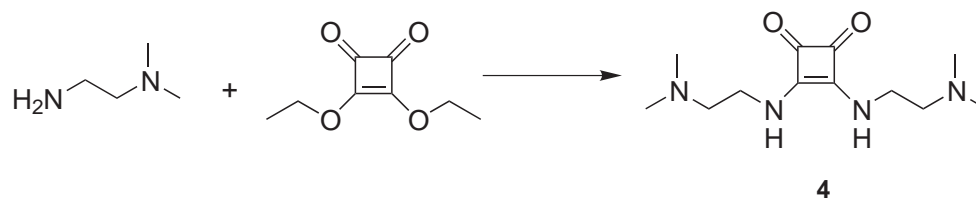


Fig. 6.5: Synthesis of 3,4-Bis(2-dimethylamino-ethylamino)-cyclobut-3-ene-1,2-dione

2-*N,N*-ethyldiamine (3.09 mL, 28.29 mmol) was added to a solution of diethylsquarate (1.60 g, 9.43 mmol) in absolute ethanol (66 mL) at r.t. under vigorous stirring and argon atmosphere. After 24 hours, the resulting white solid was filtered and washed with cold absolute ethanol (2 x 10 mL). The solid was dried under vacuum to yield 84% (2.01 g).

Characterization of 4:

$^1\text{H-NMR}$ ($\text{DMSO-}d_6$, 400 MHz) δ : 7.45 (s, 2H); 3.59 (m, $J = 4$ Hz, 4H); 2.37 (t, $J = 4$ Hz, 4H); 2.15 (s, 6H) ppm. $^{13}\text{C-NMR}$ ($\text{DMSO-}d_6$, 100 MHz) δ : 184.2, 169.7, 58.5, 43.1, 38.4 ppm. MS (ESI) m/z (%): 255.3 ($\text{M}+\text{H}^+$, 100).

6.2.5 Synthesis of compound 5

A solution of methylamine 33% in ethanol (3.1 mL, 24 mmol, 0.75 g/mL) was added to a solution of diethylsquarate (1.39 g, 8 mmol) in ethanol (10 mL), at r.t. under vigorous stirring and argon atmosphere. A yellowish solid precipitated immediately and after 24 hours the solid was filtered and washed with ethanol (2 x 5 mL). The resulting solid was dried under vacuum to yield 87% (0.99 g).

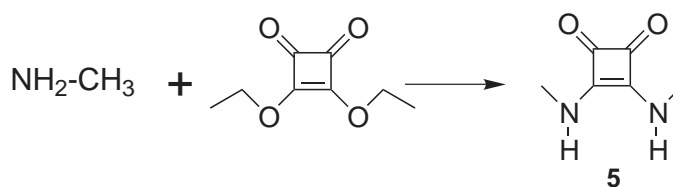


Fig. 6.6: Synthesis of 3,4-Bis-methylamino-cyclobut-3-ene-1,2-dione

Characterization of 5:

$^1\text{H-NMR}$ (DMSO- d_6 , 400 MHz) δ : 7.3 (br, NH), 3.09 (d, $J = 4$ Hz, 6H) ppm.
 $^{13}\text{C-NMR}$ (DMSO- d_6 , 100 MHz) δ : 183.3, 169.0, 30.9 ppm. MS (ESI) m/z (%):
 141.1 (M+H $^+$, 100).

6.2.6 Synthesis of compound 6

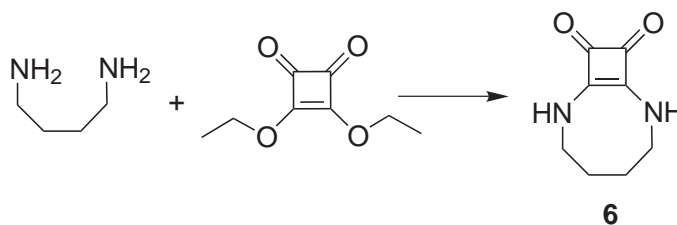


Fig. 6.7: Synthesis of 2,7-Diaza-bicyclo(6.2.0)dec-1(8)-ene-9,10-dione

A solution of 1,4-diaminobutane (0.27 g, 3 mmol) in ethanol (30 mL) was added dropwise to a stirring solution of diethylsquarate (0.52 g, 3 mmol) in ethanol (62 mL) at r.t. under nitrogen atmosphere. After stirring overnight, a white pale solid was filtered, washed with ethanol (2 x 10 mL) and dried under vacuum to yield 78% (0.39 g).

Characterization of 6:

$^1\text{H-NMR}$ (DMSO- d_6 , 400 MHz) δ : 8.31 (br, 2H), 3.19 (m, 4H), 1.25 (m, 4H) ppm. $^{13}\text{C-NMR}$ (DMSO- d_6 , 100 MHz) δ : 183.1, 169.1, 40.6, 24.8 ppm. MS (ESI) m/z (%): 167 (M+H $^+$, 100).

6.2.7 Synthesis of compound 7

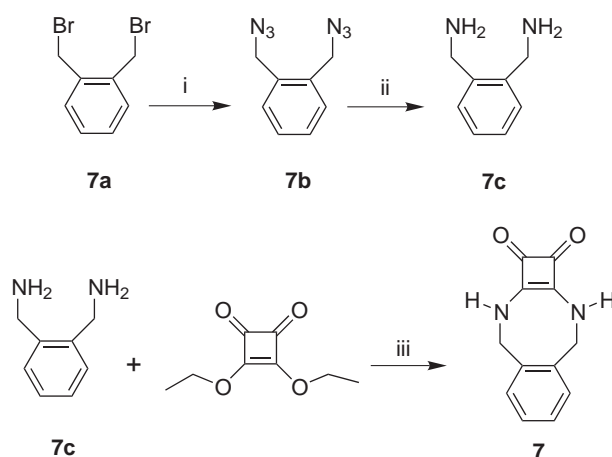


Fig. 6.8: Synthesis of 3,4,9,10-Tetrahydro-3,10-diaza-benzocyclobuta-cyclooctene-1,2-dione

Compound **7** was obtained in a three-step synthetic route. Dibromide **7a** was converted into the corresponding diazide **7b** in toluene/DMF, then reduced to the amine **7c** with LiAlH_4 , and finally condensed with one equivalent of diethyl squarate in ethanol. (ii) Sodium nitride (3.72 g, 0.07 mol) was added to a stirring solution of α, α' -Dibromo-*o*-xylene **7a** (5.02 g, 0.02 mol) in toluene (125 mL) and DMF (125 mL) and the mixture was refluxed at 110 °C for 1.5 hours under nitrogen atmosphere. The red suspension was cooled down to r.t., filtered, and washed with cold toluene (30 mL). After washing with water (3 x 50 mL) and drying with anhydrous sodium sulfate, the combined organic phases were evaporated under vacuum yielding a viscous brown tinge oil **7b** (88%). (ii) In a second step synthesis, LiAlH_4 (20 mL, 1M in THF) was added dropwise to a solution of 1,2-Bis(azidomethyl)benzene **7b** (3 g, 0.016 mol) in THF (180 mL). After adding water (10 mL), the mixture was stirred for 15 min and the suspension was filtered over celite. The solid was washed with THF (3 x 20 mL) and the combined organic fractions were evaporated under vacuum yielding a viscous yellowish oil **7c** (90%). (iii) In the last step of the synthesis, a solution of 2-aminomethylbenzylamine **7c** (2g, 0.015 mol) in ethanol (550 mL) was added to a stirring solution of diethylsquarate (2.5 g, 0.015 mol) in ethanol (10 mL) at r.t. under nitrogen atmosphere. The solid was filtered, washed with acetone (2 x 10 mL), and dried under vacuum to yield 30%.

Characterization of 7:

$^1\text{H-NMR}$ ($\text{DMSO-}d_6$, 400 MHz) δ : 8.81 (s, br, 2H), 7.21 (m, $J = 4$ Hz, 4H), 4.37 (s, 4H) ppm. $^{13}\text{C-NMR}$ ($\text{DMSO-}d_6$, 100 MHz) δ : 187.9, 173.6, 143.3, 136.2, 134.4, 50.1 ppm. MS (ESI) m/z (%): 215.3 ($\text{M}+\text{H}^+$).

6.2.8 Synthesis of compound 8

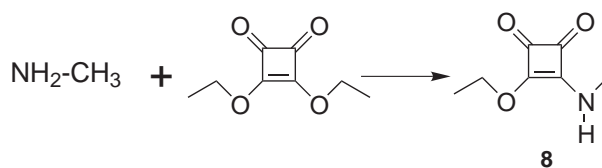


Fig. 6.9: Synthesis of 3-ethoxy-4-methylamino-cyclobut-3-ene-1,2-dione

2-ethylaminopyridine (0.69 mL, 5.9 mmol) diluted in diethylether (60 mL) was added dropwise for three hours to a stirred solution of diethylsquarate (1.01 g, 5.9 mmol) in diethylether (5 mL), at r.t. under argon atmosphere. A white solid precipitated immediately and after 24 hours of stirring it was filtered and washed with diethylether (2 x 20 mL). The resulting solid was dried under vacuum to yield 72% (1.04 g)

Characterization of 8:

$^1\text{H-NMR}$ (CDCl_3 , 400 MHz) δ : 7.61 (br, 1H), 4.62 (q, $J = 8\text{Hz}$, 2H), 3.08 (s, 3H), 1.35 (t, $J = 8\text{ Hz}$, 3H) ppm. MS (ESI) m/z (%): 156.1 ($\text{M}+\text{H}^+$, 50), 178.1 ($\text{M}+\text{Na}^+$, 50).

6.2.9 Synthesis of compound 9

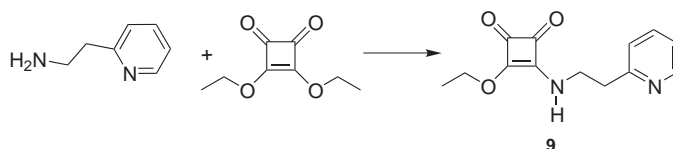


Fig. 6.10: Synthesis of 3-ethoxy-4-(2-pyridin-2-yl-ethylamino)-cyclobut-3-ene-1,2-dione

A solution of 1,4-bis(3-aminopropyl)piperazine (0.68 g, 3.4 mmol) in diethylether (60 mL) was added dropwise for three hours to a stirred solution of diethylsquarate (1.72 g, 10.1 mmol) in diethylether (10 mL), at r.t. under argon atmosphere. A white solid precipitated immediately and after 24 hours of stirring it was filtered and washed with diethylether (3 x 10 mL). The resulting solid was dried under vacuum to yield 87% (3.95 g).

Characterization of 9:

$^1\text{H-NMR}$ (CDCl_3 , 400 MHz) δ : 8.45 (br, 1H), 7.75 (br, 1H), 7.29 (br, 1H), 7.19 (br, 1H), 4.76 (m, 2H), 4.10 (s, 1H), 3.89 (m, 1H), 3.08 (m, 2H), 1.46 (m, 3H) ppm. MS (ESI) m/z (%): 247.25 ($\text{M}+\text{H}^+$, 100).

6.2.10 Synthesis of compound 10

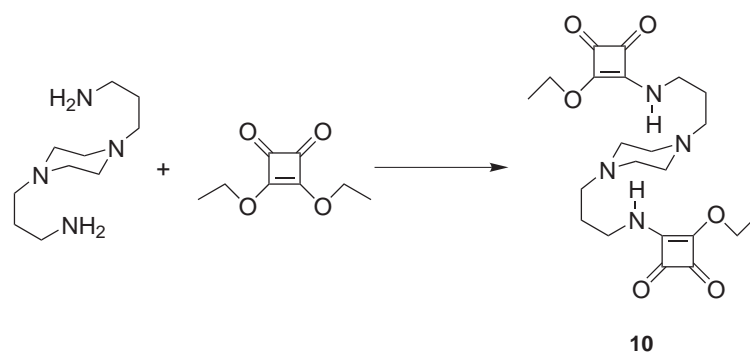


Fig. 6.11: Synthesis of 1,4-Bis-(3-aminopropyl)piperazine-bis-monosquaramide ester

A solution of 1,4-bis(3-aminopropyl)piperazine (0.68 g, 3.4 mmol) in diethylether (60 mL) was added dropwise for three hours to a stirred solution of diethylsquarate (1.72 g, 10.1 mmol) in diethylether (10 mL), at r.t. under argon atmosphere. A white solid precipitated immediately and after 24 hours of stirring it was filtered and washed with diethylether (3 x 10 mL). The resulting solid was dried under vacuum to yield 87% (3.95 g).

Characterization of 10:

$^1\text{H-NMR}$ (CDCl_3 , 400 MHz) δ : 8.21 (br, 1H), 8.01 (br, 1H), 7.94 (br, 1H), 7.75 (br, 1H), 4.76 (q, $J = 8$ Hz, 4H), 3.82 (m, 2H), 3.60 (m, 2H), 2.61 (m, 12H), 1.79 (m, 4H), 1.46 (t, $J = 8$ Hz, 6H) ppm. $^{13}\text{C-NMR}$ (CDCl_3 , 100 MHz) δ : 183.4, 182.2, 69.6, 57.7, 53.1, 45.7, 25.1, 16.1 ppm. MS (ESI) m/z (%): 449.25 ($\text{M}+\text{H}^+$, 100).

6.2.11 Synthesis of compound 11

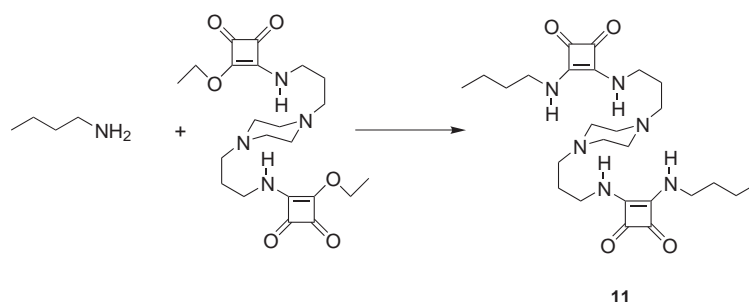


Fig. 6.12: Synthesis of 1,4-Bis-(3-aminopropyl)piperazine-bis-squaramide

Butylamine (0.25 g, 3.42 mmol) was added to a solution of compound 10 (0.5 g, 1.11 mmol) in ethanol (60 mL) at 50°C under stirring and argon atmosphere. A white solid precipitates after 10 minutes and the suspension. After three hours, it

was filtered, washed with absolute ethanol (3 x 10 mL) and dried under vacuum to yield 87% (0.49 g).

Characterization of 11:

$^1\text{H-NMR}$ ($\text{DMSO-}d_6$, 100 MHz) δ : 8.8 (br, 1H), 8.6 (br, 1H), 8.4 (br, 1H), 7.8 (br, 1H), 4.6 (q, $J=8\text{Hz}$), 1.25 (m, H), 1.37 (m, H), 1.50 (m, H), 0.89 (6H, $J=8\text{Hz}$) ppm. MS (ESI) m/z (%): 503.3 ($\text{M}+\text{H}^+$).¹

6.2.12 Synthesis of compound 12

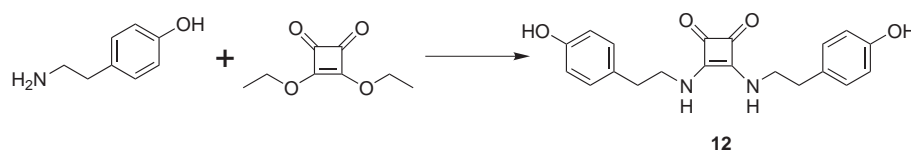


Fig. 6.13: Synthesis of 3,4-Bis-(2-(4-hydroxy-phenyl)-ethylamino)-cyclobut-3-ene-1,2-dione

A solution of tyramine (1.25 g, 8.85 mmol) in 15 mL of dichloromethane/MeOH (3:2) was added to a stirring solution of diethylsquarate (0.5 g, 2.94 mmol) in ethanol (20 mL), at r.t. under argon atmosphere. After stirring the suspension overnight, the white solid was filtered, washed with ethanol (2 x 5 mL) and dried under vacuum to yield 97% (1.01 g).

Characterization of 12:

$^1\text{H-NMR}$ ($\text{DMSO-}d_6$, 100 MHz) δ : 7.28 (br, 1H), 6.98 (d, 4H, $J = 8\text{ Hz}$), 6.67 (d, 4H, $J = 8\text{ Hz}$), 3.63 (br, 1H), 3.2 (br, 1H), 2.67 (t, 4H, $J = 8\text{ Hz}$) ppm. $^{13}\text{C-NMR}$ ($\text{DMSO-}d_6$, 400 MHz) δ : 183.11, 168.3, 156.5, 130.2, 129.2, 115.8, 45.6, 36.9 ppm. MS (ESI) m/z (%): 354.1 ($\text{M}+\text{H}^+$).

6.2.13 Synthesis of compound 13

Compound **13** was synthesized through a two-step selective condensation of *N,N*-dimethylethylenediamine and tyramine with diethylsquarate under mild conditions. A solution of *N,N*-dimethylethylenediamine (0.42 g, 4.76 mmol) in diethylether (60 mL) was added dropwise to a solution of diethylsquarate (0.81 g, 4.76 mmol) in diethylether (5 mL) at r.t. under stirring and argon atmosphere. A white solid precipitated and the suspension was stirred overnight. The solid was filtered, washed with diethylether (2 x 5 mL) and dried under vacuum to yield 56 %. In a second step, a solution of tyramine (0.45 g, 3.3 mmol) in 5 mL of MeOH:DCM (2:3) was

¹No $^{13}\text{C-NMR}$ analysis was performed due to the very low solubility of **11** in $\text{DMSO-}d_6$

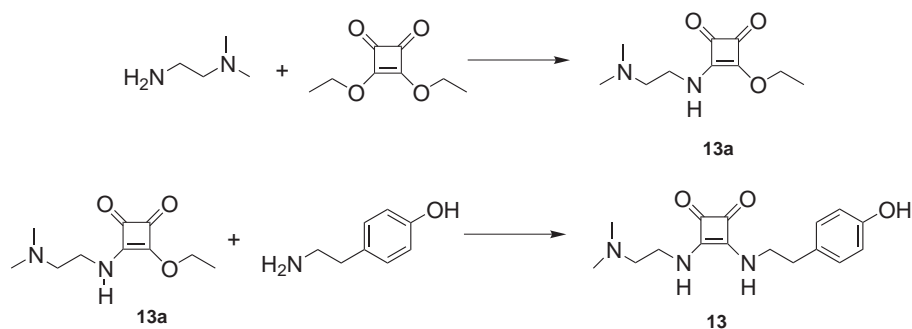


Fig. 6.14: Synthesis of 3-(2-Dimethylamino-ethylamino)-4-(2-(4-hydroxy-phenyl)-ethylamino)cyclobut-3-ene-1,2-dione

added to a solution of squaramide ester **13a** (0.35 g, 1.6 mmol) in ethanol (10 mL). After five minutes a solid precipitated and the suspension was stirred overnight under argon atmosphere. The solid was filtered, washed with diethyleter (3 x 10 mL) to yield 89% (0.30 g).

Characterization of **13a**:

¹H-NMR (CDCl₃, 400MHz) δ: 6.45 (br, 1H), 6.39 (br, 1H), 4.75 (m, 2H), 3.77 (s, 1H), 3.50 (s, 1H), 2.53 (m, J = 8 Hz, 2H), 2.27 (s, 6H), 1.44 (t, J = 8 Hz, 3H) ppm. ¹³C-NMR (CDCl₃, 400MHz) δ: 183.2, 183.1, 168.3, 156.5, 130.3, 129.2, 115.9, 59.9, 45.7, 45.5, 36.9 ppm. MS (ESI) m/z (%): 213.2 (M+H⁺, 100).

Characterization of **13**:

¹H-NMR (DMSO-*d*₆, 400 MHz) δ: 9.17 (br, 1H), 7.43 (br, 1H), 7.34 (br, 1H), 7.0 (d, J=8Hz, 2H) 6.67 (d, J=8Hz, 2H), 3.66 (m, 4H), 2.69 (t, J=8Hz, 2H), 2.35 (t, J=8Hz, 2H) ppm. ¹³C-NMR (DMSO-*d*₆, 400 MHz) δ: 183.2, 183.1, 168.3, 156.5, 130.3, 129.2, 115.9, 59.9, 45.7, 45.5, 36.9 ppm. MS (ESI) m/z (%): 304.2 (M+H⁺, 100).

6.2.14 Synthesis of compound **14**

A solution of aminobutane (0.55 g, 6 mmol) in ethanol (3 mL) was added to a stirring solution of diethylsquarate (1.07 g, 6 mmol) in ethanol (25 mL) under argon atmosphere. A white solid precipitated in a few minutes and the suspension was stirred overnight. The white solid was filtered, washed with diethyleter (2 x 5 mL) and dried in the oven under vacuum to yield 89% (0.93 g).

Characterization of **14**:

MS (ESI) m/z (%): 333.2 (M+H⁺), 355.1 (M+Na).²

²No ¹H-NMR nor ¹³C-NMR was performed due to insolubility of **14** in DMSO-*d*₆ and D₂O.

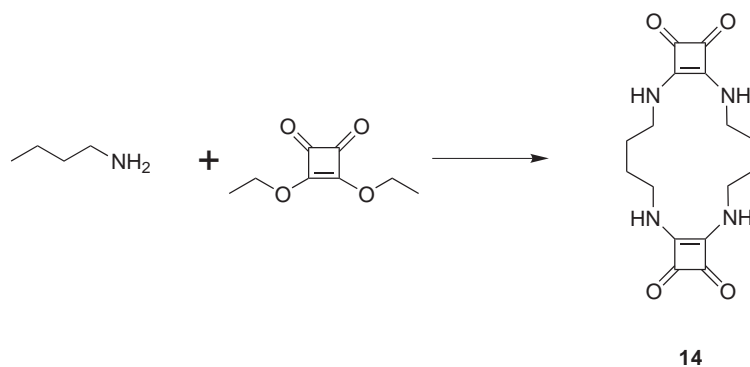


Fig. 6.15: Synthesis of 2,7,12,17-Tetraaza-tricyclo(16.2.0.0^{8,11})eicosa-1(18),8(11)-diene-9,10,19,20-tetraone

6.2.15 Synthesis of compound 15

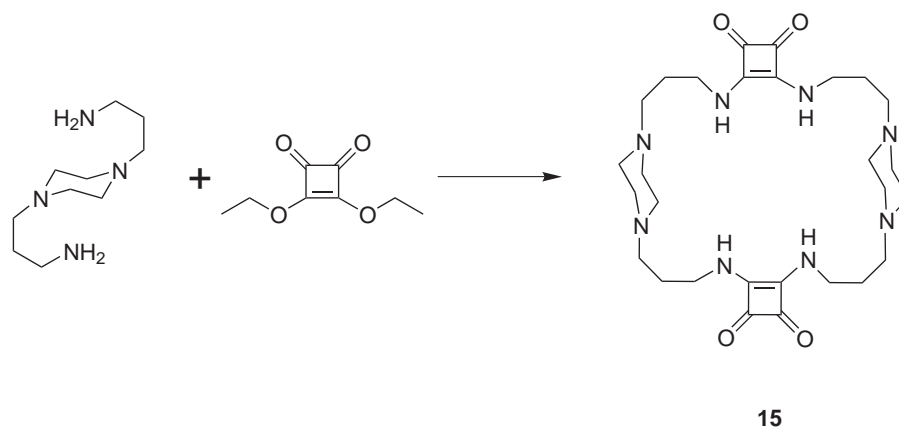


Fig. 6.16: Synthesis of cycloaminopropylpiperazinesquaramide

A solution of 1,4-bis(3-aminopropyl)-piperazine (2.13 g, 10.63 mmol) in ethanol (3 mL) was added to a stirring solution of diethylsquarate (1.09 g, 6.4 mmol) in ethanol (41 mL) under argon atmosphere. A white solid precipitated in a few minutes and the suspension was stirred overnight. The white solid was filtered, washed with ethanol (2 x 10 mL) and dried in the oven under vacuum to yield 49% (0.87 g).

Characterization of 15:

MS (ESI) m/z (%): 557.1 ($M+H^+$).³

³No ¹H-NMR nor ¹³C-NMR was performed due to insolubility of **15** in DMSO-*d*₆ and D₂O.

6.2.16 Synthesis of compound 16

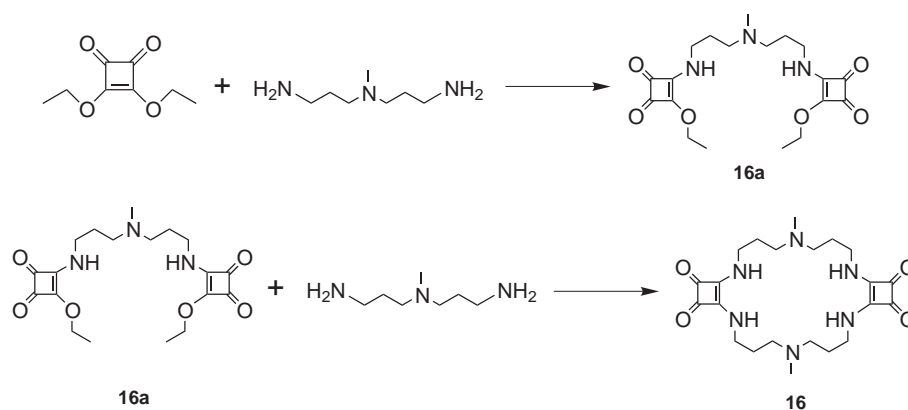


Fig. 6.17: Synthesis of cycloaminopropylpiperazinesquaramide

A solution of *N,N*-diethylethylenediamine (0.57 g, 3.9 mmol) in diethyl ether (85 mL) was added dropwise to a stirring solution of diethylsquarate (2.01 g, 11.8 mmol) in diethyl ether (2 mL) under argon atmosphere. A white solid precipitated and the suspension was stirred overnight. The white solid was filtered, washed with ethanol (2 x 10 mL) and dried in the oven under vacuum to yield 92% (1.43 g).

A solution of *N,N*-diethylethylenediamine (0.49 g, 3.4 mmol) in ethanol (30 mL) was added dropwise to a stirring solution of **16a** (1.34 g, 3.40 mmol) in ethanol (130 mL) under argon atmosphere. A white solid precipitated and the suspension was stirred overnight. The white solid was filtered, washed with ethanol (2 x 10 mL) and acetone (2 x 10 mL) dried in the oven under vacuum to yield 82% (1.25 g).

Characterization of 16:

$^1\text{H-NMR}$ (DMSO- d_6 , 400 MHz) δ : 7.20 (br, NH), 2.41 (m, 8H), 2.21 (m, 4H), 2.10 (s, 6H), 1.68 (m, 14H) ppm. MS (ESI) m/z (%): 448.2 ($\text{M}+\text{H}^+$, 100).

6.3 Synthesis of squarate salts and amidosquaric acid derivatives

In this work, derivatives of squaric acid have also been synthesized in order to analyze their solid state properties and interesting chemical effects. Since squaramides are very difficult to hydrolyze and diethylsquarate hydrolyzes easily to squaric acid, amidosquaric acids were synthesized from squaric acid under aqueous conditions. [184,400] Squaric acid (*i*) reacts with 1 equivalent of a primary amine in water under reflux (it is insoluble in water at r.t.) for minimum three hours to generate a monoamidosquaric acid (*ii*). It has been noted that the salt formation between

squaric acid and the corresponding amine (*iii*) [401] is a kinetically competitive reaction which is faster and in some cases longer periods of time were required to obtain amidosquaric acid instead of the salt. All the products are obtained by *insitu* crystallization and they can be isolated and purified by filtration and subsequent washes with ethanol or diethylether. Their purity was confirmed by NMR comparing with data from the literature when possible. A scheme summarizing the synthesis is shown in figure 6.18.

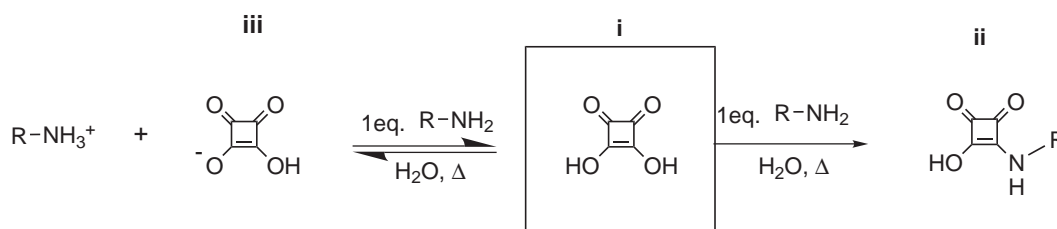


Fig. 6.18: Scheme of hydrolyzed squaramides' synthesis and their salts

6.3.1 Synthesis of compound 17

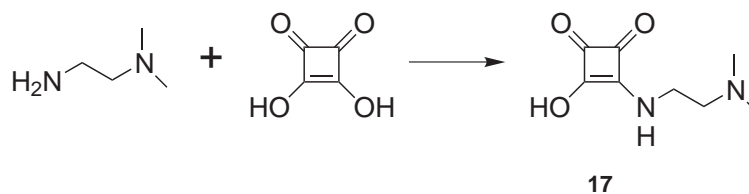


Fig. 6.19: Synthesis of 3-(2-Dimethylamino-ethoxy)-4-hydroxy-cyclobut-3-ene-1,2-dione

Compound **12** was prepared from a mixture of N,N -dimethylethylenediamine (0.47 g, 7.34 mmol) and squaric acid (0.84 g, 8.86 mmol) in water (25 mL). After refluxing the solution at 100 °C for three hours, the yellowish solution was cooled down to r.t. and yellowish needles crystallized in 24h. The solid was filtered and washed with diethylether (3 x 2 mL) to yield 90% (1.47 g).

Characterization of 17:

1H -NMR (DMSO- d_6 , 400 MHz) δ : 7.97 (t, $J = 8$ Hz, 1H), 3.70 (q, $J = 8$ Hz, 2H), 3.25 (q, $J = 8$ Hz, 2H), 2.80 (s, 6H) ppm. ^{13}C -NMR (DMSO- d_6 , 100 MHz) δ : 194.8, 190.3, 176.8, 57.7, 43.2, 40.0 ppm. MS (ESI) m/z (%): 185.1 ($M+H^+$, 100).

6.3.2 Synthesis of compound 18

A mixture of squaric acid (2.01 g, 17.6 mmol) and benzylamine (1.89 g, 17.6 mmol) in water (25 mL) was refluxed for three hours at 100 °C and after that time it was

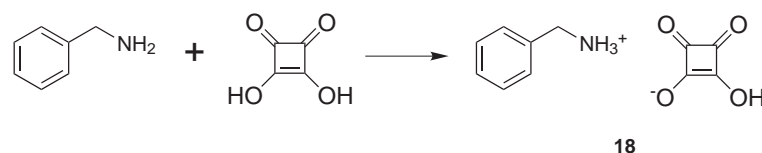


Fig. 6.20: Synthesis of squarate : dibenzylamine salt

slowly cooled down to r.t. The resulting crystals were filtered, washed with acetone (2 x 5 mL) and dried under vacuum overnight to yield 97% (3.21 g).

Characterization of 18:

$^1\text{H-NMR}$ (DMSO- d_6 , 400 MHz) δ : 8.18 (br, NH), 7.42 (m, 6H), 4.03 (s, 2H) ppm. $^{13}\text{C-NMR}$ (DMSO- d_6 , 100 MHz) δ : 197.1, 134.7, 129.3, 43.1 ppm. MS (ESI) m/z (%): 108.2 ($\text{C}_7\text{H}_9\text{N}+\text{H}^+$, 100), 112.1 ($\text{C}_4\text{H}_2\text{O}_4-2\text{H}^+$, 100).

6.3.3 Synthesis of compound 19

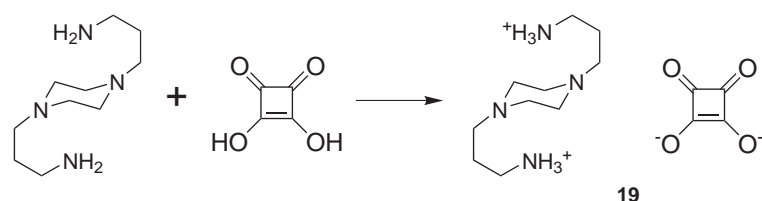


Fig. 6.21: Synthesis of squarate : 1,4-bis(3-aminopropyl)piperazine salt

A mixture of squaric acid (0.50 g, 4.4 mmol) and 1,4-bis(3-aminopropyl)piperazine (0.44 g, 2.2 mmol) in water (25 mL) was refluxed for three hours at 100 °C and after that time it was slowly cooled down to r.t. The resulting crystals were filtered, washed with acetone (2 x 5 mL) and dried under vacuum overnight to yield 80% (0.54 g).

Characterization of 19:

$^1\text{H-NMR}$ (DMSO- d_6 , 400 MHz) δ : 4.65 (s, 8H), 3.06 (m, 8H), 2.92 (t, J=8 Hz, 4H), 2.85 (t, J=8 Hz, 4H), 1.89 (m, 4H) ppm. $^{13}\text{C-NMR}$ (DMSO- d_6 , 100 MHz) δ : 202.5, 53.7, 37.2, 22.6 ppm.

6.3.4 Synthesis of compound 20

A mixture of squaric acid (0.20 g, 1.7 mmol) and diethylamine (1.28 g, 1.7 mmol) in water (10 mL) was refluxed for four hours at 100°C and it was slowly cooled down to r.t. The resulting yellowish oil was recrystallized in water at 70°C and the

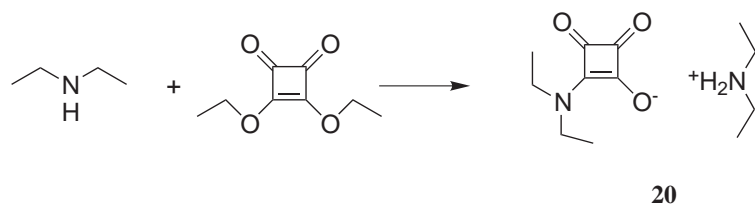


Fig. 6.22: Synthesis of diethylamidosquaric acid : diethylamine salt

solution was slowly cooled down to 5-8°C. Single crystals of **20** were filtered and analyzed by SXRD.

Characterization of **20**:

By single X-ray diffraction (see appendix C.2.19).

6.3.5 Synthesis of compound **21**

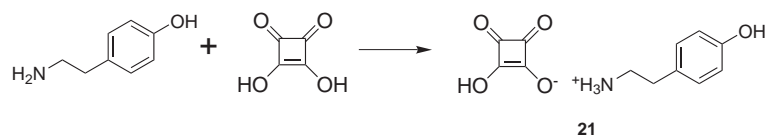


Fig. 6.23: Synthesis of squarate : tyramine salt

A mixture of squaric acid (1.09 g, 9.6 mmol) and tyramine (0.94g, 8.7 mmol) in water (25 mL) was refluxed for three hours at 100 °C and it was slowly cooled down to r.t. The resulting crystals were filtered, washed with acetone (2 x 5 mL) and dried under vacuum overnight to yield 80% (1.93 g).

Characterization of **21**:

¹H-NMR (DMSO-*d*₆, 400 MHz) δ : 7.91 (br, OH), 7.0 (d, *J* = 8Hz, 1H), 6.7 (d, *J* = 8 Hz, 2H), 2.9 (m, 2H), 2.5 (m, 2H) ppm. ¹³C-NMR (DMSO-*d*₆, 100 MHz) δ : 197.0, 156.9, 130.3, 127.8, 116.0, 32.9 ppm.

6.3.6 Synthesis of compound **22**

Compound **22** was obtained by recrystallization of **18** and it was characterized only by SXRD.

Chapter 7

Conclusions

This thesis has contributed to a better understanding of the solid state structural issues of squaric acid derivatives and their applicability to the design of new materials. A multidisciplinary work has been developed combining approaches from areas such as crystal engineering, supramolecular chemistry and crystallography. 47 polymorphs, solvates, cocrystals and salts from 22 squaric acid derivative compounds have been obtained and 31 crystal structures have been solved and analyzed. The optimization of a methodology for solving crystal structures from laboratory powder diffraction data by means of direct space methods has permitted to overcome the difficulty of disubstituted squaramides to crystallize as good quality single-crystals. The following conclusions can be extracted:

- Cooperativity in hydrogen-bonded catemers plays a crucial role in defining the robust solid-state synthon in anti/anti configuration of disubstituted squaramides, overriding the preferred association mode in solution. Consequently, the self assembling of the squaramide rings is a very strong binding motif, which has been proven difficult to be perturbed by other competing functional groups in the solid state.
- Disubstituted squaramides can act as molecular scaffolds in the design of new cocrystals with a suitable functionalization of the secondary squaramide substituents.
- Self-assembling squaramides can be used for the formation of new helicoidal topologies in the solid state.
- Electrostatic compression phenomenon observed in zwitterionic squaramides is responsible for a robust supramolecular synthon which allows the formation of multicomponent solids.

In summary, all these conclusions show that the squaric/squaramide functional group, poorly studied in the solid state, has interesting properties which can be exploited for the design and synthesis of new and diverse crystalline materials.

Bibliography

- [1] Pepinsky, R. *Phys. Rev.* **1955**, *100*, 971-971.
- [2] Schmidt, G. M. J. *Pure Appl. Chem* **1971**, *27*, 647-678.
- [3] Tiekink, E. R. T. Crystal Engineering. In *Supramolecular Chemistry*; John Wiley and Sons, Ltd: New York, 2012.
- [4] Desiraju, G. *Angew. Chem. Int. Ed.* **2007**, *46*, 8342–8356.
- [5] Evans, O. R.; Lin, W. *Chemistry of materials* **2001**, *13*, 2705–2712.
- [6] Evans, O. R.; Lin, W. *Acc. Chem. Res.* **2002**, *35*, 511–522.
- [7] Biradha, K.; Sarkar, M.; Rajput, L. *Chem. Commun.* **2006**, 4169-4179.
- [8] Remenar, J. F.; Morissette, S. L.; Peterson, M. L.; Moulton, B.; MacPhee, J. M.; Guzmán, H. R.; Almarsson, Ö. *J. Am. Chem. Soc.* **2003**, *125*, 8456-8457.
- [9] Desiraju, G. R.; Braga, D.; Miller, J. S.; Orpen, A. G.; Price, S. S. L. *CrystEngComm* **2002**, *4*, 500–509.
- [10] Sekhon, B. *Ars Pharm*, **2009**, *50*, 99–117.
- [11] Desiraju, G. R. *Angew. Chem. Int. Ed.* **2007**, *46*, 8342–8356.
- [12] Bernstein, J. *Polymorphism in Molecular Crystals*; Oxford University Press: New York, 2002.
- [13] Bernstein, J. *Cryst. Growth Des.* **2011**, *11*, 632–650.
- [14] Hilfiker, R.; Blatter, F.; Raumer, M. *Polymorphism in the pharmaceutical industry*; Wiley-VCH: Weinheim, Germany, 2006.
- [15] Halebian, J.; McCrone, W. *J. Pharm. Sci.* **1969**, *58*, 911–929.
- [16] Prohens, R.; Puigjaner, C. *El Farmacéutico.* **2007**, *373*, 58-68.

- [17] Remenar, J. F.; Morissette, S. L.; Peterson, M. L.; Moulton, B.; MacPhee, J. M.; Guzmán, H. R.; Almarsson, Ö. *J. Am. Chem. Soc.* **2003**, *125*, 8456–8457.
- [18] Griesser, U. J. *The importance of solvates*; volume 225 Wiley-VCH: Weinheim, 2006.
- [19] Ogienko, A. G.; Boldyreva, E. V.; Manakov, A. Y.; Boldyrev, V. V.; Yunoshchev, A. S.; Ogienko, A. A.; Myz, S. A.; Ancharov, A. I.; Achkasov, A. F.; Drebushchak, T. N. *Pharmaceutical research* **2011**, *28*, 3116–3127.
- [20] Chen, A. M.; Ellison, M. E.; Peresypkin, A.; Wenslow, R. M.; Variankaval, N.; Savarin, C. G.; Natishan, T. K.; Mathre, D. J.; Dormer, P. G.; Euler, D. H.; Ball, R. G.; Ye, Z.; Wang, Y.; Santos, I. *Chem. Commun.* **2007**, 419–421.
- [21] Blagden, N.; De Matas, M.; Gavan, P.; York, P. *Advanced Drug Delivery Reviews* **2007**, *59*, 617–630.
- [22] Byrn, S. R.; Pfeiffer, R.; Stowell, J. G. *Solid State Chemistry of Drugs*; SSCI Inc.: New York, 2nd ed.; West Lafayette, 1999.
- [23] Brittain, H. G. *Polymorphism In Pharmaceutical Solids*; Marcel Dekker, Inc.: New York, 1999.
- [24] Pudipeddi, M.; Serajuddin, A. *J. Pharm. Sci.* **2005**, *94*, 929–939.
- [25] Llinàs, A.; Goodman, J. M. *Drug Discovery Today* **2008**, *13*, 198 - 210.
- [26] Wöhler,; Liebig, *Annalen der Pharmacie* **1832**, *3*, 249–282.
- [27] Bauer, J.; Spanton, S.; Henry, R.; Quick, J.; Dziki, W.; Porter, W.; Morris, J. *Pharmaceutical Research* **2001**, *18*, 249–282.
- [28] Quere, L.; Riedner, J.; Wolff, H. M. *U.S. Patent 8232414* **2012**, B2, -.
- [29] Groom, C. R. “www.chem.ucl.ac.uk/cposs/openday/2011groom.pdf”, CCD-C, 2011.
- [30] Lemmerer, A.; Bernstein, J.; Griesser, U. J.; Kahlenberg, V.; Többens, D. M.; Lapidus, S. H.; Stephens, P. W.; Esterhuysen, C. *Chem. Eur. J.* **2011**, *17*, 13445–13460.
- [31] Cabri, W.; Ghetti, P.; Pozzi, G.; Alpegiani, M. *Org. Process Res. Dev.* **2007**, *11*, 64–72.

- [32] Rafilovich, M.; Bernstein, J. *J. Am. Chem. Soc.* **2006**, *128*, 12185-12191.
- [33] Yu, L. *Acc. Chem. Res.* **2010**, *43*, 1257-1266.
- [34] Dunitz, J. D.; Bernstein, J. *Acc. Chem. Res.* **1995**, *28*, 193-200.
- [35] Rodríguez-Hornedo, N.; Murphy, D. *J. Pharm. Sci.* **1999**, *88*, 651-660.
- [36] Mangin, D.; Puel, F.; Veessler, S. *Org. Process Res. Dev.* **2009**, *13*, 1241-1253.
- [37] Price, S. L. *Phys. Chem. Chem. Phys.* **2008**, *10*, 1996-2009.
- [38] Filippini, G.; Gavezzotti, A.; Novoa, J. *Act. Cryst. Sect. B* **1999**, *55*, 543-553.
- [39] Barbas, R.; Martí, F.; Prohens, R.; Puigjaner, C. *Cryst. Growth Des.* **2006**, *6*, 1463-1467.
- [40] Giron, D. *J. Therm. Anal. Calorim.* **2001**, *64*, 37-60.
- [41] Behme, R. J.; Brooke, D.; Farney, R. F.; Kensler, T. T. *J. Pharm. Sci.* **1985**, *74*, 1041-1046.
- [42] Burger, A.; Ramberger, R. *Microchimica Acta* **1979**, *72*, 273-316.
- [43] Yu, L. *J. Pharm. Sci.* **1995**, *84*, 966-974.
- [44] Kitaigorodskii, I. *Molecular Crystals and Molecules*; Academic Press: New York, 1973.
- [45] Datta, S.; Grant, D. *Nat. Rev.* **2004**, *3*, 42-57.
- [46] Morris, K. R. *Polymorphism in Pharmaceutical Solids*; Marcel Dekker: Switzerland, 1999.
- [47] Puigjaner, C.; Barbas, R.; Portell, A.; Font-Bardia, M.; Alcobé, X.; Prohens, R. *Cryst. Growth Des.* **2010**, *10*, 2948-2953.
- [48] Weyna, D. R.; Shattock, T.; Vishweshwar, P.; Zaworotko, M. J. *Cryst. Growth Des.* **2009**, *9*, 1106-1123.
- [49] Stahl, P. H.; Wermuth, C. G. *Pharmaceutical salts: Properties, selection, and use*; Wiley: Weinheim, Germany, 2002.
- [50] Ling, A. R.; Baker, J. L. *J. Chem. Soc., Trans.* **1893**, *63*, 1314-1327.
- [51] Aakeröy, C. B.; Salmon, D. J. *CrystEngComm* **2005**, *7*, 439-448.

- [52] Qiao, N.; Li, M.; Schlindwein, W.; Malek, N.; Davies, A.; Trappitt, G. *Int. J. Pharm.* **2011**, *419*, 1 - 11.
- [53] Administration, <http://www.fda.gov/downloads/Drugs/Guidances/UCM281764.pdf>, accessed August 2013.
- [54] Mohamed, S.; Tocher, D. A.; Vickers, M.; Karamertzanis, P. G.; Price, S. L. *Cryst. Growth Des.* **2009**, *9*, 2881-2889.
- [55] Aakeröy, C. B.; Fasulo, M. E.; Desper, J. *Mol. Pharm.* **2007**, *4*, 317-322.
- [56] Childs, S. L.; Hardcastle, K. I. *Cryst. Growth Des.* **2007**, *7*, 1291-1304.
- [57] Variankaval, N.; Wenslow, R.; Murry, J.; Hartman, R.; Helmy, R.; Kwong, E.; Clas, S.-D.; Dalton, C.; Santos, I. *Cryst. Growth Des.* **2006**, *6*, 690-700.
- [58] Childs, S. L.; Stahly, G. P.; Park, A. *Mol. Pharm.* **2007**, *4*, 323-338.
- [59] Johnson, S. L.; Rumon, K. A. *J. Phys. Chem.* **1965**, *69*, 74-86.
- [60] Vishweshwar, P.; McMahon, J. A.; Bis, J. A.; Zaworotko, M. J. *J. Pharm. Sci.* **2006**, *95*, 499-516.
- [61] Asaji, T.; Seliger, J.; Žagar, V.; Sekiguchi, M.; Watanabe, J.; Gotoh, K.; Ishida, H.; Vrtnik, S.; Dolinšek, J. *J. Phys.: Condens. Matter* **2007**, *19*, 226203.
- [62] Macchi, P.; Casati, N.; Marshall, W. G.; Sironi, A. *CrystEngComm* **2010**, *12*, 2596-2603.
- [63] Martins, D. M. S.; Middlemiss, D. S.; Pulham, C. R.; Wilson, C. C.; Weller, M. T.; Henry, P. F.; Shankland, N.; Shankland, K.; Marshall, W. G.; Ibberson, R. M.; Knight, K.; Moggach, S.; Brunelli, M.; Morrison, C. A. *J. Am. Chem. Soc.* **2009**, *131*, 3884-3893.
- [64] Desiraju, G. R. *J. Am. Chem. Soc.* **2013**, *135*, 9952-9967.
- [65] FDA, "GRAS", <http://www.ecfr.gov/cgi-bin/text-idx?c=ecfr&SID=4f70083a7e458a879baeaf15975a0166&rgn=div5&view=text&node=21:3.0.1.1.13&idno=21#21:3.0.1.1.14.2.1.2,>
- [66] FDA, "GRAS", [http://www.fda.gov/Food/IngredientsPackagingLabeling/FoodAdditivesIngredients/ucm091048.htm,](http://www.fda.gov/Food/IngredientsPackagingLabeling/FoodAdditivesIngredients/ucm091048.htm)

- [67] FDA, "EAFUS: Everything Added to Food in the United States", <http://www.biobased.us/eafus.pdf>.
- [68] Smith, A. J.; Kavuru, P.; Wojtas, L.; Zaworotko, M. J.; Shytle, R. D. *Mol. Pharm.* **2011**, *8*, 1867-1876.
- [69] Shiraki, K.; Takata, N.; Takano, R.; Hayashi, Y.; Terada, K. *Pharmaceutical research* **2008**, *25*, 2581-2592.
- [70] Trask, A. V.; Motherwell, W. D. S.; Jones, W. *Cryst. Growth Des.* **2005**, *5*, 1013-1021.
- [71] Babu, N. J.; Sanphui, P.; Nangia, A. *Chem. Asian J.* **2012**, *7*, 2274-2285.
- [72] Karki, S.; Friscic, T.; Fabian, L.; Laity, P. R.; Day, G. M.; Jones, W. *Advanced Materials* **2009**, *21*, 3905-3909.
- [73] Reutzel-Edens, S. M.; Newman, A. W. Physical Characterization of Hygroscopicity in Pharmaceutical Solids. In *Polymorphism*; Wiley-VCH Verlag GmbH & Co. KGaA: Weinheim, 2006.
- [74] Fucke, K.; Myz, S. A.; Shakhtshneider, T. P.; Boldyreva, E. V.; Griesser, U. J. *New J. Chem.* **2012**, *36*, 1969-1977.
- [75] Connelly, P. R.; Vuong, T. M.; Murcko, M. A. *Nat Chem* **2011**, *3*, 692-695.
- [76] Babu, N.; Reddy, L.; Aitipamula, S.; Nangia, A. *Chem. Asian J.* **2008**, *3*, 1122-1133.
- [77] Schultheiss, N.; Roe, M.; Boerrigter, S. X. M. *CrystEngComm* **2011**, *13*, 611-619.
- [78] Schultheiss, N.; Bethune, S.; Henck, J.-O. *CrystEngComm* **2010**, *12*, 2436-2442.
- [79] Halasz, I.; Rubcic, M.; Uzarevic, K.; Dilovic, I.; Mestrovic, E. *New J. Chem.* **2011**, *35*, 24-27.
- [80] Peterson, M. L.; Stanton, M. K.; Kelly, R. C.; Staples, R.; Cheng, A. *CrystEngComm* **2011**, *13*, 1170-1180.
- [81] Porter III, W. W.; Elie, S. C.; Matzger, A. J. *Cryst. Growth Des.* **2008**, *8*, 14-16.
- [82] Aitipamula, S.; Chow, P. S.; Tan, R. B. H. *Cryst. Growth Des.* **2010**, *10*, 2229-2238.

- [83] Gryl, M.; Krawczuk, A.; Stadnicka, K. *Act. Cryst. Sect. B* **2008**, *64*, 623–632.
- [84] Braga, D.; Palladino, G.; Polito, M.; Rubini, K.; Grepioni, F.; Chierotti, M.; Gobetto, R. *Chem. Eur. J.* **2008**, *14*, 10149–10159.
- [85] Sreekanth, B. R.; Vishweshwar, P.; Vyas, K. *Chem. Commun.* **2007**, 2375–2377.
- [86] Vishweshwar, P.; McMahon, J. A.; Peterson, M. L.; Hickey, M. B.; Shattock, T. R.; Zaworotko, M. J. *Chem. Commun.* **2005**, 4601–4603.
- [87] Schultheiss, N.; Newman, A. *Cryst. Growth Des.* **2009**, *9*, 2950–2967.
- [88] Madusanka, N.; Eddleston, M. D.; Arhangelskis, M.; Jones, W. *Act. Cryst. Sect. B* **2014**, *70*, 72–80.
- [89] Aitipamula, S.; Chow, P. S.; Tan, R. B. H. *CrystEngComm* **2014**, *16*, 3451–3465.
- [90] Eddleston, M. D.; Sivachelvam, S.; Jones, W. *CrystEngComm* **2013**, *15*, 175–181.
- [91] Braga, D.; Grepioni, F.; Lampronti, G. I.; Maini, L.; Turrina, A. *Cryst. Growth Des.* **2011**, *11*, 5621–5627.
- [92] Smith, A. J.; Kim, S.-H.; Duggirala, N. K.; Jin, J.; Wojtas, L.; Ehrhart, J.; Giunta, B.; Tan, J.; Zaworotko, M. J.; Shytle, R. D. *Mol. Pharm.* **2013**, *10*, 4728–4738.
- [93] Lehn, J.-M. *Pure Appl. Chem.* **1978**, *50*, 871–892.
- [94] Steed, J. W.; Atwood, J. L. *Supramolecular chemistry*; John Wiley and Sons, Ltd: Chichester: New York, 2nd ed.; 2009.
- [95] Dunitz, J. D. *Pure Appl. Chem.* **1991**, *63*, 177–185.
- [96] Pedersen, C. J. *J. Am. Chem. Soc.* **1967**, *89*, 2495–2496.
- [97] Lehn, J.-M. *Angew. Chem. Int. Ed. in English* **1988**, *27*, 89–112.
- [98] Cram, D. J. *Angew. Chem. Int. Ed. in English* **1988**, *27*, 1009–1020.
- [99] Lee, J. W.; Samal, S.; Selvapalam, N.; Kim, H.-J.; Kim, K. *Acc. Chem. Res.* **2003**, *36*, 621–630.

- [100] Whitesell, J. K.; Davis, R. E.; Saunders, L. L.; Wilson, R. J.; Feagins, J. P. *J. Am. Chem. Soc.* **1991**, *113*, 3267-3270.
- [101] Gavezzotti, A.; Simonetta, M. *Act. Cryst. Sect. A* **1976**, *32*, 997-1001.
- [102] Wood, P. A.; Borwick, S. J.; Watkin, D. J.; Motherwell, W. D. S.; Allen, F. H. *Act. Cryst. Sect. B* **2008**, *64*, 393-396.
- [103] Nishio, M. *CrystEngComm* **2004**, *6*, 130-158.
- [104] Nishio, M.; Umezawa, Y.; Honda, K.; Tsuboyama, S.; Suezawa, H. *CrystEngComm* **2009**, *11*, 1757-1788.
- [105] Parsegian, V. A. *Van der waals forces : A handbook for biologists, chemists, engineers, and physicists.*; Cambridge University Press: New York, 2006.
- [106] Paulini, R.; Müller, K.; Diederich, F. *Angew. Chem. Int. Ed.* **2005**, *44*, 1788-1805.
- [107] Etter, M. C. *Acc. Chem. Res.* **1990**, *23*, 120-126.
- [108] Pauling, L. *J. Am. Chem. Soc.* **1931**, *53*, 1367-1400.
- [109] Pauling, L. *The nature of the chemical bond and the structure of molecules and crystals; an introduction to modern structural chemistry*; Cornell University Press; H. Milford, Oxford University Press: Ithaca: N.Y., London, 1939.
- [110] Steiner, T. *Angew. Chem. Int. Ed.* **2002**, *41*, 48-76.
- [111] Desiraju, G. R. *Acc. Chem. Res.* **2002**, *35*, 565-573.
- [112] Etter, M. C.; MacDonald, J. C.; Bernstein, J. *Act. Cryst. Sect. B* **1990**, *46*, 256-262.
- [113] Sarma, J. A. R. P.; Desiraju, G. R. *Acc. Chem. Res.* **1986**, *19*, 222-228.
- [114] Brammer, L.; Bruton, E. A.; Sherwood, P. *Cryst. Growth Des.* **2001**, *1*, 277-290.
- [115] Saha, B. K.; Nangia, A.; Jaskolski, M. *CrystEngComm* **2005**, *7*, 355-358.
- [116] Metrangolo, P.; Resnati, G.; Pilati, T.; Biella, S. Halogen bonding in crystal engineering. In *Halogen Bonding*; Springer: New York, 2008.
- [117] Churchill, C. D. M.; Rutledge, L. R.; Wetmore, S. D. *Phys. Chem. Chem. Phys.* **2010**, *12*, 14515-14526.

- [118] Anslyn, E. V.; Dougherty, D. A. *Modern Physical Organic Chemistry*; University Science Books: Sausalito, California, 1st ed.; 2006.
- [119] Hunter, C. A.; Sanders, J. K. M. *J. Am. Chem. Soc.* **1990**, *112*, 5525-5534.
- [120] Hunter, C. A. *Chem. Soc. Rev.* **1994**, *23*, 101-109.
- [121] Hunter, C. A.; Lawson, K. R.; Perkins, J.; Urch, C. J. *J. Chem. Soc., Perkin Trans. 2* **2001**, 651-669.
- [122] Sunner, J.; Nishizawa, K.; Kebarle, P. *J. Phys. Chem.* **1981**, *85*, 1814-1820.
- [123] Dougherty, D. A. *Science* **1996**, *271*, 163-168.
- [124] Quiñonero, D.; Garau, C.; Rotger, C.; Frontera, A.; Ballester, P.; Costa, A.; Deyà, P. M. *Angew. Chem. Int. Ed.* **2002**, *41*, 3389-3392.
- [125] Allen, F. H. *Act. Cryst. Sect. B* **2002**, *58*, 380-388.
- [126] Desiraju, G. R. *Angew. Chem. Int. Ed. in English* **1995**, *34*, 2311-2327.
- [127] Walsh, R. D. B.; Bradner, M. W.; Fleischman, S.; Morales, L. A.; Moulton, B.; Rodríguez-Hornedo, N.; Zaworotko, M. J. *Chem. Commun.* **2003**, 186-187.
- [128] Reddy, L. S.; Babu, N. J.; Nangia, A. *Chem. Commun.* **2006**, 1369-1371.
- [129] Fischer, E. *Berichte der deutschen chemischen Gesellschaft* **1894**, *27*, 2985-2993.
- [130] Desiraju, G. R. *Nature* **2001**, *412*, 397-400.
- [131] Bis, J. A.; Vishweshwar, P.; Weyna, D.; Zaworotko, M. J. *Mol. Pharm.* **2007**, *4*, 401-416.
- [132] Dale, S. H.; Elsegood, M. R. J.; Hemmings, M.; Wilkinson, A. L. *CrystEngComm* **2004**, *6*, 207-214.
- [133] Issa, N.; Karamertzanis, P. G.; Welch, G. W. A.; Price, S. L. *Cryst. Growth Des.* **2009**, *9*, 442-453.
- [134] Karamertzanis, P. G.; Kazantsev, A. V.; Issa, N.; Welch, G. W.; Adjiman, C. S.; Pantelides, C. C.; Price, S. L. *J. Chem. Theory Comput.* **2009**, *5*, 1432-1448.
- [135] Mohammad, M. A.; Alhalaweh, A.; Velaga, S. P. *Int. J. Pharm.* **2011**, *407*, 63 - 71.

- [136] Abramov, Y. A.; Loschen, C.; Klamt, A. *J. Pharm. Sci.* **2012**, *101*, 3687–3697.
- [137] Musumeci, D.; Hunter, C. A.; Prohens, R.; Scuderi, S.; McCabe, J. F. *Chem. Sci.* **2011**, *2*, 883–890.
- [138] Hunter, C. A. *Angew. Chem. Int. Ed.* **2004**, *43*, 5310–5324.
- [139] Grecu, T.; Adams, H.; Hunter, C. A.; McCabe, J. F.; Portell, A.; Prohens, R. *Cryst. Growth Des.* **2014**, *14*, 1749–1755.
- [140] Gdanitz, R. J. *Current Opinion in Solid State and Materials Science* **1998**, *3*, 414–418.
- [141] Lommerse, J. P. M.; Motherwell, W. D. S.; Ammon, H. L.; Dunitz, J. D.; Gavezzotti, A.; Hofmann, D. W. M.; Leusen, F. J. J.; Mooij, W. T. M.; Price, S. L.; Schweizer, B.; Schmidt, M. U.; van Eijck, B. P.; Verwer, P.; Williams, D. E. *Act. Cryst. Sect. B* **2000**, *56*, 697–714.
- [142] Neumann, M.; Leusen, F.; Kendrick, J. *Angew. Chem. Int. Ed.* **2008**, *47*, 2427–2430.
- [143] Sarma, J. A. R. P.; Desiraju, G. R. *Cryst. Growth Des.* **2002**, *2*, 93–100.
- [144] Palmore, G. T. R.; Luo, T. M.; McBride-Wieser, M. T.; Picciotto, E. A.; Reynoso-Paz, C. M. *Chemistry of Materials* **1999**, *11*, 3315–3328.
- [145] Schwiebert, K. E.; Chin, D. N.; MacDonald, J. C.; Whitesides, G. M. *J. Am. Chem. Soc.* **1996**, *118*, 4018–4029.
- [146] Bowes, K. F.; Ferguson, G.; Lough, A. J.; Zakaria, C. M.; Glidewell, C. *Act. Cryst. Sect. B* **2003**, *59*, 87–99.
- [147] Trask, A. V.; van de Streek, J.; Motherwell, W. D. S.; Jones, W. *Cryst. Growth Des.* **2005**, *5*, 2233–2241.
- [148] Chadwick, K.; Davey, R.; Cross, W. *CrystEngComm* **2007**, *9*, 732–734.
- [149] Nehm, S. J.; Rodríguez-Spong, B.; Rodríguez-Hornedo, N. *Cryst. Growth Des.* **2006**, *6*, 592–600.
- [150] Chiarella, R. A.; Davey, R. J.; Peterson, M. L. *Cryst. Growth Des.* **2007**, *7*, 1223–1226.
- [151] Rager, T.; Hilfiker, R. *Zeit. Phys. Chem.* **2009**, *223*, 793–813.

- [152] Callister, W. D. *Materials science and engineering : an introduction*; John Wiley & Sons, Inc.: New York, 7th ed.; 2007.
- [153] Childs, S. L.; Rodriguez-Hornedo, N.; Reddy, L. S.; Jayasankar, A.; Maheshwari, C.; McCausland, L.; Shipplett, R.; Stahly, B. C. *CrystEngComm* **2008**, *10*, 856-864.
- [154] Mukherjee, A.; Grobelny, P.; Thakur, T. S.; Desiraju, G. R. *Cryst. Growth Des.* **2011**, *11*, 2637-2653.
- [155] Sarma, D.; Ramanujachary, K. V.; Stock, N.; Natarajan, S. *Cryst. Growth Des.* **2011**, *11*, 1357-1369.
- [156] Cohen, S.; Lacher, J.; Park, J. *J. Am. Chem. Soc.* **1959**, *81*, 3480.
- [157] Seio, K.; Miyashita, T.; Sato, K.; Sekine, M. *Eur. J. Org. Chem.* **2005**, *2005*, 5163-5170.
- [158] Schwartz, L.; Howard, J. *Phys. Chem.* **1971**, *75*, 1798-1803.
- [159] Mathew, S.; Paul, G.; Shivasankar, K.; Choudhury, A.; Rao, C. *J. Mol. Struct.* **2002**, *641*, 263 - 279.
- [160] Semmingsen, D.; Groth, P. *Acta chemica Scandinavica. Series B:* **1988**, *42*, 1-6.
- [161] Lim, N. C.; Morton, M. D.; Jenkins, H. A.; Brückner, C. *J. Org. Chem.* **2003**, *68*, 9233-9241.
- [162] MacLean, E. J.; Wheatley, P. S.; Ferguson, G.; Glidewell, C.; Lough, A. J. *Act. Cryst. Sect. C* **1999**, *55*, 1896-1899.
- [163] Braga, D.; Bazzi, C.; Maini, L.; Grepioni, F. *CrystEngComm* **1999**, *1*, 15-20.
- [164] Akhriff, Y.; Server-Carri, J.; GarcíÁa-Lozano, J.; Folgado, J. V.; Sancho, A.; EscriváÁ , E.; Vitoria, P.; Soto, L. *Cryst. Growth Des.* **2006**, *6*, 1124-1133.
- [165] Liu, Y.; Lam, A. H.; Fowler, F. W.; Lauher, J. W. *Molecular Crystals and Liquid Crystals* **2002**, *389*, 39-46.
- [166] Uçar, İ.; Bulut, A.; Yeşilel, O. Z.; Büyükgüngör, O. *Act. Cryst. Sect. C* **2004**, *60*, 0585-0588.
- [167] Onaran, M. B.; Comeau, A. B.; Seto, C. T. *J. Org. Chem.* **2005**, *70*, 10792-10802.

- [168] Ikeda, R.; Kurosawa, M.; Okabayashi, T.; Takei, A.; Yoshiwara, M.; Kumakura, T.; Sakai, N.; Funatsu, O.; Morita, A.; Ikekita, M.; Nakaike, Y.; Konakahara, T. *Bioorg. Med. Chem. Lett.* **2011**, *21*, 4784 - 4787.
- [169] Zaman, M. B.; Tomura, M.; Yamashita, Y. *Act. Cryst. Sect. C* **2001**, *57*, 621–624.
- [170] Verniest, G.; Colpaert, J.; Tornoos, K.; De Kimpe, N. *J. Org. Chem.* **2005**, *70*, 4549–4552.
- [171] Malerich, J. P.; Hagihara, K.; Rawal, V. H. *J. Am. Chem. Soc.* **2008**, *130*, 14416–14417.
- [172] Ian Storer, R.; Aciro, C.; Jones, L. H. *Chem. Soc. Rev.* **2011**, *40*, 2330–2346.
- [173] Bang-Andersen, B.; Ahmadian, H.; Lenz, S. M.; Stensbøl, T. B.; Madsen, U.; Bøgesø, K. P.; Krosgaard-Larsen, P. *J. Med. Chem.* **2000**, *43*, 4910–4918.
- [174] Porter, J. R.; Archibald, S. C.; Childs, K.; Critchley, D.; Head, J. C.; Linsley, J. M.; Parton, T. A.; Robinson, M. K.; Shock, A.; Taylor, R. J.; Warrelow, G. J.; Alexander, R. P.; Langham, B. *Bioorg. Med. Chem. Lett.* **2002**, *12*, 1051 - 1054.
- [175] Butera, J. A. *et al. J. Med. Chem.* **2000**, *43*, 1187–1202.
- [176] Kumar, S. P.; Gloria, P. M. C.; Goncalves, L. M.; Gut, J.; Rosenthal, P. J.; Moreira, R.; Santos, M. M. M. *Med. Chem. Commun.* **2012**, *3*, 489–493.
- [177] Villalonga, P.; Fernandez Mattos, S.; Ramis, G.; Obrador-Hevia, A.; Sampeador, A.; Rotger, C.; Costa, A. *ChemMedChem* **2012**, *7*, 1472–1480.
- [178] Xie, J.; Comeau, A. B.; Seto, C. T. *Organic Letters* **2004**, *6*, 83–86.
- [179] Busschaert, N.; Kirby, I. L.; Young, S.; Coles, S. J.; Horton, P. N.; Light, M. E.; Gale, P. A. *Angew. Chem. Int. Ed.* **2012**, *51*, 4426–4430.
- [180] Tomàs, S.; Prohens, R.; Deslongchamps, G.; Ballester, P.; Costa, A. *Angew. Chem. Int. Ed.* **1999**, *38*, 2208–2211.
- [181] Tomàs, S.; Prohens, R.; Vega, M.; Rotger, M. C.; Deyà, P. M.; Ballester, P.; Costa, A. *J. Org. Chem.* **1996**, *61*, 9394–9401.
- [182] Prohens, R.; Martorell, G.; Ballester, P.; Costa, A. *Chemical Communications* **2001**, 1456–1457.

- [183] Piña, M. N.; Rotger, C.; Soberats, B.; Ballester, P.; Deya, P. M.; Costa, A. *Chem. Commun.* 963-965.
- [184] Sanna, E.; Martínez, L.; Rotger, C.; Blasco, S.; González, J.; García-España, E.; Costa, A. *Organic Letters* **2010**, *12*, 3840-3843.
- [185] Delgado-Pinar, E.; Rotger, C.; Costa, A.; Piña, M. N.; Jimenez, H. R.; Alarcon, J.; Garcia-Espana, E. *Chem. Commun.* **2012**, *48*, 2609-2611.
- [186] Zhou, H.-B.; Zhang, J.; Lu, S.-M.; Xie, R.-G.; Zhou, Z.-Y.; Choi, M. C.; Chan, A. S.; Yang, T.-K. *Tetrahedron* **2001**, *57*, 9325 - 9333.
- [187] De Rosa, C. *Macromolecules* **2003**, *36*, 6087-6094.
- [188] Baran, R.; Veverkova, E.; Skvorcova, A.; Sebesta, R. *Org. Biomol. Chem.* **2013**, *11*, 7705-7711.
- [189] Qian, Y.; Ma, G.; Lv, A.; Zhu, H.; Zhao, J.; Rawal, V. H. *Chem. Commun.* **2010**, *46*, 3004-3006.
- [190] Konishi, H.; Lam, T. Y.; Malerich, J. P.; Rawal, V. H. *Organic Letters* **2010**, *12*, 2028-2031.
- [191] Woong Lee, J.; Hi Ryu, T.; Suk Oh, J.; Yong Bae, H.; Bin Jang, H.; Eui Song, C. *Chem. Commun.* **2009**, 7224-7226.
- [192] Rotger, M. C.; Piña, M. N.; Frontera, A.; Martorell, G.; Ballester, P.; Deyà, P. M.; Costa, A. *J. Org. Chem.* **2004**, *69*, 2302-2308.
- [193] Cerioni, G.; Janoschek, R.; Rappoport, Z.; Tidwell, T. T. *J. Org. Chem.* **1996**, *61*, 6212-6217.
- [194] Frontera, A.; Orell, M.; Garau, C.; Quiñonero, D.; Molins, E.; Mata, I.; Morey, J. *Organic Letters* **2005**, *7*, 1437-1440.
- [195] Quiñonero, D. Q.; Frontera, A.; Ballester, P.; Deyà, P. M. *Tetrahedron Letters* **2000**, *41*, 2001 - 2005.
- [196] Quiñonero, D.; Garau, C.; Frontera, A.; Ballester, P.; Costa, A.; Deyà, P. M. *Chem. Eur. J.* **2002**, *8*, 433-438.
- [197] Alemà, J.; Parra, A.; Jiang, H.; Jørgensen, K. A. *Chem. Eur. J.* **2011**, *17*, 6890-6899.
- [198] Amendola, V.; Bergamaschi, G.; Boiocchi, M.; Fabbrizzi, L.; Milani, M. *Chem. Eur. J.* **2010**, *16*, 4368-4380.

- [199] Amendola, V.; Fabbrizzi, L.; Mosca, L. *Chem. Soc. Rev.* **2010**, *39*, 3889-3915.
- [200] Rostami, A.; Colin, A.; Li, X. Y.; Chudzinski, M. G.; Lough, A. J.; Taylor, M. S. *J. Org. Chem.* **2010**, *75*, 3983-3992.
- [201] Fan, E.; Van Arman, S. A.; Kincaid, S.; Hamilton, A. D. *J. Am. Chem. Soc.* **1993**, *115*, 369-370.
- [202] Jin, C.; Zhang, M.; Wu, L.; Guan, Y.; Pan, Y.; Jiang, J.; Lin, C.; Wang, L. *Chem. Commun.* **2013**, *49*, 2025-2027.
- [203] Deyà, P. M.; Frontera, A.; ner, G. A. S.; nonero, D. Q.; Garau, C.; Costa, A.; Ballester, P. *Theor. Chem. Acc.* **2002**, *108*, 157-167.
- [204] Rotger, C.; Piña, M. N.; Vega, M.; Ballester, P.; Deyà, P. M.; Costa, A. *Angewandte Chemie* **2006**, *118*, 6998-7002.
- [205] Rotger, C.; Soberats, B.; Quiñonero, D.; Frontera, A.; Ballester, P.; Benet-Buchholz, J.; Deyà, P. M.; Costa, A. *Eur. J. Org. Chem.* **2008**, *2008*, 1864-1868.
- [206] P. Davis, A.; M. Draper, S.; Dunne, G.; Ashton, P. *Chem. Commun.* **1999**, 2265-2266.
- [207] Roy, S.; Aitipamula, S.; Nangia, A. *Cryst. Growth Des.* **2005**, *5*, 2268-2276.
- [208] Görbitz, C. H. *Act. Cryst. Sect. B* **2010**, *66*, 253-259.
- [209] Desiraju, G. R. *CrystEngComm* **2007**, *9*, 91-92.
- [210] Bernstein, J. *Cryst. Growth Des.* **2011**, *11*, 632-650.
- [211] Anderson, K. M.; Steed, J. W. *CrystEngComm* **2007**, *9*, 328-330.
- [212] McKinnon, J. J.; Spackman, M. A.; Mitchell, A. S. *Act. Cryst. Sect. B* **2004**, *60*, 627-668.
- [213] Jha, S.; Silversides, J. D.; Boyle, R. W.; Archibald, S. J. *CrystEngComm* **2010**, *12*, 1730-1739.
- [214] Wolff, S. K.; Grimwood, D. J.; McKinnon, J. J.; Jayatilaka, D.; Spackman, N. A. University of Western Australia, Perth, Australia, 2007.
- [215] Spackman, M. A.; McKinnon, J. J. *CrystEngComm* **2002**, *4*, 378-392.
- [216] Zyss, J.; Chemla, D. S. *Non-linear optical properties of organic and molecular crystals*; New York, 1987, Vol 1 and 2: 1st ed.; 1987.

- [217] Hollingsworth, M. D. *Science*. **2002**, 2410-2413.
- [218] Timofeeva, T. V.; Nesterov, V. N.; Clark, R. D.; Penn, B.; Frazier, D.; Antipin, M. Y. *J. Mol. Struct.* **2003**, 647, 181 - 202 Polymorphism, prediction, transformations and activity in organic crystal chemistry.
- [219] Maity, S. K.; Kumar, R.; Ambast, D. K. S.; Pal, B.; Haldar, D. *J. Mater. Chem.* **2012**, 22, 22198-22203.
- [220] Glaser, R.; Knotts, N.; Wu, Z.; Barnes, C. L. *Cryst. Growth Des.* **2006**, 6, 235-240.
- [221] Dey, A.; Desiraju, G. R. *Chem. Commun.* **2005**, 2486-2488.
- [222] Spackman, M. A.; Munshi, P.; Dittrich, B. *ChemPhysChem* **2007**, 8, 2051-2063.
- [223] Thallapally, P. K.; Jetti, R. K. R.; Katz, A. K.; Carrell, H. L.; Singh, K.; Lahiri, K.; Kotha, S.; Boese, R.; Desiraju, G. R. *Angew. Chem. Int. Ed.* **2004**, 43, 1149-1155.
- [224] Puigjaner, C.; Barbas, R.; Portell, A.; Valverde, I.; Vila, X.; Alcobe, X.; Font-Bardia, M.; Prohens, R. *CrystEngComm* **2012**, 14, 362-365.
- [225] Musumeci, D.; Hunter, C. A.; McCabe, J. F. *Cryst. Growth Des.* **2010**, 10, 1661-1664.
- [226] Davey, R. J.; Allen, K.; Blagden, N.; Cross, W. I.; Lieberman, H. F.; Quayle, M. J.; Righini, S.; Seton, L.; Tiddy, G. J. T. *CrystEngComm* **2002**, 4, 257-264.
- [227] Tomàs, S.; Prohens, R.; Vega, M.; Rotger, M. C.; Deyà, P. M.; Ballester, P.; Costa, A. *J. Org. Chem.* **1996**, 61, 9394-9401.
- [228] Prohens, R. "Reconocimiento molecular de oxoaniones mediante receptores basados en escuaramidas", Ph. D. Thesis,.
- [229] Bisson, A. P.; Carver, F. J.; Eggleston, D. S.; Haltiwanger, R. C.; Hunter, C. A.; Livingstone, D. L.; McCabe, J. F.; Rotger, C.; Rowan, A. E. *J. Am. Chem. Soc.* **2000**, 122, 8856-8868.
- [230] Hunter, C.; Anderson, H. *Angew. Chem. Int. Ed.* **2009**, 48, 7488-7499.
- [231] Vishweshwar, P.; Nangia, A.; Lynch, V. M. *Chem. Commun.* **2001**, 179-180.

- [232] Kozmutza, C.; Varga, I.; Udvardi, L. *J. Mol. Struct.: {THEOCHEM}* **2003**, 666-667, 95 - 97 The Role of Chemistry in the Evolution of Molecular Medicine. A Tribute to Professor Albert Szent-Gyorgyi to Celebrate his 110th Birthday.
- [233] Welch, G. W. A.; Karamertzanis, P. G.; Misquitta, A. J.; Stone, A. J.; Price, S. L. *J. Chem. Theory Comput.* **2008**, 4, 522-532.
- [234] Kobko, N.; Paraskevas, L.; del Rio, E.; Dannenberg, J. J. *J. Am. Chem. Soc.* **2001**, 123, 4348-4349.
- [235] Dannenberg, J. **2005**, 72, 227 - 273.
- [236] Masunov, A.; Dannenberg, J. J. *J. Phys. Chem. B* **2000**, 104, 806-810.
- [237] Dunitz, J. D.; Gavezzotti, A. *Chem. Soc. Rev.* **2009**, 38, 2622-2633.
- [238] Whitehead, M.; Turega, S.; Stephenson, A.; Hunter, C. A.; Ward, M. D. *Chem. Sci.* **2013**, 4, 2744-2751.
- [239] Blight, B. A.; Hunter, C. A.; Leigh, D. A.; McNab, H.; Thomson, P. I. T. *Nat. Chem.* **2011**, 3, 244-248.
- [240] Amenta, V.; Cook, J. L.; Hunter, C. A.; Low, C. M. R.; Sun, H.; Vinter, J. G. *J. Am. Chem. Soc.* **2013**, 135, 12091-12100.
- [241] Hunter, C. A.; Misuraca, M. C.; Turega, S. M. *Chem. Sci.* **2012**, 3, 2462-2469.
- [242] Cook, J.; Hunter, C.; Low, C.; Perez-Velasco, A.; Vinter, J. *Angew. Chem. Int. Ed.* **2007**, 46, 3706-3709.
- [243] Amenta, V.; Cook, J. L.; Hunter, C. A.; Low, C. M. R.; Vinter, J. G. *J. Phys. Chem. B* **2012**, 116, 14433-14440.
- [244] Grecu, T.; Hunter, C. A.; Gardiner, E. J.; McCabe, J. F. *Cryst. Growth Des.* **2014**, 14, 165-171.
- [245] Abraham, M. H.; Platts, J. A. *J. Org. Chem.* **2001**, 66, 3484-3491.
- [246] Hunter, C. A.; Low, C. M. R.; Rotger, C.; Vinter, J. G.; Zonta, C. *Chem. Commun.* **2003**, 834-835.
- [247] "Spartan'10, Wavefunction Inc.", .
- [248] Simon, S.; Duran, M.; Berg, J. J. *J. Phys. Chem. A* **1999**, 103, 1640-1643.

- [249] De Greef, T. F. A.; Smulders, M. M. J.; Wolffs, M.; Schenning, A. P. H. J.; Sijbesma, R. P.; Meijer, E. W. *Chemical Reviews* **2009**, *109*, 5687-5754.
- [250] Paisner, K.; Zakharov, L. N.; Doxsee, K. M. *Cryst. Growth Des.* **2010**, *10*, 3757-3762.
- [251] Liu, Y.; Lam, A. H. W.; Fowler, F. W.; Lauher, J. W. *Molecular Crystals and Liquid Crystals* **2002**, *389*, 39-46.
- [252] Kolev, T.; Koleva, B. B.; Spassov, T.; Cherneva, E.; Spiteller, M.; Mayer-Figge, H.; Sheldrick, W. S. *J. Mol. Struct.* **2008**, *875*, 372 - 381.
- [253] Albrecht, M. *Angew. Chem. Int. Ed.* **2005**, *44*, 6448-6451.
- [254] Speck, A. K.; Meixner, M.; Fong, D.; McCullough, P. R.; Moser, D. E.; Ueta, T. *The Astronomical Journal* **2002**, *123*, 346.
- [255] Park, K. H.; Noh, T. H.; Shim, Y.-B.; Jung, O.-S. *Chem. Commun.* **2013**, *49*, 4000-4002.
- [256] Guan, Y.-F.; Li, Z.-Y.; Ni, M.-F.; Lin, C.; Jiang, J.; Li, Y.-Z.; Wang, L. *Cryst. Growth Des.* **2011**, *11*, 2684-2689.
- [257] Oda, R.; Huc, I.; Schmutz, M.; Candau, S. J.; MacKintosh, F. C. *Nature* **1999**, *104*, 566-569.
- [258] Sewald, N.; Jakubke, H.-D. *Peptides: Chemistry and Biology*; Wiley-VCH: Weinheim: 1st ed.; 2002.
- [259] Yashima, E.; Maeda, K.; Iida, H.; Furusho, Y.; Nagai, K. *Chemical Reviews* **2009**, *109*, 6102-6211.
- [260] Balbo Block, M.; Kaiser, C.; Khan, A.; Hecht, S. Discrete Organic Nanotubes Based on a Combination of Covalent and Non-Covalent Approaches. In *Functional Molecular Nanostructures*, Vol. 245; Schlüter, A., Ed.; Springer Berlin Heidelberg: 2005.
- [261] Gutov, O. V. *Cryst. Growth Des.* **2013**, *13*, 3953-3957.
- [262] Pantos, G.; Pengo, P.; Sanders, J. *Angew. Chem. Int. Ed.* **2007**, *46*, 194-197.
- [263] Krämer, R.; Lehn, J. M.; Marquis-Rigault, A. *Proc. Natl. Acad. Sci.* **1993**, *90*, 5394-5398.
- [264] Huang, X.; Li, C.; Jiang, S.; Wang, X.; Zhang, B.; Liu, M. *J. Am. Chem. Soc.* **2004**, *126*, 1322-1323.

- [265] Kataoka, K.; Yanagi, M.; Katagiri, T. *CrystEngComm* **2011**, *13*, 6342-6344.
- [266] Atwood, J. L.; Steed, J. W. *Organic Nanostructures*; Wiley VCH, Weinheim: 1st ed.; 2008.
- [267] Moorthy, J. N.; Natarajan, R.; Savitha, G.; Venugopalan, P. *Cryst. Growth Des.* **2006**, *6*, 919-924.
- [268] Yang, Y.; Yang, Z.-Y.; Yi, Y.-P.; Xiang, J.-F.; Chen, C.-F.; Wan, L.-J.; Shuai, Z.-G. *J. Org. Chem.* **2007**, *72*, 4936-4946.
- [269] Korevaarl, P.; George, S. J.; Markvoort, A. J.; Smulders, M. M. J.; Hilbers, P. A. J.; Schenning, A. P. H. J.; Greef, T. F. A. D.; Meijer, E. W. *Nature* **2012**, 492-497.
- [270] G. A., Jeffrey, W. S. *Hydrogen bonding in biological structures.*; Springer-Verlag: Berlin; New York: 1st ed.; 1994.
- [271] Nishio, M.; Hirota, M.; Umezawa, Y. *In The C-H/ π Interaction: Evidence, Nature, Consequences*; Wiley-VCH: New York: 1st ed.; 1998.
- [272] Zhang, Z.; Zhang, Y.; Yao, D.; Bi, H.; Javed, I.; Fan, Y.; Zhang, H.; Wang, Y. *Cryst. Growth Des.* **2009**, *9*, 5069-5076.
- [273] Jeffrey, G. A.; Saenger, W. *Hydrogen bonding in biological structures*; Jeffrey, George A.; Springer-Verlag: Berlin; New York: 1st ed.; 1994.
- [274] Li, S.; Wang, K.; Zhou, M.; Li, Q.; Liu, B.; Zou, G.; Zou, B. *J. Phys. Chem.B* **2011**, *115*, 8981-8988.
- [275] Salonen, L. M.; Ellermann, M.; Diederich, F. *Angew. Chem. Int. Ed.* **2011**, *50*, 4808-4842.
- [276] Braga, D.; Grepioni, F. *Acc. Chem. Res.* **2000**, *33*, 601-608.
- [277] Braga, D.; Grepioni, F. *Chem. Commun.* **1998**, 911-912.
- [278] Jesus, A. J. L.; Redinha, J. S. *J. Phys. Chem.A* **2011**, *115*, 14069-14077.
- [279] Novoa, J. J.; Braga, D.; Addadi, L. *Engineering of Crystalline Materials Properties: State of the Art in Modeling, Design and Applications*; The Netherlands, Springer: 1st ed.; 2008.
- [280] Gilli, G.; Gilli, P. *The Nature of the Hydrogen Bond.*; Oxford University Press Inc., New York: 1st ed.; 2009.

- [281] Braga, D.; Bazzi, C.; Grepioni, F.; J. Novoa, J. *New J. Chem.* **1999**, *23*, 577-579.
- [282] Braga, D.; Grepioni, F.; Tagliavini, E.; J. Novoa, J.; Mota, F. *New J. Chem.* **1998**, *22*, 755-757.
- [283] Braga, D.; Grepioni, F.; J. Novoa, J. *Chem. Commun.* **1998**, 1959-1960.
- [284] Braga, D.; Maini, L.; Grepioni, F. *Chem. Eur. J.* **2002**, *8*, 1804-1812.
- [285] S. Miller, J.; J. Epstein, A. *Chem. Commun.* **1998**, 1319-1325.
- [286] Braga, D.; Maini, L.; Prodi, L.; Caneschi, A.; Sessoli, R.; Grepioni, F. *Chem. Eur. J.* **2000**, *6*, 1310-1317.
- [287] Gillard, R. E.; Raymo, F. M.; Stoddart, J. F. *Chem. Eur. J.* **1997**, *3*, 1933-1940.
- [288] Hunter, C. A. *J. Mol. Biol.* **1993**, *230*, 1025 - 1054.
- [289] Bertolasi, V.; Gilli, P.; Ferretti, V.; Gilli, G. *Act. Cryst. Sect. B* **2001**, *57*, 591-598.
- [290] Georgopoulos, S. L.; Diniz, R.; Yoshida, M. I.; Speziali, N. L.; Santos, H. F. D.; Junqueira, G. M. A.; de Oliveira, L. F. *J. Mol. Struct.* **2006**, *794*, 63 - 70.
- [291] Meyer, E. A.; Castellano, R. K.; Diederich, F. *Angew. Chem. Int. Ed.* **2003**, *42*, 1210-1250.
- [292] Burley, S.; Petsko, G. *Science* **1985**, *229*, 23-28.
- [293] Kim, K. S.; Tarakeshwar, P.; Lee, J. Y. *Chemical Reviews* **2000**, *100*, 4145-4186.
- [294] Ma, J. C.; Dougherty, D. A. *Chemical Reviews* **1997**, *97*, 1303-1324.
- [295] Kim, K. S.; Lee, J. Y.; Lee, S. J.; Ha, T.-K.; Kim, D. H. *J. Am. Chem. Soc.* **1994**, *116*, 7399-7400.
- [296] Frontera, A.; Gamez, P.; Mascal, M.; Mooibroek, T. J.; Reedijk, J. *Angew. Chem. Int. Ed.* **2011**, *50*, 9564-9583.
- [297] Seth, S. K.; Sarkar, D.; Roy, A.; Kar, T. *CrystEngComm* **2011**, *13*, 6728-6741.

- [298] Prohens, R.; Portell, A.; Font-Bardia, M.; Bauzà, A.; Frontera, A. *Cryst. Growth Des.* **2014**, *14*, 2578-2587.
- [299] Threlfall, T. *Org. Process Res. Dev.* **2000**, *4*, 384-390.
- [300] Barbas, R.; Polito, M.; Prohens, R.; Puigjaner, C. *Chem. Commun.* **2007**, 3538-3540.
- [301] Weissbuch, I.; Lahav, M.; Leiserowitz, L. *Cryst. Growth Des.* **2003**, *3*, 125-150.
- [302] Mirmehrabi, M.; Rohani, S. *J. Pharm. Sci.* **2005**, *94*, 1560-1576.
- [303] Carlson, R. *Design and optimization in organic synthesis*; Elsevier: Amsterdam: 1992.
- [304] Snyder, L. *Journal of Chromatographic Science* **1978**, *16*, 223-234.
- [305] Milligan, G. W. *Multivariate Behavioral Research* **1981**, *16*, 379-407.
- [306] Gu, C.; Li, H.; Gandhi, R. B.; Raghavan, K. *Int. J. Pharm.* **2004**, *283*, 117-125.
- [307] Gu, C.-H.; Young, V.; Grant, D. J. *J. Pharm. Sci.* **2001**, *90*, 1878-1890.
- [308] Marcus, Y. *Chem. Soc. Rev.* **1993**, *22*, 409-416.
- [309] Lide, D. *Handbook of organic solvents*; Boca Raton [etc.]: CRC: 1995.
- [310] Winget, P.; Dolney, D. M.; Giesen, D. J.; Cramer, C. J.; Truhlar, D. G. *Minnesota Solvent Descriptor Database*; University of Minnesota, Minneapolis, MN 55455-0431: 1999.
- [311] Abraham, M. H. *J. Phys. Org. Chem.* **1993**, *6*, 660-684.
- [312] Aaltonen, J.; Allesø, M.; Mirza, S.; Koradia, V.; Gordon, K. C.; Rantanen, J. *Eur. J. Pharm. Biopharm.* **2009**, *71*, 23-37.
- [313] Aakeröy, C. B.; Grommet, A. B.; Desper, J. *Pharmaceutics* **2011**, *3*, 601-614.
- [314] Friscic, T.; Childs, S. L.; Rizvi, S. A. A.; Jones, W. *CrystEngComm* **2009**, *11*, 418-426.
- [315] Mukherjee, A. K. *J. Indian Chem. Soc.* **2005**, *87*, 221-235.

- [316] David, W. I. F.; Shankland, K.; McCusker, L.; Baerlocher, C. "Structure Determination from Powder Diffraction Data", 2002.
- [317] Shankland, K.; David, W. I. F.; Csoka, T.; McBride, L. *Int. J. Pharm.* **1998**, *165*, 117-126.
- [318] Le Bail, A.; Duroy, H.; Fourquet, J. L. *Math.Res.Bull.* **1988**, *23*, 447-452.
- [319] J.I. Langford, D. L. *Rep. Prog. Phys.* **1996**, *59*, 131-234.
- [320] Hammond, R.; Roberts, K.; Doherty, R.; M., E. *J. Phys. Chem.* **1997**, *B101*, 6532-6536.
- [321] Cernik, R. J.; Cheetham, A. K.; Prout, C. K.; Watkin, D. J.; Wilkinson, A. P.; Willis, B. T. M. *J. App. Cryst.* **1991**, *24*, 222-226.
- [322] Knudsen, K. D.; Pattison, P.; Fitch, A. N.; Cernik, R. J. *Angew. Chem. Int. Ed.* **1998**, *37*, 2340-2343.
- [323] Cheung, E. Y.; Harris, K. D.; Johnston, R. L.; Hadden, K. L.; Zakrzewski, M. *J. Pharm. Sci.* **2003**, *92*, 2017-2026.
- [324] Tedesco, E.; Sala, F. D.; Favaretto, L.; Barbarella, G.; Albesa-Jové, D.; Pisignano, D.; Gigli, G.; Cingolani, R.; Harris, K. D. M. *J. Am. Chem. Soc.* **2003**, *125*, 12277-12283.
- [325] Colquhoun, H. M.; Aldred, P. L.; Zhu, Z.; Williams, D. J. *Macromolecules* **2003**, *36*, 6416-6421.
- [326] Kiang, Y. H.; Huq, A.; Stephens, P. W.; Xu, W. *J. Pharm. Sci.* **2003**, *92*, 1844-1853.
- [327] Brunelli, M.; Wright, J. P.; Vaughan, G. B. M.; Mora, A. J.; Fitch, A. N. *Angew. Chem. Int. Ed.* **2003**, *42*, 2029-2032.
- [328] Wunschel, M.; Dinnebier, R. E.; Carlson, S.; Bernatowicz, P.; van Smaalen, S. *Act. Cryst. Sect. B* **2003**, *59*, 60-71.
- [329] Nowell, H.; Shan, N.; Attfield, J.; Jones, W.; Motherwell, W. *Crystal Engineering* **2003**, *6*, 57 - 67.
- [330] Masciocchi, N.; Sironi, A. *J. Chem. Soc., Dalton Trans.* **1997**, 4643-4650.
- [331] K.D.M. Harris, M. T. *Chem. Mater.* **1996**, *8*, 2554-2570.
- [332] D. M. Poojary, A. C. *Acc. Chem. Res.* **1997**, *30*, 414-422.

- [333] Tremayne, M. J.; Kariuki, B. M.; Harris, K. D. M.; Shankland, K.; Knight, K. S. *J. Appl. Cryst.* **1997**, *30*, 968-974.
- [334] Seaton, C. C.; Tremayne, M. *Chem. Commun.* **2002**, 880-881.
- [335] Prohens, R.; Portell, A.; Alcobé, X. *Cryst. Growth Des.* **2012**, *12*, 4548-4553.
- [336] Florence, A. J.; Shankland, N.; Shankland, K.; David, W. I. F.; Pidcock, E.; Xu, X.; Johnston, A.; Kennedy, A. R.; Cox, P. J.; Evans, J. S. O.; Steele, G.; Cosgrove, S. D.; Frampton, C. S. *J. App. Cryst.* **2005**, *38*, 249-259.
- [337] Lightfoot, P.; Tremayne, M.; Harris, K. D. M.; Bruce, P. G. *J. Chem. Soc., Chem. Commun.* **1992**, 1012-1013.
- [338] Fujii, K.; Young, M. T.; Harris, K. D. M. *J Struct Biol.* **2011**, 461-467.
- [339] Giacovazzo, C. "Direct methods in Crystallography", 1980.
- [340] Visser, J. W. *J. Appl. Cryst.* **1969**, *2*, 968-974.
- [341] P. E. Werner, L. Eriksson, M. W. *J. Appl. Cryst.* **1985**, *18*, 367.
- [342] Boultif, A.; Louër, D. *J. App. Cryst.* **1991**, *24*, 987-993.
- [343] Boultif, A.; Louër, D. *J. App. Cryst.* **2004**, *37*, 724-731.
- [344] de Wolff, P. M. *J. App. Cryst.* **1968**, *1*, 108-113.
- [345] Pawley, G. S. *J. App. Cryst.* **1981**, *14*, 357-361.
- [346] Thompson, P.; Cox, D. E.; Hastings, J. B. *J. App. Cryst.* **1987**, *20*, 79-83.
- [347] Young, R. A. *The Rietveld Method*; International Union of Crystallography: , 1995.
- [348] Clegg, W.; Blake, A. J.; Cole, J. M.; Evans, J. S. O.; Main, P.; Parsons, S.; Watkin, D. J. *Crystal Structure Analysis: Principles and Practice*; Oxford University Press: Oxford, 2009.
- [349] Baerlocher, C.; McCusker, L. B.; Palatinus, L. *Acta Cryst. A62* **2006**, 231.
- [350] Cascarano, G.; Giacovazzo, C.; Camalli, M.; Spagna, R.; Burla, M. C.; Nunzi, A.; Polidori, G. *Act. Cryst. Sect. A* **1984**, *40*, 278-283.
- [351] Altomare, A.; Giacovazzo, C.; Moliterni, G.; Grazia, A.; Rizzi, R. *J. Res. Natl. Inst. Stand. Technol.* **2004**, *109*, 125.

- [352] Harris, K. D. M.; Tremayne, M.; Kariuki, B. M. *Angew. Chem. Int. Ed.* **2001**, *40*, 1626–1651.
- [353] Favre-Nicolin Vincent, R. e. *Zeitschrift für Kristallographie* **2007**, *222*, 105–113.
- [354] Chernyshev, V. V. *Russ. Chem. Bull.* **2001**, *50*, 2273–2292.
- [355] Rius, J. *Act. Cryst. Sect. A* **2011**, *67*, 63–67.
- [356] Harris, K. D. M.; Cheung, E. Y. *Chem. Soc. Rev.* **2004**, *33*, 526–538.
- [357] Hodeau, J. L.; Bordet, P.; Anne, M.; Prat, A.; Fitch, A. N.; Dooryheé, E.; Vaughan, G.; Freund, A. “Part of the SPIE Conference on Crystal and Multilayer Optics”, .
- [358] Schmitt, B.; Brönnimann, C.; Eikenberry, E. F.; Gozzo, F.; Hörmann, C.; Horisberger, R.; Patterson, B. *Nucl. Instr. Meth. Phys. Res.* **2003**, *A501*, 267–272.
- [359] Altomare, A.; Caliandro, R.; Camalli, M.; Cuocci, C.; da Silva, I.; Giacovazzo, C.; Moliterni, A. G. G.; Spagna, R. *J. App. Cryst.* **2004**, *37*, 957–966.
- [360] Favre-Nicolin, V.; Černý, R. *J. App. Cryst.* **2002**, *35*, 734–743.
- [361] Favre-Nicolin, V.; Černý, R. *Zeitschrift für Kristallographie* **2004**, *219*, 773–901.
- [362] Shankland, K. *Newsletter of the Comision on Crystallographic Computing of the International Union of Crystallography* **2004**, *4*, 46–51.
- [363] Reck, G.; Kretschmer, R.-G.; Kutschabsky, L.; Pritzkow, W. *Act. Cryst. Sect. A* **1988**, *44*, 417–421.
- [364] Dinnebier, R. E.; Stephens, P. W.; Carter, J. K.; Lommen, A. N.; Heiney, P. A.; McGhie, A. R.; Brard, L.; Smith, III, A. B. *J. App. Cryst.* **1995**, *28*, 327–334.
- [365] Harris, K. D. M.; Tremayne, M.; Lightfoot, P.; Bruce, P. G. *J. Am. Chem. Soc.* **1994**, *116*, 3543–3547.
- [366] Kirkpatrick, S.; Gelatt, C. D.; Vecchi, M. P. *Science* **1983**, *220*, 671–680.
- [367] Andreev, Y. G.; MacGlashan, G. S.; Bruce, P. G. *Phys. Rev. B* **1997**, *55*, 12011–12017.

- [368] Andreev, Y. G.; Lightfoot, P.; Bruce, P. G. *J. App. Cryst.* **1997**, *30*, 294–305.
- [369] Newsam, J. W.; Deem, M. W.; Freeman, C. M. *Accuracy in Powder Diffraction II, NIST Special Publication* **1992**, *846*, 80–91.
- [370] Earl, D. J.; Deem, M. W. *Phys. Chem. Chem. Phys.* **2005**, *7*, 3910–3916.
- [371] Harris, K. D. M.; Johnston, R. L.; Kariuki, B. M. *Act. Cryst. Sect. A* **1998**, *54*, 632–645.
- [372] Immirzi, A.; Erra, L.; Tedesco, C. *J. App. Cryst.* **2008**, *41*, 784–790.
- [373] Tremayne, M.; Seaton, C. C.; Glidewell, C. *Act. Cryst. Sect. B* **2002**, *58*, 823–834.
- [374] Metropolis, N.; Rosenbluth, A. W.; Rosenbluth, M. N.; Teller, A. H.; Teller, E. *J. Chem. Phys.* **1953**, *21*, 1087–1092.
- [375] Coelho, A. “Coelho Software, Brisbane, Asustralia, p. Topas Academic v4.1”, 2007.
- [376] David, W. I. F.; Shankland, K.; van de Streek, J.; Pidcock, E.; Motherwell, W. D. S.; Cole, J. C. *J. App. Cryst.* **2006**, *39*, 910–915.
- [377] Kariuki, B. M.; Serrano-González, H.; Johnston, R. L.; Harris, K. D. M. *Chemical Physics Letters* **1997**, *280*, 189–195.
- [378] Brodski, V.; Peschar, R.; Schenk, H. *J. App. Cryst.* **2005**, *38*, 688–693.
- [379] Toby, B. H. *Powder diffraction* **2006**, *21*, 67.
- [380] Dovesi, R.; Saunders, V. R.; Roetti, C.; Causa, M.; Harrison, N. M.; Orlando, R.; Apra, E. University of Torino, 1996.
- [381] Beyer, T.; Lewis, T.; Price, S. L. *CrystEngComm* **2001**, *3*, 178–212.
- [382] Schön, J. C.; Jansen, M. *Z. Kristallogr.* **2001**, *216*, 307–325.
- [383] Schön, J. C.; Jansen, M. *Z. Kristallogr.* **2001**, *216*, 361–383.
- [384] Le Bail, A. *J. App. Cryst.* **2005**, *38*, 389–395.
- [385] Mc Greevy, R. L. Pusztai, L. *Mol. Simul.* **1988**, *1*, 359–367.
- [386] Lasocha, W.; Gawel, B.; Rafalska-Lasocha, A.; Pawłowski, M.; Talik, P.; Paszkowicz, W. *J. App. Cryst.* **2010**, *43*, 163–167.

- [387] Roy, S.; Chakraborty, A.; Chattopadhyay, B.; Bhattacharya, A.; Mukherjee, A. K.; Ghosh, R. *Tetrahedron* **2010**, *66*, 8512 - 8521.
- [388] Derollez, P.; Dudognon, E.; Affouard, F.; Danède, F.; Correia, N. T.; Descamps, M. *Act. Cryst. Sect. B* **2010**, *66*, 76–80.
- [389] Al-Ktaifani, M.; Rukiah, M. *Act. Cryst. Sect. C* **2010**, *66*, o479–o483.
- [390] “Openbabel”, <http://openbabel.org/>.
- [391] Rietveld, H. M. *J. App. Cryst.* **1969**, *2*, 65–71.
- [392] Dollase, W. A. *J. App. Cryst.* **1986**, *19*, 267–272.
- [393] Rodriguez-Carvajal, J. “FULLPROF: A program for Rietveld refinement and pattern matching analysis. Powder Diffraction, satellite meeting of the XVth IUCr congress”, 1990.
- [394] Finger, L. W.; Cox, D. E.; Jephcoat, A. P. *J. App. Cryst.* **1994**, *27*, 892–900.
- [395] Sheldrick, G. M. *Act. Cryst. Sect. A* **2007**, *64*, 112–122.
- [396] Sheldrick, G. M. *Act. Cryst. Sect. A* **2008**, *64*, 112–122.
- [397] Hübschle, C. B.; Sheldrick, G. M.; Dittrich, B. *J. App. Cryst.* **2011**, *44*, 1281–1284.
- [398] Schmidt, A. H. *Synthesis* **1980**, 961-994.
- [399] Mukkanti, A.; Periasamy, M. *ARKIVOC* **2005**, 48–77.
- [400] Singh, L.; Ram, R. N. *J. Org. Chem.* **1994**, *59*, 710–711.
- [401] Neuse, E. W.; Green, B. R. *J. Org. Chem.* **1974**, *39*, 3881-3887.

Appendix A

Experimental polymorph screening

The experiments performed in the polymorph screening for each squaric acid derivative are summarized in this appendix, in which an experimental method example for each new solid form is also described. Their PXRD, DSC, TGA, ¹H-NMR and crystallographic data are shown in appendix C.2.19. In all tables the following nomenclature has been used; X: no experiment was performed, - : experiment performed but no solid crystallized, 1: evidences of a new phase, 2: single crystal, CSS: crystallization experiments of the dissolutions obtained from the solubility study, PHT: precipitation experiments by rapid cooling from high to low temperature, CHT: crystallization experiments by slow cooling from high temperature to r.t., CRT: crystallization experiments by evaporation at r.t., CSE: crystallization experiments by seeding at r.t., PAA: precipitation experiments by rapid addition of antisolvent at r.t. and CAD: crystallization experiments by antisolvent diffusion at r.t. In the solubility tables the following nomenclature has been used; S: soluble, I: insoluble and PS: partially soluble.

A.1 Compound 1

Tab. A.1: Solubility of **1**

Solvent	B.p. (°C)	V (mL)	Result
MeOH	65	1.0	I
EtOH	78	1.0	I
ETG	197	1.0	I
ACN	82	1.0	I
Acetone	56	1.0	I
H ₂ O	100	1.0	S (r.t.)
DMF	153	1.0	S (70°C)
DMSO	189	1.0	S (40°C)
Heptane	98	1.0	I
Toluene	111	1.0	I
Et ₂ O	34	1.0	I
THF	66	1.0	I
Dioxane	101	1.0	I
DCM	39	1.0	I
CHCl ₃	61	1.0	I

Tab. A.2: Slurry experiments of **1** from the solubility study

Solvent	Result
MeOH	Forms II/III ^a
EtOH	Forms II/III
ETG	Forms II/III
ACN	Forms II/III
Acetone	Forms II/III
H ₂ O	Forms II/III
Heptane	Forms II/III
Toluene	Forms II/III
Et ₂ O	Forms II/III
THF	Forms II/III
Dioxane	Forms II/III
DCM	Forms II/III
CHCl ₃	Forms II/III

^aResult from DSC analysisTab. A.3: Precipitation and crystallization experiments of **1**

Solvent	PHT	CHT	CRT
DMF	Form I	Form I	2 (Form I)
DMSO	Form II/III	Form II/III	Form I

Tab. A.4: Precipitation and crystallization experiments of **1** by antisolvent addition

Antisolvent	PAA		CAD	
H ₂ O	Form II/III	Form II/III	Form I	X
DCM	Form I	Form I	X	1
Dioxane	Form I	Form I	X	2 (Form III)
Toluene	Form I	Form I	X	2 (Form III)
ETG	Form I	Form II/III	X	X
EtOH	Form I	Form II/III	X	X
THF	Form I	Form I	X	X
ACN	Form I	Form II/III	X	X
Acetone	Form I	Form II/III	Form I	X
MeOH	Form I	Form I	Form I	X
Et ₂ O	Form I	Form II/III	X	2 (Form II)
Solvent	DMF	DMSO	DMF	DMSO

Preparation of the new forms of **1**

- **Form I**

Compound **1** (10.2 mg, 0.03 mmol) was dissolved in DMF (0.5 mL) at 70°C and the solution was slowly cooled down to r.t. Needle-shaped crystals of form I appeared after 13 days.

- **Form II**

Diethyl ether (2 mL) was let to diffuse into a solution of **1** (10.9 mg, 0.03 mmol) in DMSO (1.0 mL) at r.t. Needle-shaped crystals of form II appeared after 15 days.

- **Form III**

Dioxane (2 mL) was let to diffuse into a solution of **1** (10.1 mg, 0.03 mmol) in DMSO (1.0 mL) at r.t. Needle-shaped crystals of form III appeared after 30 days.

A.2 Compound 2

Tab. A.5: Solubility of **2**

Solvent	B.p. (°C)	V (mL)	Result
MeOH	65	1.0	S (40°C)
EtOH	78	1.0	S (40°C)
ETG	197	1.0	S (70°C)
ACN	82	1.0	S (70°C)
Acetone	56	1.0	I
H ₂ O	100	1.0	S (70°C)
DMF	153	0.4	S (r.t.)
DMSO	189	0.4	S (r.t.)
Heptane	98	1.0	I
Toluene	111	1.0	I
Et ₂ O	34	1.0	I
THF	66	1.0	S (50°C)
Dioxane	101	1.0	S (80°C)
DCM	39	1.0	I
CHCl ₃	61	1.0	I

Tab. A.6: Slurry experiments of **1** from the solubility study

Solvent	Result
Acetone	Form I
Heptane	Form I
Toluene	Form I
Et ₂ O	Form I
DCM	Form I
CHCl ₃	Form I

Tab. A.7: Precipitation and crystallization experiments of **2**

Solvent	CSS	PHT	CHT	CRT	CSE
MeOH	Form I	Form I	Form I	X	X
EtOH	Form I	Form I	Form I	X	X
ETG	-	-	Form I	X	X
ACN	Form I	Form I	Form I	X	X
H ₂ O	Form I	Form I	Form I	X	X
DMF	-	-	-	Form I	X
DMSO	-	-	-	Form I	X
THF	Form I	Form I	Form I	X	2 (Form I)
Dioxane	Form I	Form I	Form I	X	X

Tab. A.8: Precipitation and crystallization experiments of **2** by antisolvent addition

Antisolvent	PAA		CAD	
H ₂ O	Form I	Form I	Form I	-
DCM	-	-	X	X
Dioxane	Form I	-	X	X
Toluene	Form I	-	-	2 (Form I)
ETG	-	-	X	X
EtOH	Form I	-	-	-
THF	-	-	X	X
ACN	Form I	-	-	-
Acetone	-	-	X	X
MeOH	-	-	X	X
Et ₂ O	Form I	-	-	Form I
Solvent	DMF	DMSO	DMF	DMSO

Preparation of the new forms of **2**

- **Form I**

Toluene (2 mL) was let to diffuse into a solution of **2** (10.3 mg, 0.03 mmol) in DMF (1.0 mL) at r.t. Plate-shaped crystals of form I appeared after 15 days.

- **Form II**

Form II of **2** could only be obtained by heating form I from r.t. to 175°C in the DSC crucible under nitrogen.

A.3 Compound **3**

Tab. A.9: Solubility of **3**

Solvent	B.p. (°C)	V (mL)	Result
MeOH	65	1.0	S (35°C)
EtOH	78	1.0	S (70°C)
ETG	197	1.0	S(50°C)
ACN	82	1.0	I
Acetone	56	1.0	I
H ₂ O	100	1.0	PS (90°C)
DMF	153	0.5	S (r.t.)
DMSO	189	0.5	S (r.t.)
Heptane	98	1.0	I
Toluene	111	1.0	I
Et ₂ O	34	1.0	I
THF	66	1.0	I
Dioxane	101	1.0	I
DCM	39	1.0	I
CHCl ₃	61	1.0	I

Tab. A.10: Slurry experiments of **3** from the solubility study

Solvent	Result
Acetone	Form I
ACN	Form I
Heptane	Form I
Toluene	Form I
Et ₂ O	Form I
THF	Form I
Dioxane	Form I
DCM	Form I
CHCl ₃	Form I

Tab. A.11: Precipitation and crystallization experiments of **3**

Solvent	CSS	PHT	CHT	CRT	CSE
MeOH	Form I	Form I	Form I	Form I	X
EtOH	Form I	Form III	Form I	Form I	X
ETG	Form I	-	Form I	Form I	X
H ₂ O	X	Form IV	Form I	Form I	X
DMF	-	Form I	Form I	Form I	-
DMSO	-	Form I	Form I	Form I	2 (Form I)

Tab. A.12: Precipitation and crystallization experiments of **3** by antisolvent addition

Antisolvent	PAA	CAD
H ₂ O	-	Form I
DCM	-	-
Dioxane	Form I	-
Toluene	Form I	Form I
THF	-	Form I
ACN	Form I	Form I
Acetone	Form I	Form I
Et ₂ O	Form I	-
Solvent	DMF	DMSO

Preparation of the new forms of **3**

• Form I

A solution of **3** (10.5 mg, 0.03 mmol) in DMSO (0.5 mL) was kept in an opened vial at r.t. Needle-shaped crystals of form I crystallized after 21 days.

• Form II

Form II of **3** could only be obtained by heating form I from r.t. to 215°C in the DSC crucible under nitrogen.

• Form III

A solution of **3** (10.3 mg, 0.03 mmol) in ethanol (1.0 mL) at 70°C was rapidly cooled down to 0°C. The solid was filtered and dried under vacuum.

• Form IV

A solution of **3** (10.3 mg, 0.03 mmol) in water (1.5 mL) at 90°C was rapidly cooled down to 5-10°C. The solid was filtered and dried under vacuum.

A.4 Compound 4

Tab. A.13: Solubility of 4

Solvent	B.p. (°C)	V (mL)	Result
MeOH	65	1.0	S (r.t.)
EtOH	78	1.0	S (r.t.)
ETG	197	1.0	S (60°C)
ACN	82	1.0	S (70°C)
Acetone	56	1.0	I
H ₂ O	100	0.5	S (r.t.)
DMF	153	0.5	S (r.t.)
DMSO	189	0.5	S (r.t.)
Heptane	98	1.0	I
Toluene	111	1.0	I
Et ₂ O	34	1.0	I
THF	66	1.0	I
Dioxane	101	1.0	I
DCM	39	1.0	I
CHCl ₃	61	1.0	PS (50°C)

Tab. A.14: Slurry experiments of 4 from the solubility study

Solvent	Result
Acetone	Forms I+α
Heptane	Forms I+α
Toluene	Forms I+α
Et ₂ O	Forms I+α
THF	Forms I+α
Dioxane	Forms I+α
DCM	Forms I+α
CHCl ₃	Forms I+α

Tab. A.15: Crystallization experiments of 4

Solvent	CSS	CHT
MeOH	Forms I+α	Forms I+α
EtOH	Forms I+α	Forms I+α
ETG	Forms I+α	Forms I+α
ACN	Forms I+α	2 (Form III)
H ₂ O	Forms I+α	Forms I+α
DMF	Forms I+α	Forms I+α
DMSO	Forms I+α	Forms I+α

Tab. A.16: Crystallization experiments of 4 by antisolvent addition

Antisolvent	CAD						
DCM	Forms I+α	Forms I+α	-	17 (form III)	X	Forms I+α	-
THF	Forms I+α	Forms I+α	X	17 (form III)	-	Forms I+α	Forms I+α
Acetone	Forms I+α	Forms I+α	-	-	X	Forms I+α	Forms I+α
Et ₂ O	Forms I+α	-	Forms I+α	X	X	Forms I+α	Forms I+α
Pentane	X	X	Forms I+α	X	X	X	X
Heptane	X	X	X	-	-	X	X
Dioxane	X	X	X	-	-	X	X
Toluene	X	X	X	-	-	X	X
Solvent	ACN	EtOH	MeOH	H ₂ O	ETG	DMF	DMSO

Preparation of the new forms of 4

- **Form II¹**

Form II of 4 was obtained from the cocrystallization experiments. (See appendix B.8).

¹Form I could not be obtained pure.

- **Form III**

A solution of **4** (10.1 mg, 0.03 mmol) in ACN (1.0 mL) at 70°C was slowly cooled down to r.t. The vial containing the solution was kept sealed until needle-shaped crystals appeared after 15 days.

- **Form III of 17**

Interestingly, form III of **17** was obtained from the polymorph screening of **4**. DCM or THF (2 mL) were let to diffuse at r.t. into a solution of **4** in water (10.4 mg, 0.04 mmol). After 18 months needle-shaped crystals appeared.²

A.5 Compound 5

Tab. A.17: Solubility of **5**

Solvent	B.p. (°C)	V (mL)	Result
MeOH	65	1.0	I
EtOH	78	1.0	I
ETG	197	1.0	S (90°C)
ACN	82	1.0	I
Acetone	56	1.0	I
H ₂ O	100	1.0	S (70°C)
DMF	153	1.0	S (60°C)
DMSO	189	1.0	S (40°C)
Heptane	98	1.0	I
Toluene	111	1.0	I
Et ₂ O	34	1.0	I
THF	66	1.0	I
Dioxane	101	1.0	I
DCM	39	1.0	I
CHCl ₃	61	1.0	I

Tab. A.18: Slurry experiments of **5** from the solubility study

Solvent	Result
MeOH	Form I
EtOH	Form I
ACN	Form I
Acetone	Form I
Heptane	Form I
Toluene	Form I
Et ₂ O	Form I
THF	Form I
Dioxane	Form I
DCM	Form I
CHCl ₃	Form I

Tab. A.19: Precipitation and crystallization experiments of **5**

Solvent	CSS	PHT ^a	CHT
DMSO	Form I	Form I	Form I
DMF	Form I	Form I	X
ETG	-	-	X
H ₂ O	Form I	Form I	Form I

^aPrecipitations from high T to 10°C

²Since disquaramides are so difficult to hydrolyze, we suspect that traces of squaric acid reacted with traces of amine to produce **17** contaminated with **4** in the same batch.

Tab. A.20: Precipitation and crystallization experiments of **5** by antisolvent diffusion

Antisolvent	PAA	CAD
DCM	Form I	Form I
Dioxane	Form I	Form I
Toluene	Form I	Form I
CHCl ₃	Form I	Form I
THF	Form I	Form I
ACN	Form I	Form I
MeOH	Form I	Form I
Et ₂ O	Form I	Form I
MEK	Form I	Form I
AcOEt	Form I	2 (Form I)
MTBE	Form I	Form I
Pentane	Form I	Form I
Solvent	DMSO	

Preparation of the new form of **5**

- **Form I**

AcOEt was let to diffuse at r.t. into a solution of **5** (5.1 mg, 0.03 mmol) in DMSO (0.5 mL), which was prepared at 40°C and cooled down to r.t. Needle-shaped crystals of form I appeared after 30 days.

A.6 Compound **7**

Tab. A.21: Solubility of **7**

Solvent	B.p. (°C)	V (mL)	Result
MeOH	65	1.0	I
EtOH	78	1.0	I
ETG	197	1.0	I
ACN	82	1.0	I
Acetone	56	1.0	I
H ₂ O	100	1.0	I
DMF	153	1.0	S (r.t.)
DMSO	189	0.2	S (r.t.)
Heptane	98	1.0	I
Toluene	111	1.0	I
Et ₂ O	34	1.0	I
THF	66	1.0	I
Dioxane	101	1.0	I
DCM	39	1.0	I
CHCl ₃	61	1.0	I
Acetic acid	118	0.1	S (r.t.)
TFE	74.0	0.5	S (r.t.)

Tab. A.22: Slurry experiments of **7** from the solubility study

Solvent	Result
MeOH	Form I
EtOH	Form I
ETG	Form I
ACN	Form I
Acetone	Form I
H ₂ O	Form I
Heptane	Form I
Toluene	Form I
Et ₂ O	Form I
THF	Form I
Dioxane	Form I
DCM	Form I
CHCl ₃	Form I

Tab. A.23: Crystallization experiments of **7** by antisolvent diffusion

Antisolvent	CAD	
DCM	Form I	Form I
Dioxane	Form I	Form I
Toluene	Form I	Form I
EtOH	-	X
ACN	-	2 (Form I)
Acetone	Form I	Form I
MeOH	-	Form I
Et ₂ O	Form I	Form I
DIE	-	X
MEK	Form I	X
AcOEt	Form I	Form I
Solvent	DMSO	Acetic acid

Preparation of the new form of **7**

- Form I

Acetonitrile was let to diffuse at r.t. into a solution of **7** (6.5 mg, 0.046 mmol) in acetic acid (0.5 mL). Needle-shaped crystals of form I appeared after 60 days.

A.7 Compound 8

Tab. A.24: Solubility of **8**

Solvent	B.p. (°C)	V (mL)	Result
MeOH	65	0.1	S (r.t.)
EtOH	78	0.1	S (r.t.)
ACN	82	1.0	PS (70°C)
DMF	153	0.1	S (r.t.)
DMSO	189	0.1	S (r.t.)
DCM	39	1.0	I
CHCl ₃	61	1.0	I

Tab. A.25: Slurry experiments of **8** from the solubility study

Solvent	Result
DCM	Form I
CHCl ₃	Form I

Tab. A.26: Precipitation and crystallization experiments of **8**

Solvent	CSS	PHT	CHT
MeOH	Form I	Form I	Form I
EtOH	Form I	Form I	2 (Form I)
ACN	Form I	Form I	Form I
DMSO	Form I	X	Form I
DMF	Form I	X	Form I

Tab. A.27: Crystallization experiments of **8** by antisolvent diffusion

Antisolvent	PAA	CAD
Et ₂ O	Form I	Form I
Pentane	Form I	Form I
Solvent	MeOH	

Preparation of the new form of **8**

• Form I

A solution of **8** (20.1 mg, 0.13 mmol) in ethanol (0.1 mL) at 50°C was cooled down to r.t. Needle-shaped crystals of form I appeared after 3 days.

A.8 Compound **9**

Tab. A.28: Solubility of **9**

Solvent	B.p. (°C)	V (mL)	Result
MeOH	65	1.0	S (r.t.)
EtOH	78	1.0	S (50°C)
ETG	197	1.0	S (r.t.)
ACN	82	1.0	PS (80°C)
Acetone	56	1.0	PS (50°C)
H ₂ O	100	1.0	S (60°C)
DMF	153	1.0	S (70°C)
DMSO	189	1.0	S (40°C)
Heptane	98	1.0	I
Toluene	111	1.0	PS (90°C)
Et ₂ O	34	1.0	I
THF	66	1.0	PS (60°C)
Dioxane	101	1.0	PS (90°C)
DCM	39	1.0	PS (r.t.)
CHCl ₃	61	1.0	S (r.t.)
MIBK	116	1.0	I
Cyclohexane	81	1.0	I
Pentane	36	1.0	I
MTBE	55	1.0	I
Xylene	138	1.0	I
ⁱ pOH	82	1.0	PS (80°C)
AcOEt	77	1.0	PS (80°C)
n-BuOH	118	1.0	S (80°C)
MIBK	116	1.0	PS (90°C)

Tab. A.29: Slurry experiments of **9** from the solubility study

Solvent	Result
Et ₂ O	Form I
Heptane	Form I
Cyclohexane	Form I
Pentane	Form I
MEK	Form I
MIBK	Form I
MTBE	Form I
Xylene	Form I

Tab. A.30: Precipitation and crystallization experiments of **9**

Solvent	CSS	PHT	CHT
MeOH	Form I	Form I	X
EtOH	Form I	Form I	2 (Form I)
ETG	-	X	X
ACN	Form I	Form I	Form I
Acetone	Form I	Form I	Form I
H ₂ O	Form I	X	Form I
DMF	Form I	X	Form I
DMSO	Form I	X	Form I
Toluene	Form I	Form I	Form I
THF	Form I	Form I	Form I
DCM	Form I	X	Form I
CHCl ₃	Form I	-	Form I
Dioxane	Form I	X	Form I
ⁱ pOH	Form I	Form I	Form I
AcOEt	Form I	Form I	Form I
n-BuOH	Form I	X	Form I
MIBK	Form I	Form I	Form I

Preparation of the new form of **9**

- **Form I**

Compound **9** (10.1 mg, 0.041 mmol) was dissolved in ethanol (1.8 mL) at 50°C. The solution was slowly cooled down to r.t. Needle-shaped crystals appeared after two days.

A.9 Compound 10

Tab. A.31: Solubility of **10**

Solvent	B.p. (°C)	V (mL)	Result
MeOH	65	1.0	S (r.t.)
EtOH	78	1.0	S (40°C)
ETG	197	1.0	S (90°C)
ACN	82	1.0	S (40°C)
Acetone	56	1.0	S (40°C)
H ₂ O	100	1.0	S (90°C)
DMF	153	1	S (r.t.)
DMSO	189	1	S (70°C)
Heptane	98	1.0	I
Toluene	111	1.0	I
Et ₂ O	34	1.0	I
THF	66	1.0	S (60°C)
Dioxane	101	1.0	S (70°C)
DCM	39	1.0	S (r.t.)
CHCl ₃	61	1.0	S (r.t.)
ⁱ pOH	82	1.0	S (50°C)
^t BuOH	82	1.0	S (90°C)
n-BuOH	118	1.0	S (50°C)
MIBK	116	1.0	S (90°C)
DME	85	1.0	S (70°C)
MEK	55	1.0	PS (60°C)

Tab. A.32: Slurry experiments of **10** from the solubility study

Solvent	Result
Heptane	Form I
Et ₂ O	Form I
Toluene	Form II
Cyclohexane	Form I
MEK	Form I
Pentane	Form I
MIBK	Form I
AcOEt	Forms I+II
DIE	Forms I+II
Xylene	Forms I+II
MTBE	Form II

Tab. A.33: Precipitation and crystallization experiments of **10**

Solvent	CSS	PHT	CHT
MeOH	Form II	Form I	X
EtOH	Form II	Form I	Form II
ETG	1	-	X
ACN	Form II	Form I	X
Acetone	Form II	Form I	X
H ₂ O	Form III	X	X
DMF	-	X	X
DMSO	1	X	X
THF	Form I	Forms I+II	X
Dioxane	X	X	Form II
DCM	Forms I+II	Form I	X
CHCl ₃	Form I	Forms I+II	X
ⁱ pOH	Form II	Form I	Form I
^t BuOH	Form II	X	X
n-BuOH	Form II	Form I	Form I
MIBK	Form II	1	X
DME	Form II	Form I	X
MEK	Form II	Form I	X

Tab. A.34: Crystallization experiments of **10** by antisolvent diffusion

Antisolvent	CAD
Et ₂ O	Form II
Pentane	Form II
AcOEt	Form II
MEK	Form II
MTBE	Form II
DIE	Form II
Solvent	EtOH

Preparation of the new forms of **10**

- **Form I**

Form I was obtained from the synthesis of **10**. (See 6.3.6)

- **Form II**

Diethyl ether was let to diffuse into a solution of **10** (10.1 mg, 0.02 mmol) in ethanol (1.5 mL) at r.t. The solid was filtered and dried under vacuum.

A.10 Compound 11

Tab. A.35: Solubility of **11**

Solvent	B.p. (°C)	V (mL)	Result
MeOH	65	1.0	I
EtOH	78	1.0	I
ETG	197	1.0	I
ACN	82	1.0	I
Acetone	56	1.0	I
H ₂ O	100	1.0	I
DMF	153	1.0	S (120°C)
DMSO	189	1.0	S (120°C)
Heptane	98	1.0	I
Toluene	111	1.0	I
THF	66	1.0	I
Dioxane	101	1.0	I
CHCl ₃	61	1.0	I
ⁱ pOH	82	1.0	I
^t BuOH	82	1.0	I
n-BuOH	118	1.0	I
MIBK	116	1.0	I
DME	85	1.0	I
MEK	55	1.0	I
TFE	78	1.0	S (r.t.)
Acetic acid	118	1.0	S (70°C)

Tab. A.36: Slurry experiments of **11** from the solubility study

Solvent	Result
MeOH	Form I
EtOH	Form I
ETG	Form I
ACN	Form I
Acetone	Form I
H ₂ O	Form I
Heptane	Form I
Toluene	Form I
THF	Form I
Dioxane	Form I
CHCl ₃	Form I
ⁱ pOH	Form I
^t BuOH	Form I
n-BuOH	Form I
MIBK	Form I
DME	Form I
MEK	Form I

Tab. A.37: Precipitation and crystallization experiments of **11**

Solvent/s	CSS	CHT
DMSO	Form I	X
ETG/DMF	X	Form I
DMF	Form I	Form I
DMSO/DMF	X	Form I
Acetic acid	Form I	Form I
TFE	Form I	Form I
Acetic acid/H ₂ O	X	Form I

Tab. A.38: Crystallization experiments of **11** by antisolvent diffusion

Antisolvent	PAA	CAD	
Et ₂ O	X	Form I	Form I
DCM	X	Form I	Form I
MIBK	X	Form I	X
Pentane	X	Form I	Form I
MeOH	X	Form I	Form I
MEK	X	X	Form I
Acetone	X	X	Form I
THF	X	X	Form I
CHCl ₃	X	X	Form I
DMSO	Form I	X	Form I
Solvent	TFE	Acetic acid	TFE

Preparation of the new form of **11**

- **Form I**

A solution of **14** (10.3 mg, 0.02 mmol) with DMSO (2 mL) was prepared at 120°C and it was let to cool down to r.t. The solid was filtered and dried under vacuum.

A.11 Compound **12**

Tab. A.39: Solubility of **12**

Solvent	B.p. (°C)	V (mL)	Result
MeOH	65	1.0	I
EtOH	78	1.0	I
ETG	197	1.0	I
ACN	82	1.0	I
Acetone	56	1.0	I
H ₂ O	100	1.0	PS (90°C)
DMF	153	1	S (90°C)
DMSO	189	1	S (60°C)
Heptane	98	1.0	I
Toluene	111	1.0	I
Et ₂ O	34	1.0	I
THF	66	1.0	I
Dioxane	101	1.0	I
DCM	39	1.0	I
CHCl ₃	61	1.0	I

Tab. A.40: Slurry experiments of **12** from the solubility study

Solvent	Result
MeOH	Form II
EtOH	Form II
ETG	Form II
ACN	Form II
Acetone	Form II
Heptane	Form II
Toluene	Form II
Et ₂ O	Form II
THF	Form II
Dioxane	Form II
DCM	Form II
CHCl ₃	Form II

Tab. A.41: Crystallization experiments of **12** by antisolvent diffusion

Antisolvent	CAD
MeOH	1
DIE	1
THF	1
Et ₂ O	1
Pentane	1
AcOEt	-
MEK	1
MTBE	-
DIE	1
DCM	1
CHCl ₃	1
THF	-
ACN	-
ⁱ pOH	1
H ₂ O	1
EtOH	2 (Form III)
Solvent	DMSO

Preparation of the new forms of **12**

- **Form I**

Form I was obtained from the cocrystallization experiments with pyridine (See appendix B.8).

- **Form II**

Form II was obtained from the synthesis of **12** in ethanol (See chapter 6.3.6).

- **Form III**

Ethanol (2 mL) was let to diffuse into a solution of **12** in DMSO at r.t. Needle-shaped crystals appeared after three months.

- **Form IV**

Form IV was obtained from the cocrystallization experiments (See appendix B.8).

A.12 Compound 17

Tab. A.42: Solubility of **17**

Solvent	B.p. (°C)	V (mL)	Result
H ₂ O	100	1.0	S (80°C)
DMSO	189	1.0	S (r.t.)

Tab. A.43: Crystallization experiments of **17**

Solvent	CSS	CHT
H ₂ O	Form I	1
DMSO	Form I	Form I

Tab. A.44: Crystallization experiments of **17** by antisolvent diffusion

Antisolvent	CAD
MeOH	-
THF	Form I
Et ₂ O	Form I
Pentane	-
AcOEt	Form I
MEK	Forms I+II
MTBE	2 (Form II)
DIE	1
DCM	1
CHCl ₃	1
ACN	Form I
Toluene	1
Dioxane	2 (Form I)
Solvent	DMSO

Preparation of the new forms of **17**

- **Form I**

Dioxane (2 mL) was let to diffuse at r.t. into a solution of **17** (5.0 mg, 0.03 mmol) in DMSO (0.5 mL), which was prepared at 40°C and cooled down to r.t. Needle-shaped crystals of form I appeared after 15 days.

- **Form II**

MTBE (2 mL) was let to diffuse at r.t. into a solution of **17** (5.0 mg, 0.03 mmol) in DMSO (0.5 mL), which was prepared at 40°C and cooled down to r.t. Needle-shaped crystals of form II appeared after 15 days.

- **Form III**

Form III of **17** was obtained during the polymorph screening of **4** (See A.4).

Appendix B

Experimental cocrystal screening

The experiments performed in the cocrystal screening for each squaric acid derivative are summarized in this annex, in which an experimental method example for the obtention of each new solid form is also described. Their PXRD, DSC, TGA, $^1\text{H-NMR}$ or $^{13}\text{C-NMR}$ and crystallographic data are shown in annex III. The crystal structure solution of the new forms is described in annex IV. In all tables the following nomenclature has been used; X: no experiment was performed, - : experiment performed but no solid crystallized, 0: no cocrystal obtained, 1: evidences of a new phase or mixture of phases, 2: single crystal, DG: drop grinding experiments, RC: reaction crystallization experiments, CHT: crystallization experiments by slow cooling from high temperature to r.t., CAD: crystallization experiments by antisolvent diffusion at r.t., PHT: precipitation experiments by rapid cooling from high T to r.t., CRT: crystallization experiments by evaporation at r.t.

Each new form is confirmed by SXRD or PXRD and $^1\text{H-NMR}$ and it is identified by the number of squaric acid derivative (1,2...), number of coformer (I, II...) and polymorphic form (A, B...).

B.1 Cofomers

Number	Name	Scheme	Description
I	Fumaric acid (FA)		Linear formula: C ₄ H ₄ O ₄ MW: 116.07 g/mol Melting point: 287°C
II	<i>p</i> -nitrobenzoic acid (PNBA)		Linear formula: C ₇ H ₅ NO ₄ MW: 167.12 g/mol Melting point: 237°C
III	Glutaric acid (GRA)		Linear formula: C ₅ H ₈ O ₄ MW: 132.12 g/mol Melting point: 95-98°C
IV	Glutamic acid (GMA)		Linear formula: C ₅ H ₉ NO ₄ MW: 147.13 g/mol Melting point: 199°C
V	Oxalic acid (OA)		Linear formula: C ₂ H ₂ O ₄ MW: 90.03 g/mol Melting point: 102°C
VI	Citric acid (CA)		Linear formula: C ₆ H ₈ O ₇ MW: 192.12 g/mol Melting point: 153-159°C
VII	Squaric acid (SQA)		Linear formula: C ₄ H ₂ O ₄ MW: 114.06 g/mol Melting point: >300°C
VIII	Resorcinol (RE)		Linear formula: C ₆ H ₆ O ₂ MW: 110.11 g/mol Melting point: 109-112°C
IX	Urea (UR)		Linear formula: CH ₄ N ₂ O MW: 60.06 g/mol Melting point: 132-135°C
X	Nicotinamide (NA)		Linear formula: C ₆ H ₆ N ₂ O MW: 122.12 g/mol Melting point: 129°C
XI	Hydroquinone (HY)		Linear formula: C ₆ H ₆ O ₂ MW: 110.12 g/mol Melting point: 172°C
XII	3,5-dihydroxybenzoic acid (DHBA)		Linear formula: C ₇ H ₆ CO ₄ MW: 154.12 g/mol Melting point: 236-238°C
XIII	Carbamazepine (CBZ)		Linear formula: C ₁₅ H ₁₂ N ₂ O MW: 236.27 g/mol Melting point: 190-192°C
XIV	Dimethylurea (DMU)		Linear formula: C ₃ H ₈ N ₂ O MW: 88.11 g/mol Melting point: 104°C
XV	Dibenzylsulfoxide (DBS)		Linear formula: C ₁₄ H ₁₄ C ₂ SO MW: 230.33 g/mol Melting point: 130-132°C
XVI	Triphenylphosphine oxide (TPPO)		Linear formula: C ₁₈ H ₁₅ OP MW: 278.29 g/mol Melting point: 154-158°C
XVII	Bipyridine (BIP)		Linear formula: C ₁₀ H ₈ N ₂ MW: 151.18 g/mol Melting point: 114°C
XVIII	Pyridine (PY)		Linear formula: C ₅ H ₅ N MW: 79.1 g/mol Melting point: -41.6°C
XIX	Isonicotinamide (ISNA)		Linear formula: C ₆ H ₆ N ₂ O MW: 122.12 g/mol Melting point: 156°C
XX	Propionic acid (PA)		Linear formula: C ₃ H ₆ O ₂ MW: 74.08 g/mol Melting point: -20.5°C
XXI	Lactic acid (LA)		Linear formula: C ₃ H ₆ O ₃ MW: 90.08 g/mol Melting point: 16.8°C
XXII	Gluconic acid (GLA)		Linear formula: C ₆ H ₁₂ O ₇ MW: 131.0 g/mol Melting point: 196.16°C
XXIII	Formic acid (FRA)		Linear formula: CH ₂ O ₂ MW: 46.03 g/mol Melting point: 8.4°C
XXIV	Isethionic acid (IA)		Linear formula: C ₂ H ₆ O ₄ S MW: 126.13 g/mol Melting point: 191-194°C
XXV	Phosphoric acid (PHA)		Linear formula: H ₃ O ₄ P MW: 98.0 g/mol Melting point: 42.35°C

Fig. B.1: List of cofomers used in this work (Description according to Sigma Aldrich)

B.2 Compound 2

Tab. B.1: Drop grinding experiments of **2** and selected cofomers (**DG**)

Solvent	Cofomer		
	FA	RE	NA
EtOH	1	0	-

Tab. B.2: Reaction crystallization experiments of **2** and selected cofomers (**RC**)

Solvent	Cofomer							
	FA	PNBA	GRA	GMA	OA	CA	SQA	RE
EtOH	2-I-A	2-II	-	0	1	-	1	0

Tab. B.3: Crystallization experiments of **2** and selected cofomers from high temperature to r.t. (**CHT**)

Solvents	Cofomer	
	FA	NA
MeOH	0	X
EtOH	0	-
ACN	2 (2-I-A)	X
H ₂ O	0	X
ratio (2:coformer)	1:1	1:2

Tab. B.4: Crystallization experiments of **2** and selected cofomers by antisolvent diffusion at r.t. (**CAD**)

Antisolvent	Cofomer					
	FA	RE	NA	FA	RE	NA
MEK	1	1	-	-	-	0
Acetone	-	-	-	-	X	-
Pentane	X	X	X	-	-	X
Et ₂ O	1	1	0	-	-	0
THF	X	X	X	-	-	X
MTBE	1	1	0	0	0	0
DIE	1	1	1	-	-	0
DCM	-	1	-	-	-	0
ACN	X	X	X	-	-	X
Solvent	THF/ CHCl ₃	THF/ CHCl ₃	THF/ CHCl ₃	EtOH/ DMSO	THF/ CHCl ₃	
ratio (2:coformer)	1:1	1:2	1:1	1:1	1:1	

Tab. B.5: Recrystallization experiments from reaction crystallization solids of **2** and selected cofomers from high temperature to r.t. (**RRC**)

Solvent	Cofomer									
	FA	PNBA	GRA	GMA	OA	CA	SQA	RE	UR	NA
EtOH	0	-	X	X	0	X	0	0	-	-

Preparation of the new multicomponent forms of **2**

- **Cocrystal of 2:fumaric acid, form A (2-I-A)**

Compound **2** (13 mg, 0.04 mmol) was added to a saturated solution of fumaric acid in ethanol (2.0 mL) and the suspension was stirred during one day at r.t. The solid was filtered and dried under vacuum.

- **Cocrystal of 2:fumaric acid, form B (2-I-B)**

A mixture of **2** (20.2 mg, 0.07 mmol) and fumaric acid (15.7 mg, 0.14 mmol) were dissolved in ACN (30 mL) at 60°C. The heater was switched off and thin needles crystallized overnight.

- **Cocrystal of 2:*p*-nitrobenzoic acid (2-II)**

Compound **2** (10 mg, 0.03 mmol) was added to a saturated solution of *p*-nitrobenzoic acid in ethanol (2.0 mL) and the suspension was stirred during one day at r.t. The solid was filtered and dried under vacuum.

B.3 Compound **4**

Tab. B.6: Drop grinding experiments of **4** and selected cofomers (**DG**)

Solvent	Cofomer									
	FA	PNBA	GRA	GMA	OA	CA	SQA	RE	UR	NA
MeOH	X	X	X	X	X	X	X	4-VIII-A ^a	X	X
EtOH	1	0	-	0	1	-	1	1	1	1
IPA	X	X	X	X	X	X	X	1	X	X
THF	X	X	X	X	X	X	X	4-VIII-B ^a	X	X
H ₂ O	X	X	X	X	X	X	X	1	X	X
ACN	X	X	X	X	X	X	X	4-VIII-B ^a	X	X
DMF	X	X	X	X	X	X	X	1	X	X
DMSO	X	X	X	X	X	X	X	1	X	X

^aNo single crystals were obtained from recrystallization of these samples

Tab. B.7: Reaction crystallization experiments of **4** and selected cofomers (**RC**) (**FII** of **4** meaning polymorph **II** of **4**)

Solvent	Cofomer									
	FA	PNBA	GRA	GMA	OA	CA	SQA	RE	UR	NA
MeOH	X	X	X	X	X	X	X	4-VIII-A	X	X
EtOH	4-I-A	1	1	FII of 4	1	1	4-VII-A	X	FII+FII of 4	FII+FII of 4
ACN	X	X	X	X	X	X	X	4-VIII-B	X	X

Tab. B.8: Crystallization experiments of **4** and selected coformers from high temperature to r.t. (CHT)

Solvent/s	Coformer										
	FA	PNBA	GRA	GMA	OA			UR	NA		
ACN/DMSO	X	X	X	0	X	X	X	X	-	X	X
ACN/TFE	X	X	X	X	1	X	1	X	X	-	-
EtOH/DMSO	1	0	X	X	X	X	X	1	X	X	X
ACN/TFE/DMSO	X	X	1	X	X	X	X	X	X	X	X
H ₂ O	X	X	X	X	X	X	X	2 (4-VII-B)	X	X	X
ratio 4 :coformer	1:1	1:1	1:2	1:2	1:2	1:1	1:2	1:1	1:2	1:2	1:2

Tab. B.9: Recrystallization experiments of the solids obtained by drop grinding between **4** and resorcinol

Solvent	Result
MeOH	4-VIII-A
EtOH	4-VIII-A
IPA	1
THF	0
Chloroform	4-VIII-A
Acetone	0
Dioxane	4-VIII-B
MEK	1
ETG	-

Tab. B.10: Crystallization experiments of **4** and selected coformers by antisolvent diffusion at r.t. (CAD)

Antisolvent	Coformer										
	FA	PNBA	GRA	GMA	OA	RE	UR	NA			
MeOH	2 (4-I-B)	-	-	X	X	X	X	X	0	X	0
MEK	needles ^a	-	-	X	X	-	-	-	0	-	0
Acetone	0	-	-	X	X	-	-	X	0	X	0
Pentane	0	-	0	4-VIII-A	-	0	-	0	0	-	0
Et ₂ O	0	-	-	4-VIII-A	-	0	-	-	0	1	0
THF	0	-	-	X	X	0	-	0	0	0	0
MTBE	0	-	-	1	-	4-VIII-A	-	0	0	-	0
DIE	0	-	0	4-VIII-A	-	-	-	-	0	-	0
DCM	0	-	-	4-VIII-A	-	4-VIII-A	-	0	0	-	0
ACN	-	-	-	4-VIII-A	-	X	X	0	0	1	0
-	twins ^a	-	-	X	-	-	-	0	0	-	0
Solvent/s	EtOH/H ₂ O/ DMSO	EtOH/ DMSO	EtOH/ DMSO	EtOH	EtOH	ACN	ACN	EtOH	EtOH	EtOH	EtOH
ratio (4 :coformer)	1:1	1:1	1:2	1:1	1:2	1:1	1:2	1:1	1:2	1:1	1:2

^aNo good quality single crystalsTab. B.11: Crystallization experiments of the reaction crystallization solids of **4** and selected coformers by antisolvent diffusion at r.t. (CAD)

Solvent	Antisolvent	Coformer				
		FA	PNBA	GMA	OA	RE
EtOH	-	1	1	0	1	-
ACN	-	X	X	X	X	4-VIII-A
Toluene	-	X	X	X	X	0
EtOH	DCM	X	X	X	X	-
ACN	DCM	X	X	X	X	-
Toluene	DCM	X	X	X	X	-

Preparation of the new forms of 4

- **Form II of 4**

Compound 4 (55 mg, 0.21 mmol) was added to a saturated solution of glutamic acid in ethanol (1.0 mL) and the suspension was stirred overnight. The solid was filtered and dried under vacuum.

- **Cocrystal of 4 : fumaric acid, form A (4-I-A)**

Compound 4 (10 mg, 0.04 mmol) was added to a saturated solution of fumaric acid in ethanol (1.0 mL) and the suspension was stirred overnight. The solid was filtered and dried under vacuum.

- **New phase 4 : fumaric acid, form B (4-I-B)**

A solution of 4 (50.2 mg, 0.20 mmol) and fumaric acid (22.8 mg, 0.20 mmol) in ethanol (6 mL) was prepared. Since the solid did not completely dissolve, DMSO (8 mL) and water (1 mL) were added at 40 °C until a total dissolution. An aliquot was placed at r.t. in a thin vial and it was sealed with a septum and a needle, through which methanol was let to diffuse into the solution. After one month thin needles crystallized.

- **Salt of 4 : squaric acid, form A (4-VII-A)**

Compound 4 (12 mg, 0.05 mmol) was added to a saturated solution of squaric acid in ethanol (1.0 mL) and the suspension was stirred overnight. The solid was filtered and dried under vacuum.

- **Salt of 4 : squaric acid, form B (4-VII-B)**

Compound 4 (12 mg, 0.05 mmol) and squaric acid were dissolved in water (1.0 mL) at 80 °C and the solution was slowly cooled down to r.t. Crystals were isolated and analyzed by SXRD.

- **Cocrystal of 4 : resorcinol, form A (4-VIII-A)**

Resorcinol (30.7 mg, 0.28 mmol) was added to a saturated solution of 4 in ACN (0.5 mL) and the suspension was heated to 50 °C. Since it did not completely dissolve, ACN (0.5 mL) was added and the solid was filtered at r.t. The solution was kept in a sealed vial with a needle at r.t. until a solid crystallized. It was filtered and dried under vacuum.

- **Cocrystal of 4 : resorcinol, form B (4-VIII-B)**

Resorcinol (8.7 mg, 0.08 mmol) was added to a saturated solution of 4 in ACN (0.2 mL) and the suspension was stirred overnight. The solid was filtered and dried under vacuum.

B.4 Compound 5

Tab. B.12: Drop grinding experiments of **7** and selected coformers in a 1:1 molar ratio (**DG**)

Solvent/s	Coformer						
	FA	PNBA	RE	NA	CBZ	DMU	DBS
DMF	0	0	0	0	0	0	0
EtOH	0	0	0	0	0	0	0
DMSO	0	0	0	0	0	0	0

Tab. B.13: Reaction crystallization experiments of **5** and selected coformers (**RC**)

Solvent/s	Coformer						
	FA	PNBA	RE	NA	CBZ	DMU	DBS
ACN/DMF	0	0	0	0	0	0	0
EtOH	0	0	0	0	0	0	0

B.5 Compound 7

Tab. B.14: Drop grinding experiments of **7** and selected coformers (**DG**)

Solvent/s	Coformer				
	SQA	RE	TPPO		
DMF	1	0	0	0	0
DMSO	0	0	0	0	0
Acetic acid	0	0	0	0	0
TFE	1	0	0	0	0
MeOH/DCM	0	0	0	0	0
ratio (7:coformer)	1:1	1:2	2:1	1:1	1:1

Tab. B.15: Reaction crystallization experiments of **7** and selected coformers (**RC**)

Solvent	Coformer							
	FA	PNBA	GRA	GMA	OA	CA	SQA	DHBA
DMF	X	X	X	X	X	X	0	X
DMSO	X	X	0	0	X	X	0	X
Acetic acid	X	X	X	X	X	X	0	X
TFE	X	X	X	X	X	X	1	0
MeOH/DCM	X	X	0	0	X	X	0	X
EtOH	0	0	0	0	0	0	0	0

Tab. B.16: Crystallization experiments of **7** and oxalic acid in a 1:1 molar ratio by antisolvent diffusion (**CAD**)

Antisolvent	Solvent	Result
DCM	DMSO	0
Et ₂ O	DMSO	0
EtOH	DMSO	0
Acetone	DMSO	0

Tab. B.17: Crystallization experiments of **7** and selected cofomers in a 1:1 molar ratio from high temperature to r.t. (CHT)

Solvent	Cofomer							
	GRA	GMA	PA	LA	GLA	FRA	IA	PHA
DMSO	0	0	X	X	X	X	X	X
TFE	0	0	X	X	X	X	X	X
-	X	X	-	-	-	0	-	1

Tab. B.18: Crystallization experiments of **7** and phosphoric acid (PHA) in a 1:1 molar ratio by antisolvent diffusion (CAD)

Antisolvent	Result
AcOEt	1
MTBE	1

B.6 Compound 10

Tab. B.19: Drop grinding experiments of **10** and selected cofomers (DG)

Solvent	Cofomer		
	RE	HI	
MeOH	10-VIII-A,B	FI of 10 + 10-XI-A	10-XI-A
EtOH	10-VIII-A,B	X	X
Acetone	10-VIII-A,B	FI of 10 + 10-XI-A	FI of 10 + 10-XI-A
CHCl ₃	FI of 10 + 10-VIII-B	X	X
Dioxane	10-VIII-A,B	X	X
Toluene	10-VIII-A,B	FI of 10 + 10-XI-A	10-XI-A
DCM	FI of 10 + 10-VIII-B	X	X
^t BuOH	1	FI of 10	X
ACN	10-VIII-A,B	FI of 10 + 10-XI-A	FI of 10 + 10-XI-A
MEK	10-VIII-A,B	X	X
THF	10-VIII-A,B	X	X
IPA	10-VIII-A,B	X	X
MIBK	10-VIII-A,B	X	X
H ₂ O	10-VIII-B	X	X
TFE	FI of 10 + 10-VIII-A	X	X
ratio (10:coformer)	1:2	1:1	1:2

Tab. B.20: Reaction crystallization experiments of **10** and selected cofomers (**RC**)

Solvent	Cofomer	
	RE	HY
MeOH	0	10-XI-B
EtOH	0	X
Acetone	0	0
CHCl ₃	0	1
DMF	-	X
Toluene	1	1
DCM	0	X
^t BuOH	1	1
ACN	X	10-XI-B
IPA	X	X

Tab. B.21: Precipitation experiments of **10** and resorcinol by rapid cooling from high temperature to 0°C (**PHT**)

Solvent/s	Result
MeOH	0
EtOH	0
Acetone	0
CHCl ₃ /MeOH	0
THF	0
Toluene	0
DCM/MeOH	10-VIII-B
IPA	0
ACN	0
ratio (10:coformer)	1:2

Tab. B.22: Crystallization experiments of **10** and selected cofomers from high temperature to r.t. (**CHT**)

Solvent	Cofomer			
	RE	HI		
MeOH	0	X	X	0
Acetone	0	X	X	0
DCM	1	X	X	X
H ₂ O	0	X	X	X
THF	X	X	0	X
CHCl ₃	X	X	1	X
H ₂ O	X	10-VIII-B	X	X
ratio (10:coformer)	1:1	1:2	1:1	1:2

Tab. B.23: Crystallization experiments of **10** and selected cofomers by solvent evaporation at r.t. (CRT)

Solvent	Cofomer		
	RE	HY	
MeOH	1	-	X
Toluene	1	1	X
ACN	X	X	0
^t BuOH	X	X	0
Dioxane	X	X	-
ratio (10:coformer)	1:1	1:2	1:1

Tab. B.24: Crystallization experiments of **10** and resorcinol in a 1:2 molar ratio by antisolvent diffusion (CAD)

Antisolvent	Solvent								
	MeOH	Acetone	EtOH	IPA	THF	DCM/ MeOH	CHCl ₃ / MeOH	ACN	H ₂ O
Pentane	0	0	0	0	FI of 10 + 10-VIII-B	10-VIII-A	10-VIII-A	10-VIII-B	1

Tab. B.25: Crystallization experiments of **10** and hydroquinone by antisolvent diffusion (CAD)

Antisolvent	Solvent			
	THF	ACN	MeOH	
MEK	1	X	X	X
Pentane	1	FI of 10 + 10-XI-A	1	-
Et ₂ O	1	0	-	-
MTBE	1	X	1	-
DIE	10-XI-A	X	0	-
DCM	-	-	-	-
ratio (10:coformer)	1:1	1:2	1:2	1:2

Preparation of the new multicomponent forms of **10**

- **Cocrystal of **10** : resorcinol, form A (10-VIII-A)**

A mixture of **10** (20.1 mg, 0.04 mmol) and resorcinol (10.0 mg, 0.09 mmol) was dissolved in a solvent mixture of DCM/MeOH 10:1 (1 mL) at 50°C. The solution was cooled down to r.t. and pentane (2 mL) was rapidly added. A white powder precipitated immediately.

- **Cocrystal of **10** : resorcinol, form B (10-VIII-B)**

A mixture of **10** (10.1 mg, 0.02 mmol) and resorcinol (4.8 mg, 0.04 mmol) was dissolved in a water (1.0 mL) at 70°C. The solution was slowly cooled down to r.t. and a white powder crystallized.

- **Cocrystal of **10** : hydroquinone, form A (10-XI-A)**

A mixture of **10** (10.2 mg, 0.02 mmol) and hydroquinone (5.1 mg, 0.04 mmol) with a drop of toluene was grinded for 30 minutes at 30Hz.

- Cocrystal of **10** : hydroquinone, form B (**10-XI-B**)

Compound **10** (12 mg, 0.02 mmol) was added to a saturated solution of hydroquinone in methanol (0.1 mL) at r.t. The suspension was stirred for two days and the solid was filtered and dried under vacuum.

B.7 Compound 12

Tab. B.26: Drop grinding experiments of **12** and selected cofomers (**DG**)

Solvent	Cofomer									
	OA		RE		NA		ISNA		BIP	
DMSO	-	-	0	0	1	1	1	X	1	1
DMF	1	1	0	0	1	1	X	X	1	1
ACN	X	X	X	X	1	1	X	X	1	X
THF	X	X	0	0	X	X	X	X	1	X
H ₂ O	X	X	X	X	X	X	X	X	1	1
Dioxane	X	X	X	X	X	X	X	X	1	X
Acetone	X	X	X	X	X	X	X	X	1	X
ratio (12:coformer)	1:1	1:2	1:1	1:2	1:1	1:2	1:1	1:2	1:1	1:2

Tab. B.27: Reaction crystallization experiments of **12** and selected cofomers (**RC**)

Solvent	Cofomer		
	NA	ISNA	BIP
DMSO	1	1	X
ACN	1	0	X
H ₂ O	X	X	1
TFE	X	X	0

Tab. B.28: Crystallization experiments of **12** and selected cofomers from high temperature to r.t. (**CHT**)

Solvent	Result		
BIP	1	1	X
BIP	1	1	X
PY	X	X	FI of 12
Solvent	DMSO	DMF	-
ratio (12:coformer)	1:1	1:2	-

Tab. B.29: Crystallization experiments of **12** and selected cofomers in a 1:2 molar ratio in DMSO by antisolvent diffusion (**CAD**)

Antisolvent	Cofomer	
	OA	BIP
MeOH	1	1
DIE	-	2 FIV of 12
THF	1	1
Et ₂ O	-	-
Pentane	1	-
MTBE	1	1
DCM	1	1
MEK	1	-
AcOEt	1	1
CHCl ₃	0	1

Preparation of the new forms of **12**

- **Form I of 12**

Form I was obtained from a cocrystallization experiment of **12** with pyridine. Compound **12** (10.0 mg, 0.03 mmol) was dissolved in pyridine (0.5 mL) at 50°C and the solution was cooled down slowly to r.t. A white solid crystallized after one month.

- **Form IV of 12**

The single crystal of form IV was obtained from a cocrystallization experiment of **12** with 4,4'-bipyridine. A mixture of **12** (10.6 mg, 0.03 mmol) and 4,4'-bipyridine (8.8 mg, 0.06 mmol) was dissolved in DMSO (0.8 mL) at 50°C. The vial containing the solution was kept sealed at r.t. and DIE (2 mL) was let to diffuse through a needle. Needle-shaped crystals were obtained after four months.

B.8 Compound 17

Tab. B.30: Crystallization experiments of **17** and selected cofomers by antisolvent diffusion (CAD)

Antisolvent	Cofomer			
	CA	RE	RE	RE
ACN	-	1	0	0
THF	X	X	0	0
MEK	X	X	0	0
AcOEt	2	-	0	0
	17-VII^a	-	0	0
Toluene	X	X	0	0
ratio (17:coformer)	1:1	1:2	1:1	1:2
Solvent	H ₂ O		DMSO	

^aSingle crystal needles of **17** with squaric acid were obtained possibly due to traces of squaric acid from the synthesis of **17**

Preparation of the new forms of **17**

- Salt of **17** : squaric acid (**17-VII**)

The single crystal of this form was obtained from a cocrystallization experiment of **17** (containing traces of squaric acid) with citric acid. A mixture of **17** (10.1 mg, 0.09 mmol) and citric acid (17.3 mg, 0.09 mmol) was dissolved in water at 70°C. The vial containing the solution was kept sealed at r.t. and AcOEt (2 mL) was let to diffuse through a needle. Needle-shaped crystals were obtained after one month.

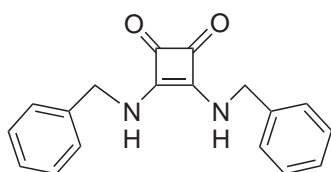
Appendix C

Figures

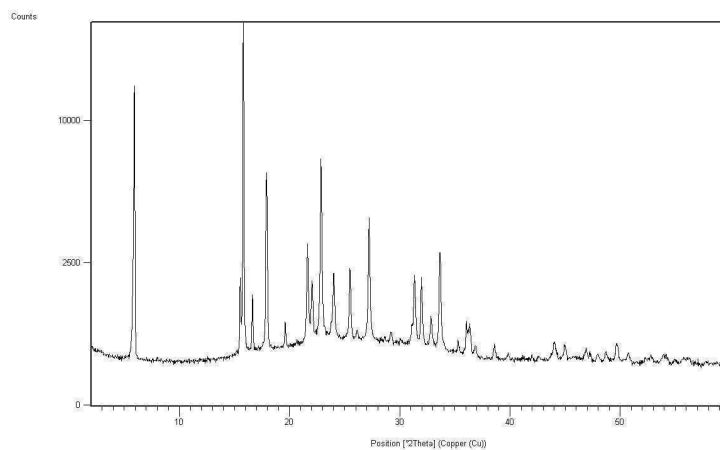
C.1 Polymorphs

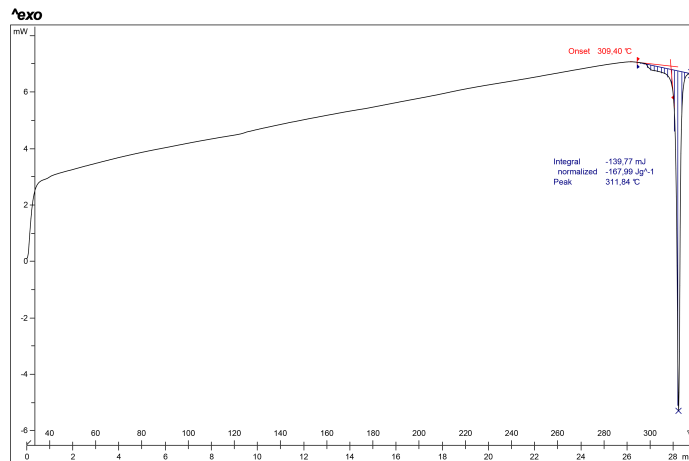
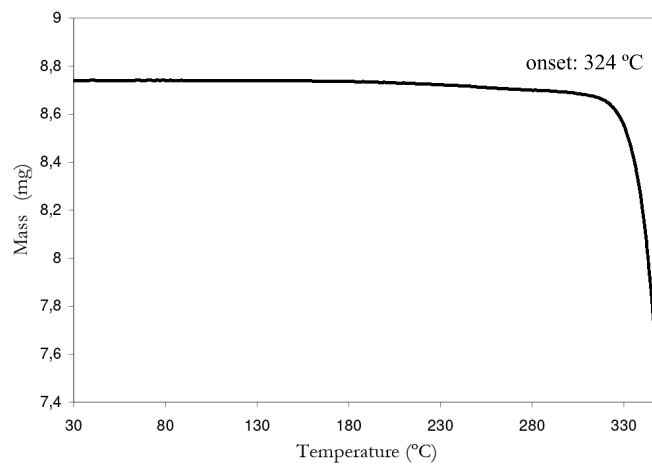
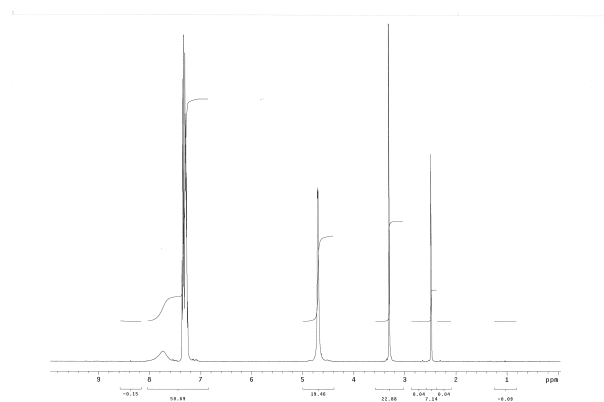
The powder X-ray diffractogram, DSC and TGA thermograms, $^1\text{H-NMR}$ or $^{13}\text{C-NMR}$ spectra and crystallographic data of the new forms obtained in the present work are included in this appendix. In some cases, $^1\text{H-NMR}$, $^{13}\text{C-NMR}$ or TGA data are missing due to lack of sample availability or because the form was sufficiently characterized by the rest of the techniques.

C.1.1 Compound 1, form I

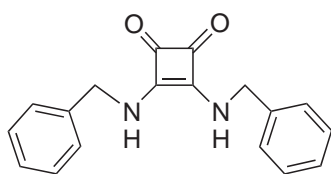
**1**

Structure	Form I of 1
Empirical formula	C ₁₈ H ₁₆ N ₂ O ₂
Formula Weight	292.20
Temperature (K)	293 (2)
Wavelength (Å)	1.7173
Crystal system	Monoclinic
Space group	C2
a, b, c (Å)	11.403(2), 4.401(10), 30.270(6)
α, β, γ (°)	90.0, 100.807(5), 90.0
Volume (Å ³)	1495.2(5)
Z, Density (calc.) (Mg/m ³)	1, 0.325
Absorption coefficient (mm ⁻¹)	0.021
F(000)	154
Crystal size (mm ³)	0.22 x 0.19 x 0.11
θ range for data collection (°)	0.68 to 26.73
Limiting indices	-14<=h<=14, -5<=k<=5, -38<=l<=38
Reflections collected / unique	7998/2327
Completeness to θ (%)	99.9
Absorption correction	Empirical
Max. and min. transmission	0.99 to 0.98
Refinement method	Full-matrix least-squares on F ²
Data/restraints/parameters	3156/ 1/ 225
Goodness-of - fit on F ²	1.057
Final R indices [I > 2σ(I)]	R1 = 0.0613, wR2 = 0.0880
R indices (all data)	R1 = 0.1546, wR2 = 0.1777
Largest diff. peak and hole (e.Å ⁻³)	0.186 to -0.202
CCDC number	676071

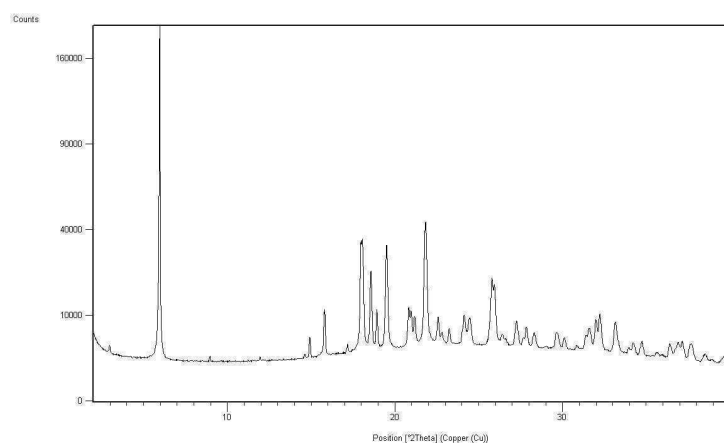
Fig. C.1: Crystallographic data of form I of **1** obtained by SXRDFig. C.2: Powder X-ray diffractogram of form I of **1**

Fig. C.3: DSC thermogram of form I of **1**Fig. C.4: TGA thermogram of form I of **1**Fig. C.5: ¹H-NMR spectrum of form I of **1**

C.1.2 Compound 1, form II

**1**

Structure	Form II of 1
Empirical formula	C ₁₈ H ₁₆ N ₂ O ₂
Formula Weight	292.0
Temperature (K)	293
Wavelength (Å)	1.54175
Crystal system	Monoclinic
Space group	<i>Pc</i>
a, b, c (Å)	29.44215 (4), 5.96429(5), 7.93757 (7)
α, β, γ (°)	90.0, 96.8480 (7), 90.0
Volume (Å ³)	1383.91 (3)
Z, Density (calc.) (Mg/m ³)	4, 1.265
Limiting indices	-
θ range for data collection (°)	2.00 to 69.98
Computer structure refinement	FullProf
Data/restraints/parameters	1675/212/117
Goodness-of - fit	2.92
Final R indices	R=0.028, Rwp= 0.037
CCDC number	914675

Fig. C.6: Crystallographic data of form II of **1** solved by PXRDFig. C.7: Powder X-ray diffractogram of form II of **1**

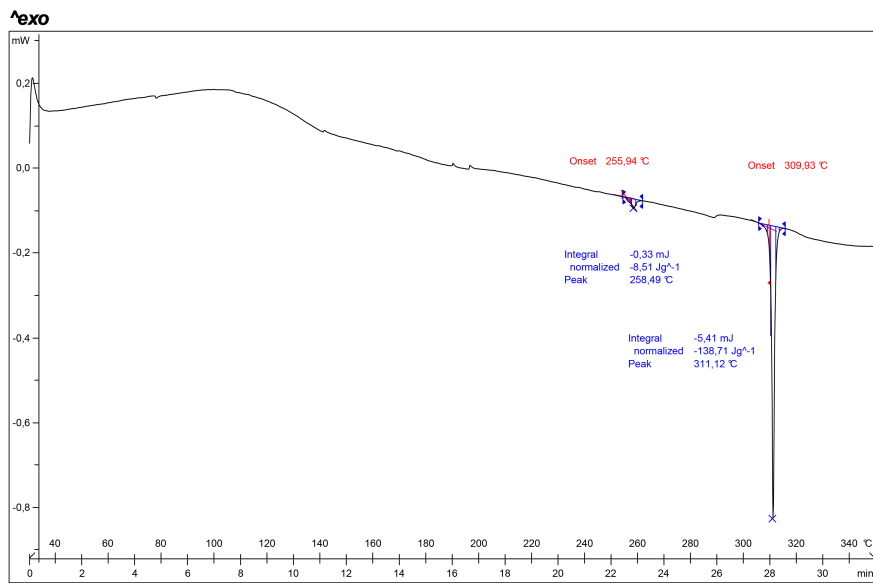


Fig. C.8: DSC thermogram of form II of 1

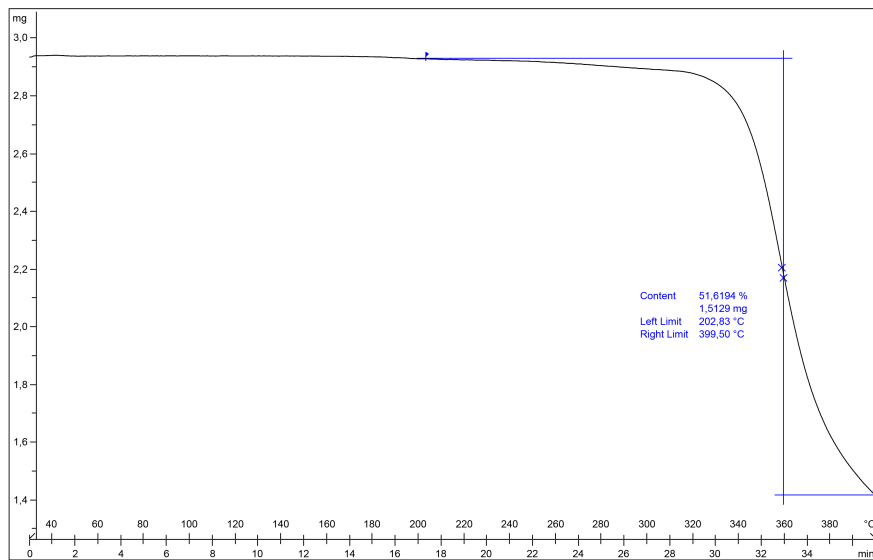
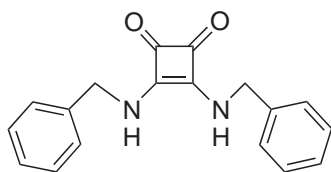


Fig. C.9: TGA thermogram of form II of 1

C.1.3 Compound 1, form III

**1**

Structure	Form III of 1
Empirical formula	C ₁₈ H ₁₆ N ₂ O ₂
Formula Weight	292.33
Temperature (K)	293 (2)
Wavelength (Å)	1.7173
Crystal system	Monoclinic
Space group	C2/c
a, b, c (Å)	30.60(3), 6.035(5), 8.197(4)
α, β, γ (°)	90.0, 96.72(4), 90.0
Volume (Å ³)	1503(2)
Z, Density (calc.) (Mg/m ³)	4, 1.292
Absorption coefficient (mm ⁻¹)	0.085
F(000)	616
Crystal size (mm ³)	0.09 x 0.07 x 0.07
θ range for data collection (°)	1.34 to 32.47
Limiting indices	-42<=h<=46, -7<=k<=9, -12<=l<=12
Reflections collected / unique	6495/2474
Completeness to θ (%)	99.9
Absorption correction	Empirical
Max. and min. transmission	0.99 to 0.98
Refinement method	Full-matrix least-squares on F ²
Data/restraints/parameters	2474/ 1/ 100
Goodness-of-fit on F ²	1.192
Final R indices [I > 2σ(I)]	R1 = 0.072, wR2 = 0.1550
R indices (all data)	R1 = 0.1619, wR2 = 0.1983
Largest diff. peak and hole (e.Å ⁻³)	0.186 to -0.202
CCDC number	686074

Fig. C.10: Crystallographic data of form III of 1 obtained by SXRD

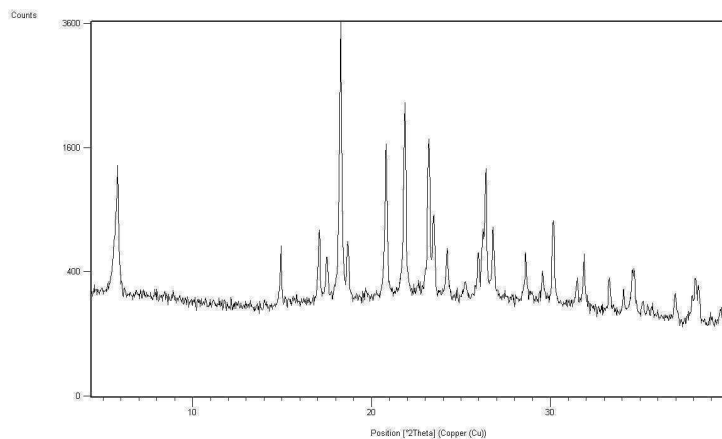
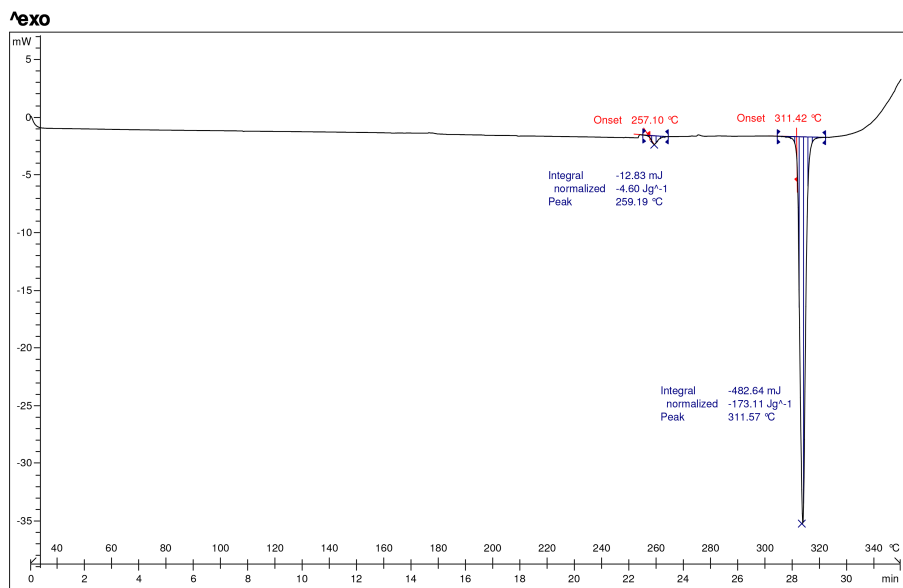
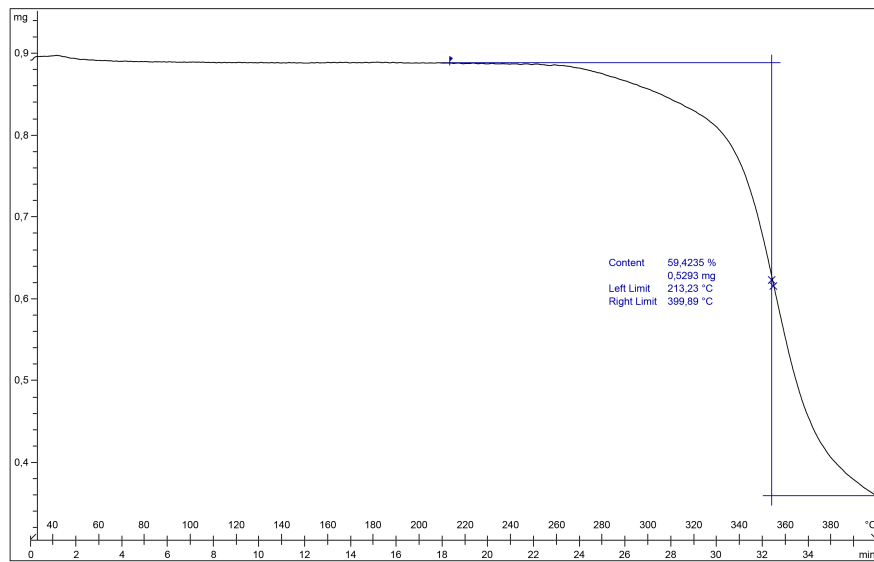
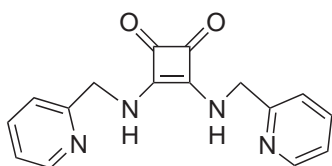


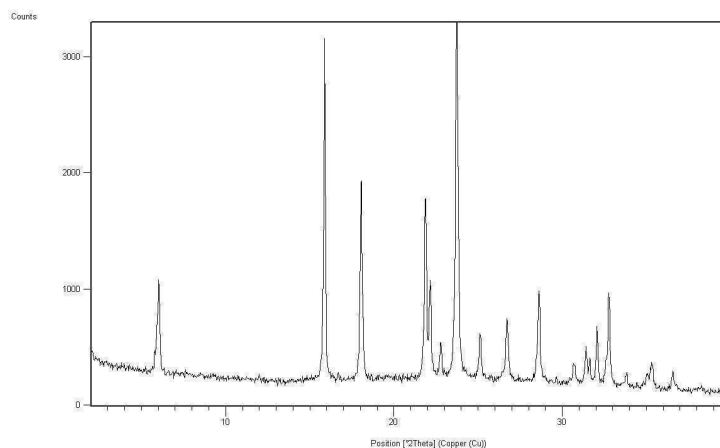
Fig. C.11: Powder X-ray diffractogram of form III of 1

Fig. C.12: DSC thermogram of form III of **1**Fig. C.13: TGA thermogram of form III of **1**

C.1.4 Compound 2, form I

**2**

Structure	Form I of 2
Empirical formula	C ₁₆ H ₁₄ N ₄ O ₂
Formula Weight	155.15
Temperature (K)	293 (2)
Wavelength (Å)	0.71073
Crystal system	Monoclinic
Space group	<i>Pc</i>
a, b, c (Å)	4.358(5), 29.45(3), 6.076(5)
α, β, γ (°)	90, 110.62(8), 90
Volume (Å ³)	729.9(13)
Z, Density (calc.) (Mg/m ³)	2, 1.339
Absorption coefficient (mm ⁻¹)	0.092
F(000)	308
Crystal size (mm ³)	0.2 x 0.2 x 0.09
θ range for data collection (°)	2.77 to 31.86
Limiting indices	-5 ≤ h ≤ 5, -39 ≤ k ≤ 39, -7 ≤ l ≤ 7
Reflections collected / unique	3800/1555
Completeness to θ (%)	90.1
Absorption correction	Empirical
Max. and min. transmission	0.99 and 0.98
Refinement method	Full-matrix least-squares on F ²
Data/restraints/parameters	2185/ 2 /199
Goodness-of-fit on F ²	1.170
Final R indices [I > 2σ(I)]	R1 = 0.0699, wR2 = 0.0930
R indices (all data)	R1 = 0.2093, wR2 = 0.2223
Largest diff. peak and hole (e.Å ⁻³)	0.123 and -0.138
CCDC number	805689

Fig. C.14: Crystallographic data of form I of **2** obtained by SXRFig. C.15: Powder X-ray diffractogram of form I of **2**

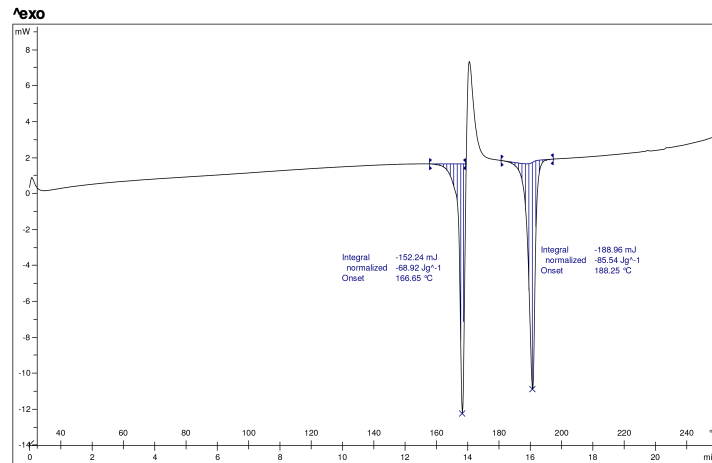


Fig. C.16: DSC thermogram of form I of 2

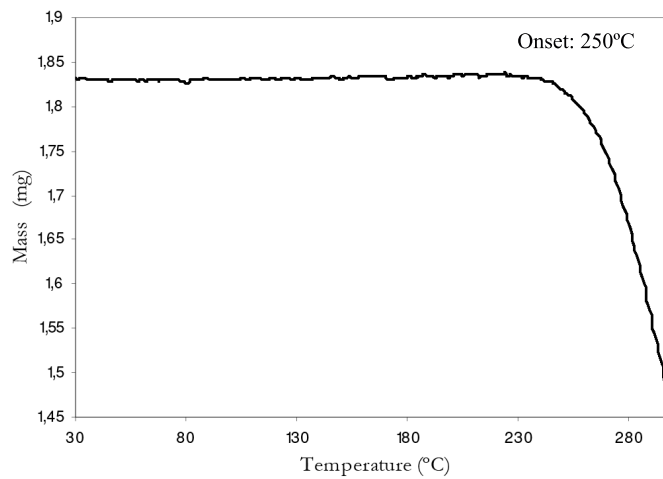
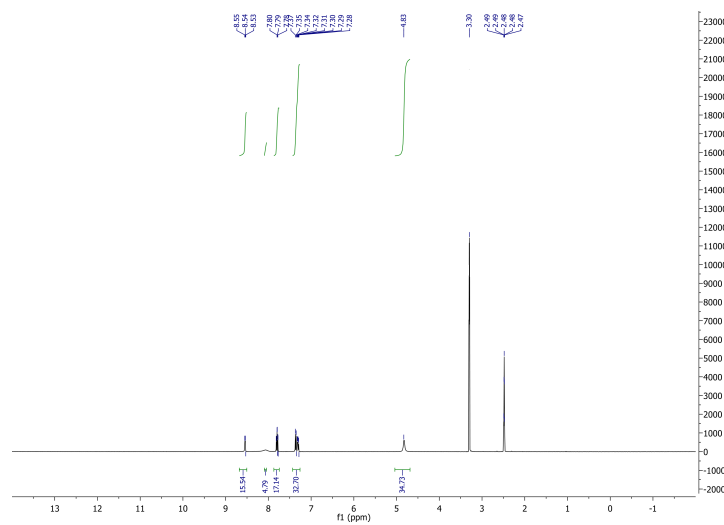
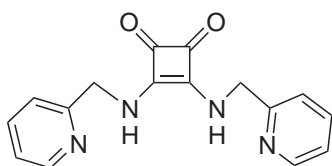


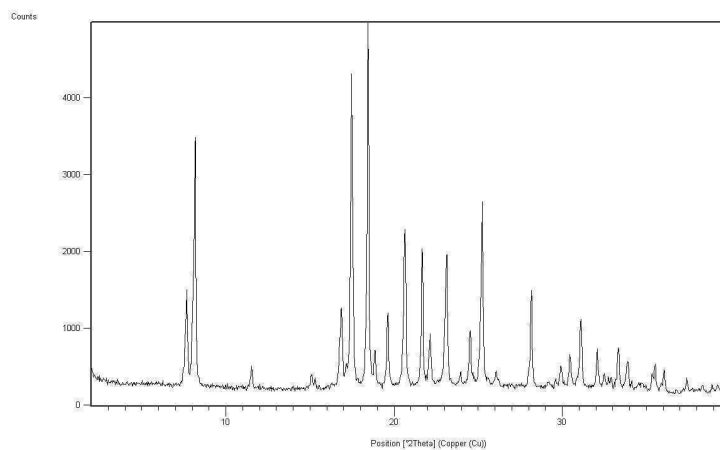
Fig. C.17: TGA thermogram of form I of 2

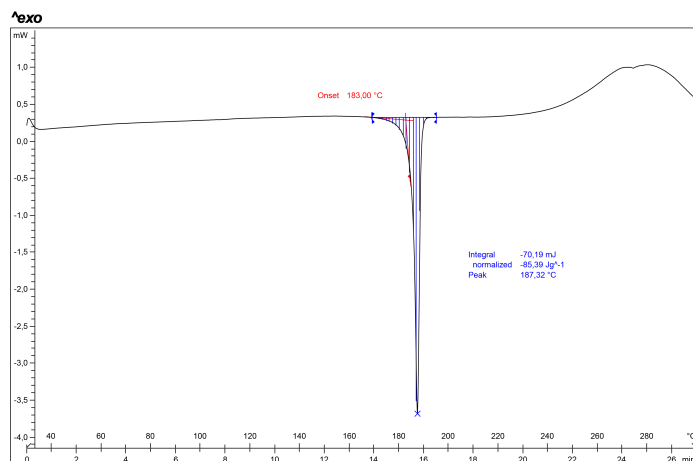
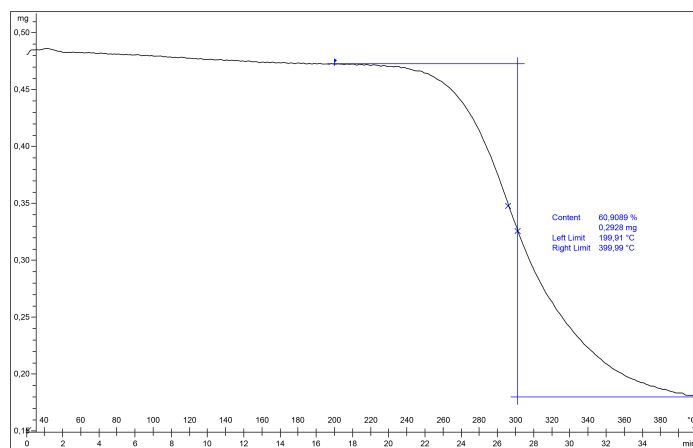
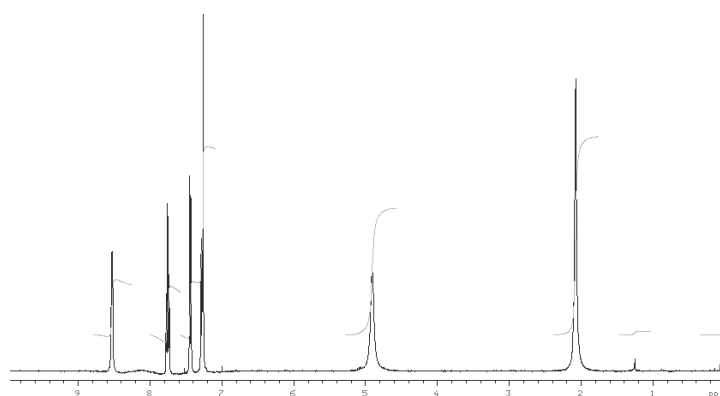
Fig. C.18: $^1\text{H-NMR}$ spectrum of form I of 2

C.1.5 Compound 2, form II

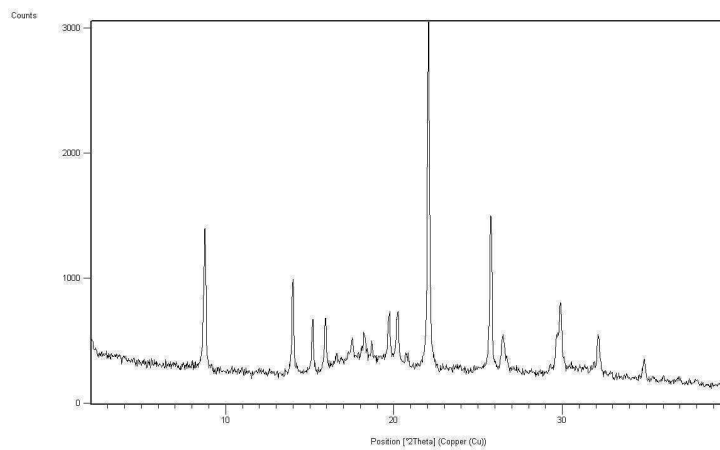
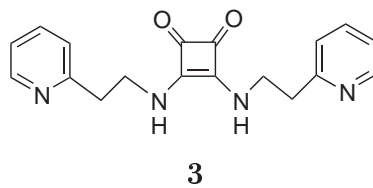
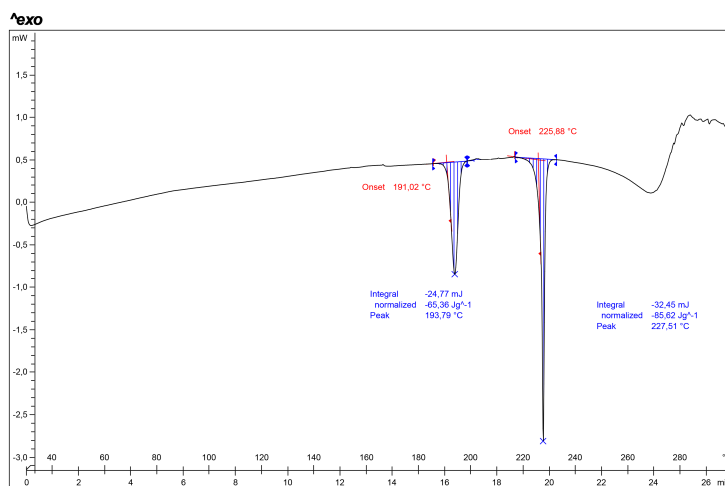
**2**

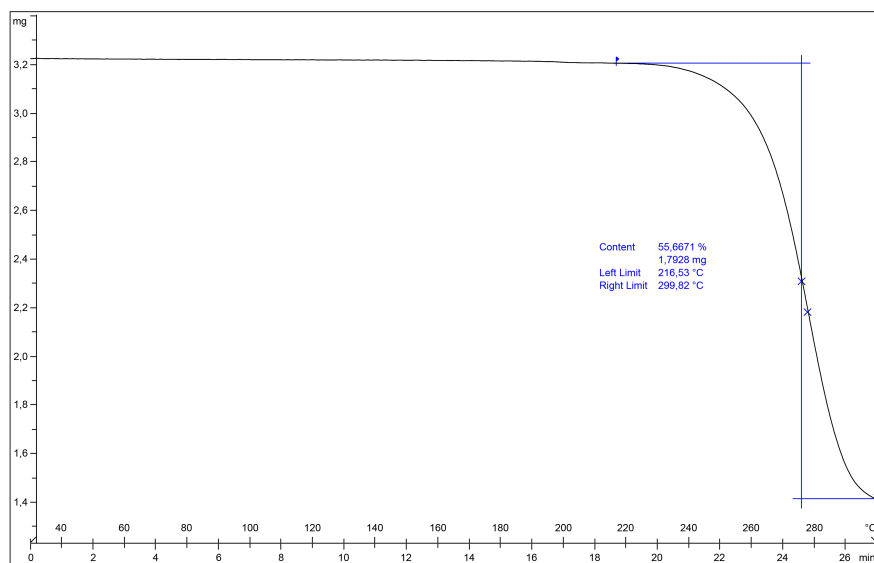
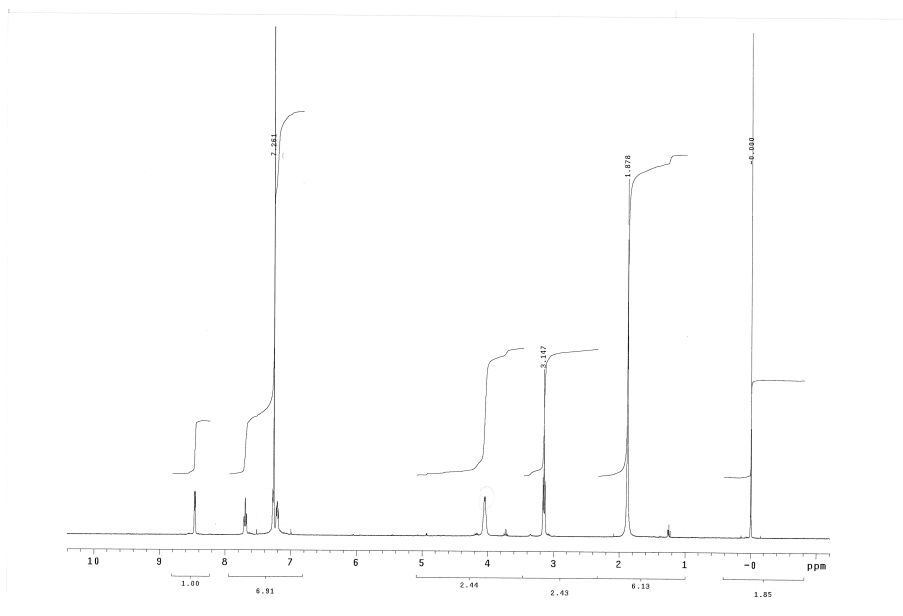
Structure	Form II of 2
Empirical formula	C ₁₆ H ₁₄ N ₄ O ₂
Formula Weight	294.31
Temperature (K)	293
Wavelength (Å)	1.5406
Crystal system	Triclinic
Space group	<i>P</i> -1
a, b, c (Å)	6.03426(25), 10.9211(5), 11.9179(6)
α , β , γ (°)	93.0202(26), 103.1757(26), 92.4776(34)
Volume (Å ³)	762.42(8)
Z, Density (calc.) (Mg/m ³)	4, 1.351
Limiting indices	0 ≤ h < 4, -8 ≤ k ≤ 8, -8 ≤ l ≤ 8
θ range for data collection (°)	4.17 to 69.91
Computer structure refinement	GSAS
Data/restraints/parameters	1304/122/167
Goodness-of-fit	2.30
Final R indices	R=0.0527, Rwp= 0.0757
CCDC number	805689

Fig. C.19: Crystallographic data of form II of **2** solved by PXRDFig. C.20: Powder X-ray diffractogram of form II of **2**

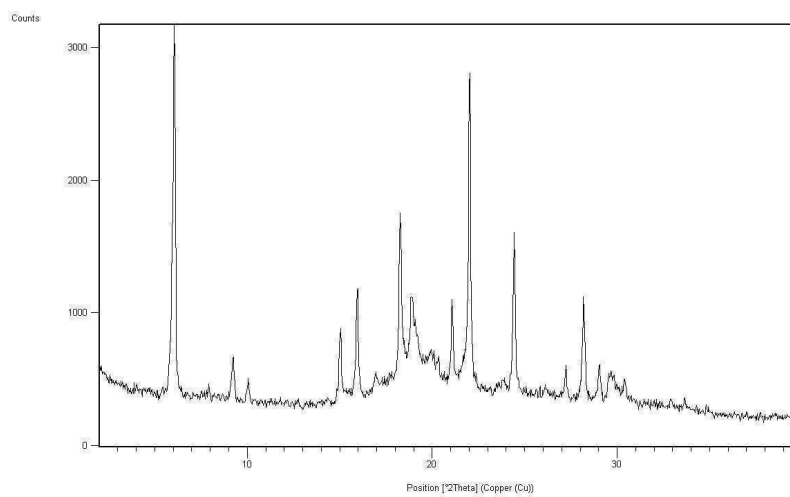
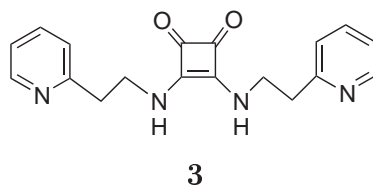
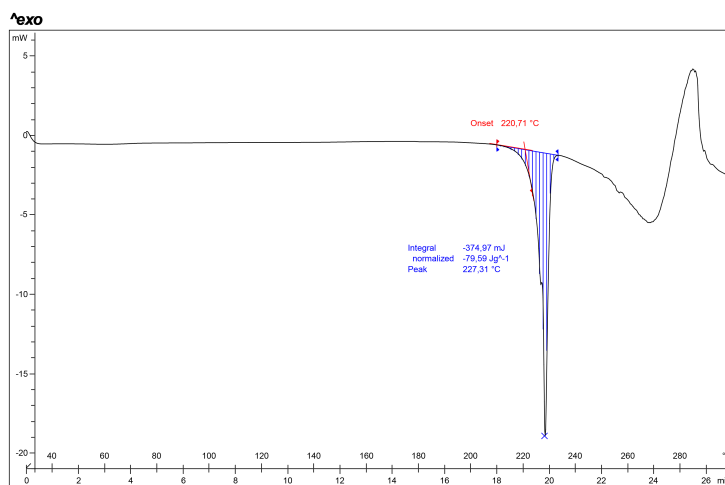
Fig. C.21: DSC thermogram of form II of **2**Fig. C.22: TGA thermogram of form II of **2**Fig. C.23: ¹H-NMR spectrum of form II of **2**

C.1.6 Compound 3, form I

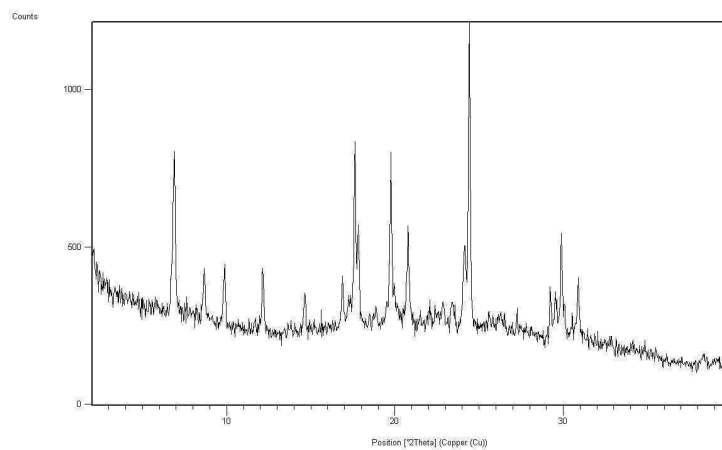
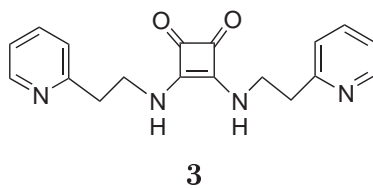
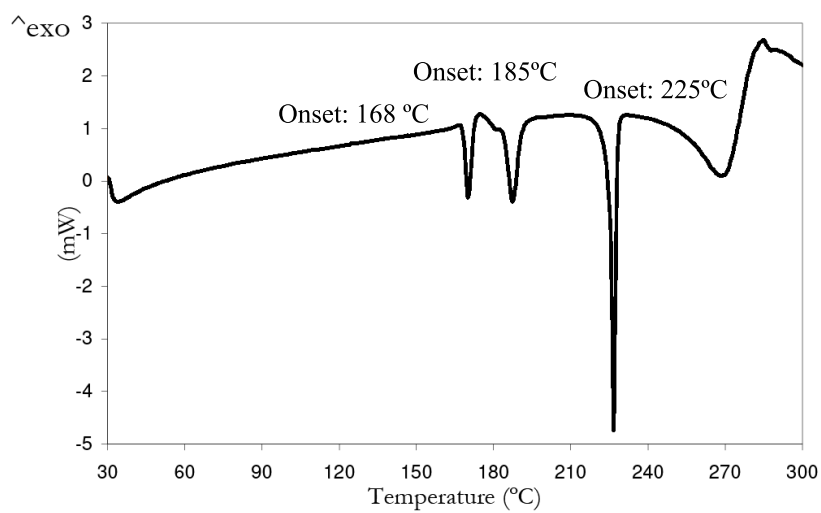
Fig. C.24: Powder X-ray diffractogram of form I of **3**Fig. C.25: DSC thermogram of form I of **3**

Fig. C.26: TGA thermogram of form I of **3**Fig. C.27: ¹H-NMR spectrum of form I of **3**

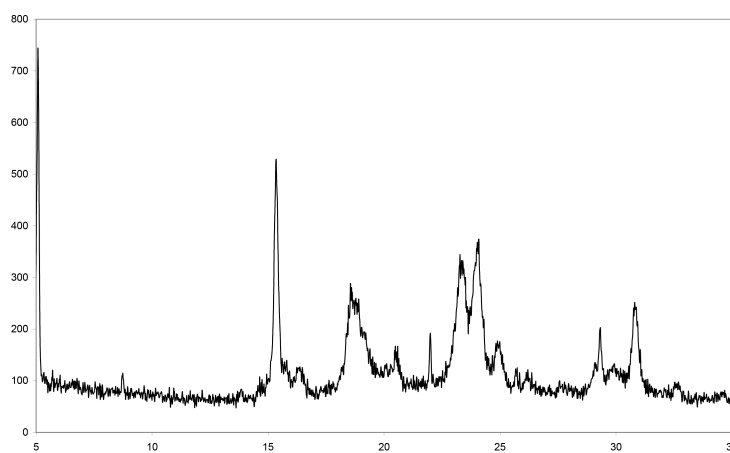
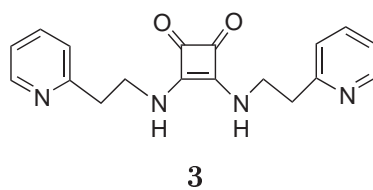
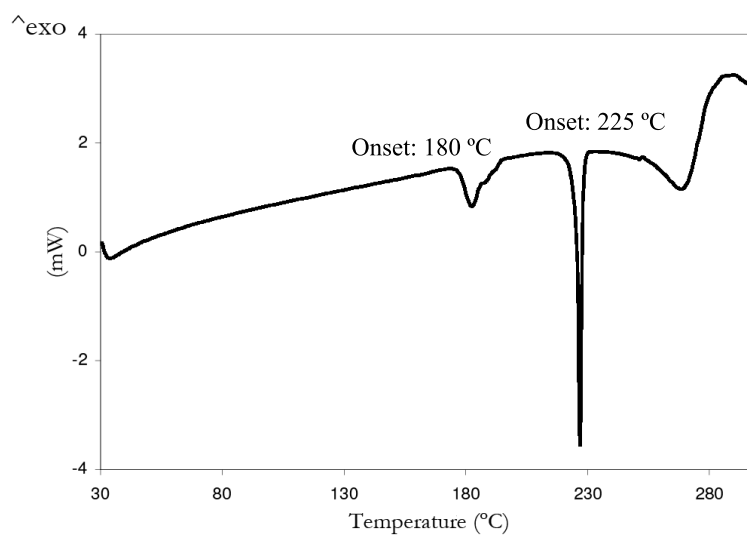
C.1.7 Compound 3, form II

Fig. C.28: Powder X-ray diffractogram of form II of **3**Fig. C.29: DSC thermogram of form II of **3**

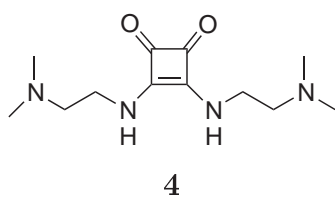
C.1.8 Compound 3, form III

Fig. C.30: Powder X-ray diffractogram of form III of **3**Fig. C.31: DSC thermogram of form III of **3**

C.1.9 Compound 3, form IV

Fig. C.32: Powder X-ray diffractogram of form IV of **3**Fig. C.33: DSC thermogram of form IV of **3**

C.1.10 Compound 4, form II



Structure	Form II of 4
Empirical formula	C ₁₂ H ₂₀ N ₄ O ₂
Formula Weight	254.34
Temperature (K)	293
Wavelength (Å)	1.54175
Crystal system	Monoclinic
Space group	<i>P2₁/c</i>
a, b, c (Å)	16.6744(11), 14.6385(8), 16.3611(3)
α, β, γ (°)	90.0, 158.826(4), 90.0
Volume (Å ³)	1442.489(15)
Z, Density (calc.) (Mg/m ³)	4, 1.171
Limiting indices	-
θ range for data collection (°)	2.01 to 69.98
Computer structure refinement	FullProf
Data/restraints/parameters	1395/112/68
Goodness-of-fit	12.8
Final R indices	R=2.6967, Rwp= 3.7524
CCDC number	1016996

Fig. C.34: Crystallographic data of form II of **4** solved by PXRD

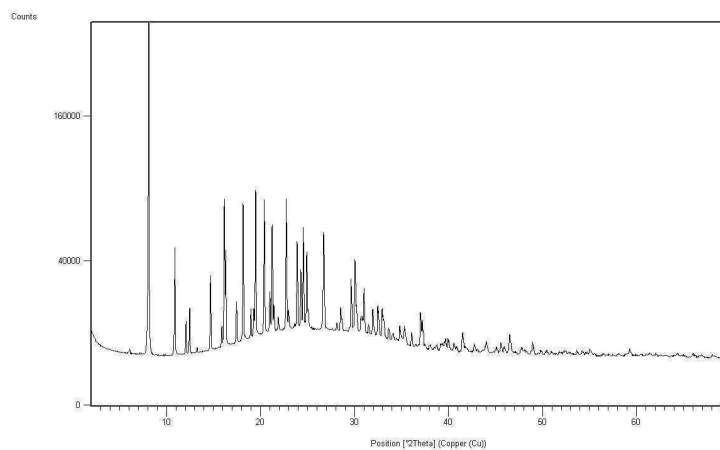


Fig. C.35: Powder X-ray diffractogram of form II of **4**

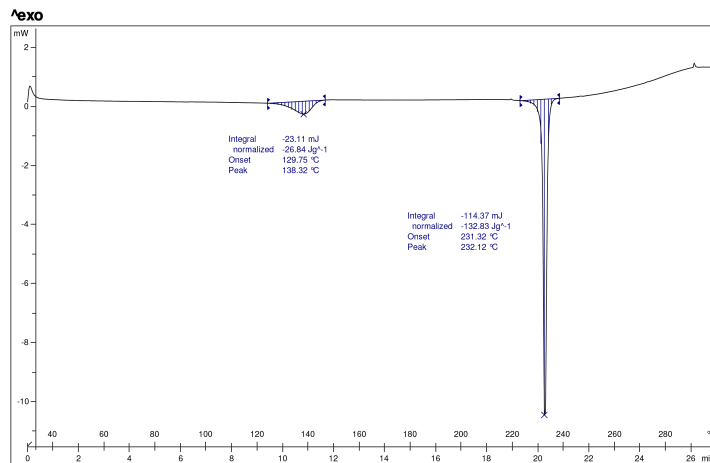


Fig. C.36: DSC thermogram of form II of 4

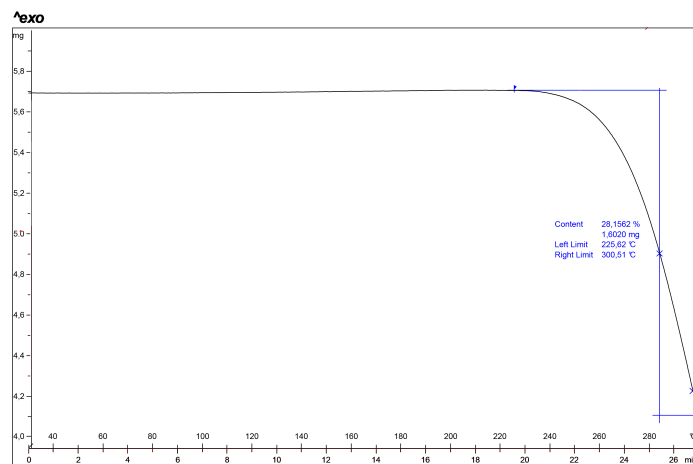
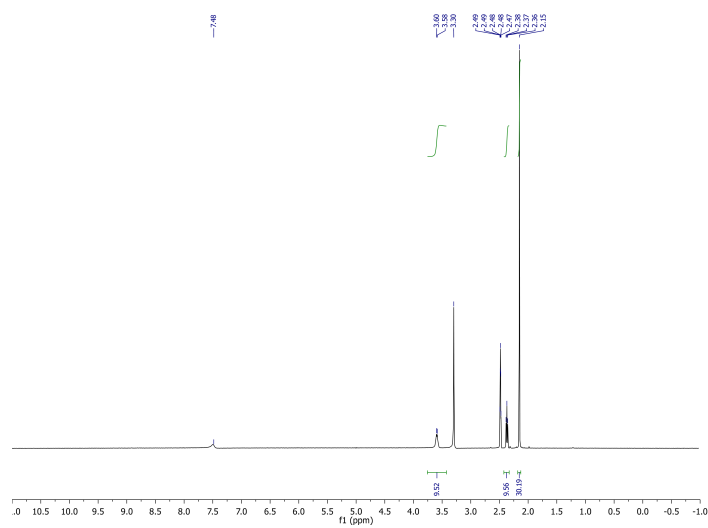
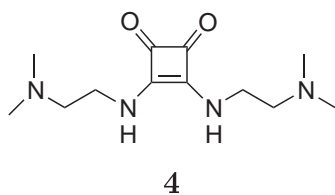


Fig. C.37: TGA thermogram of form II of 4

Fig. C.38: $^1\text{H-NMR}$ spectrum of form II of 4

C.1.11 Compound 4, form III



Structure	Form III of 4
Empirical formula	C ₁₂ H ₂₂ N ₄ O ₂
Formula Weight	254.34
Temperature (K)	293 (2)
Wavelength (Å)	0.71073
Crystal system	Orthorhombic
Space group	Fdd2
a, b, c (Å)	16.185(14), 29.012(18), 6.093(4)
α, β, γ (°)	90, 90, 90
Volume (Å ³)	2861(4)
Z, Density (calc.) (Mg/m ³)	8, 1.181
Absorption coefficient (mm ⁻¹)	0.083
F(000)	1104
Crystal size (mm ³)	0.2 x 0.1 x 0.1
θ range for data collection (°)	2.81 to 32.42
Limiting indices	-22<=h<=24, -43<=k<=42, -8<=l<=8
Reflections collected / unique	5245/1961
Completeness to θ (%)	99.6
Absorption correction	Empirical
Max. and min. transmission	0.99 and 0.98
Refinement method	Full-matrix least-squares on F ²
Data/restraints/parameters	1961/ 4 /85
Goodness-of-fit on F ²	1.137
Final R indices [I > 2σ(I)]	R1 = 0.0695, wR2 = 0.1901
R indices (all data)	R1 = 0.0950, wR2 = 0.2027
Largest diff. peak and hole (e.Å ⁻³)	0.299 and -0.163
CCDC number	1015652

Fig. C.39: Crystallographic data of form III of 4 obtained by SXRD

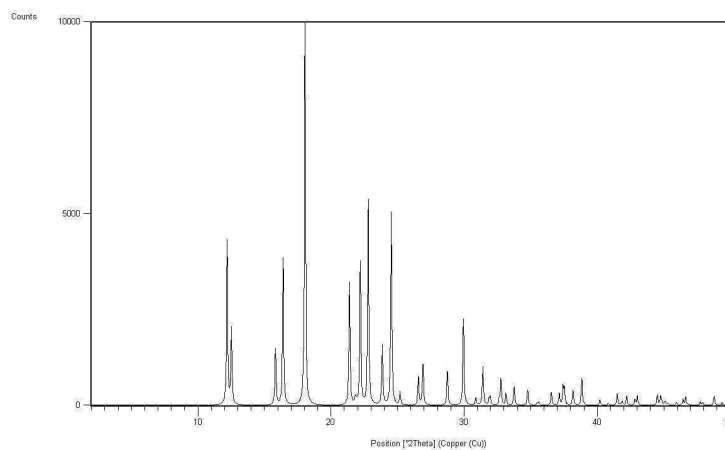


Fig. C.40: Calculated powder X-ray diffractogram of form III of 4

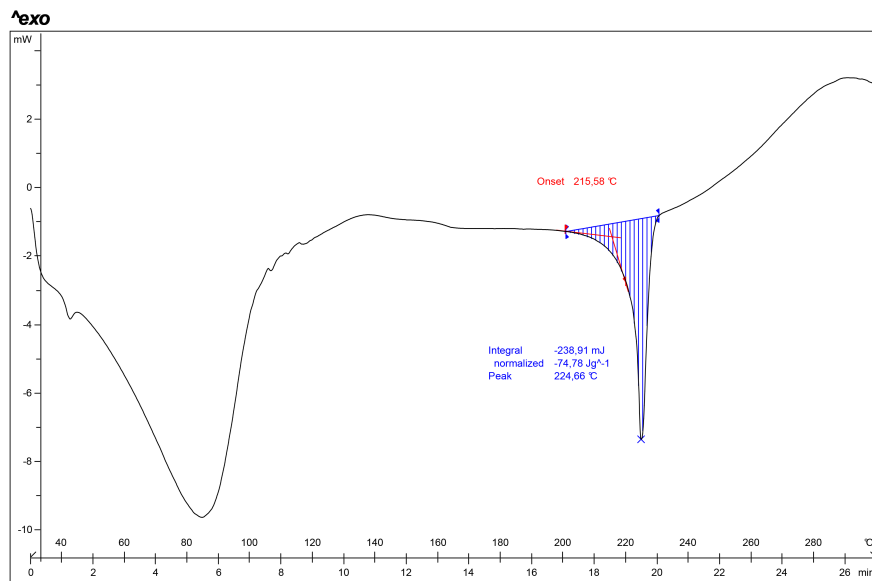


Fig. C.41: DSC thermogram of form III of 4

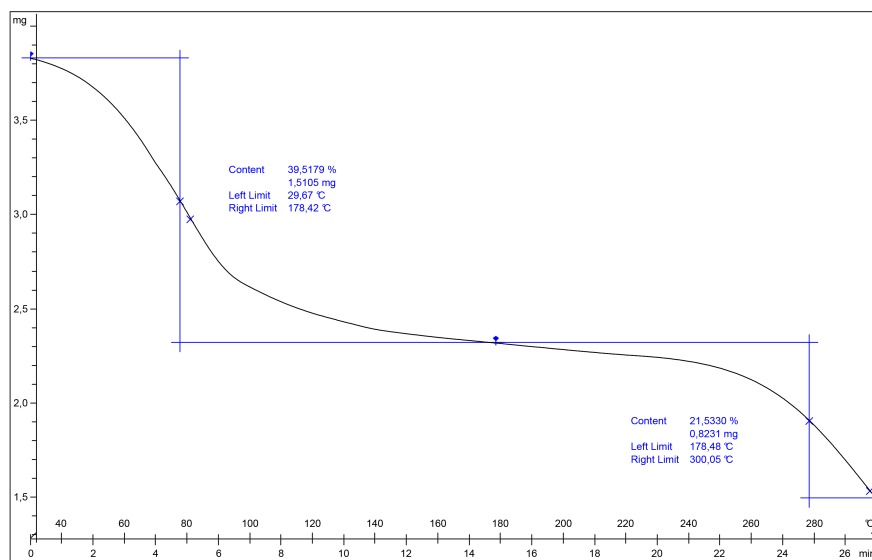
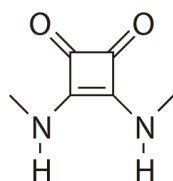


Fig. C.42: TGA thermogram of form III of 4 (The weight loss registered in the TGA analysis is attributed to a wet solid)

C.1.12 Compound 5, form I



5

Structure	Form I of 5
Empirical formula	C ₆ H ₈ N ₂ O ₂
Formula Weight	140.14
Temperature (K)	293 (2)
Wavelength (Å)	0.71073
Crystal system	Monoclinic
Space group	<i>P</i> 2 ₁ / <i>c</i>
a, b, c (Å)	6.087(4), 7.307(3), 16.041(8)
α, β, γ (°)	90, 109.98(3), 90
Volume (Å ³)	670.5(6)
Z, Density (calc.) (Mg/m ³)	4, 1.388
Absorption coefficient (mm ⁻¹)	0.106
F(000)	296
Crystal size (mm ³)	0.2 x 0.1 x 0.1
θ range for data collection (°)	3.10 to 30.47
Limiting indices	-7<=h<=7, -9<=k<=9, -20<=l<=20
Reflections collected / unique	4842/1619
Completeness to θ (%)	94.7
Absorption correction	none
Max. and min. transmission	0.99 and 0.98
Refinement method	Full-matrix least-squares on F ²
Data/restraints/parameters	1619/ 5 /92
Goodness-of-fit on F ²	1.098
Final R indices [I > 2σ(I)]	R1 = 0.0344, wR2 = 0.0920
R indices (all data)	R1 = 0.0374, wR2 = 0.0937
Largest diff. peak and hole (e.Å ⁻³)	0.135 and -0.110
CCDC number	865057

Fig. C.43: Crystallographic data of form I of 5 obtained by SXRD

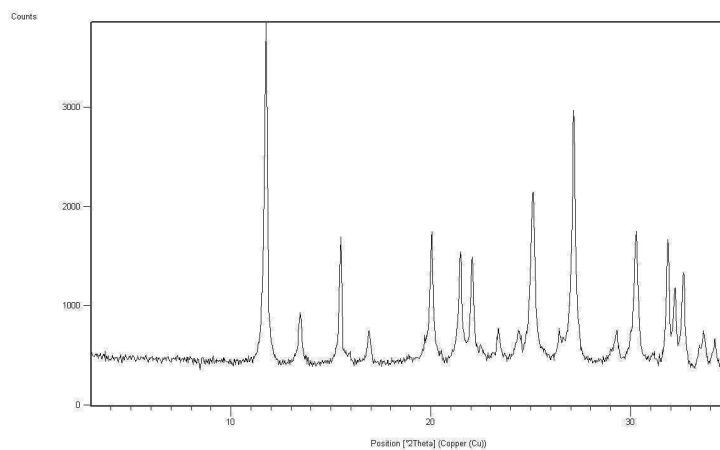
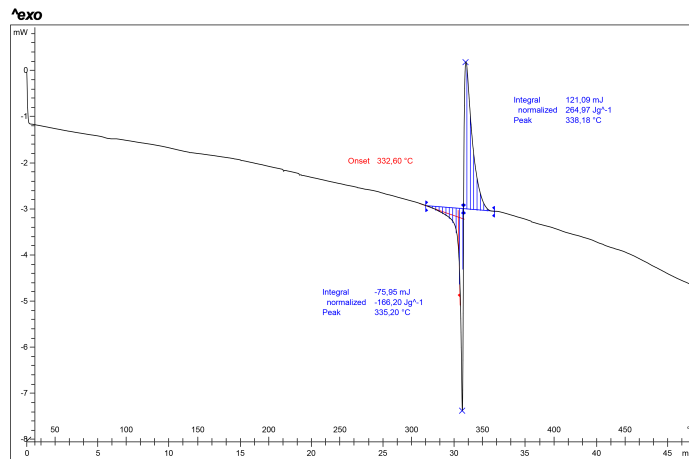
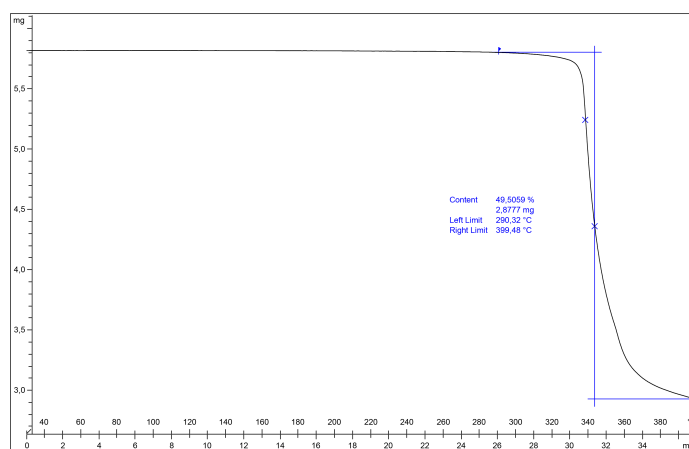
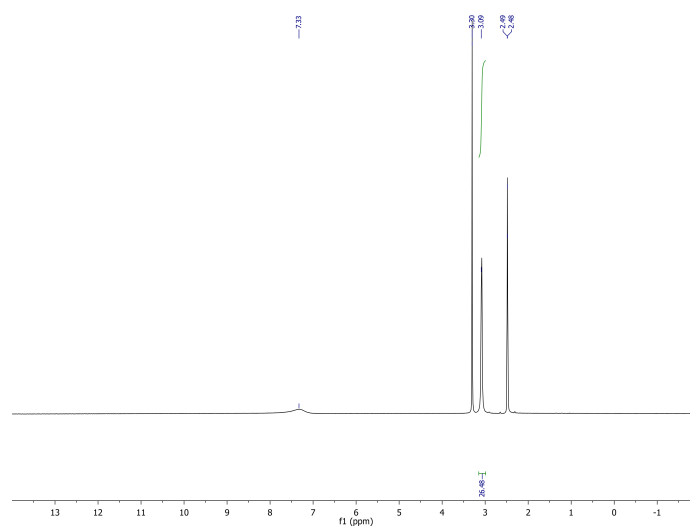
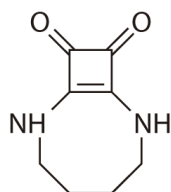


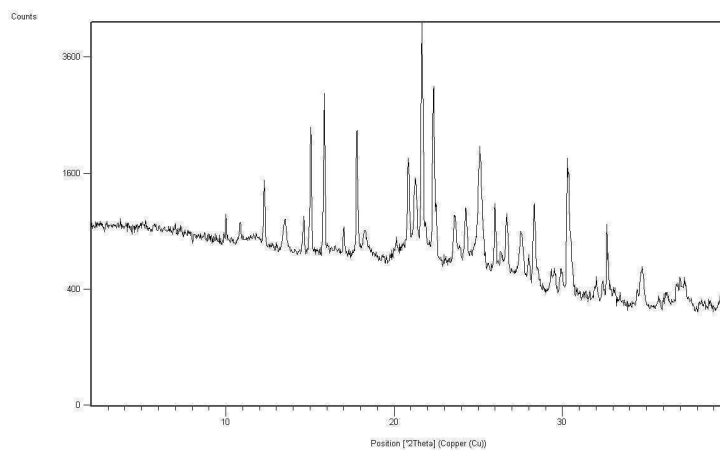
Fig. C.44: Powder X-ray diffractogram of form I of 5

Fig. C.45: DSC thermogram of form I of **5**Fig. C.46: TGA thermogram of form I of **5**Fig. C.47: ¹H-NMR spectrum of form I of **5**

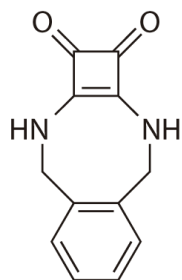
C.1.13 Compound 6, form I

**6**

Structure	Form I of 6
Empirical formula	C ₈ H ₁₀ N ₂ O ₂
Formula Weight	166.18
Temperature (K)	105 (2)
Wavelength (Å)	0.71073
Crystal system	Monoclinic
Space group	<i>P</i> 2 ₁ / <i>a</i>
a, b, c (Å)	4.995(4), 11.203(7), 14.389(8)
α, β, γ (°)	90, 90.44(4), 90
Volume (Å ³)	802.8(9)
Z, Density (calc.) (Mg/m ³)	4, 1.375
Absorption coefficient (mm ⁻¹)	0.101
F(000)	352
Crystal size (mm ³)	0.2 x 0.1 x 0.1
θ range for data collection (°)	2.31 to 32.45
Limiting indices	-7 ≤ h ≤ 6, -16 ≤ k ≤ 15, -21 ≤ l ≤ 21
Reflections collected / unique	6377/2422
Completeness to θ (%)	99.0
Absorption correction	Empirical
Max. and min. transmission	0.99 and 0.98
Refinement method	Full-matrix least-squares on F ²
Data/restraints/parameters	2422/ 0 /109
Goodness-of-fit on F ²	1.099
Final R indices [I > 2σ(I)]	R1 = 0.0470, wR2 = 0.0882
R indices (all data)	R1 = 0.0757, wR2 = 0.0972
Largest diff. peak and hole (e.Å ⁻³)	0.111 and -0.144
CCDC number	865058

Fig. C.48: Crystallographic data of form I of **6** obtained by SXRDFig. C.49: Powder X-ray diffractogram of form I of **6**

C.1.14 Compound 7, form I



7

Structure	Form I of 7
Empirical formula	C ₁₂ H ₁₀ N ₂ O ₂
Formula Weight	214.22
Temperature (K)	293 (2)
Wavelength (Å)	0.71073
Crystal system	Orthorhombic
Space group	<i>Pnma</i>
a, b, c (Å)	18.938(19), 11.841(11), 4.309(6)
α, β, γ (°)	90, 90, 90
Volume (Å ³)	966.3(19)
Z, Density (calc.) (Mg/m ³)	4, 1.473
Absorption coefficient (mm ⁻¹)	0.103
F(000)	448
Crystal size (mm ³)	0.2 x 0.08 x 0.07
θ range for data collection (°)	2.15 to 32.38
Limiting indices	-28<=h<=25, -17<=k<=17, -5<=l<=5
Reflections collected / unique	8451/1664
Completeness to θ (%)	96.9
Absorption correction	Empirical
Max. and min. transmission	0.90 and 0.89
Refinement method	Full-matrix least-squares on F ²
Data/restraints/parameters	1664/ 3 /73
Goodness-of-fit on F ²	1.180
Final R indices [I > 2σ(I)]	R1 = 0.0764, wR2 = 0.1836
R indices (all data)	R1 = 0.1362, wR2 = 0.2100
Largest diff. peak and hole (e.Å ⁻³)	0.184 and -0.423
CCDC number	865059

Fig. C.53: Crystallographic data of form I of 7 obtained by SXRD

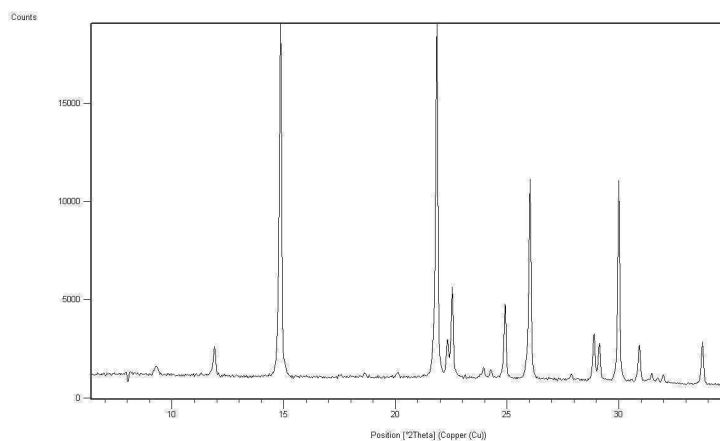
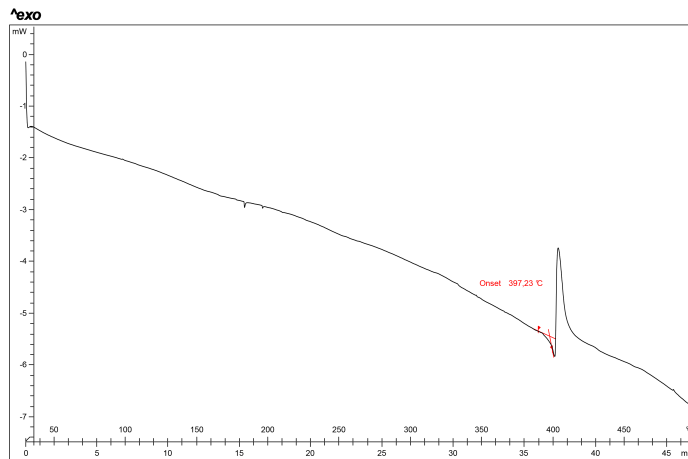
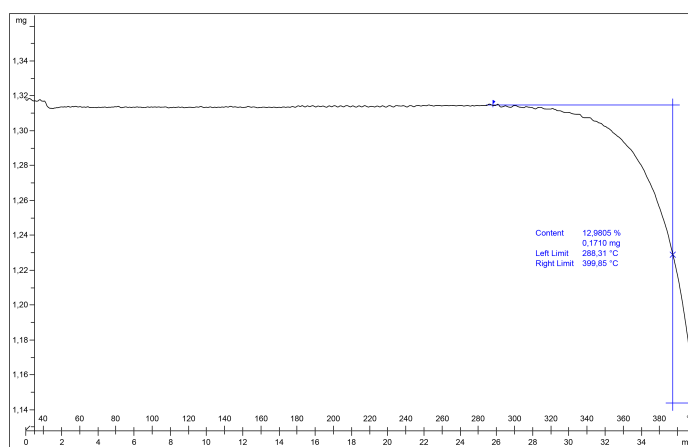
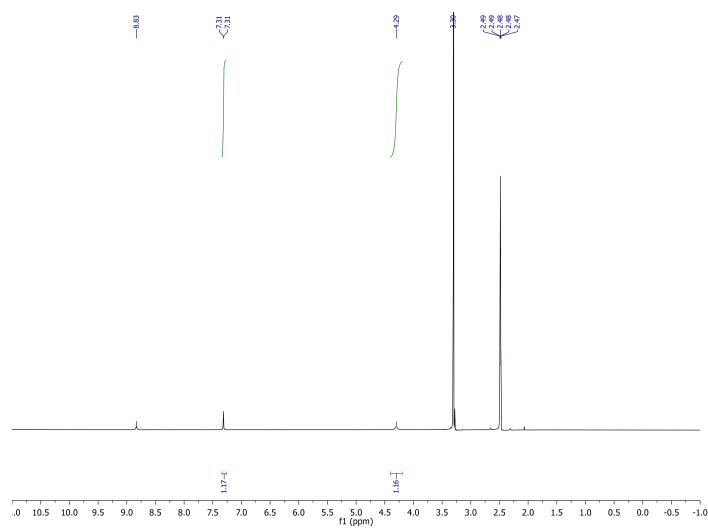
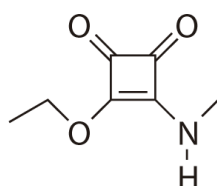


Fig. C.54: Powder X-ray diffractogram of form I of 7

Fig. C.55: DSC thermogram of form I of **7**Fig. C.56: TGA thermogram of form I of **7**Fig. C.57: ¹H-NMR spectrum of form I of **7**

C.1.15 Compound 8, form I



8

Structure	Form I of 8
Empirical formula	C ₇ H ₉ N O ₃
Formula Weight	155.15
Temperature (K)	293 (2)
Wavelength (Å)	0.71073
Crystal system	Triclinic
Space group	P-1
a, b, c (Å)	7.619(14), 7.888(11), 8.147(9)
α, β, γ (°)	65.33(9), 66.81(8), 72.58(10)
Volume (Å ³)	403.6(10)
Z, Density (calc.) (Mg/m ³)	2, 1.277
Absorption coefficient (mm ⁻¹)	0.101
F(000)	164
Crystal size (mm ³)	0.2 x 0.09 x 0.09
θ range for data collection (°)	2.88 to 32.29
Limiting indices	-11 ≤ h ≤ 11, -9 ≤ k ≤ 11, -12 ≤ l ≤ 11
Reflections collected / unique	3151/1938
Completeness to θ (%)	90.1
Absorption correction	Empirical
Max. and min. transmission	0.99 and 0.98
Refinement method	Full-matrix least-squares on F ²
Data/restraints/parameters	1938/ 3 /109
Goodness-of - fit on F ²	1.134
Final R indices [I > 2σ(I)]	R1 = 0.0746, wR2 = 0.1674
R indices (all data)	R1 = 0.1378, wR2 = 0.1910
Largest diff. peak and hole (e.Å ⁻³)	0.123 and -0.138
CCDC number	865060

Fig. C.58: Crystallographic data of form I of 8 obtained by SXRD

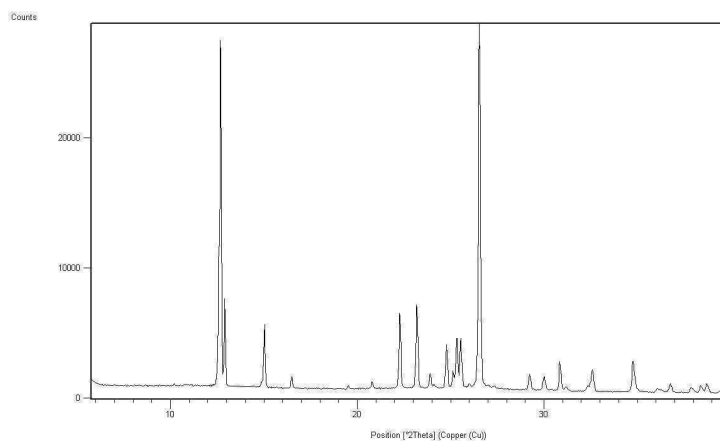


Fig. C.59: Powder X-ray diffractogram of form I of 8

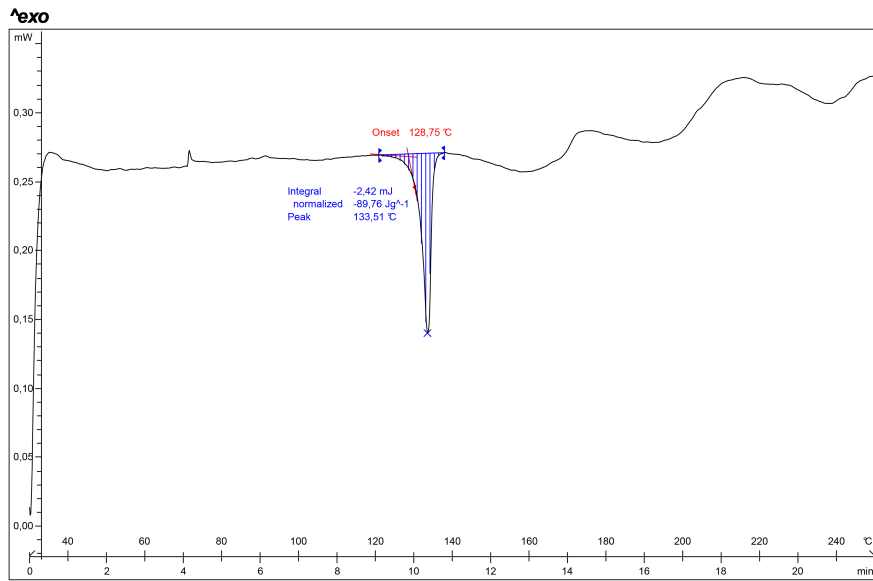


Fig. C.60: DSC thermogram of form I of 8

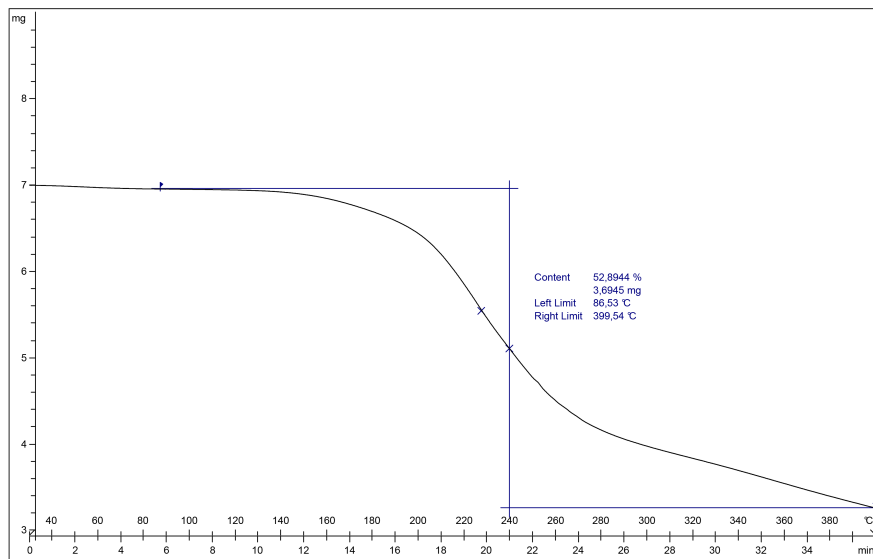
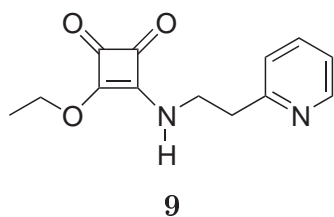


Fig. C.61: TGA thermogram of form I of 8

C.1.16 Compound 9, form I



Structure	Form I of 9
Empirical formula	C ₁₇ H ₁₄ N ₂ O ₂
Formula Weight	246.26
Temperature (K)	293 (2)
Wavelength (Å)	0.7173
Crystal system	Monoclinic
Space group	P2 ₁ /n
a, b, c (Å)	7.435(5), 14.028(7), 12.008(6)
α, β, γ (°)	90.0, 92.07(3), 90.0
Volume (Å ³)	1251.6(12)
Z, Density (calc.) (Mg/m ³)	4, 1.307
Absorption coefficient (mm ⁻¹)	0.094
F(000)	520
Crystal size (mm ³)	0.09 x 0.08 x 0.07
θ range for data collection (°)	2.90 to 30.33
Limiting indices	-8<=h<=8, -18<=k<=18, -16<=l<=16
Reflections collected / unique	11149/3058
Completeness to θ (%)	94.4
Absorption correction	none
Max. and min. transmission	0.99 to 0.98
Refinement method	Full-matrix least-squares on F ²
Data/restraints/parameters	3058/ 3/ 164
Goodness-of-fit on F ²	1.160
Final R indices [I > 2σ(I)]	R1 = 0.0475, wR2 = 0.1278
R indices (all data)	R1 = 0.0536, wR2 = 0.1312
Largest diff. peak and hole (e.Å ⁻³)	0.200 to -0.305
CCDC number	883964

Fig. C.62: Crystallographic data of form I of 9 obtained by SXRD

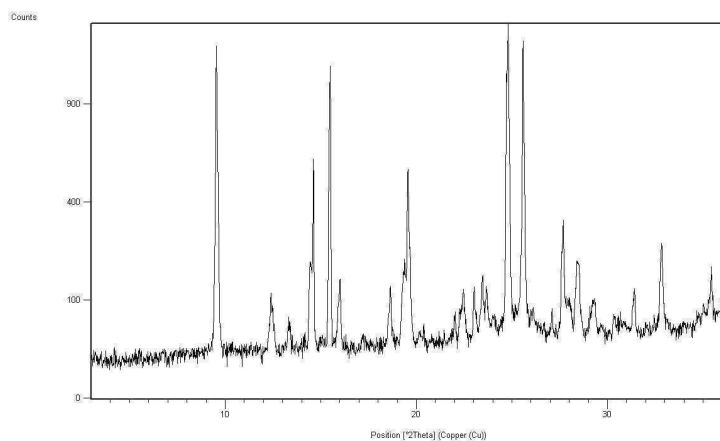
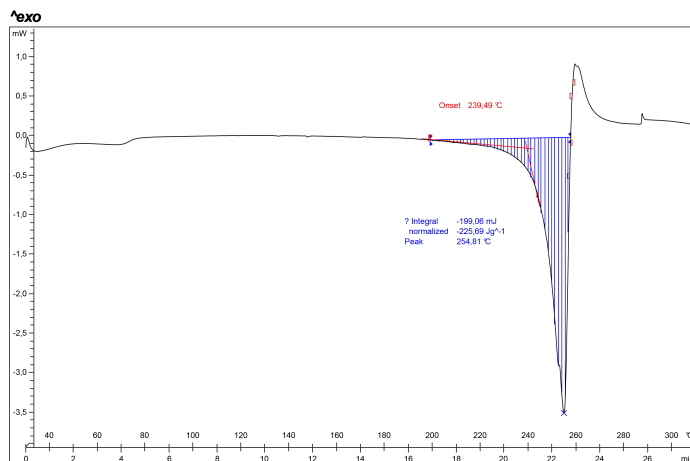
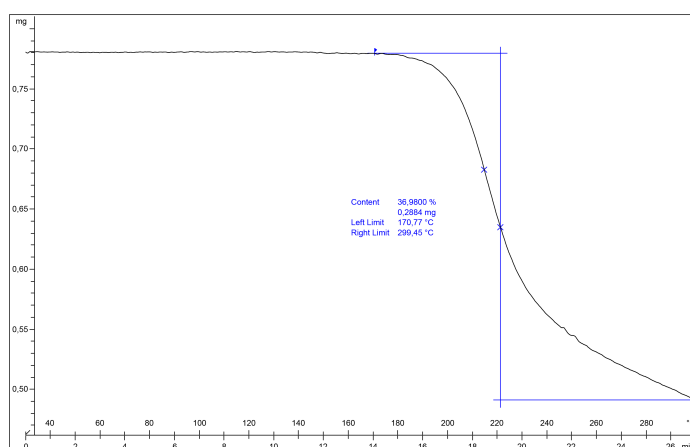
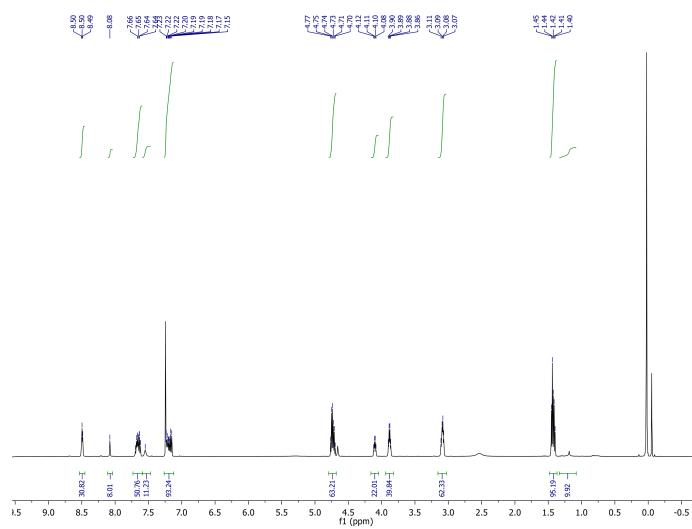
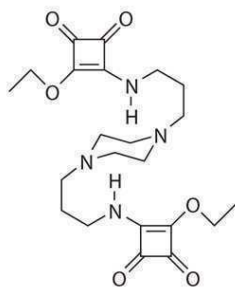


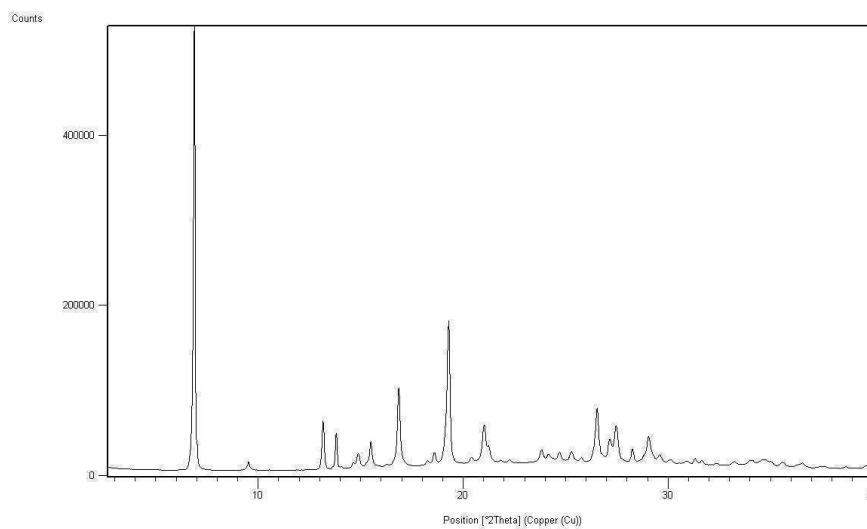
Fig. C.63: Powder X-ray diffractogram of form I of 9

Fig. C.64: DSC thermogram of form I of **9**Fig. C.65: TGA thermogram of form I of **9**Fig. C.66: ¹H-NMR spectrum of form I of **9**

C.1.17 Compound 10, form I

**10**

Structure	Form I of 10
Empirical formula	C ₂₂ H ₃₂ N ₄ O ₆
Formula Weight	448
Temperature (K)	293
Wavelength (Å)	1.54175
Crystal system	Monoclinic
Space group	<i>P2₁/c</i>
a, b, c (Å)	16.37064 (12), 10.00640(6), 7.27971(3)
α, β, γ (°)	90.0, 98.8213(5), 90.0
Volume (Å ³)	1178.392(12)
Z, Density (calc.) (Mg/m ³)	2, 1.263
Limiting indices	-
θ range for data collection (°)	4.01 to 69.98
Computer structure refinement	FullProf
Data/restraints/parameters	1205/87/139
Goodness-of - fit	10.2
Final R indices	R=0.018, Rwp= 0.026
CCDC number	883948

Fig. C.67: Crystallographic data of form I of **10** solved by PXRDFig. C.68: Powder X-ray diffractogram of form I of **10**

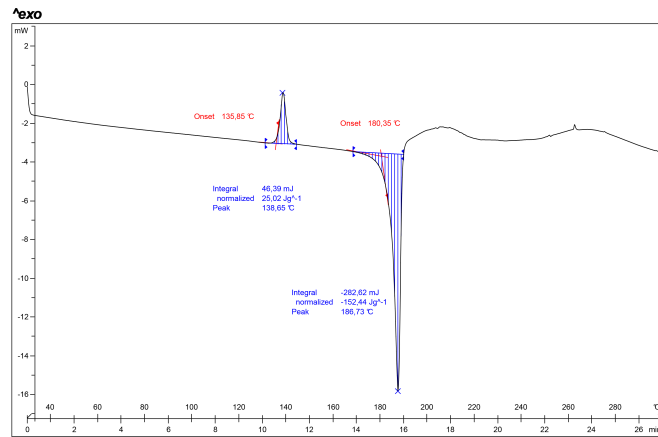


Fig. C.69: DSC thermogram of form I of 10

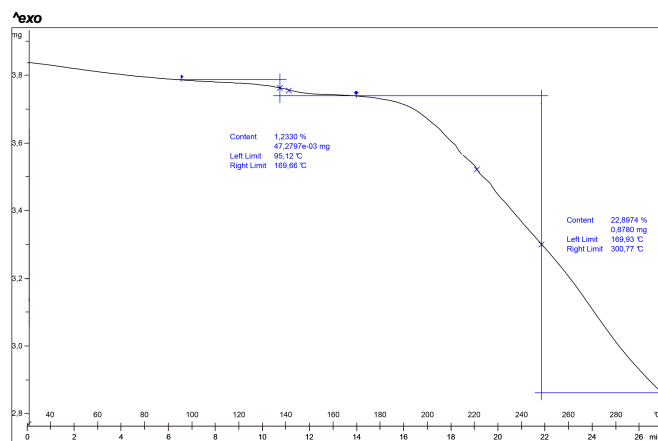
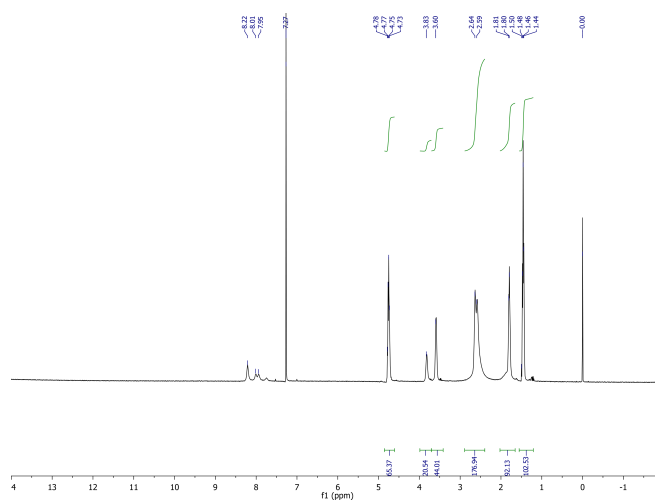
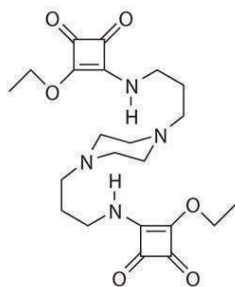


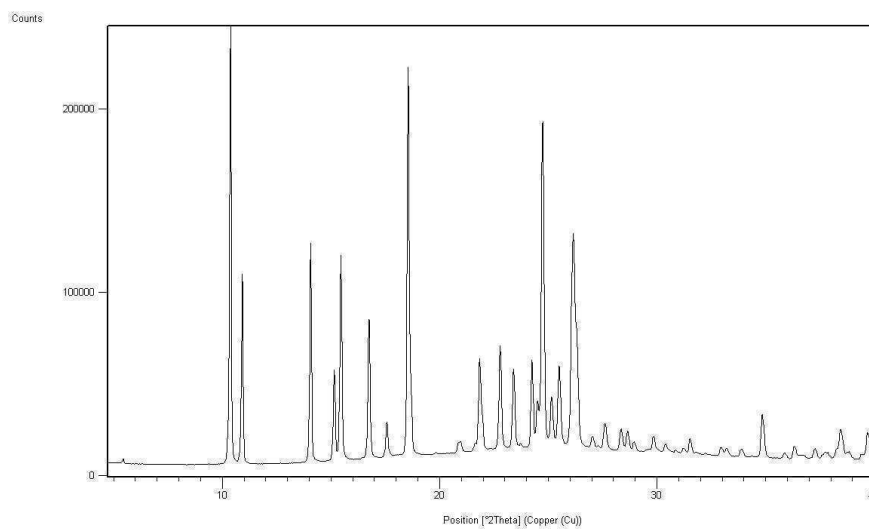
Fig. C.70: TGA thermogram of form I of 10

Fig. C.71: $^1\text{H-NMR}$ spectrum of form I of 10

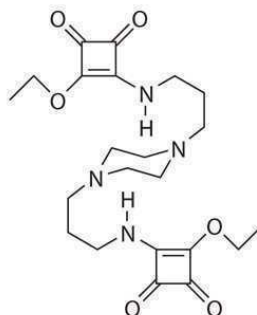
C.1.18 Compound 10, form II

**10**

Structure	Form II of 10
Empirical formula	C ₂₂ H ₃₂ N ₄ O ₆
Formula Weight	448
Temperature (K)	293
Wavelength (Å)	1.54175
Crystal system	Monoclinic
Space group	<i>P</i> 2 ₁ / <i>c</i>
a, b, c (Å)	12.9142(5), 13.4373(2), 6.82870(13)
α , β , γ (°)	90.0, 96.9271(17), 90.0
Volume (Å ³)	1176.35(5)
Z, Density (calc.) (Mg/m ³)	2, 1.265
Limiting indices	-
θ range for data collection (°)	5.01 to 69.98
Computer structure refinement	FullProf
Data/restraints/parameters	1385/87/112
Goodness-of-fit	51.15
Final R indices	R=0.041, Rwp= 0.058
CCDC number	883949

Fig. C.72: Crystallographic data of form II of **10** solved by PXRDFig. C.73: Powder X-ray diffractogram of form II of **10**

C.1.19 Compound 10, form III



10

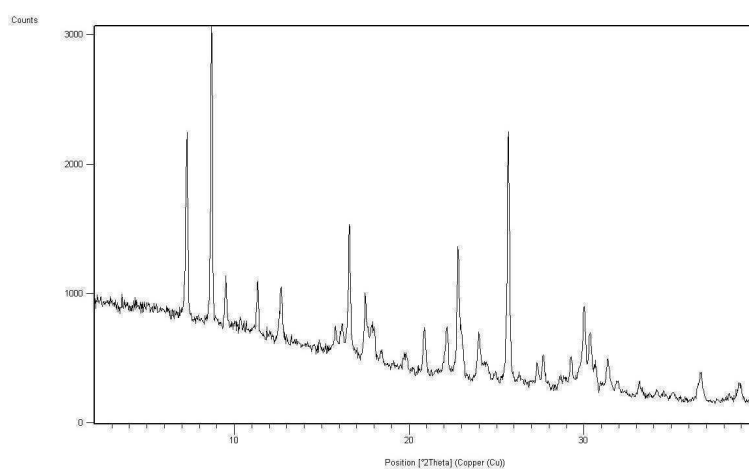


Fig. C.77: Powder X-ray diffractogram of form III of 10

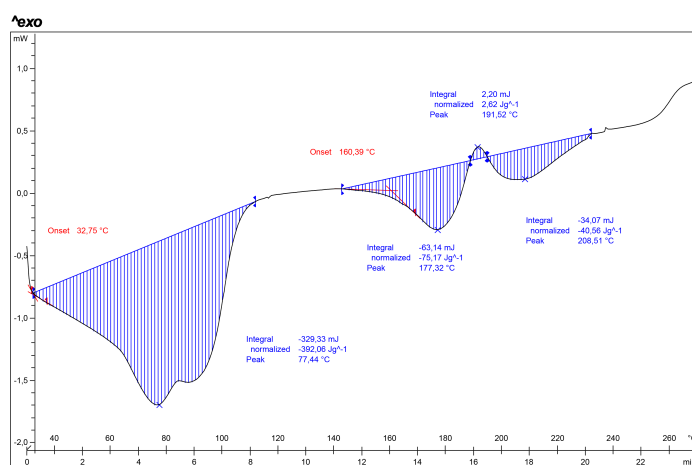
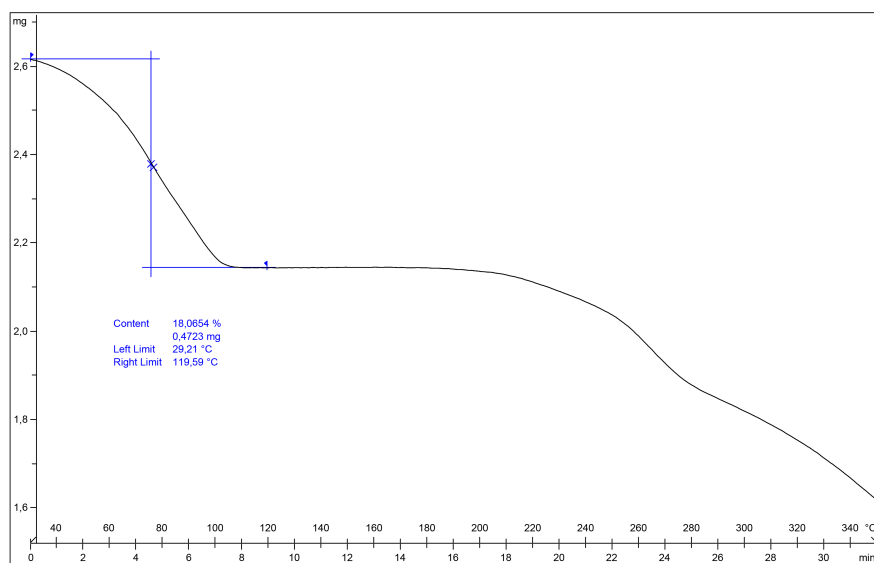
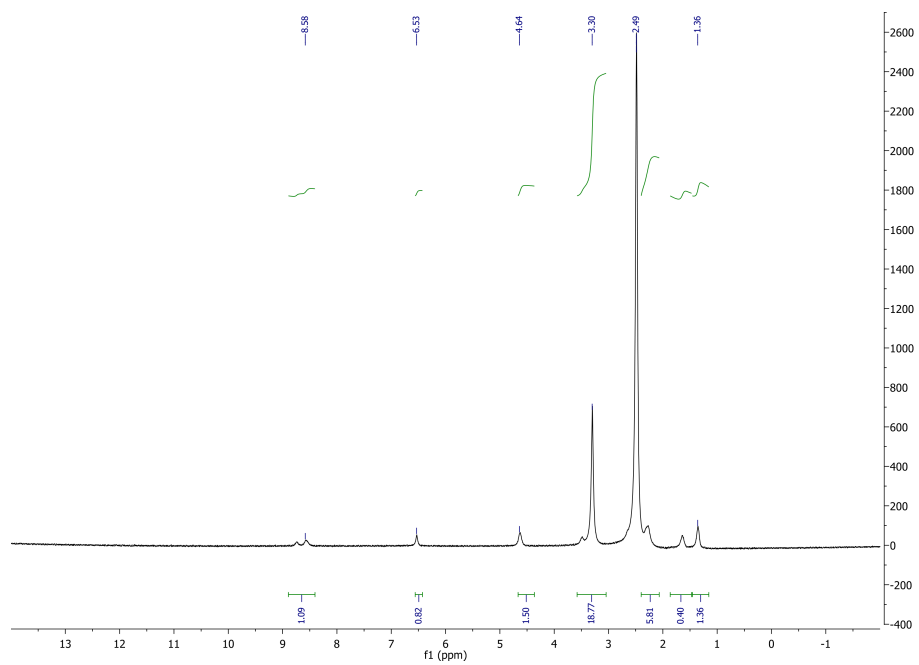
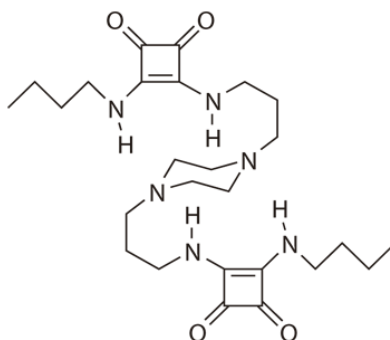


Fig. C.78: DSC thermogram of form III of 10

Fig. C.79: TGA thermogram of form III of **10**Fig. C.80: ¹H-NMR spectrum of form III of **10**

C.1.20 Compound 11, form I



11

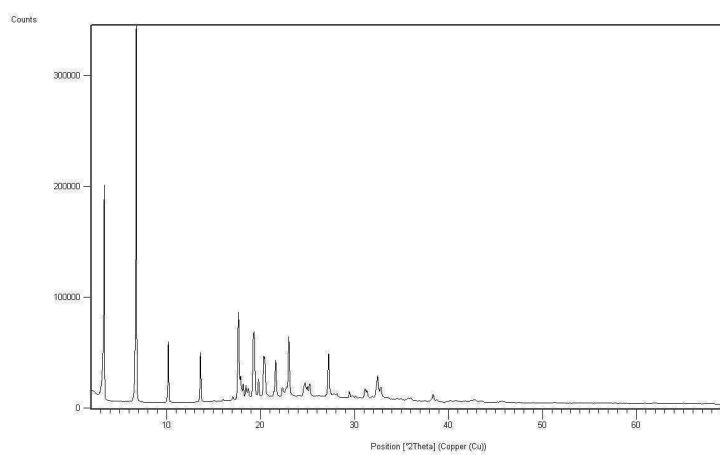


Fig. C.81: Powder X-ray diffractogram of form I of 11

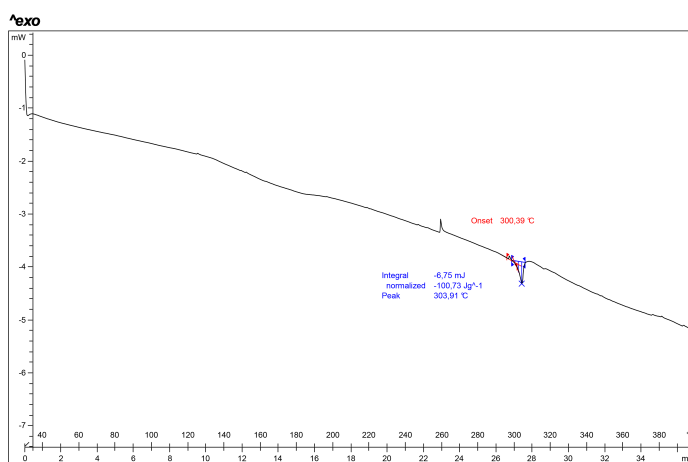


Fig. C.82: DSC thermogram of form I of 11

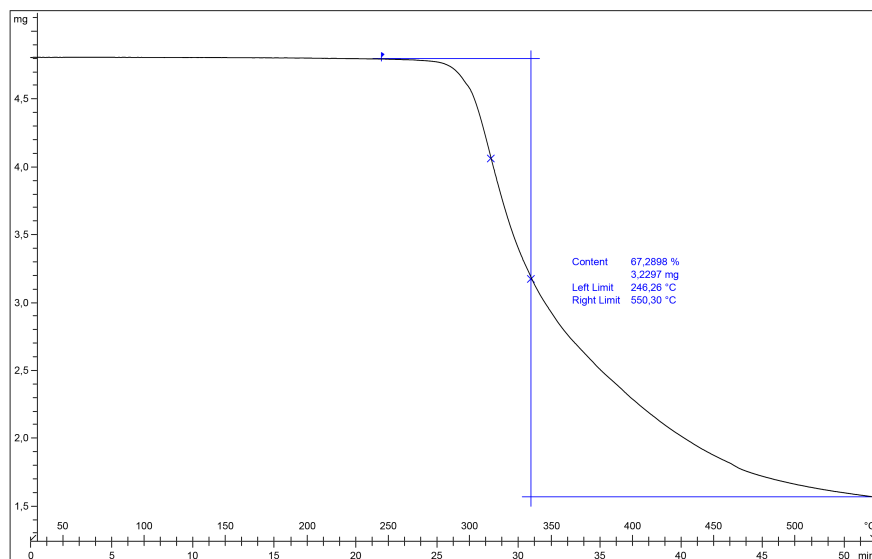
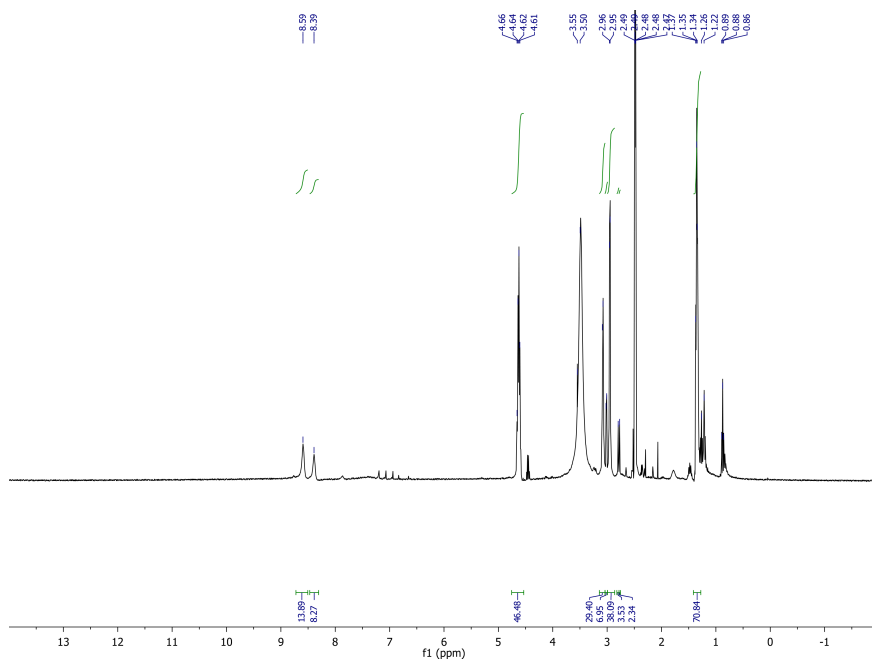
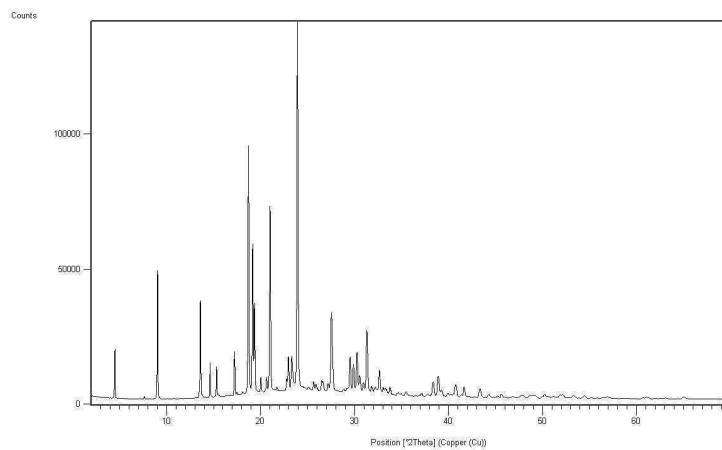
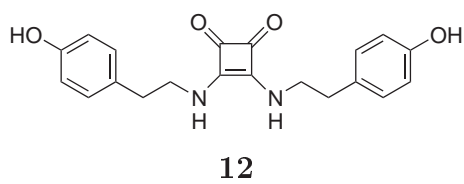
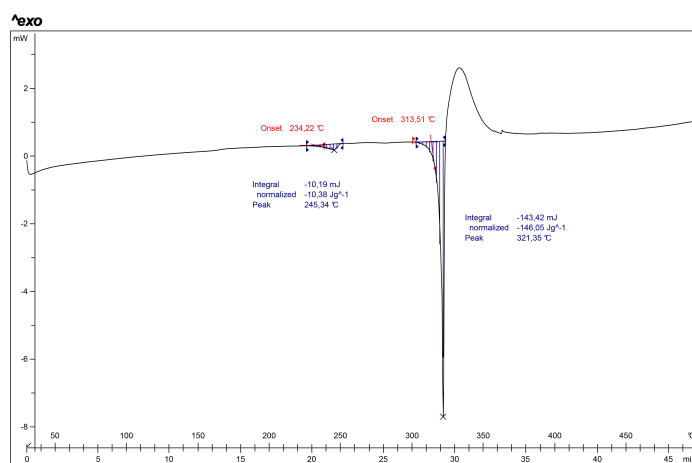


Fig. C.83: TGA thermogram of form I of 11

Fig. C.84: ¹H-NMR spectrum of form I of 11

C.1.21 Compound 12, form I

Fig. C.85: Powder X-ray diffractogram of form I of **12**Fig. C.86: DSC thermogram of form I of **12**

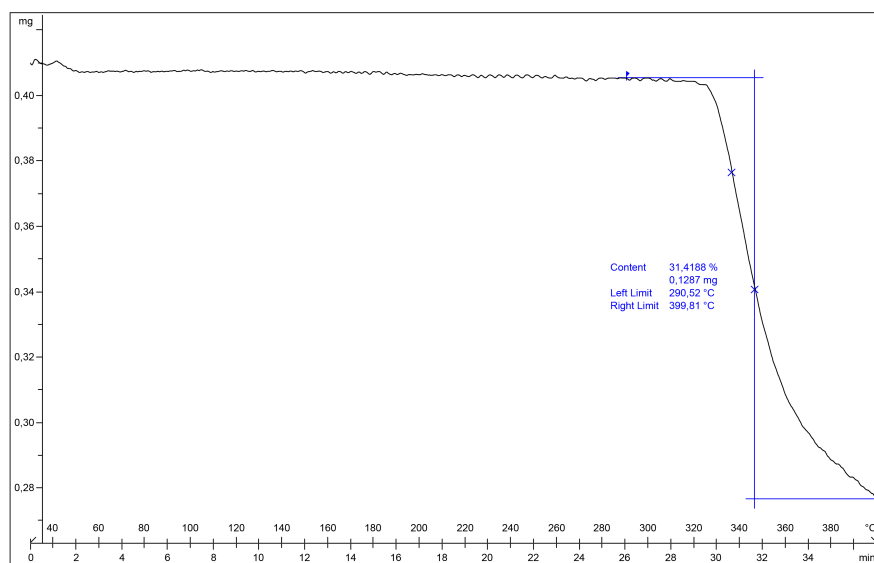
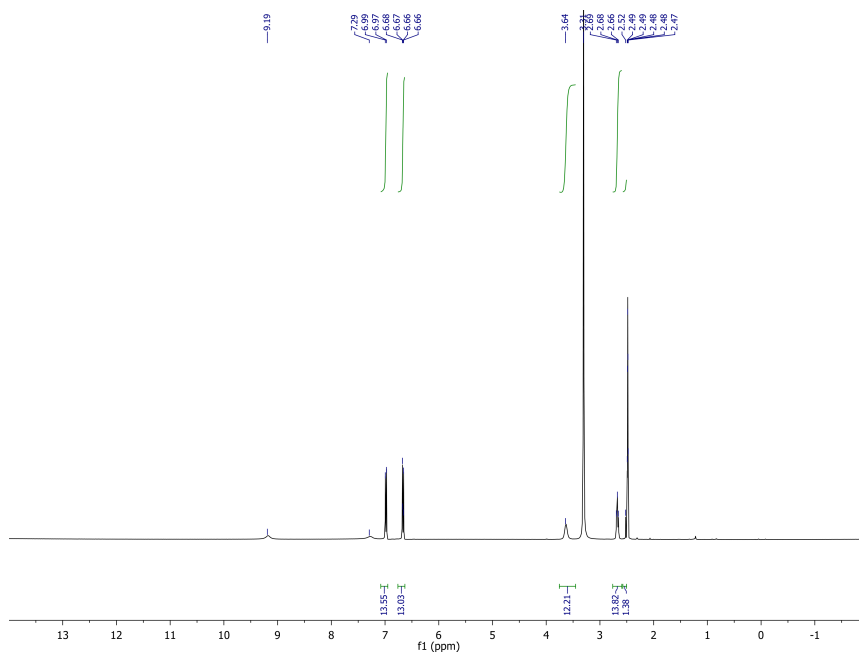
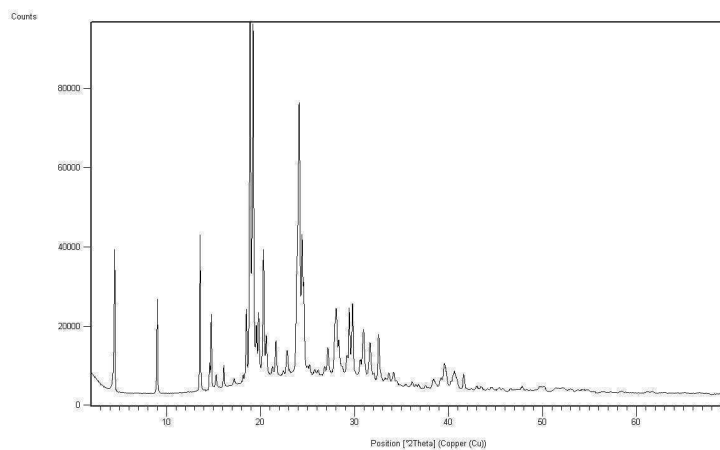
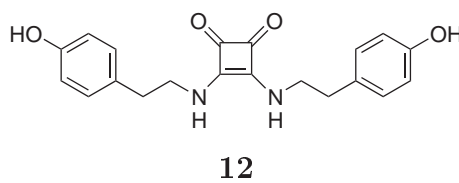
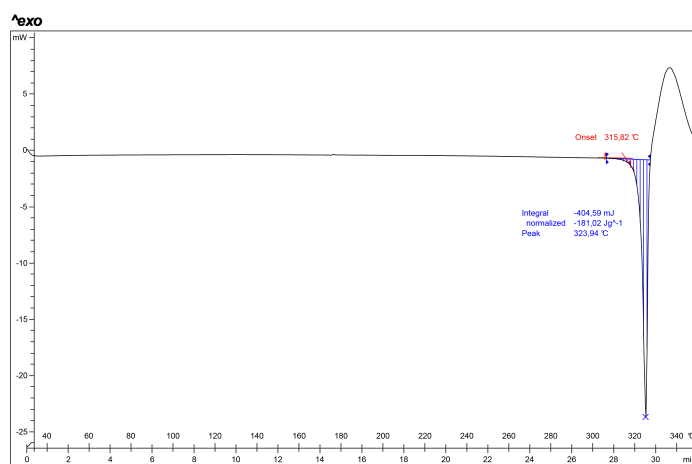
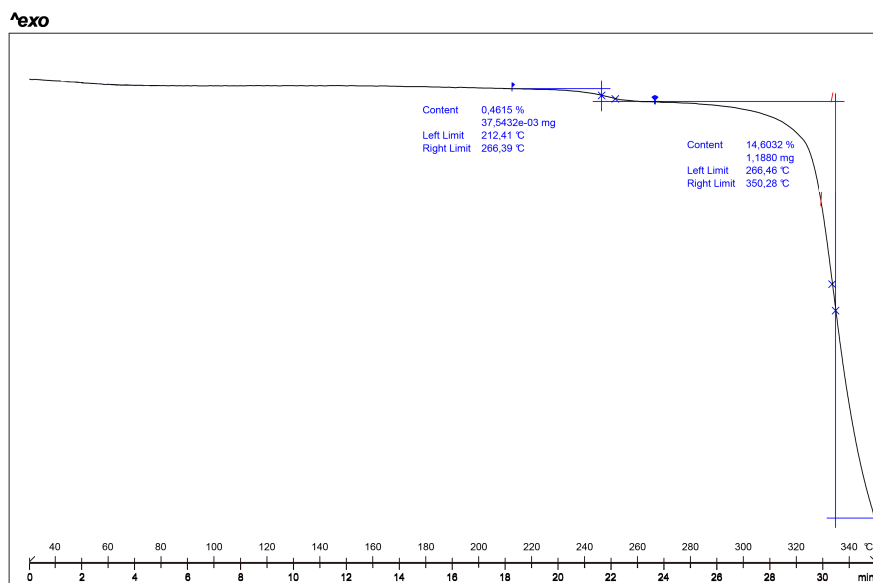
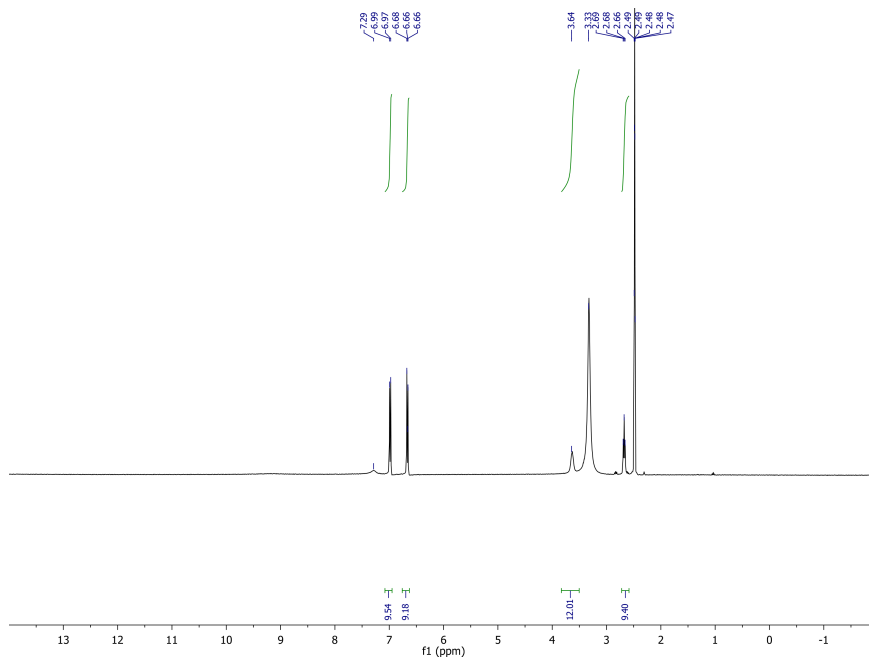


Fig. C.87: TGA thermogram of form I of 12

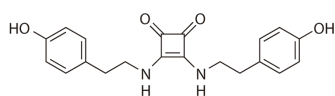
Fig. C.88: ¹H-NMR spectrum of form I of 12

C.1.22 Compound 12, form II

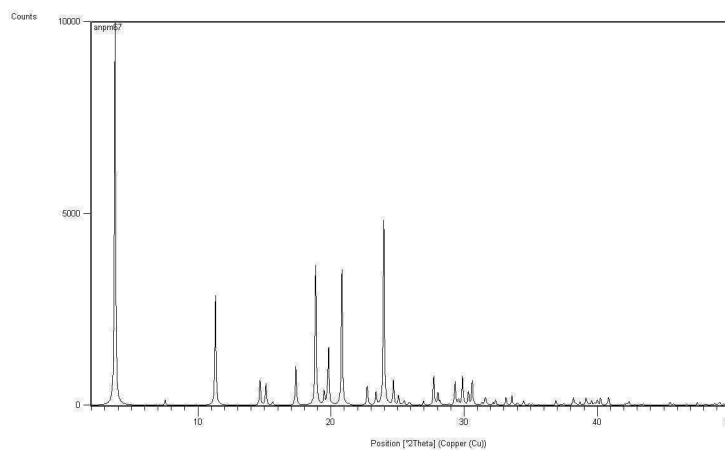
Fig. C.89: Powder X-ray diffractogram of form II of **12**Fig. C.90: DSC thermogram of form II of **12**

Fig. C.91: TGA thermogram of form II of **12**Fig. C.92: ¹H-NMR spectrum of form II of **12**

C.1.23 Compound 12, form III

**12**

Structure	Form III of 12
Empirical formula	C ₂₀ H ₂₀ N ₂ O ₄ · C ₂ H ₅ OH
Formula Weight	398.30
Temperature (K)	293 (2)
Wavelength (Å)	0.71073
Crystal system	Monoclinic
Space group	Cc
a, b, c (Å)	46.92(5), 6.086(4), 7.467(8)
α, β, γ (°)	90, 92.72(6), 90
Volume (Å ³)	2130(4)
Z, Density (calc.) (Mg/m ³)	2, 1.243
Absorption coefficient (mm ⁻¹)	0.088
F(000)	848
Crystal size (mm ³)	0.2 x 0.1 x 0.1
θ range for data collection (°)	1.74 to 32.31
Limiting indices	-69<=h<=57, -9<=k<=9, -10<=l<=10
Reflections collected / unique	6362/3820
Completeness to θ (%)	89.7
Absorption correction	Empirical
Max. and min. transmission	0.5 and 0.5
Refinement method	Full-matrix least-squares on F ²
Data/restraints/parameters	3820/ 13 /241
Goodness-of - fit on F ²	0.973
Final R indices [I > 2σ(I)]	R1 = 0.0758, wR2 = 0.2012
R indices (all data)	R1 = 0.1222, wR2 = 0.2424
Largest diff. peak and hole (e.Å ⁻³)	0.479 and -0.452
CCDC number	1015653

Fig. C.93: Crystallographic data of form III of **12** obtained by SXRDFig. C.94: Calculated powder X-ray diffractogram of form III of **12**

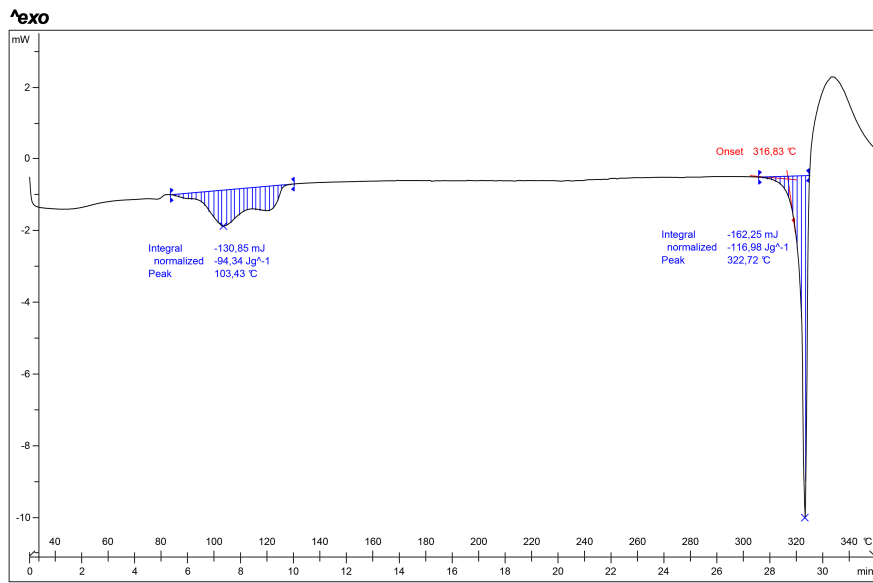


Fig. C.95: DSC thermogram of form III of 12

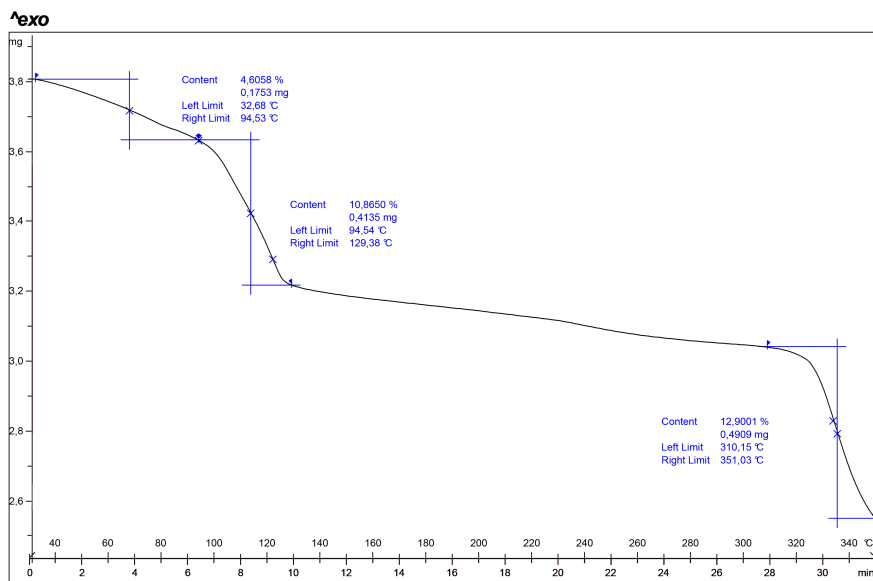
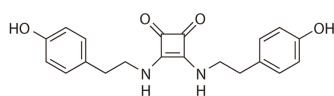
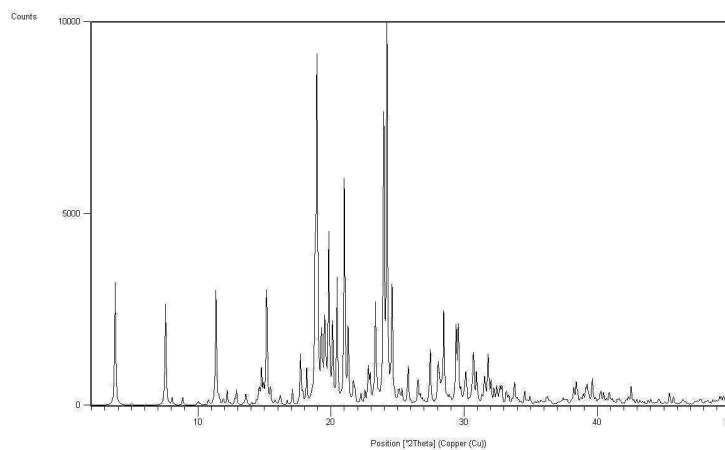


Fig. C.96: TGA thermogram of form III of 12

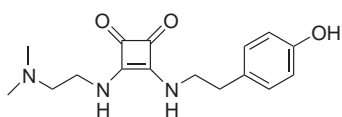
C.1.24 Compound 12, form IV

**12**

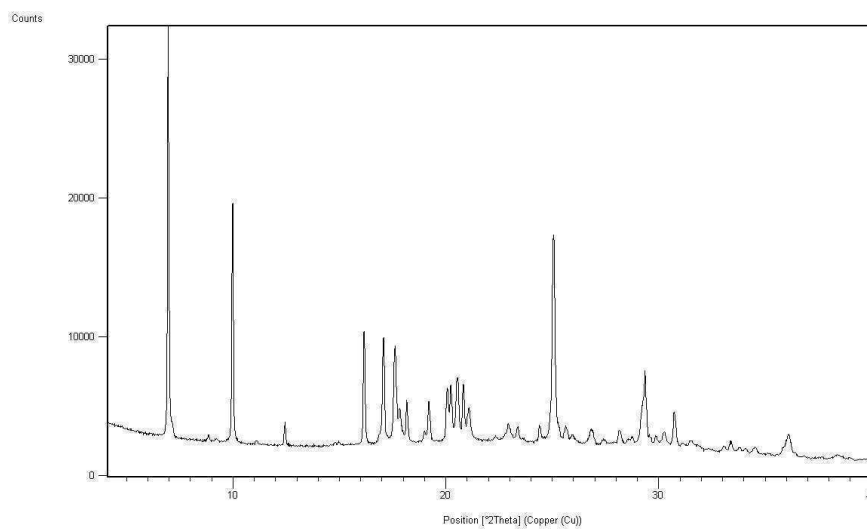
Structure	Form IV of 12
Empirical formula	5(C ₂₀ H ₂₀ N ₂ O ₄), 4(C ₂ H ₆ OS), 2(H ₂ O)
Formula Weight	2110.44
Temperature (K)	303 (2)
Wavelength (Å)	0.71073
Crystal system	Monoclinic
Space group	P2 ₁ /c
a, b, c (Å)	23.485(10), 9.632(4), 47.030(19)
α, β, γ (°)	90, 96.764(10), 90
Volume (Å ³)	10564(8)
Z, Density (calc.) (Mg/m ³)	4, 1.327
Absorption coefficient (mm ⁻¹)	0.170
F(000)	4472
Crystal size (mm ³)	0.5 x 0.3 x 0.2
θ range for data collection (°)	2.16 to 25.00
Limiting indices	-31<=h<=31, -12<=k<=13, -63<=l<=62
Reflections collected / unique	173437/18613
Completeness to θ (%)	97.2
Absorption correction	Semi-empirical from equivalents
Max. and min. transmission	0.7457 and 0.5810
Refinement method	Full-matrix least-squares on F ²
Data/restraints/parameters	18613 / 13 / 1353
Goodness-of-fit on F ²	0.630
Final R indices [I > 2σ(I)]	R1 = 0.0364, wR2 = 0.0514
R indices (all data)	R1 = 0.1991, wR2 = 0.0626
Largest diff. peak and hole (e.Å ⁻³)	0.262 and -0.159
CCDC number	1017985

Fig. C.97: Crystallographic data of form IV of **12** obtained by SXRDFig. C.98: Calculated powder X-ray diffractogram of form IV of **12**

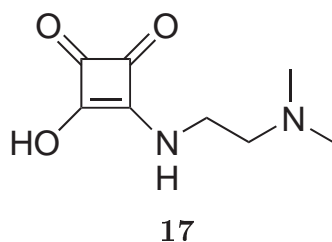
C.1.25 Compound 13, form I

**13**

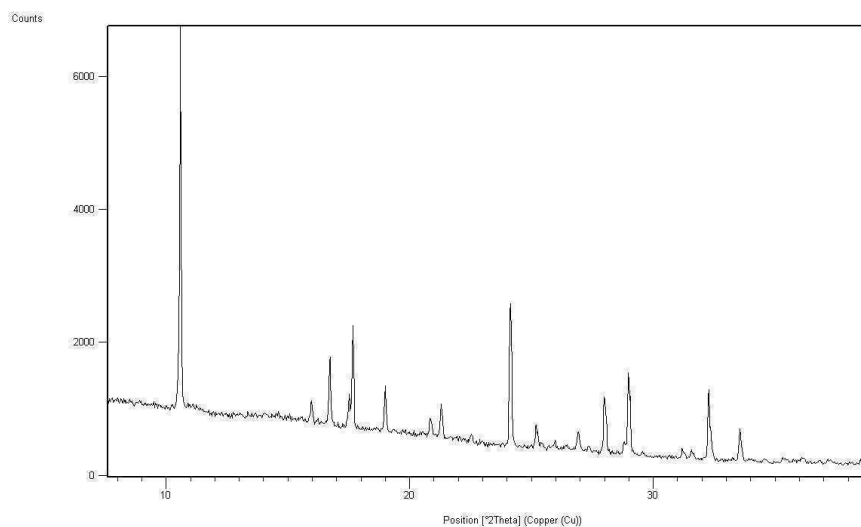
Structure	Form I of 13
Empirical formula	C ₁₆ H ₂₁ N ₃ O ₃
Formula Weight	303.0
Temperature (K)	293
Wavelength (Å)	1.54175
Crystal system	Monoclinic
Space group	<i>P</i> 2 ₁ / <i>c</i>
a, b, c (Å)	10.2164(8), 6.07487(12), 25.9781(17)
α, β, γ (°)	90.0, 102.821(16), 90.0
Volume (Å ³)	1572.09(19)
Z, Density (calc.) (Mg/m ³)	4, 1.265
Limiting indices	-
θ range for data collection (°)	2.02 to 69.98
Computer structure refinement	FullProf
Data/restraints/parameters	1765/120/94
Goodness-of-fit	2.41
Final R indices	R=0.038, Rwp= 0.055
CCDC number	953732

Fig. C.99: Crystallographic data of form I of **13** solved by PXRDFig. C.100: Powder X-ray diffractogram of form I of **13**

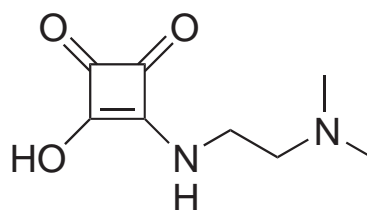
C.1.26 Compound 17, form I



Structure	Form I of 17
Empirical formula	C ₈ H ₁₂ N ₂ O ₃
Formula Weight	184.20
Temperature (K)	293 (2)
Wavelength (Å)	0.71073
Crystal system	Monoclinic
Space group	<i>P</i> 2 ₁ / <i>c</i>
a, b, c (Å)	6.249(4), 12.774(6), 11.848(5)
α, β, γ (°)	90, 111.29(3), 90
Volume (Å ³)	881.2(8)
Z, Density (calc.) (Mg/m ³)	4, 1.388
Absorption coefficient (mm ⁻¹)	0.107
F(000)	392
Crystal size (mm ³)	0.1 x 0.1 x 0.1
θ range for data collection (°)	2.44 to 32.41
Limiting indices	-7<=h<=7, -17<=k<=17, -15<=l<=16
Reflections collected / unique	6771/2152
Completeness to θ (%)	93.3
Absorption correction	none
Max. and min. transmission	0.5 and 0.5
Refinement method	Full-matrix least-squares on F ²
Data/restraints/parameters	2152/ 1 /118
Goodness-of-fit on F ²	1.150
Final R indices [I > 2σ(I)]	R1 = 0.0561, wR2 = 0.1869
R indices (all data)	R1 = 0.0610, wR2 = 0.1905
Largest diff. peak and hole (e.Å ⁻³)	0.152 and -0.346
CCDC number	938373

Fig. C.104: Crystallographic data of form I of **17** obtained by SXRDFig. C.105: Powder X-ray diffractogram of form I of **17**

C.1.27 Compound 17, form II



17

Structure	Form II of 19
Empirical formula	C ₈ H ₁₂ N ₂ O ₃
Formula Weight	184.20
Temperature (K)	293 (2)
Wavelength (Å)	0.71073
Crystal system	Monoclinic
Space group	<i>P</i> 2 ₁ / <i>c</i>
a, b, c (Å)	9.356(6), 9.541(5), 11.672(6)
α, β, γ (°)	90, 121.72(4), 90
Volume (Å ³)	886.3(9)
Z, Density (calc.) (Mg/m ³)	4, 1.380
Absorption coefficient (mm ⁻¹)	0.107
F(000)	392
Crystal size (mm ³)	0.1 x 0.1 x 0.1
θ range for data collection (°)	2.56 to 31.00
Limiting indices	-12<=h<=13, -13<=k<=13, -14<=l<=12
Reflections collected / unique	6714/1921
Completeness to θ (%)	93.3
Absorption correction	none
Max. and min. transmission	0.5 and 0.5
Refinement method	Full-matrix least-squares on F ²
Data/restraints/parameters	2160/0/119
Goodness-of-fit on F ²	1.114
Final R indices [I > 2σ(I)]	R1 = 0.0623, wR2 = 0.0694
R indices (all data)	R1 = 0.1619, wR2 = 0.1699
Largest diff. peak and hole (e.Å ⁻³)	0.152 and -0.255
CCDC number	951985

Fig. C.109: Crystallographic data of form II of 17 obtained by SXRD

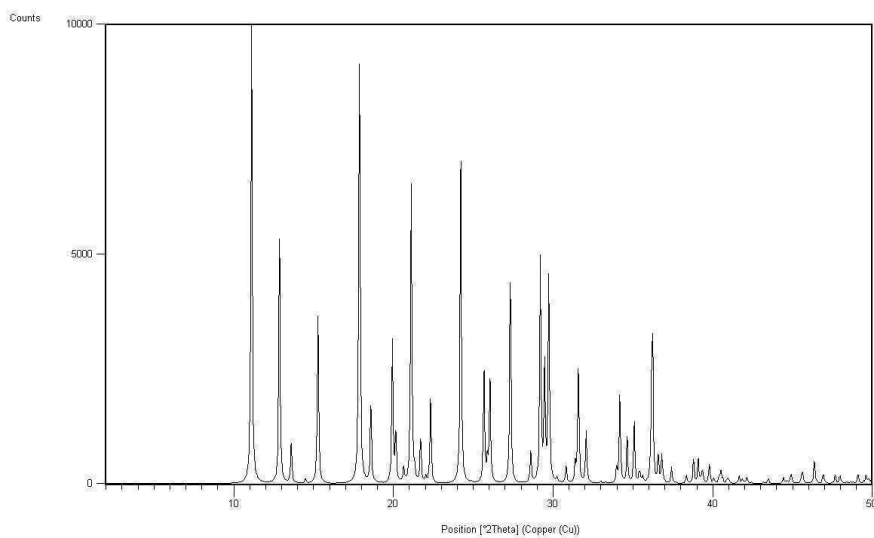


Fig. C.110: Calculated powder X-ray diffractogram of form II of **17**

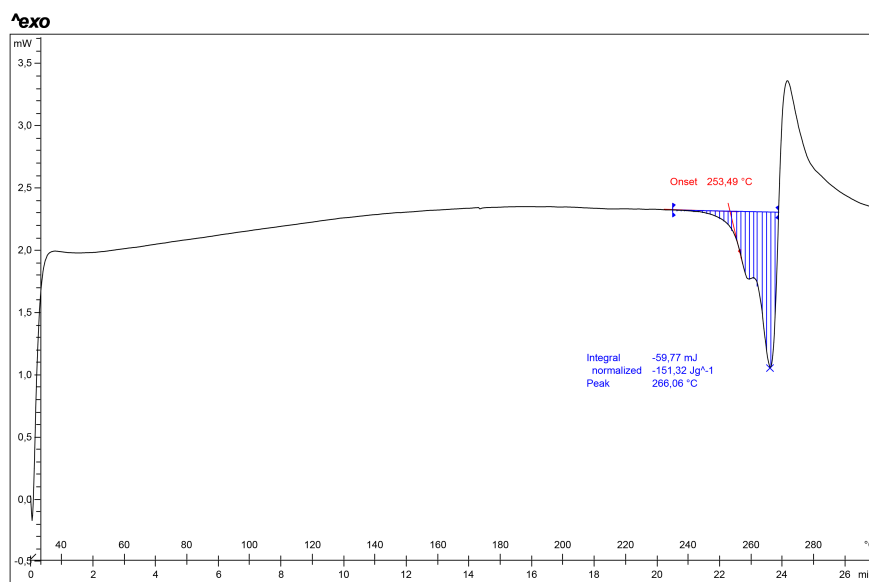
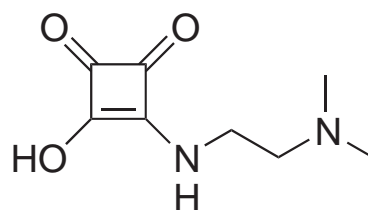


Fig. C.111: DSC thermogram of form II of **17**

C.1.28 Compound 17, form III



17

Structure	Form III of 19
Empirical formula	C ₈ H ₁₂ N ₂ O ₃ · H ₂ O
Formula Weight	202.21
Temperature (K)	105 (2)
Wavelength (Å)	0.71073
Crystal system	Monoclinic
Space group	<i>P</i> 2 ₁ / <i>c</i>
a, b, c (Å)	6.536(7), 10.844(9), 14.095(11)
α, β, γ (°)	90, 103.17(6), 90
Volume (Å ³)	972.7(15)
Z, Density (calc.) (Mg/m ³)	4, 1.381
Absorption coefficient (mm ⁻¹)	0.111
F(000)	432
Crystal size (mm ³)	0.2 x 0.09 x 0.04
θ range for data collection (°)	2.39 to 32.36
Limiting indices	-8 ≤ h ≤ 8, -16 ≤ k ≤ 16, -19 ≤ l ≤ 21
Reflections collected / unique	6841/2673
Completeness to θ (%)	93.2
Absorption correction	Empirical
Max. and min. transmission	0.99 and 0.98
Refinement method	Full-matrix least-squares on F ²
Data/restraints/parameters	2673/ 8 / 141
Goodness-of-fit on F ²	0.870
Final R indices [I > 2σ(I)]	R1 = 0.0397, wR2 = 0.0849
R indices (all data)	R1 = 0.1012, wR2 = 0.0953
Largest diff. peak and hole (e.Å ⁻³)	0.107 and -0.187
CCDC number	938372

Fig. C.112: Crystallographic data of form III of 17 obtained by SXRD

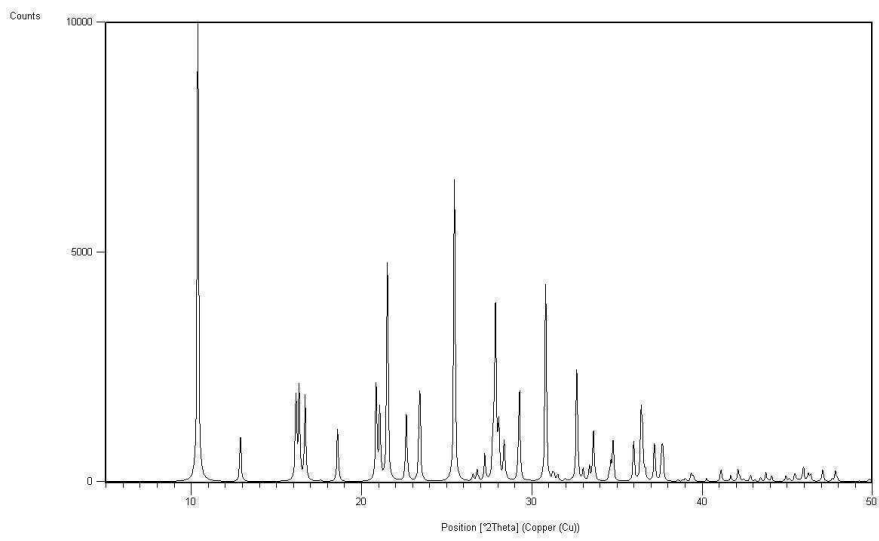


Fig. C.113: Calculated powder X-ray diffractogram of form III of **17**

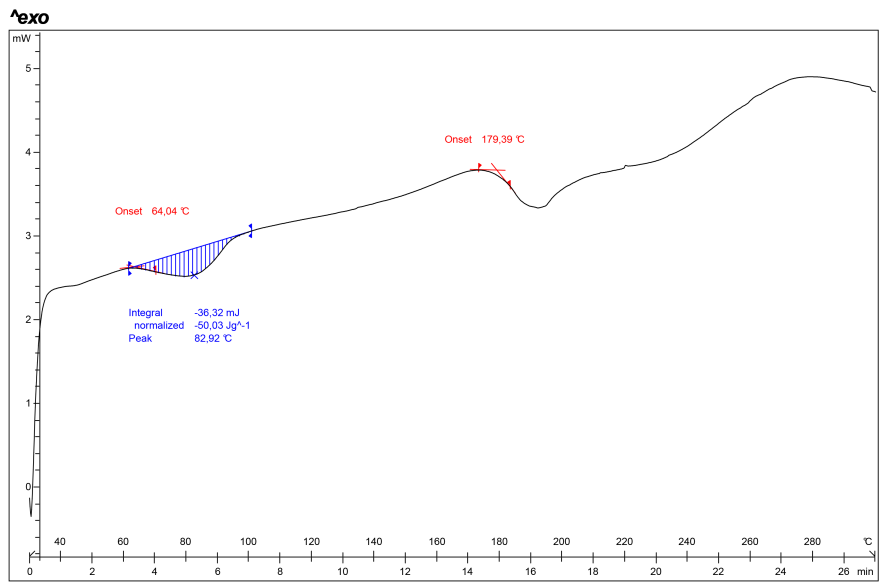
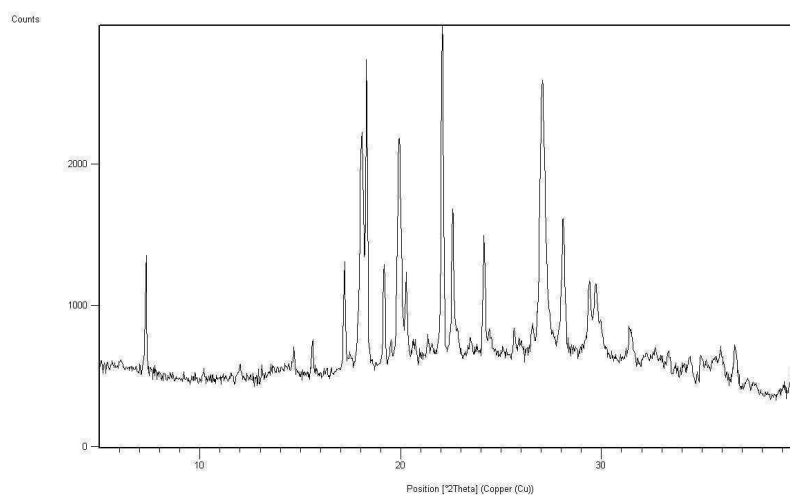
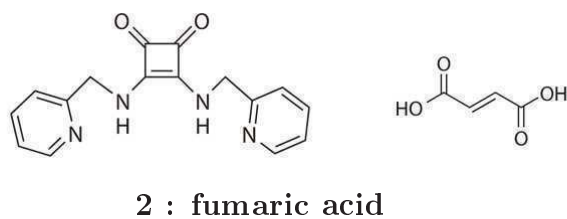
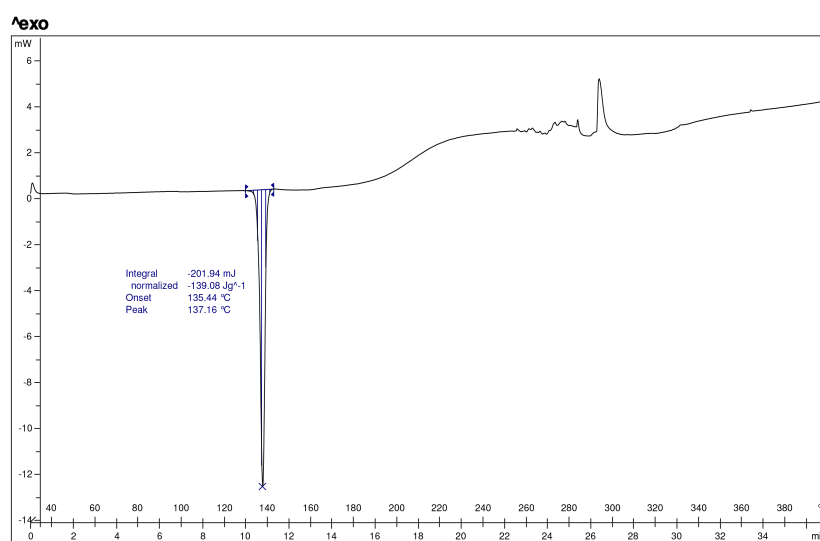


Fig. C.114: DSC thermogram of form III of **17**

C.2 Multicomponent solids

The powder X-ray diffractogram, DSC and TGA thermograms, ^1H -NMR or ^{13}C -NMR spectra and crystallographic data of the new multicomponent forms obtained in the present work are included in this appendix. In some cases, ^1H -NMR, ^{13}C -NMR or TGA data are missing due to lack of sample availability or because the form was sufficiently characterized by the rest of the techniques.

C.2.1 Cocrystal of **2** : fumaric acid, form AFig. C.115: Powder X-ray diffractogram of form A of **2:fumaric acid** cocrystalFig. C.116: DSC thermogram of form A of **2:fumaric acid** cocrystal

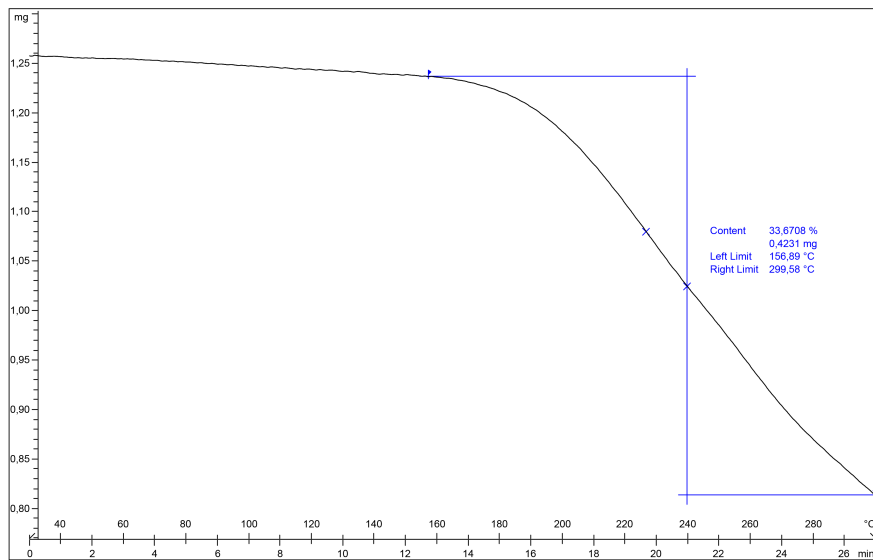


Fig. C.117: TGA thermogram of form A of **2:fumaric acid** cocrystal

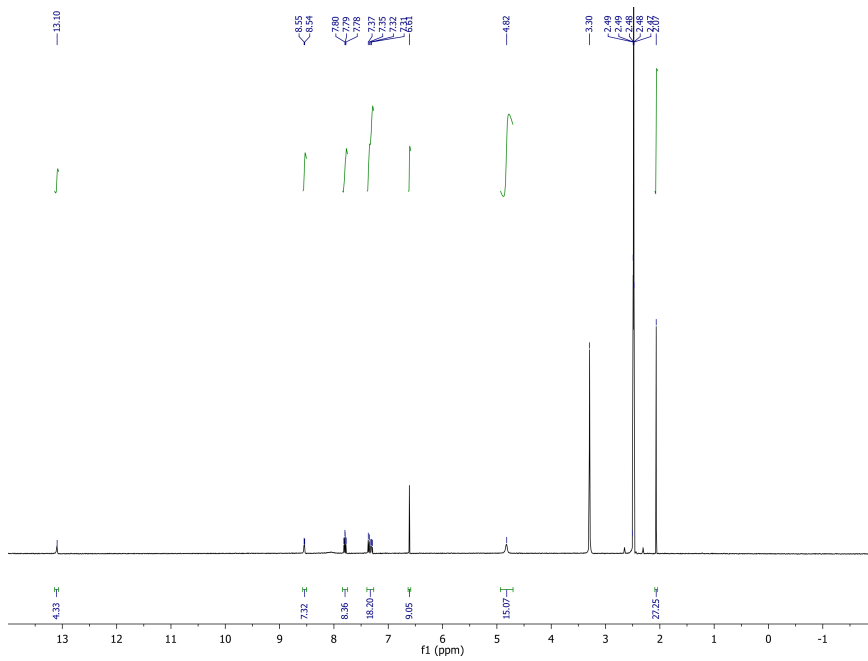
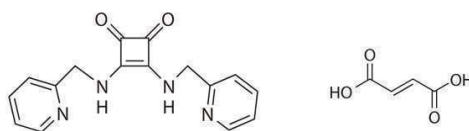


Fig. C.118: ¹H-NMR spectrum of form A of **2:fumaric acid** cocrystal

C.2.2 Cocystal of **2** : fumaric acid, form B**2** : fumaric acid

Structure	2-I-B
Empirical formula	C ₁₆ H ₁₄ N ₄ O ₂ · C ₄ H ₄ O ₄ 2(C ₂ H ₃ N)
Formula Weight	492.49
Temperature (K)	105 (2)
Wavelength (Å)	0.71073
Crystal system	Monoclinic
space group	C2/c
a, b, c (Å)	24.98(2), 5.990(5), 17.717(8)
α, β, γ (°)	90, 105.66(4), 90
Volume (Å ³)	2553(3)
Z, Density (calc.) (Mg/m ³)	4, 1.282
Absorption coefficient (mm ⁻¹)	0.095
F(000)	1032
Crystal size (mm ³)	0.2 x 0.07 x 0.07
θ range for data collection (°)	1.69 to 32.16
Limiting indices	-34 ≤ h ≤ 35, -7 ≤ k ≤ 7, -26 ≤ l ≤ 26
Reflections collected / unique	9878/3266
Completeness to θ (%)	95.5
Absorption correction	Empirical
Max. and min. transmission	0.99 and 0.98
Refinement method	Full-matrix least-squares on F ²
Data/restraints/parameters	3266/ 5 /164
Goodness-of-fit on F ²	1.156
Final R indices [I > 2σ(I)]	R1 = 0.0566, wR2 = 0.1414
R indices (all data)	R1 = 0.0881, wR2 = 0.1577
Largest diff. peak and hole (e.Å ⁻³)	0.124 and -0.192
CCDC number	1015650

Fig. C.119: Crystallographic data of form B of **2:fumaric acid** cocystal obtained by SXRD

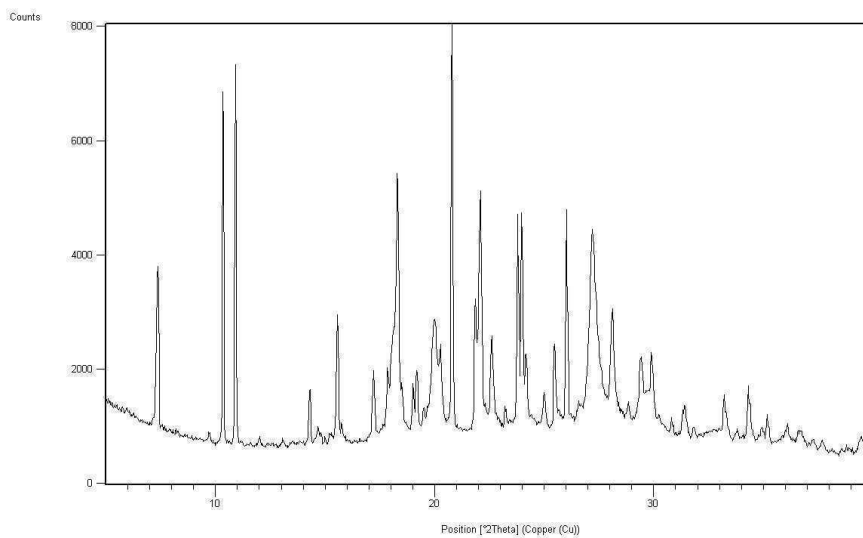


Fig. C.120: Powder X-ray diffractogram of form B of **2:fumaric acid** cocrystal

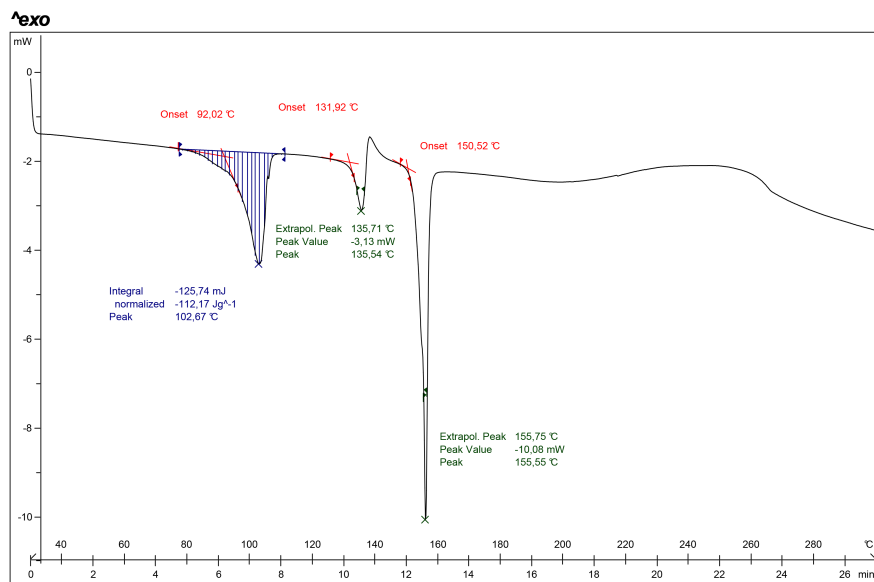
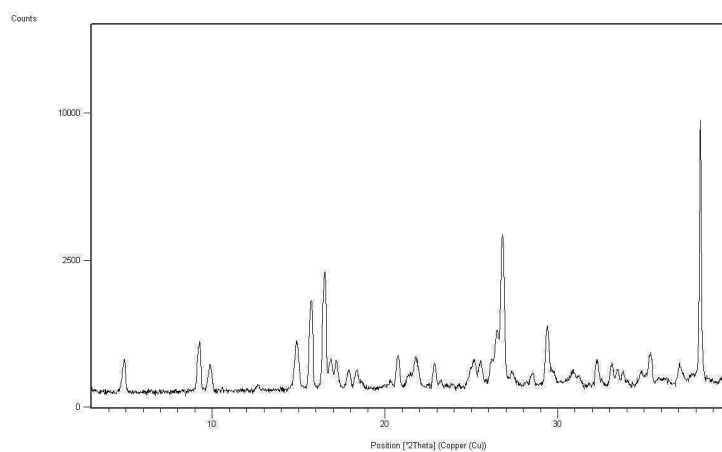
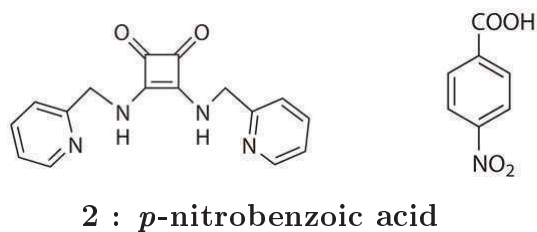
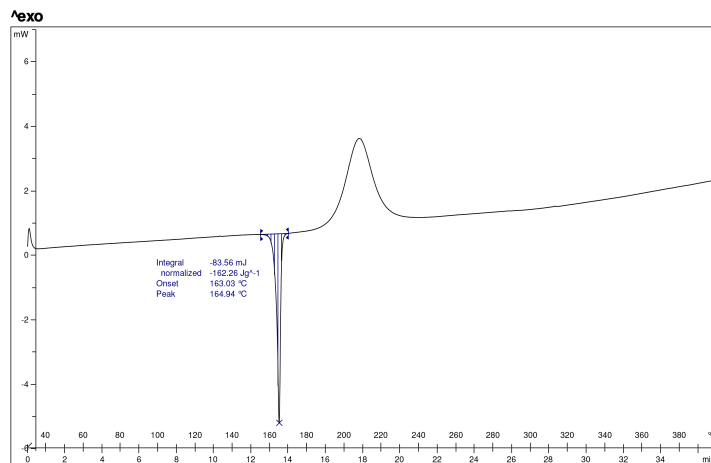
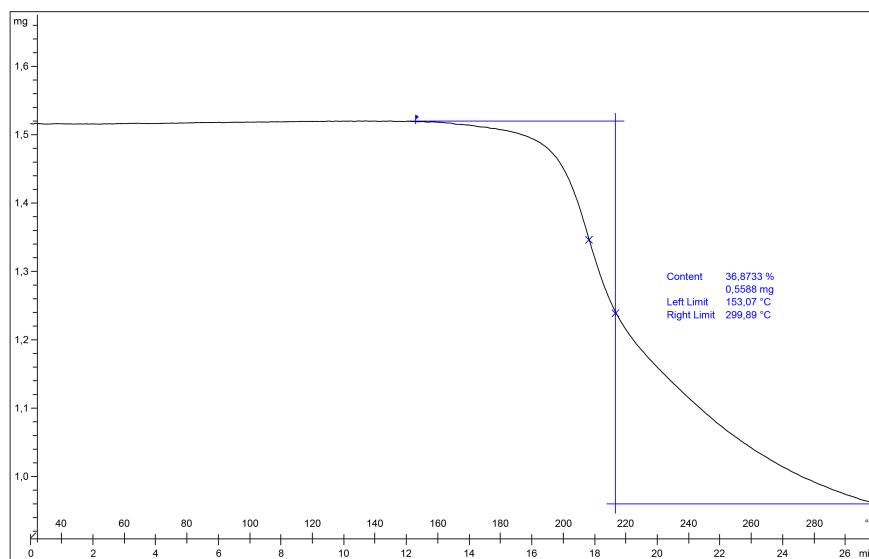
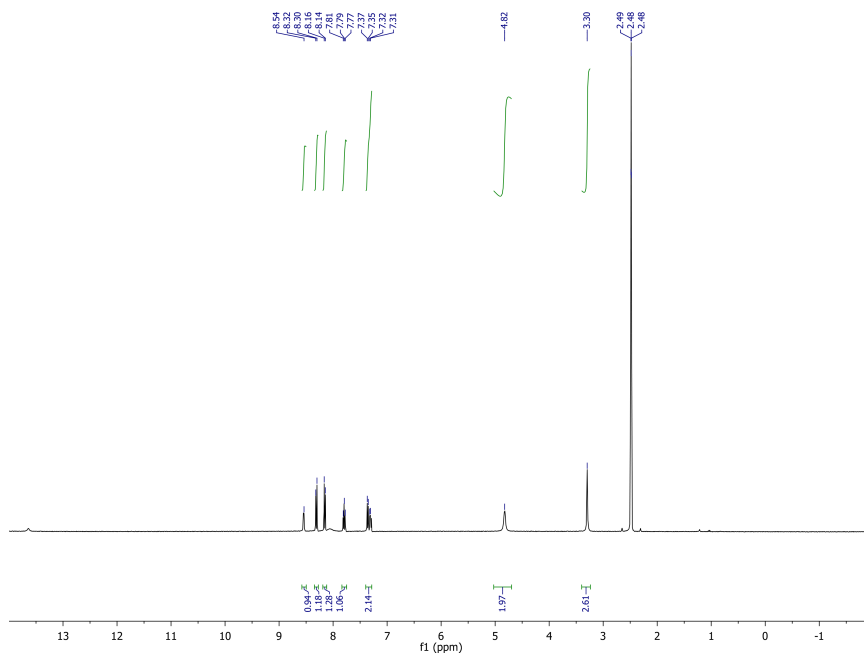
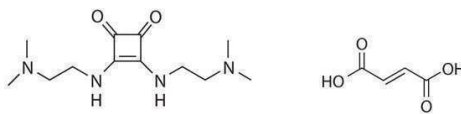


Fig. C.121: DSC thermogram of form B of **2:fumaric acid** cocrystal

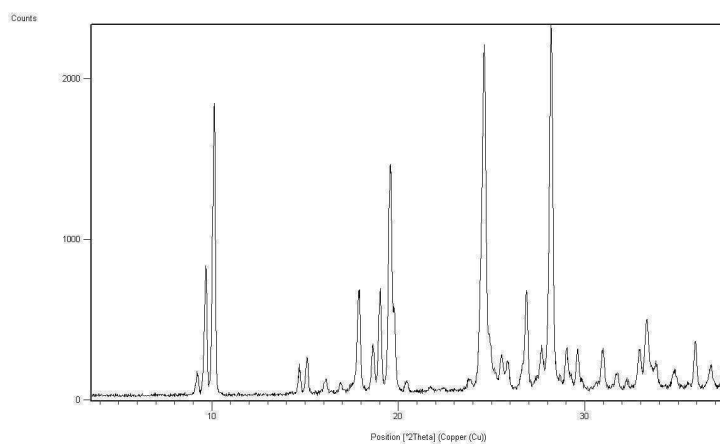
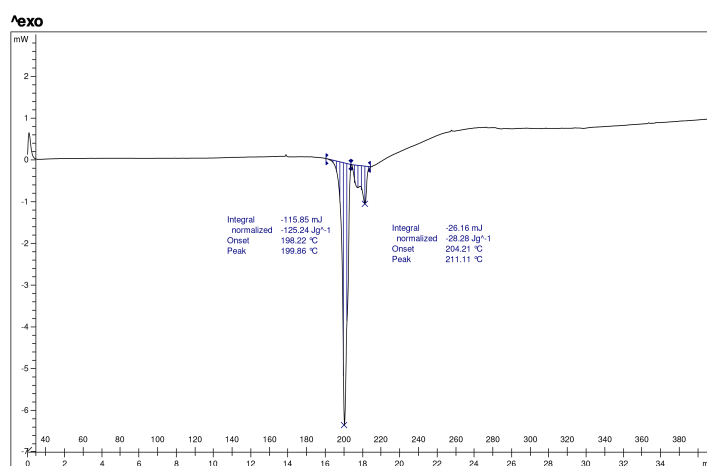
C.2.3 Cocrystal of **2** : *p*-nitrobenzoic acidFig. C.122: Powder X-ray diffractogram of **2**:*p*-nitrobenzoic acid saltFig. C.123: DSC thermogram of **2**:*p*-nitrobenzoic acid salt

Fig. C.124: TGA thermogram of **2:p-nitrobenzoic acid salt**Fig. C.125: ¹H-NMR spectrum of **2:p-nitrobenzoic acid salt**

C.2.4 Cocrystal of 4 : fumaric acid, form A



4 : fumaric acid

Fig. C.126: Powder X-ray diffractogram of form A of **4:fumaric acid** saltFig. C.127: DSC thermogram of form A of **4:fumaric acid** salt

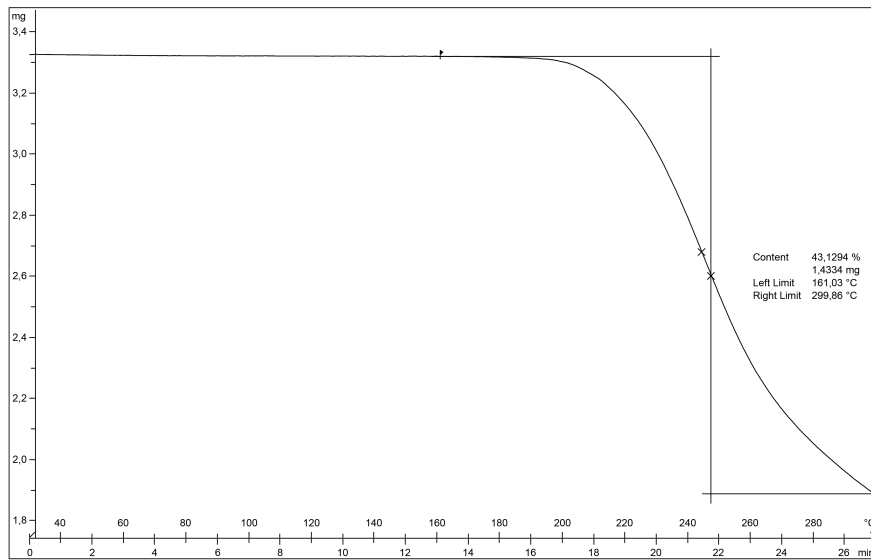
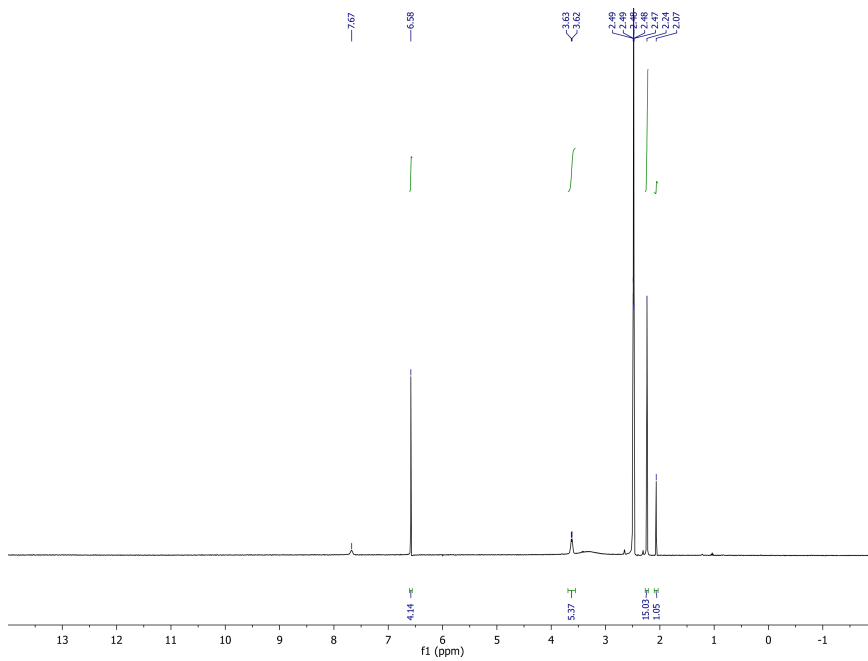
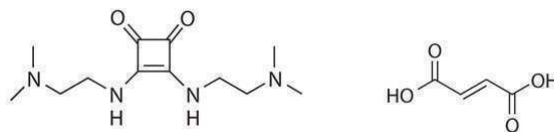


Fig. C.128: DSC thermogram of form A of 4:fumaric acid salt

Fig. C.129: ¹H-NMR spectrum of form A of 4:fumaric acid salt

C.2.5 Cocrystal of 4 : fumaric acid, form B



4 : fumaric acid

Structure	4-I-B
Empirical formula	$2(C_{12}H_{22}N_4O_2) \cdot 2(C_4H_4O_4) \cdot CH_3OH \cdot 3(H_2O)$
Formula Weight	822.87
Temperature (K)	293 (2)
Wavelength (Å)	0.71073
Crystal system	Triclinic
space group	<i>P</i> -1
a, b, c (Å)	6.196(8), 13.132(11), 13.815(13)
α, β, γ (°)	73.83(5), 83.92(6), 78.69(6)
Volume (Å ³)	1057.1(19)
Z, Density (calc.) (Mg/m ³)	1, 1.293
Absorption coefficient (mm ⁻¹)	0.103
F(000)	440
Crystal size (mm ³)	0.2 x 0.2 x 0.1
θ range for data collection (°)	1.54 to 32.52
Limiting indices	$-9 \leq h \leq 9, -18 \leq k \leq 19, 0 \leq l \leq 20$
Reflections collected / unique	6197/2151
Completeness to θ (%)	88.5
Absorption correction	Empirical
Max. and min. transmission	0.99 and 0.98
Refinement method	Full-matrix least-squares on F ²
Data/restraints/parameters	6197/7/272
Goodness-of-fit on F ²	0.882
Final R indices [$I > 2\sigma(I)$]	R1 = 0.0865, wR2 = 0.1978
R indices (all data)	R1 = 0.1786, wR2 = 0.2403
Largest diff. peak and hole (e.Å ⁻³)	-
CCDC number	1015651

Fig. C.130: Crystallographic data of form B of 4:fumaric acid salt obtained by SXRD

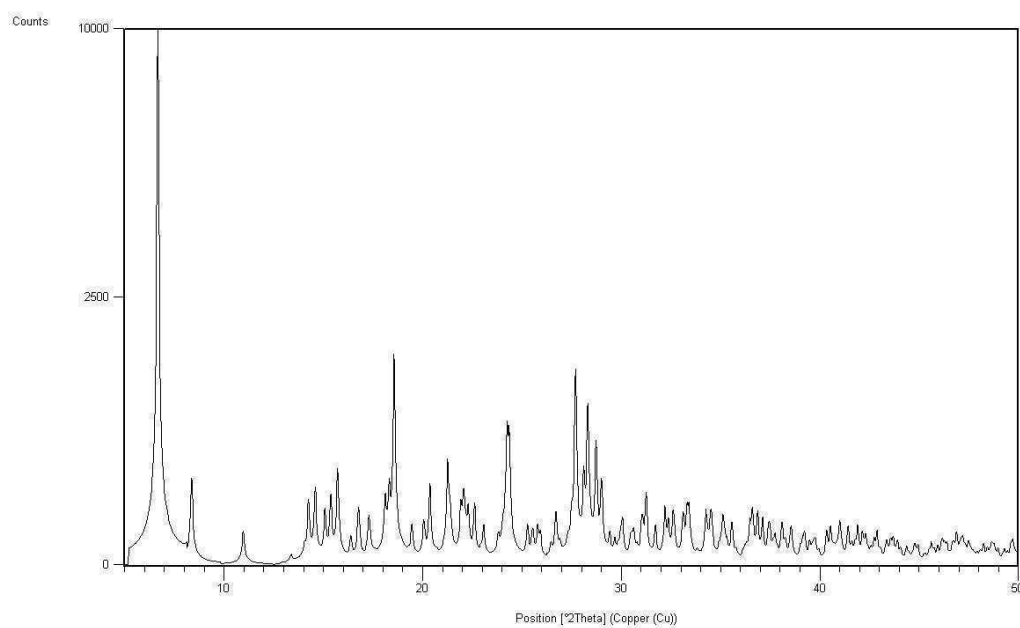
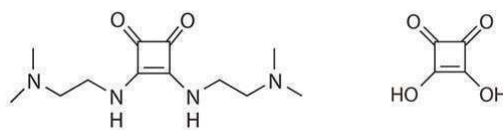


Fig. C.131: Calculated powder X-ray diffractogram of form B of **4:fumaric acid** salt

C.2.6 Salt of 4 : squaric acid, form A



4 : squaric acid

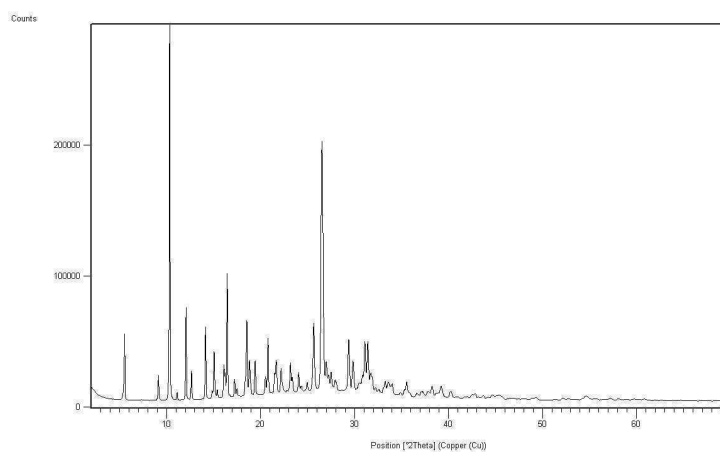


Fig. C.132: Powder X-ray diffractogram of form A of 4:squaric acid salt

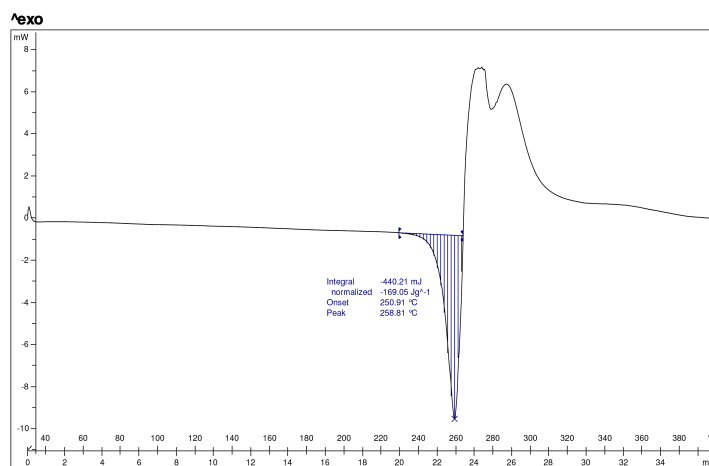


Fig. C.133: DSC thermogram of form A of 4:squaric acid salt

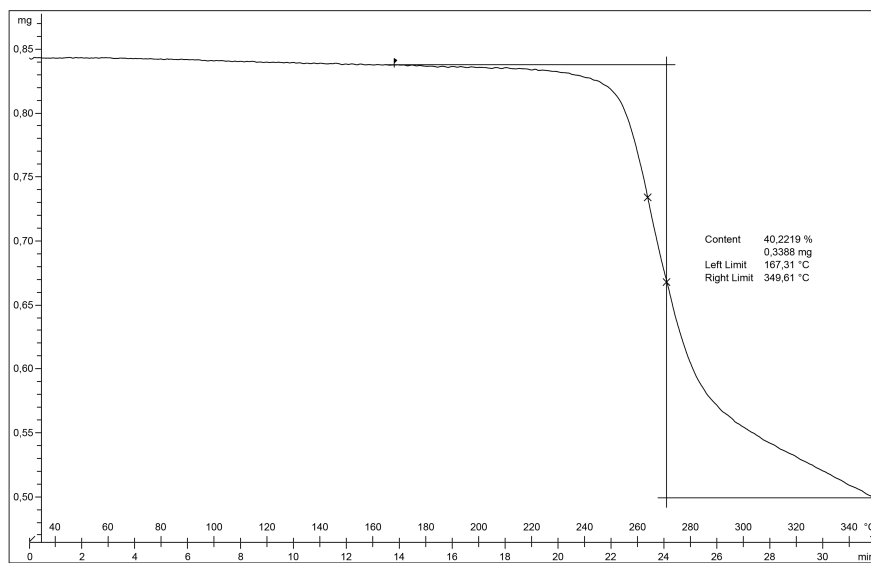
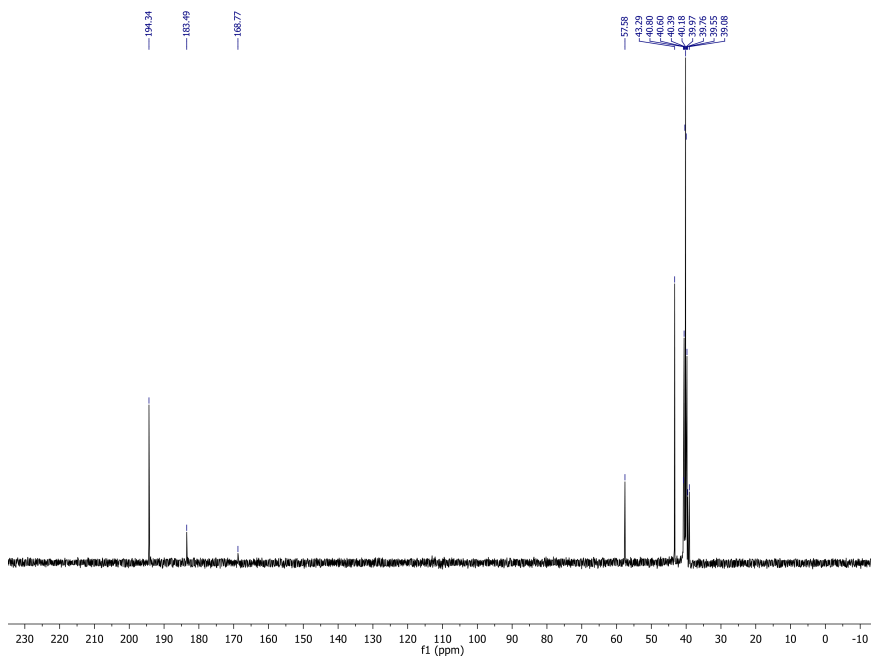
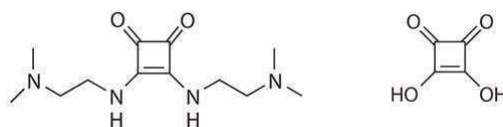


Fig. C.134: TGA thermogram of form A of 4:squaric acid salt

Fig. C.135: ^{13}C -NMR spectrum of form A of 4:squaric acid salt

C.2.7 Salt of 4 : squaric acid, form B



4 : squaric acid

Structure	4-VII-B
Empirical formula	$C_{12} H_{22} N_4 O_2 \cdot C_4 H_2 O_4 \cdot H_2 O$
Formula Weight	386.41
Temperature (K)	110 (2)
Wavelength (Å)	0.71073
Crystal system	Monoclinic
space group	$P2_1/c$
a, b, c (Å)	10.737(6), 11.931(5), 16.323(7)
α, β, γ (°)	90, 119.13(3), 90
Volume (Å ³)	1826.5(15)
Z, Density (calc.) (Mg/m ³)	4, 1.405
Absorption coefficient (mm ⁻¹)	0.111
F(000)	824
Crystal size (mm ³)	0.2 x 0.1 x 0.1
θ range for data collection (°)	2.17 to 32.49
Limiting indices	$-12 \leq h \leq 16, -17 \leq k \leq 17, -21 \leq l \leq 21$
Reflections collected / unique	13716/5911
Completeness to θ (%)	99.4
Absorption correction	Empirical
Max. and min. transmission	0.90 and 0.89
Refinement method	Full-matrix least-squares on F^2
Data/restraints/parameters	5911/ 9 /273
Goodness-of - fit on F^2	0.866
Final R indices [$I > 2\sigma(I)$]	R1 = 0.0534, wR2 = 0.1181
R indices (all data)	R1 = 0.1464, wR2 = 0.1429
Largest diff. peak and hole (e.Å ⁻³)	0.204 and -0.198
CCDC number	987595

Fig. C.136: Crystallographic data of form B of 4:squaric acid salt obtained by SXRD

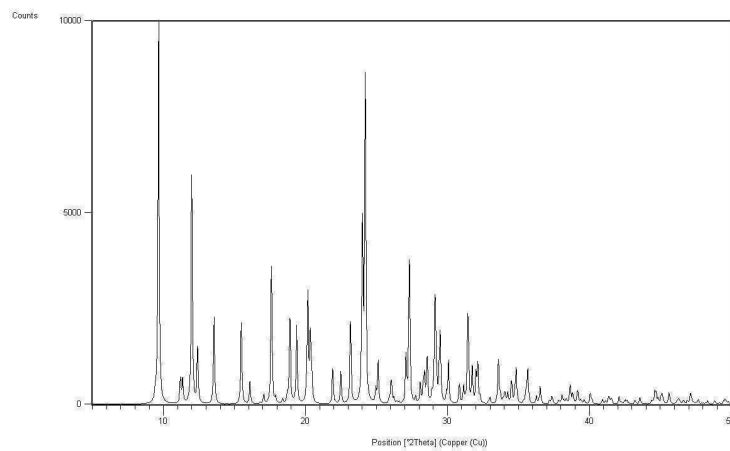


Fig. C.137: Calculated powder X-ray diffractogram of form B of **4:squaric acid salt**

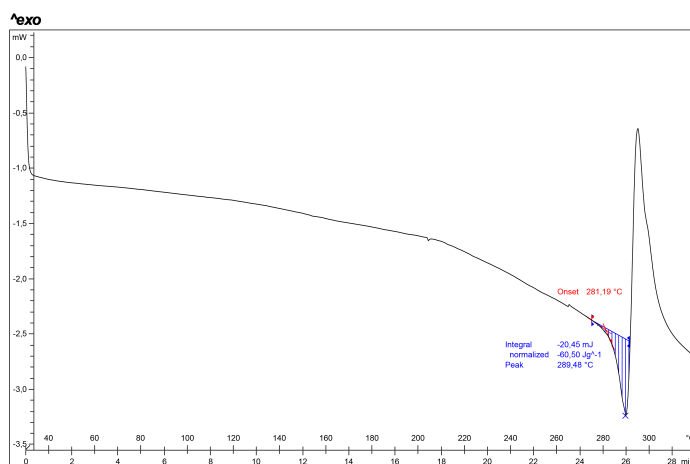


Fig. C.138: DSC thermogram of form B of **4:squaric acid salt**

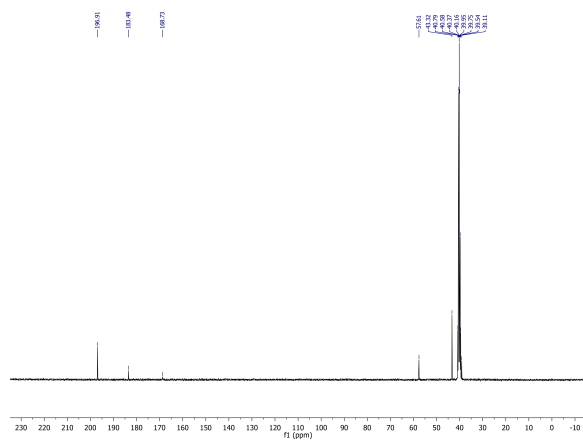
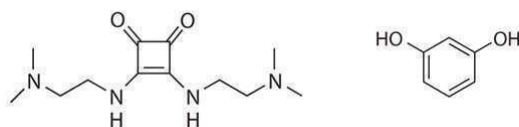


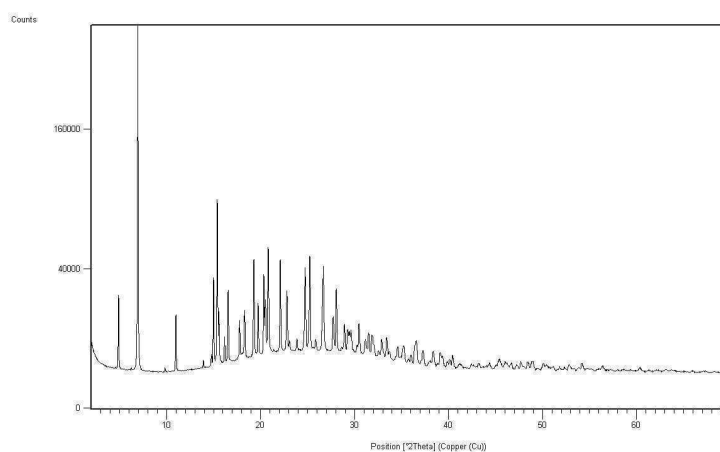
Fig. C.139: ¹³C-NMR spectrum of form B of **4:squaric acid salt**

C.2.8 Cocrystal of 4 : resorcinol, form A



4 : resorcinol

Structure	4-VIII-A
Empirical formula	$C_{12}H_{22}N_4O_2 \cdot C_6H_6O_2$
Formula Weight	364.10
Temperature (K)	293
Wavelength (Å)	1.54175
Crystal system	Tetragonal
space group	$P4_2/n$
a, b, c (Å)	25.43120(12), 25.43120(12), 6.06772(3)
α, β, γ (°)	90.0, 90.0, 90.0
Volume (Å ³)	3924.27(3)
Z, Density (calc.) (Mg/m ³)	8, 1.232
θ range for data collection (°)	2.01 to 69.98
Reflections collected	5230
Refinement program	Fullprof
Data/restraints/parameters	2060/ 146 /126
Goodness-of - fit on F ²	9.52
Final R indices [$I > 2\sigma(I)$]	R1 = 0.0289, wR2 = 0.0411
R indices (all data)	R1 = 0.0842, wR2 = 0.0853
CCDC number	1022284

Fig. C.140: Crystallographic data of form A of **4:resorcinol** cocrystal obtained by SXRDFig. C.141: Powder X-ray diffractogram of form A of **4:resorcinol** cocrystal

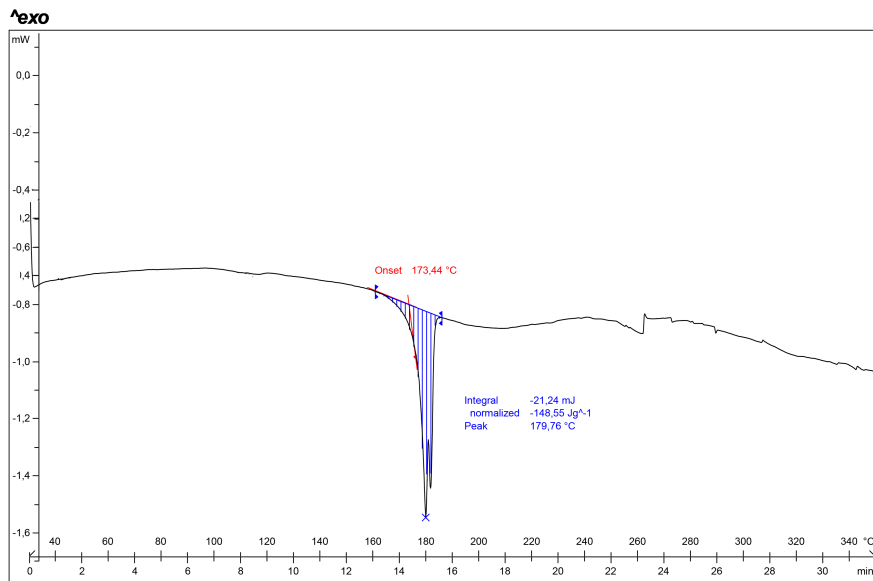


Fig. C.142: DSC thermogram of form A of 4:resorcinol cocrystal

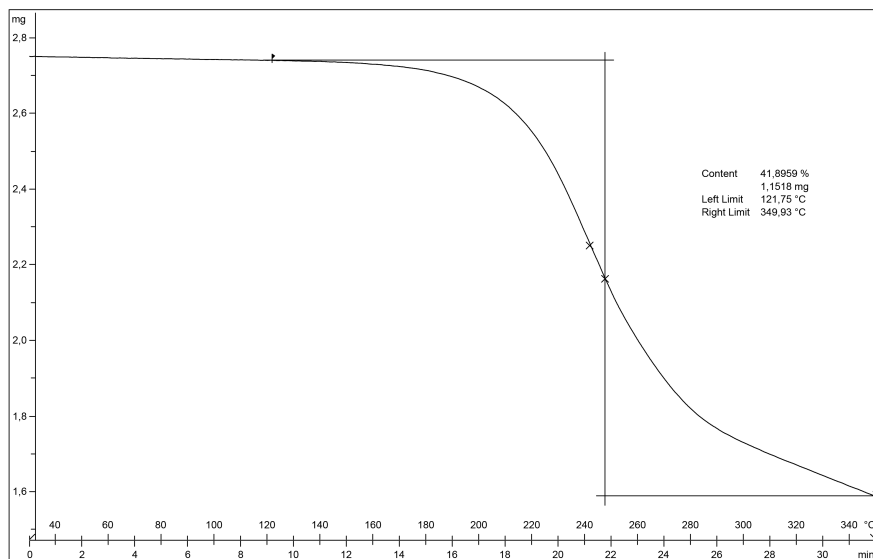
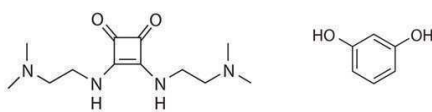
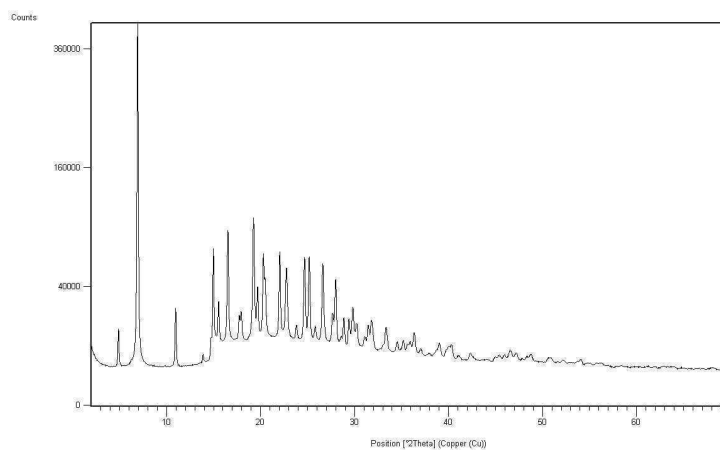
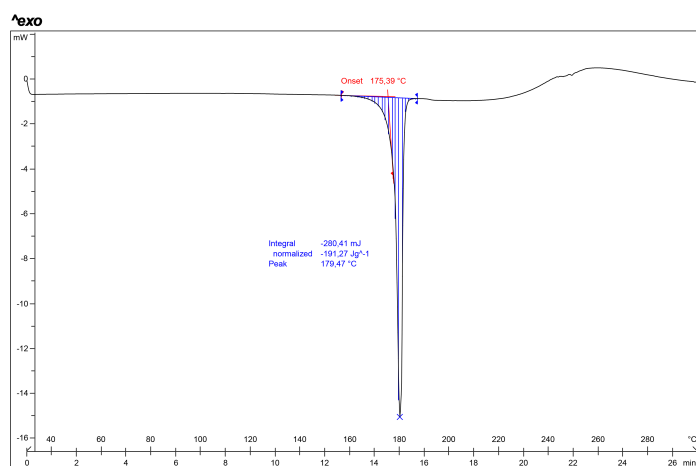


Fig. C.143: TGA thermogram of form A of 4:resorcinol cocrystal

C.2.9 Cocrystal of 4 : resorcinol, form B



4 : resorcinol

Fig. C.144: Powder X-ray diffractogram of form B of **4:resorcinol** cocrystalFig. C.145: DSC thermogram of form B of **4:resorcinol** cocrystal

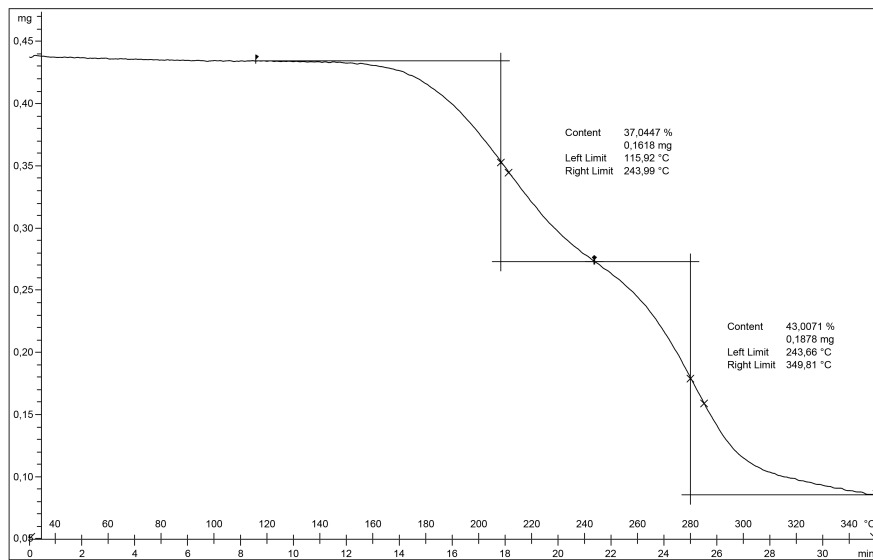
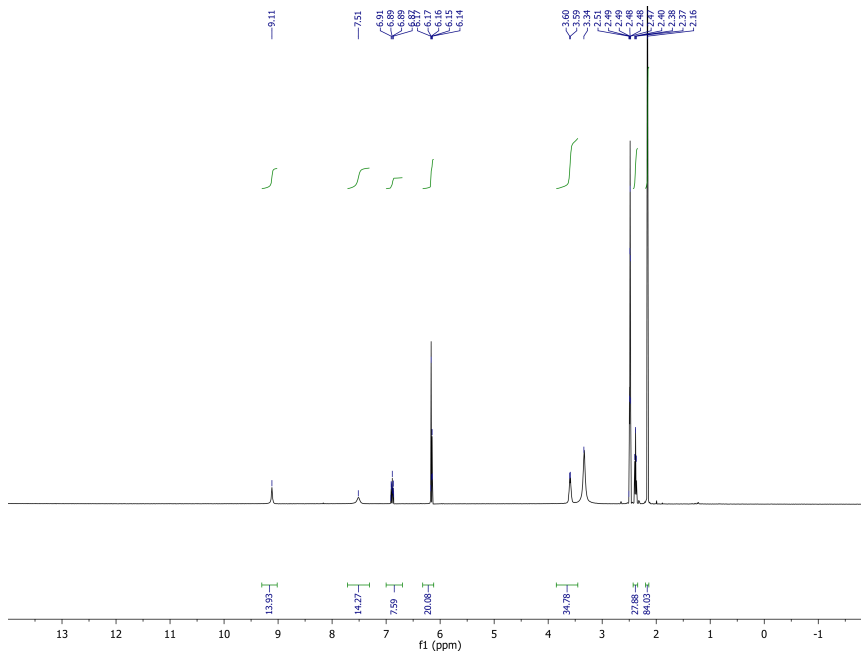
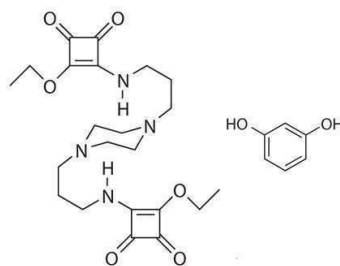


Fig. C.146: TGA thermogram of form B of 4:resorcinol cocrystal

Fig. C.147: ¹H-NMR spectrum of form B of 4:resorcinol cocrystal

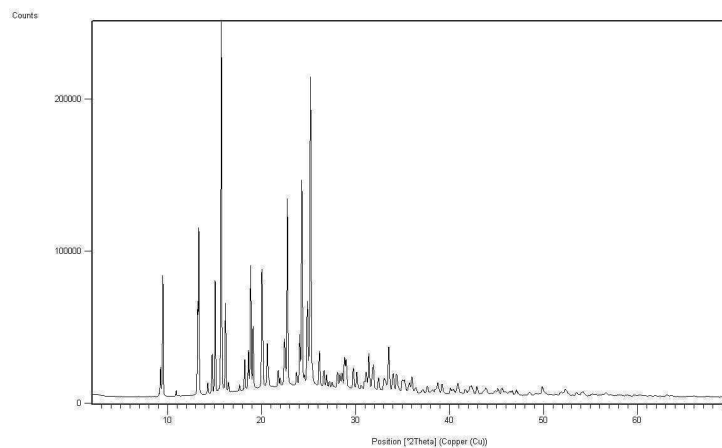
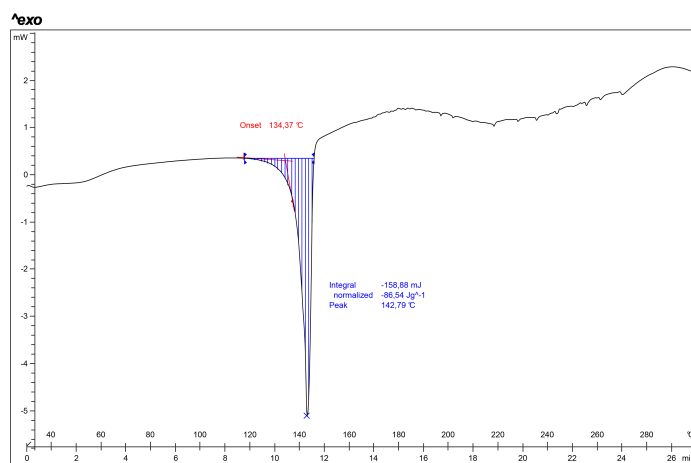
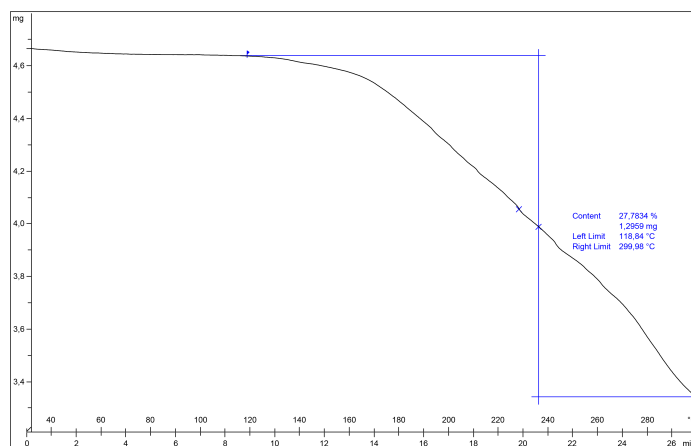
C.2.10 Cocystal of 10 : resorcinol, form A



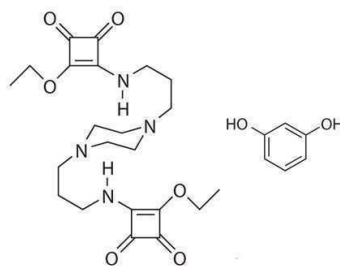
10 : resorcinol

Structure	11-VIII-A
Empirical formula	$C_{22}H_{32}N_4O_6 \cdot 2(C_6H_6O_2)$
Formula Weight	668.73
Temperature (K)	293
Wavelength (Å)	1.54175
Crystal system	Triclinic
space group	<i>P</i> -1
a, b, c (Å)	11.41571(9), 10.98858(10), 8.19298(5)
α, β, γ (°)	86.5493(4), 99.3077(4), 122.3577(4)
Volume (Å ³)	856.303(12)
Z, Density (calc.) (Mg/m ³)	1, 1.295
θ range for data collection (°)	2.02 to 69.98
Reflections collected	5229
Refinement program	Fullprof
Data/restraints/parameters	1793/ 121 /82
Goodness-of - fit on F ²	16.64
Final R indices [<i>I</i> > 2 σ (<i>I</i>)]	R1 = 0.0283, wR2 = 0.0360
R indices (all data)	R1 = 0.0673, wR2 = 0.0676
CCDC number	883950

Fig. C.148: Crystallographic data of form A of **10:resorcinol** cocystal obtained by SXR

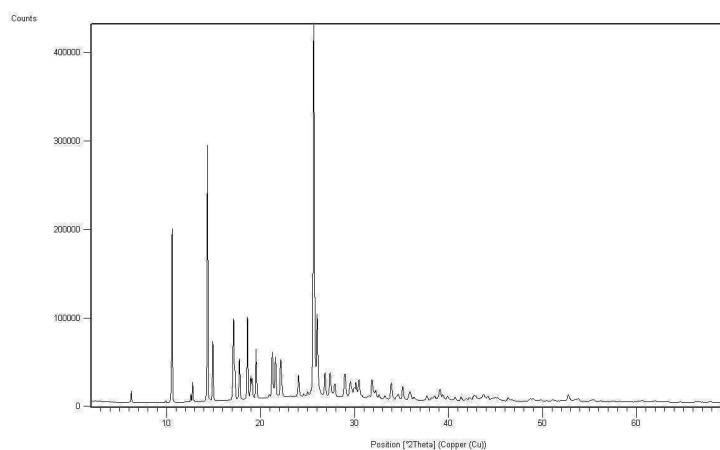
Fig. C.149: Powder X-ray diffractogram of form A of **10:resorcinol** cocrystalFig. C.150: DSC thermogram of form A of **10:resorcinol** cocrystalFig. C.151: TGA thermogram of form A of **10:resorcinol** cocrystal

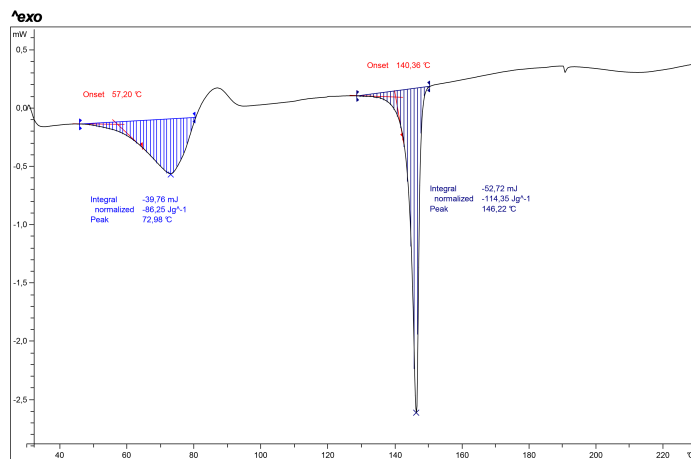
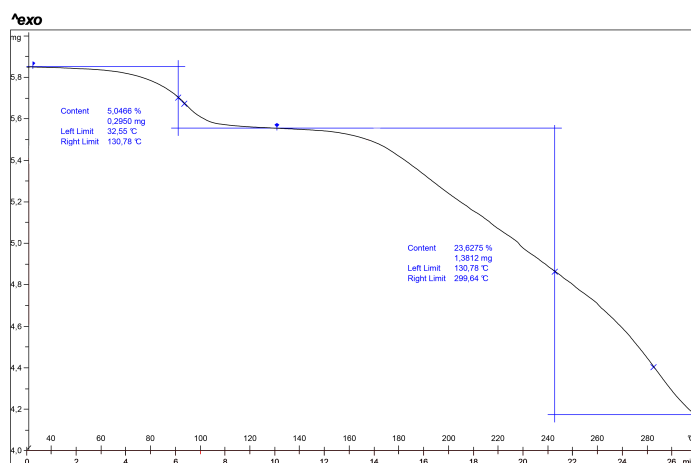
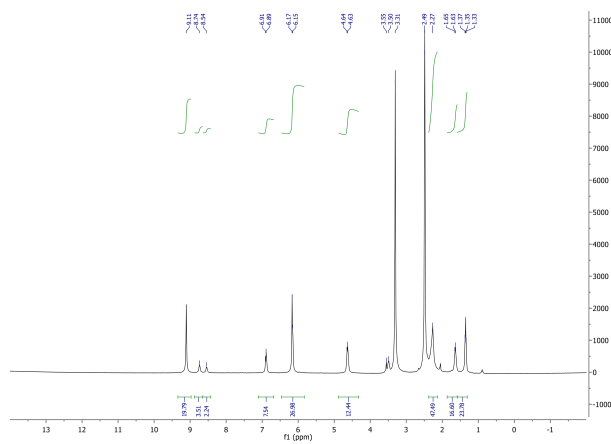
C.2.11 Cocrystal of 10 : resorcinol, form B



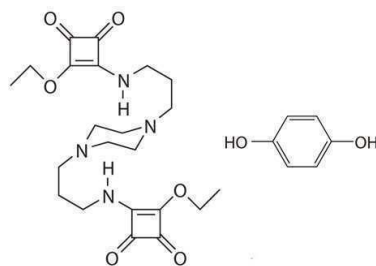
10 : resorcinol

Structure	11-VIII-B
Empirical formula	C ₂₂ H ₃₂ N ₄ O ₆ · 2(C ₆ H ₆ O ₂) · 2(H ₂ O)
Formula Weight	704.76
Temperature (K)	293
Wavelength (Å)	1.54175
Crystal system	Triclinic
space group	<i>P</i> -1
a, b, c (Å)	7.04800(6), 9.32696(15), 14.50037(19)
α, β, γ (°)	76.7937(9), 81.7078(7), 77.4380(6)
Volume (Å ³)	901.286(20)
Z, Density (calc.) (Mg/m ³)	1, 1.297
θ range for data collection (°)	2.02 to 69.98
Reflections collected	5229
Refinement program	Fullprof
Data/restraints/parameters	1940/ 124 /126
Goodness-of-fit on F ²	16.64
Final R indices [I > 2σ(I)]	R1 = 0.037, wR2 = 0.050
R indices (all data)	R1 = 0.084, wR2 = 0.089
CCDC number	883951

Fig. C.152: Crystallographic data of form B of **10:resorcinol** cocrystal obtained by SXRDFig. C.153: Powder X-ray diffractogram of form B of **10:resorcinol** cocrystal

Fig. C.154: DSC thermogram of form B of **10:resorcinol** cocrystalFig. C.155: TGA thermogram of form B of **10:resorcinol** cocrystalFig. C.156: ¹H-NMR spectrum of form B of **10:resorcinol** cocrystal

C.2.12 Cocrystal of 10 : hydroquinone, form A



10 : hydroquinone

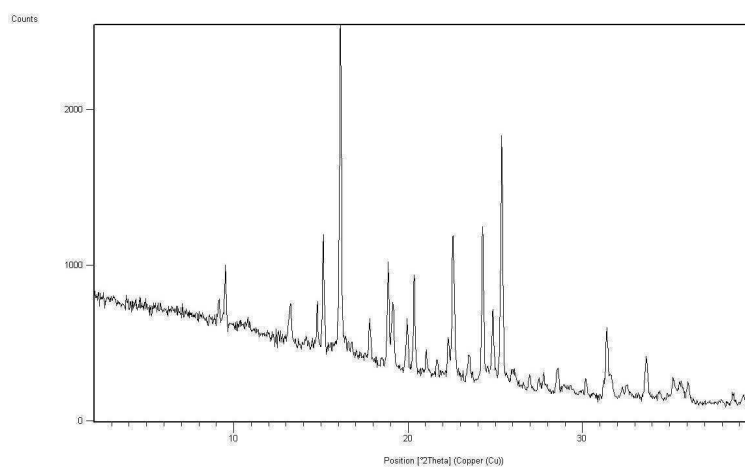


Fig. C.157: Powder X-ray diffractogram of form A of 10:hydroquinone cocrystal

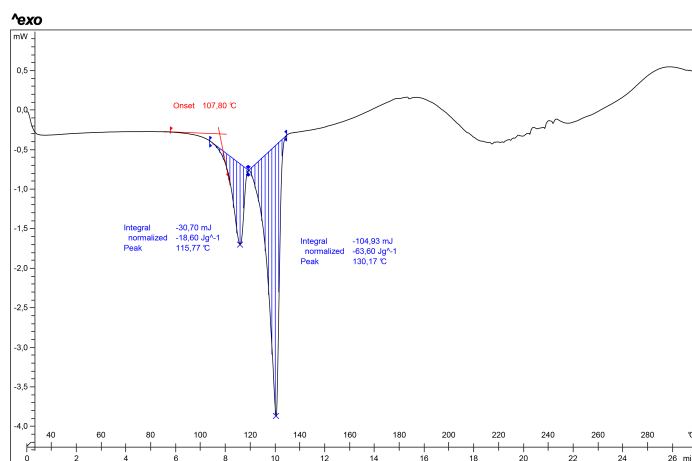


Fig. C.158: DSC thermogram of form A of 10:hydroquinone cocrystal

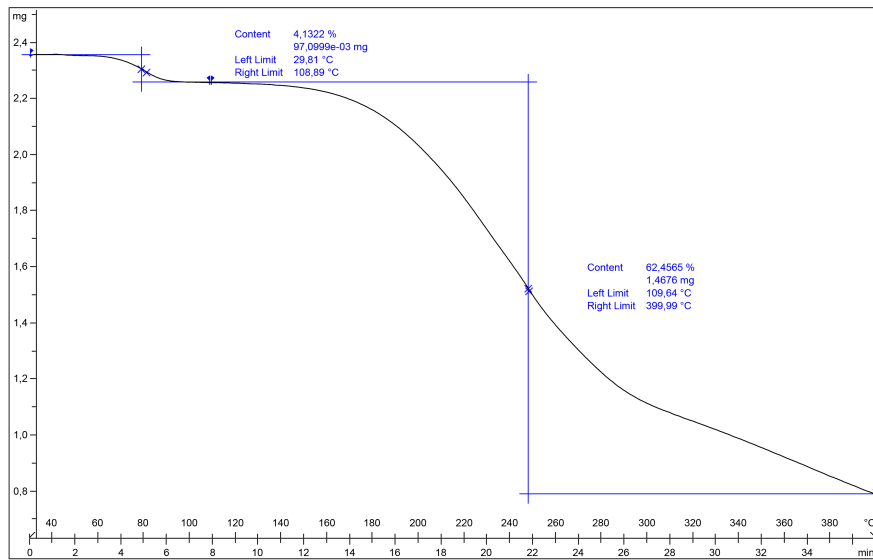
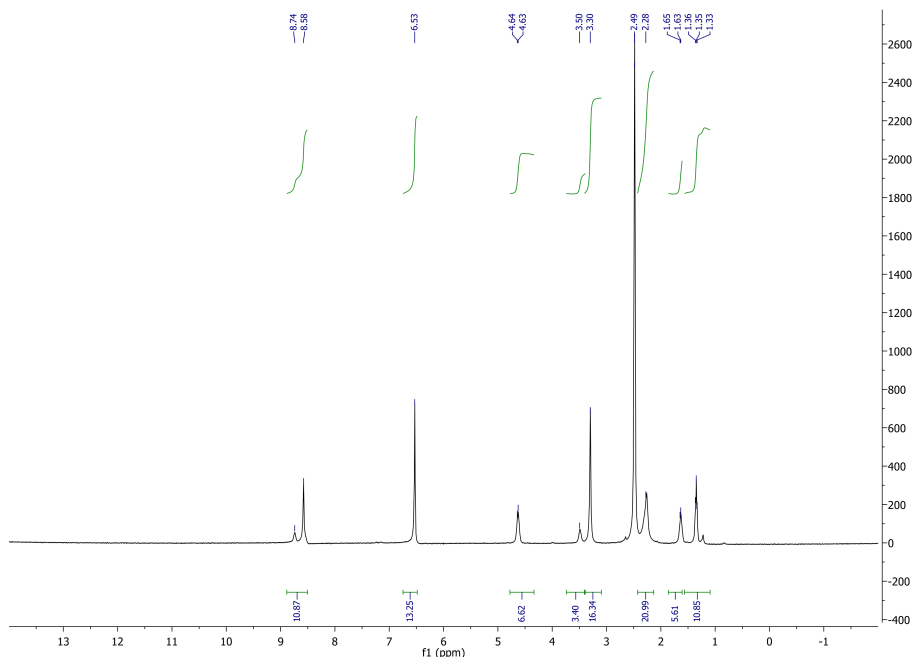
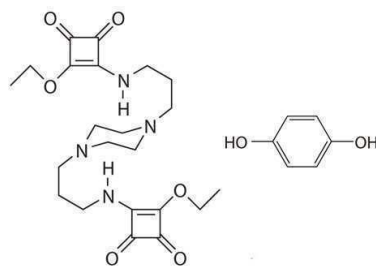


Fig. C.159: TGA thermogram of form A of 10:hydroquinone cocrystal

Fig. C.160: ¹H-NMR spectrum of form A of 10:hydroquinone cocrystal

C.2.13 Cocrystal of 10 : hydroquinone, form B



10 : hydroquinone

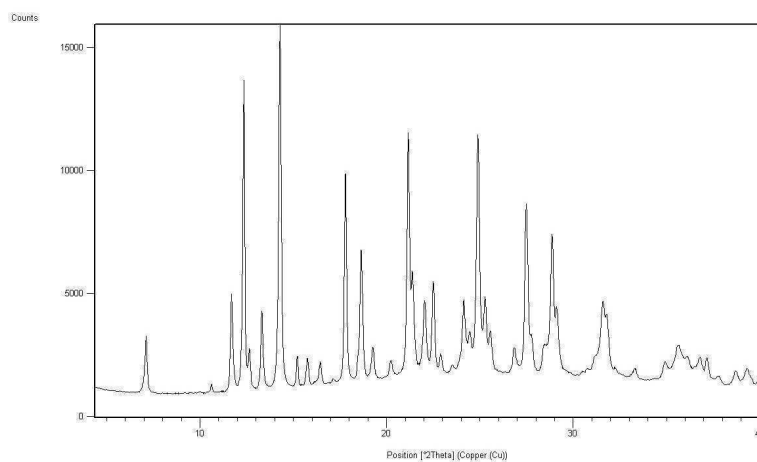


Fig. C.161: Powder X-ray diffractogram of form B of 10:hydroquinone cocrystal

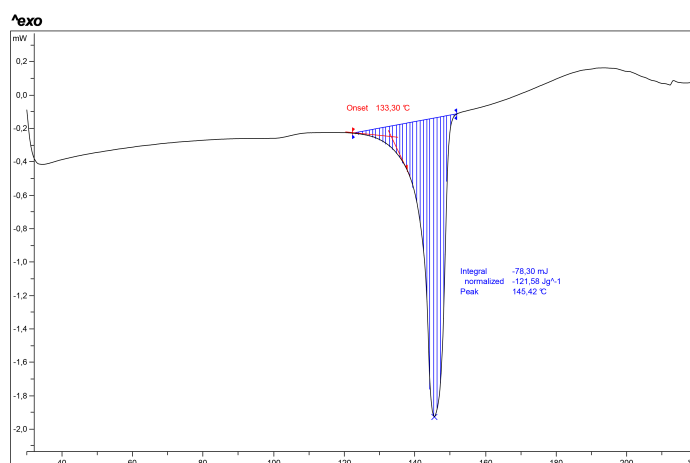


Fig. C.162: DSC thermogram of form B of 10:hydroquinone cocrystal

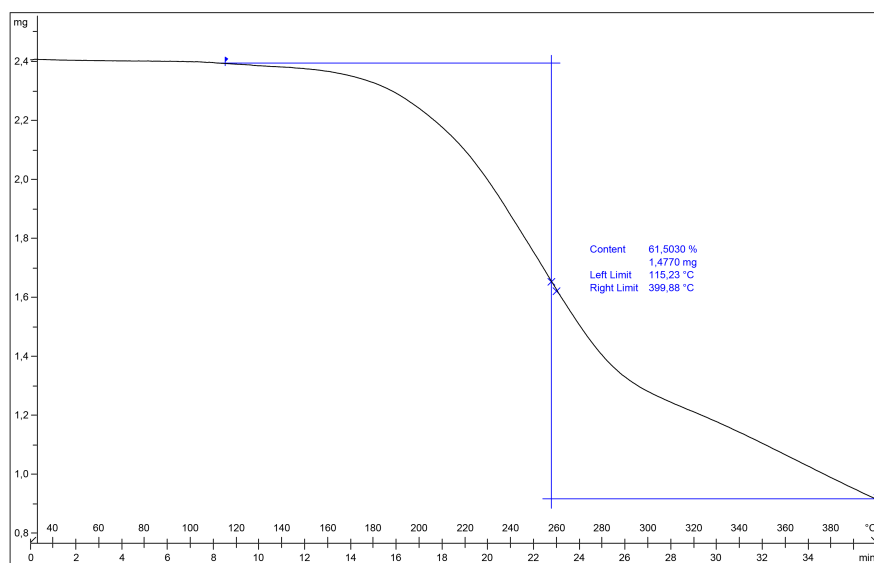


Fig. C.163: TGA thermogram of form B of **10:hydroquinone** cocrystal

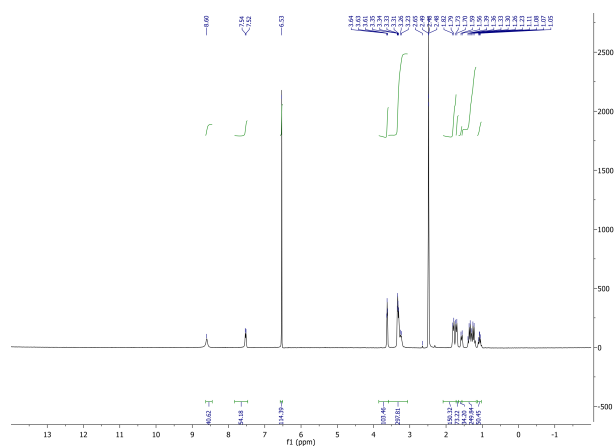
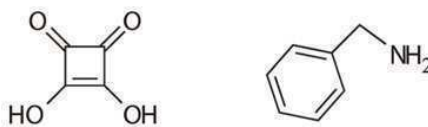


Fig. C.164: ¹H-NMR spectrum of form B of **10:hydroquinone** cocrystal

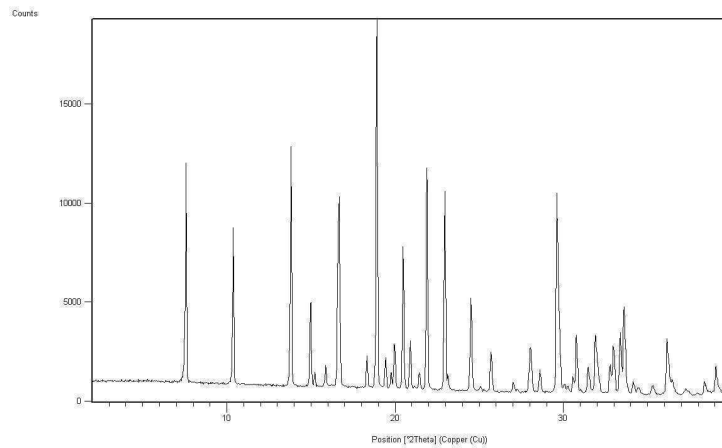
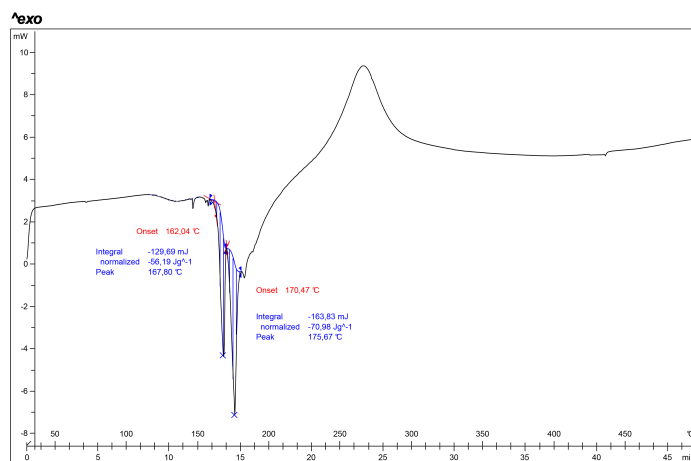
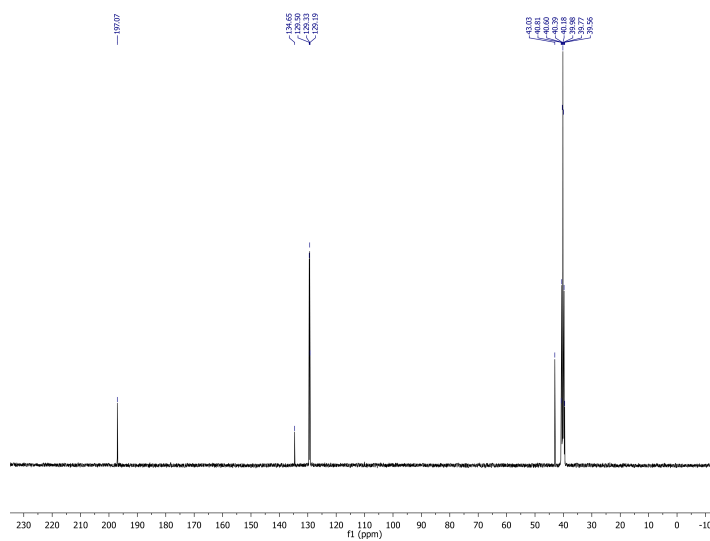
C.2.14 Salt 18



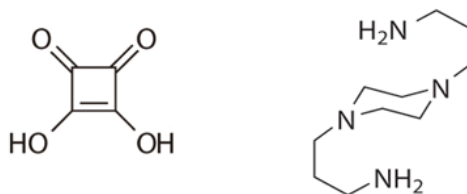
squaric acid : benzylamine

Structure	18
Empirical formula	2(C ₇ H ₁₀ N) · 2(C ₄ H ₂ O ₄) · H ₂ O
Formula Weight	495.42
Temperature (K)	293 (2)
Wavelength (Å)	0.71073
Crystal system	Monoclinic
space group	C2/c
a, b, c (Å)	23.793(11), 9.123(2), 10.925(4)
α, β, γ (°)	90, 102.60(2), 90
Volume (Å ³)	2314.3(15)
Z, Density (calc.) (Mg/m ³)	4, 1.319
Absorption coefficient (mm ⁻¹)	0.104
F(000)	964
Crystal size (mm ³)	0.2 x 0.09 x 0.09
θ range for data collection (°)	1.75 to 30.61
Limiting indices	-31 ≤ h ≤ 31, -12 ≤ k ≤ 11, -12 ≤ l ≤ 14
Reflections collected / unique	10061/3048
Completeness to θ (%)	98.6
Absorption correction	Empirical
Max. and min. transmission	0.99 and 0.98
Refinement method	Full-matrix least-squares on F ²
Data/restraints/parameters	3048/ 4 /153
Goodness-of-fit on F ²	1.132
Final R indices [I > 2σ(I)]	R1 = 0.0516, wR2 = 0.1466
R indices (all data)	R1 = 0.0558, wR2 = 0.1495
Largest diff. peak and hole (e.Å ⁻³)	0.244 and 0.1495
CCDC number	987591

Fig. C.165: Crystallographic data of 18 salt obtained by SXRD

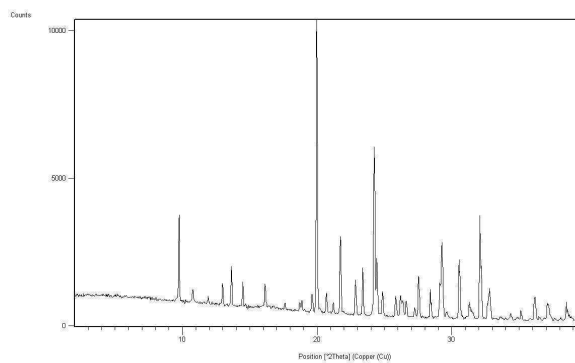
Fig. C.166: Powder X-ray diffractogram of **18** saltFig. C.167: DSC thermogram of **18** saltFig. C.168: ^{13}C -NMR spectrum of **18** salt

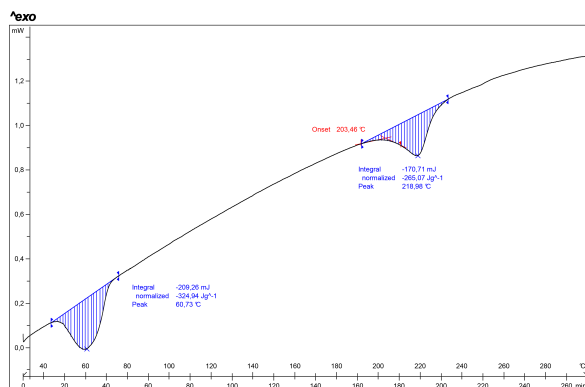
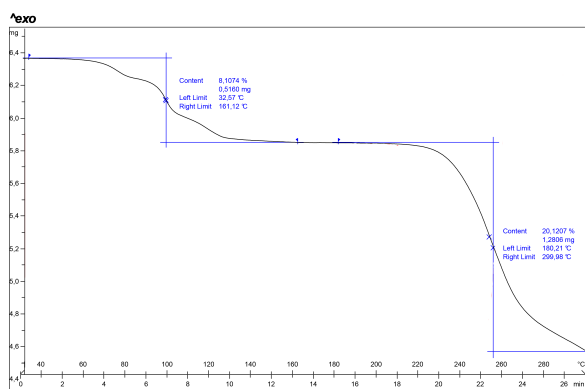
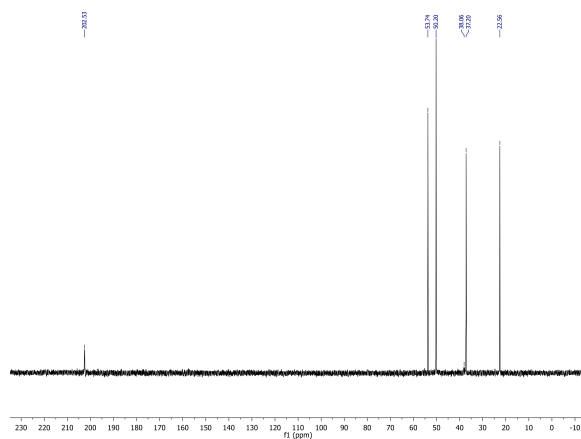
C.2.15 Salt 19



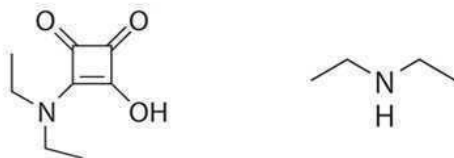
squaric acid:1,4-bis(3-aminopropyl)piperazine

Structure	19
Empirical formula	C ₁₄ H ₂₄ N ₄ ·C ₄ H ₂ O ₄ ·2(H ₂ O)
Formula Weight	392.41
Temperature (K)	296 (2)
Wavelength (Å)	0.71073
Crystal system	Monoclinic
space group	C2/c
a, b, c (Å)	18.512(11), 7.339(3), 16.768(8)
α, β, γ (°)	90, 102.90(2), 90
Volume (Å ³)	2222.6(19)
Z, Density (calc.) (Mg/m ³)	2, 1.443
Absorption coefficient (mm ⁻¹)	0.120
F(000)	1032
Crystal size (mm ³)	0.2 x 0.1 x 0.1
θ range for data collection (°)	2.26 to 29.66
Limiting indices	-25 ≤ h ≤ 25, -9 ≤ k ≤ 9, -20 ≤ l ≤ 20
Reflections collected / unique	7470/2430
Completeness to θ (%)	96.4
Absorption correction	Empirical
Max. and min. transmission	0.99 and 0.98
Refinement method	Full-matrix least-squares on F ²
Data/restraints/parameters	2430/0/171
Goodness-of-fit on F ²	1.104
Final R indices [I > 2σ(I)]	R1 = 0.0444, wR2 = 0.1146
R indices (all data)	R1 = 0.087, wR2 = 0.1184
Largest diff. peak and hole (e.Å ⁻³)	0.264 and -0.179
CCDC number	987592

Fig. C.169: Crystallographic data of **19** salt obtained by SXRDFig. C.170: Powder X-ray diffractogram of **19** salt

Fig. C.171: DSC thermogram of **19** saltFig. C.172: TGA thermogram of **19** saltFig. C.173: ¹³C-NMR spectrum of **19** salt

C.2.16 Salt 20



diethylamididosquaric acid : diethylamine

Structure	20
Empirical formula	C ₈ H ₁₀ N ₂ O ₃ C ₄ H ₁₂ N
Formula Weight	242.32
Temperature (K)	105 (2)
Wavelength (Å)	0.71073
Crystal system	Monoclinic
space group	P2 ₁ /c
a, b, c (Å)	7.041(4), 12.717(5), 16.156(7)
α, β, γ (°)	90, 104.25(3), 90
Volume (Å ³)	1402.1(11)
Z, Density (calc.) (Mg/m ³)	4, 1.148
Absorption coefficient (mm ⁻¹)	0.082
F(000)	528
Crystal size (mm ³)	0.1 x 0.09 x 0.08
θ range for data collection (°)	2.06 to 32.34
Limiting indices	-9<=h<=9, -18<=k<=18, -23<=l<=23
Reflections collected / unique	12749/4065
Completeness to θ (%)	99.4
Absorption correction	Empirical
Max. and min. transmission	0.99 and 0.98
Refinement method	Full-matrix least-squares on F ²
Data/restraints/parameters	4065/ 6 /158
Goodness-of - fit on F ²	1.113
Final R indices [I > 2σ(I)]	R1 = 0.0593, wR2 = 0.1604
R indices (all data)	R1 = 0.0803, wR2 = 0.1742
Largest diff. peak and hole (e.Å ⁻³)	0.247 and -0.282
CCDC number	987593

Fig. C.174: Crystallographic data of 20 salt obtained by SXRD

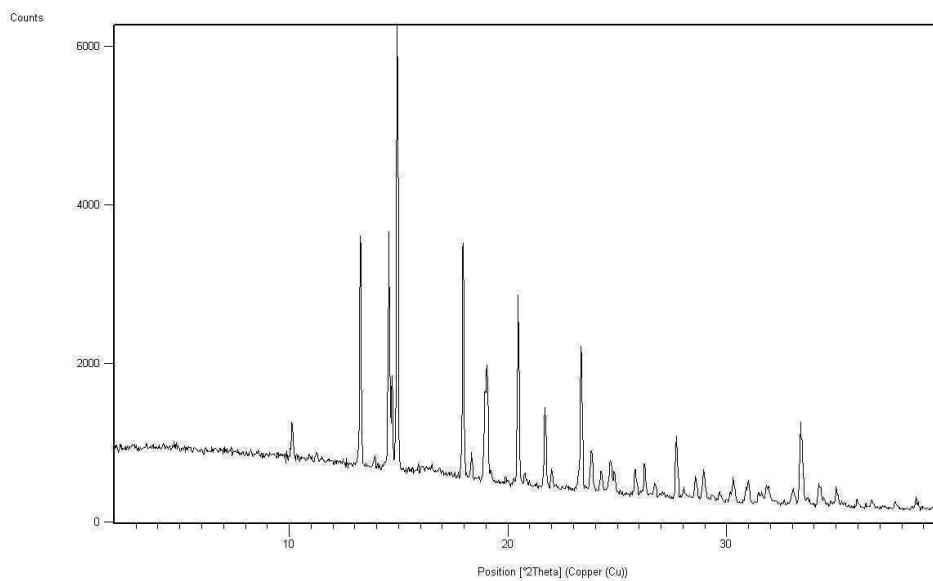


Fig. C.175: Powder X-ray diffractogram of **20** salt

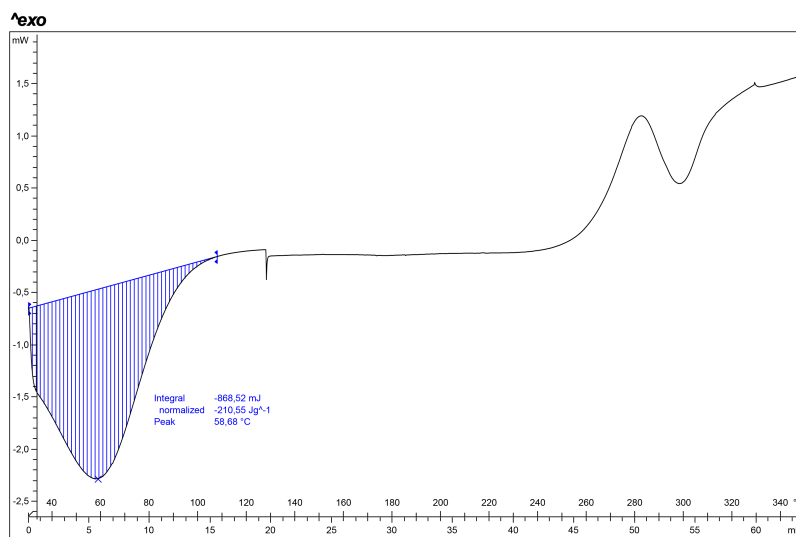
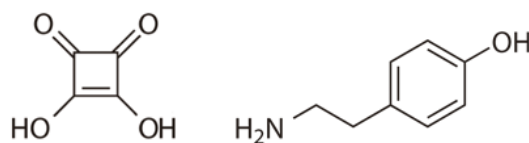


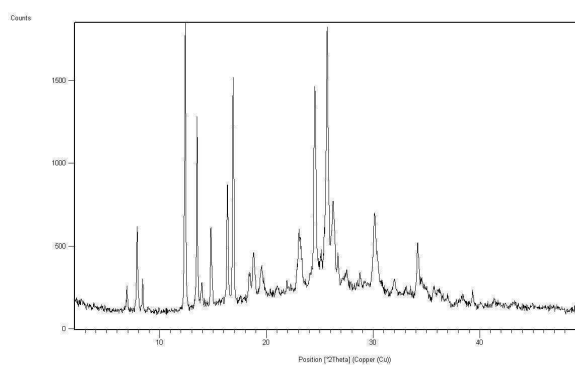
Fig. C.176: DSC thermogram of **20** salt

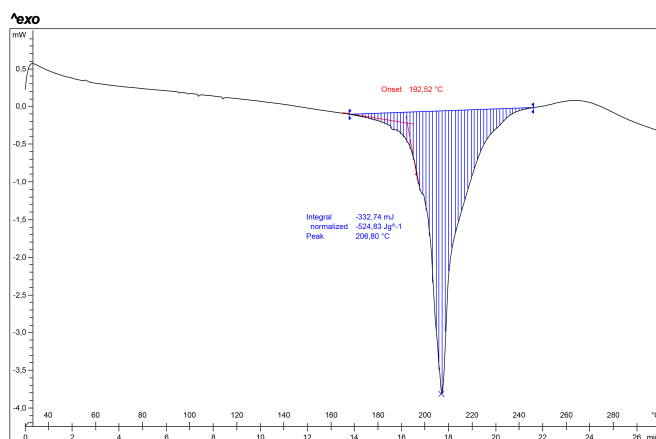
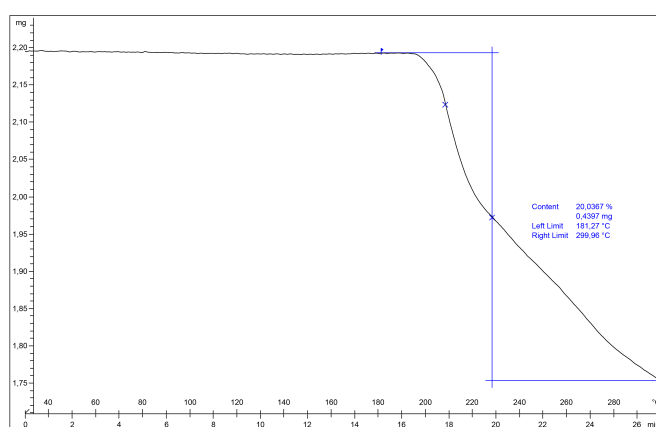
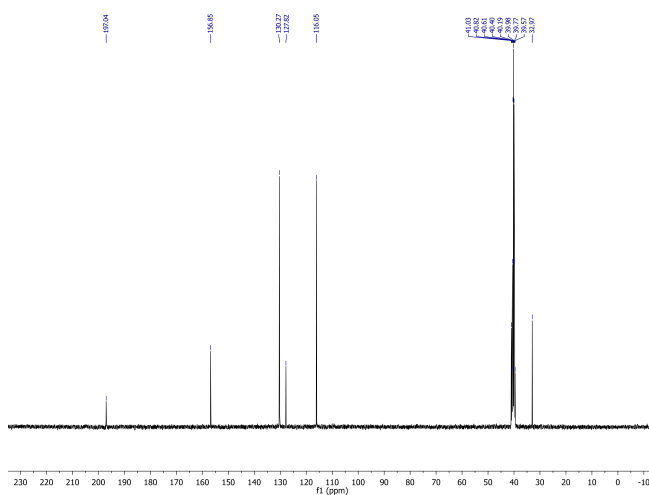
C.2.17 Salt 21



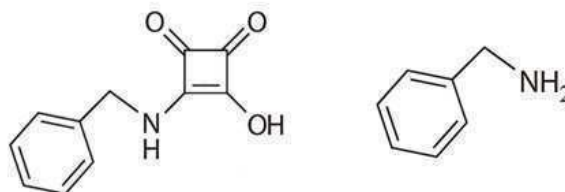
squaric acid:tyramine

Structure	21
Empirical formula	$C_{11}H_9NO_3 \cdot C_7H_9N$
Formula Weight	319.35
Temperature (K)	293 (2)
Wavelength (Å)	0.71073
Crystal system	Orthorhombic
space group	<i>Pbca</i>
a, b, c (Å)	23.15(2), 10.354(10), 29.282(10)
α, β, γ (°)	90, 90, 90
Volume (Å ³)	7018 (10)
Z, Density (calc.) (Mg/m ³)	8, 1.209
Absorption coefficient (mm ⁻¹)	0.085
F(000)	2704
Crystal size (mm ³)	0.2 x 0.2 x 0.1
θ range for data collection (°)	1.39 to 32.58
Limiting indices	$-34 \leq h \leq 33, -13 \leq k \leq 13, -44 \leq l \leq 37$
Reflections collected / unique	32155/8532
Completeness to θ (%)	88.5
Absorption correction	Empirical
Max. and min. transmission	0.99 and 0.98
Refinement method	Full-matrix least-squares on F ²
Data/restraints/parameters	8532/18/388
Goodness-of-fit on F ²	0.905
Final R indices [$I > 2\sigma(I)$]	R1 = 0.0555, wR2 = 0.1277
R indices (all data)	R1 = 0.1901, wR2 = 0.1609
Largest diff. peak and hole (e.Å ⁻³)	0.306 and -0.239
CCDC number	987596

Fig. C.177: Crystallographic data of **21** salt obtained by SXRDFig. C.178: Powder X-ray diffractogram of **21** salt

Fig. C.179: DSC thermogram of **21** saltFig. C.180: TGA thermogram of **21** saltFig. C.181: ^{13}C -NMR spectrum of **21** salt

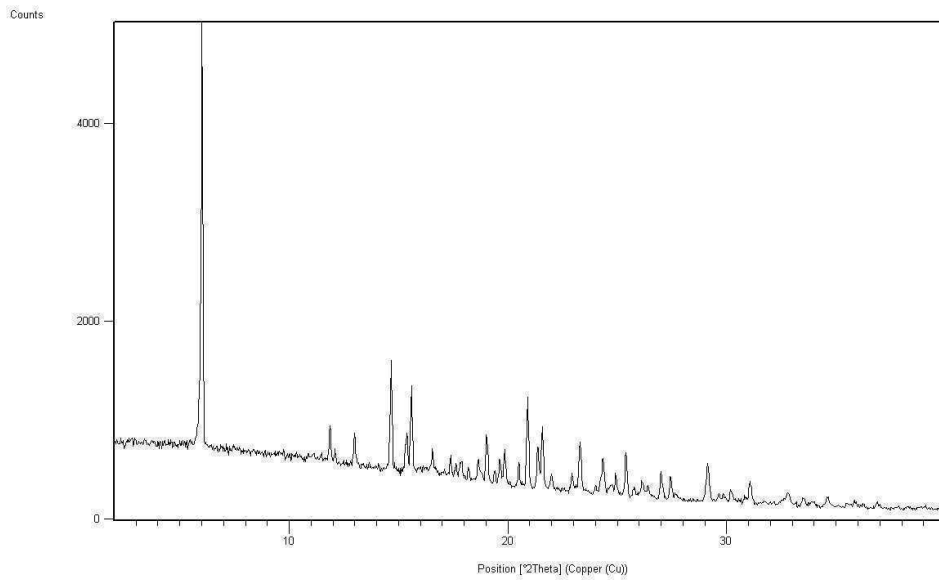
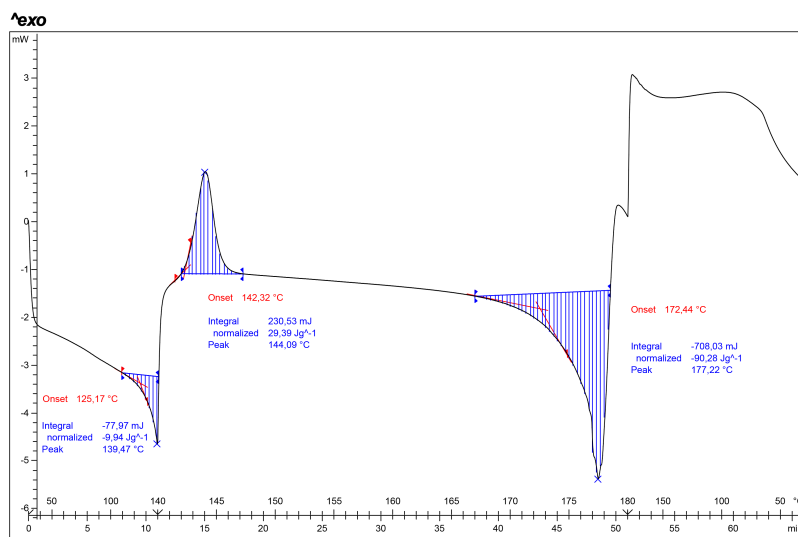
C.2.18 Salt 22



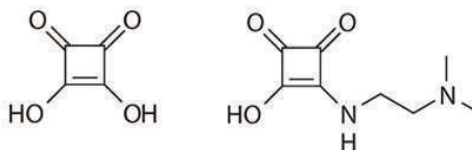
benzylamidosquaric acid : benzylamine

Structure	22
Empirical formula	$2(C_{11}H_8NO_3) \cdot 2(C_7H_{10}N) \cdot H_2O$
Formula Weight	638.70
Temperature (K)	293 (2)
Wavelength (Å)	0.71073
Crystal system	Orthorhombic
space group	Pbca
a, b, c (Å)	23.15(2), 10.354(10), 29.282(10)
α, β, γ (°)	90, 90, 90
Volume (Å ³)	7018(10)
Z, Density (calc.) (Mg/m ³)	8, 1.09
Absorption coefficient (mm ⁻¹)	0.085
F(000)	2704
Crystal size (mm ³)	0.20 x 0.19 x 0.08
θ range for data collection (°)	1.39 to 32.58
Limiting indices	$-34 \leq h \leq 33, -13 \leq k \leq 13, -44 \leq l \leq 37$
Reflections collected / unique	32155/8532
Completeness to θ (%)	88.5
Absorption correction	Empirical
Max. and min. transmission	0.99 and 0.98
Refinement method	Full-matrix least-squares on F^2
Data/restraints/parameters	8532/ 18 /388
Goodness-of - fit on F^2	0.905
Final R indices [$I > 2\sigma(I)$]	R1 = 0.0555, wR2 = 0.1277
R indices (all data)	R1 = 0.1901, wR2 = 0.1609
Largest diff. peak and hole (e.Å ⁻³)	0.306 and -0.239
CCDC number	987596

Fig. C.182: Crystallographic data of **22** salt obtained by SXRD

Fig. C.183: Powder X-ray diffractogram of **22** saltFig. C.184: DSC thermogram of **22** salt

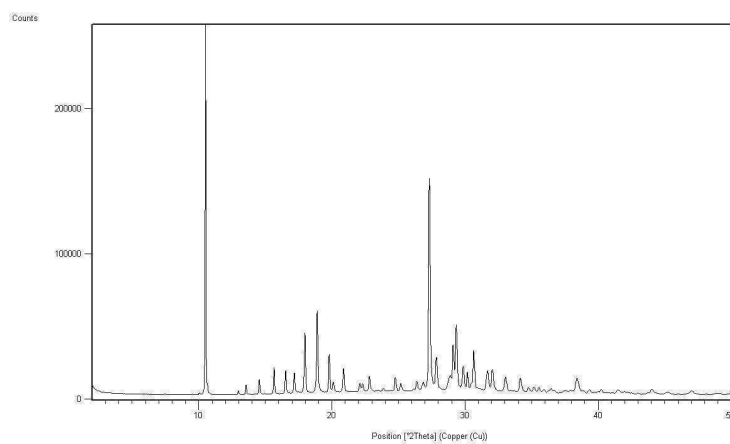
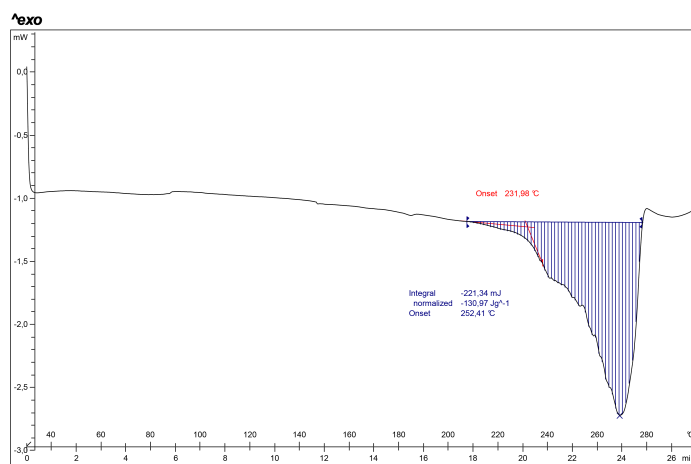
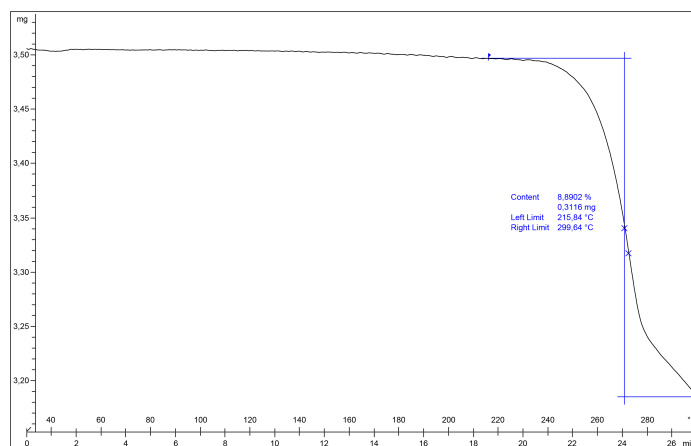
C.2.19 Salt of 17:squaric acid



17

Structure	17-VII
Empirical formula	$C_8 H_{12} N_2 O_3 \cdot C_4 H_2 O_4$
Formula Weight	298.25
Temperature (K)	105 (2)
Wavelength (Å)	0.71073
Crystal system	Monoclinic
space group	$P2_1/n$
a, b, c (Å)	7.470(3), 16.818(4), 10.286(4)
α, β, γ (°)	90, 97.37(3), 90
Volume (Å ³)	1281.6(8)
Z, Density (calc.) (Mg/m ³)	4, 1.546
Absorption coefficient (mm ⁻¹)	0.129
F(000)	624
Crystal size (mm ³)	0.1 x 0.09 x 0.08
θ range for data collection (°)	2.34 to 32.26
Limiting indices	$-10 \leq h \leq 10, -20 \leq k \leq 24, -13 \leq l \leq 13$
Reflections collected / unique	12424/3448
Completeness to θ (%)	93.5
Absorption correction	None
Max. and min. transmission	-
Refinement method	Full-matrix least-squares on F^2
Data/restraints/parameters	3448/ 0 /242
Goodness-of-fit on F^2	1.134
Final R indices [$I > 2\sigma(I)$]	R1 = 0.0594, wR2 = 0.1600
R indices (all data)	R1 = 0.0624, wR2 = 0.1640
Largest diff. peak and hole (e.Å ⁻³)	0.367 and -0.362
CCDC number	938374

Fig. C.185: Crystallographic data of 17 salt obtained by SXRD

Fig. C.186: Powder X-ray diffractogram of **17** saltFig. C.187: DSC thermogram of **17** saltFig. C.188: TGA thermogram of **17** salt

Appendix D

Resum

És conegut el fet que les esquaramides presenten una doble capacitat donadora i acceptora d'enllaços d'hidrogen en solució que les fa interessants en àrees com la química supramolecular o la química mèdica. No obstant això, la falta d'informació sobre les seves propietats en estat sòlid ens va encoratjar inicialment portar a terme un *screening* polimòrfic de diversos compostos model amb l'objectiu de conèixer els trets estructurals i les preferències conformacionals d'aquesta família de compostos. En una segona fase, vam utilitzar aquesta informació per a dissenyar noves arquitectures supramoleculares a través d'estratègies d'enginyeria cristal·lina. Finalment, l'anàlisi de les seves estructures cristal·lines, en combinació amb l'estudi d'importants fenòmens químics associats com la cooperativitat, la preorganització i la compressió electrostàtica ens van ajudar a establir relacions químiques i cristal·logràfiques entre aquests compostos.

Polimorfisme de les esquaramides

En aquesta tesi s'ha estudiat el polimorfisme de quatre compostos model els quals van ser cuidadosament dissenyats amb el seu particular interès: la dibenzilesquaramida no conté grups acceptors/donadors d'enllaç d'hidrogen addicionals a l'anell esquaramídic (**1**), les dues esquaramides que contenen grups piridina (**2** i **3**) difereixen en la llargada de la cadena alquílica i, finalment, la *N,N*-dimetiletilediesquaramida (**4**) que conté dues amines terciàries i té major flexibilitat (Fig. D.1).

Dibenzilesquaramida (**1**)

L'*screening* polimòrfic experimental del compost **1** ha resultat en l'obtenció de tres formes poli-mòrfiques (Fig. D.2), dues de les quals comparteixen una transició sòlid-

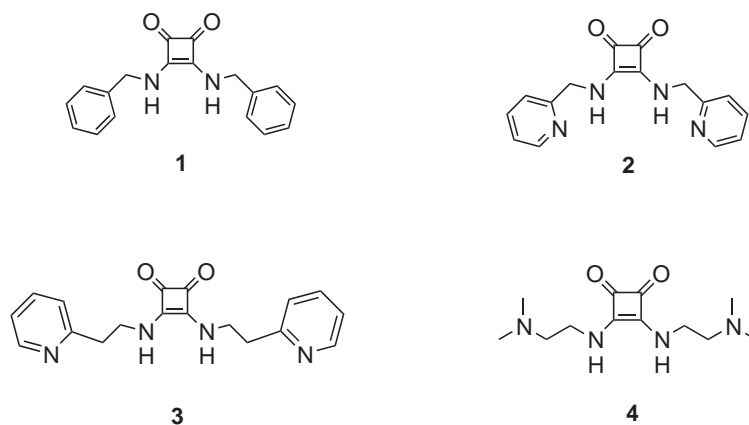


Fig. D.1: Compostos model esquaramídics: (1) Dibenzilsquaramida, (2) 3,4-bis-(2-metilaminopiridil)-1,2-dioxo-3-ciclobutè, (3) 3,4-bis-(2-etilaminopiridil)-1,2-dioxo-3-ciclobutè, (4) 3,4-bis-(2-dimetilamino-etilamino)-1,2-dioxo-3-ciclobutè

sòlid a la mateixa temperatura cap a la fase de punt de fusió més elevat (Fig. D.3).

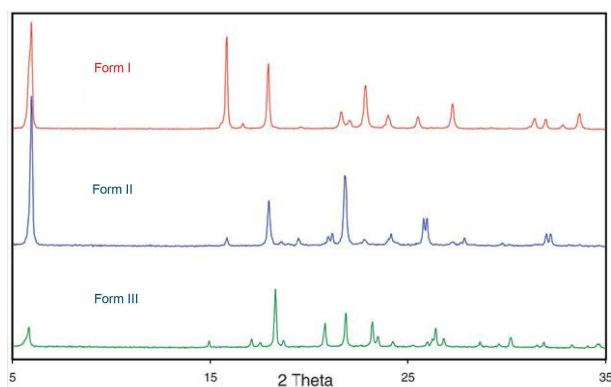


Fig. D.2: Diagrames de DRXP de les formes I, II i III de 1

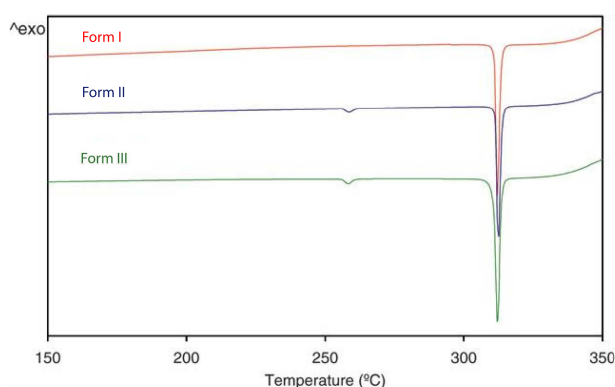


Fig. D.3: Termogrames de DSC de les formes I, II and III of 1

L'anàlisi de les seves estructures cristal·lines revela el mateix motiu estructural cap i cua en direccions paral·leles, antiparal·leles i no paral·leles dels enllaços d'hidrogen formats entre els NH amídics i els carbonils de les unitats es-

quaramídiques (Fig. D.4). La forma II es diferencia de les altres dues en el fet que conté dues molècules en diferent conformació a la unitat asimètrica (Fig. D.5).

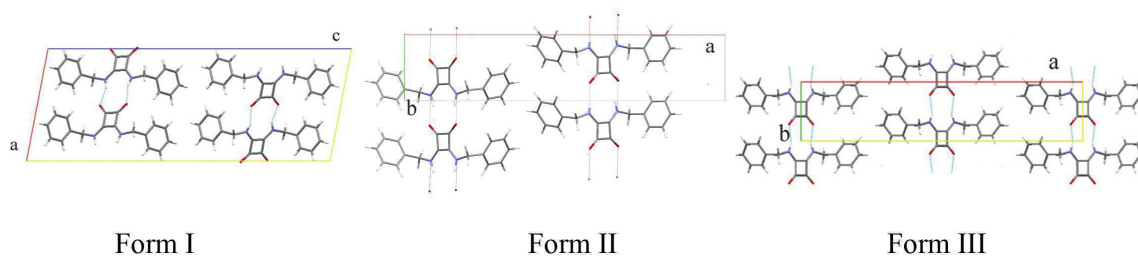


Fig. D.4: Estructures cristal·lines de les formes I, II and III del compost 1

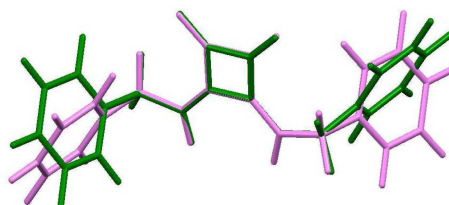


Fig. D.5: Conformers sobreposats en la unitat asimètrica de la forma II del compost 1

3,4-bis-(2-metilaminopiridil)-1,2-dioxo-3-ciclobutè (2)

L'*screening* polimòrfic del compost 2 va resultar en l'obtenció de dues formes (Fig. D.6). La forma I presenta un punt de fusió a 166°C juntament amb una cristal·lització simultània cap a la forma II, la qual fon a 186°C (Fig. D.7).

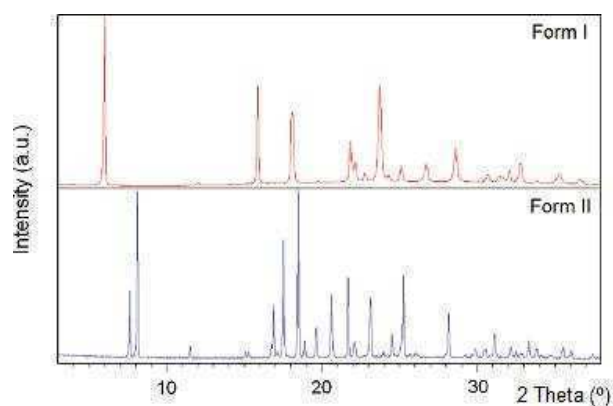


Fig. D.6: Diagrames de DRXP de les formes I i II del compost 2

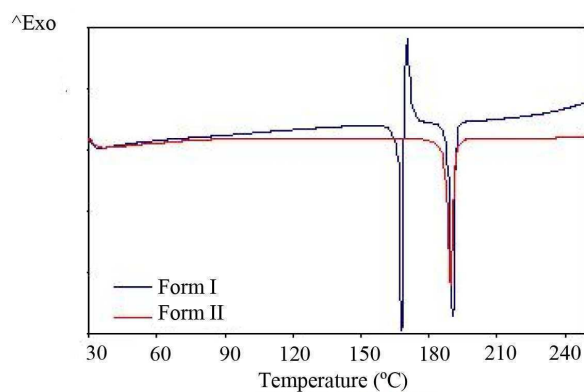


Fig. D.7: Termogrames de DSC de les formes I i II del compost **2**

Ocasionalment, es va observar una transició sòlid-sòlid endotèrmica per DSC (Fig. D.8) de la forma I a la forma II a una velocitat d'escalfament lenta (1 °C/min), revelant una relació enantiotròpica entre ambdós polimorfs, essent la forma I estable per sota de la temperatura de transició (ca. 160 °C). Aquest comportament tèrmic es va corroborar qualitativament per termomicroscopia (Fig. D.9).

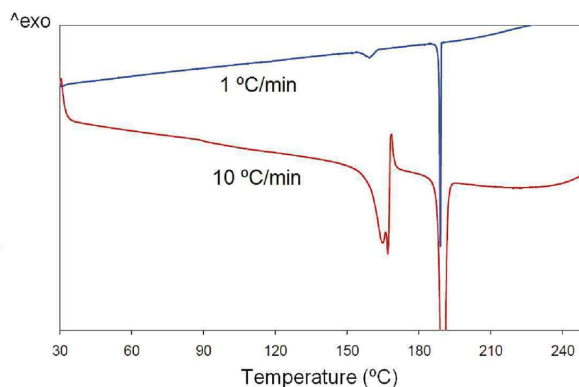


Fig. D.8: Termograma de DSC de la forma I del compost **2** mostrant la fusió/cristal·lització (vermell) i l'ocasionalment observada transició sòlid-sòlid de la forma I a la II (blau)

L'estructura cristal·lina de les dues formes (Fig. D.10) presenta el mateix motiu estructural (paral·lel i antiparal·lel) cap i cua que l'observat en el compost **1**, juntament amb interaccions secundàries de $\pi - \pi$ stacking que difereixen en les direccions en ambdues estructures. També s'observen interaccions $\text{CH}_{\text{aril}} \cdots \text{N}_{\text{piridina}}$.

3,4-bis-(2-etilaminopiridil)-1,2-dioxo-3-ciclobutè (**3**)

Quatre formes polimòrfiques es van obtenir de l'*screening* experimental del compost **3** (Fig. D.11). Curiosament, la naturalesa del fenomen tèrmic de la forma I no va poder ser confirmada ja que en l'anàlisi per DSC sembla una fusió (Fig. D.12), pero

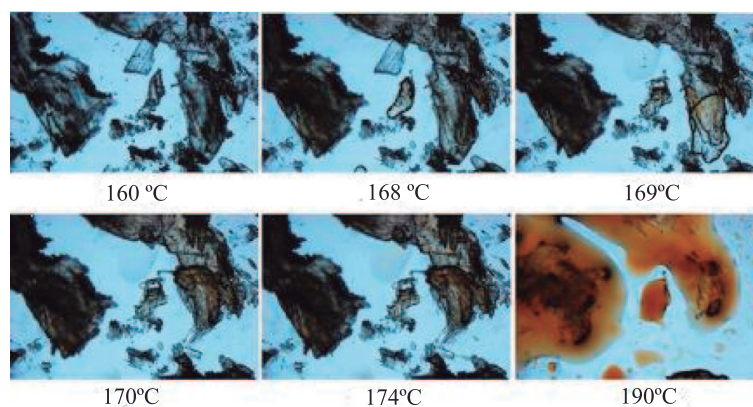


Fig. D.9: Fotogrames de termomicroscopia del compost **2**, mostrant la transició de fase sòlida de la forma I a la II juntament amb la fusió/cristal·lització durant l'escalfament a 10 °C/min

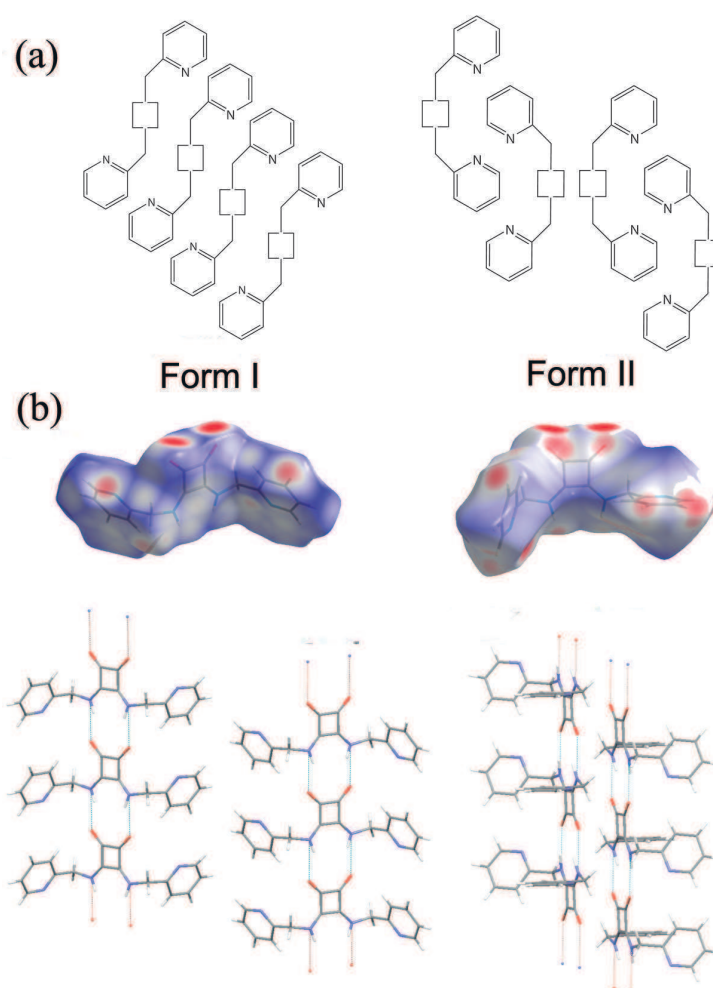


Fig. D.10: Estructures cristal·lines i superfícies de Hirshfeld de les formes I i II del compost **2**

en l'anàlisi per termomicroscopia s'observa una transició sòlid-sòlid (Fig.D.13). La fusió de la forma II s'observa a 224 °C. La forma III presenta un punt de fusió a 168 °C i la forma IV fon a 180 °C.

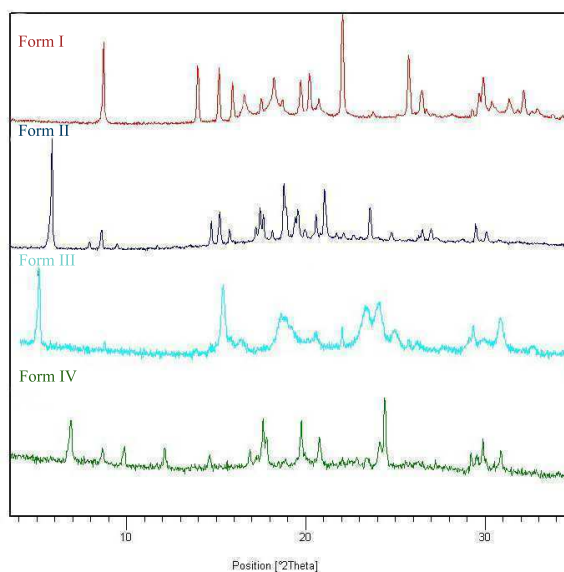


Fig. D.11: Diagrames de DRXP de les formes I, II, III i IV del compost **3**

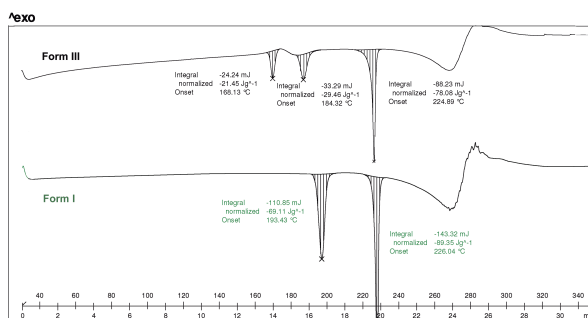


Fig. D.12: Termogrames de DSC de les formes I, II, III, IV del compost **3**

L'estructura cristal·lina de la forma I (Fig. D.14) presenta el mateix motiu cap i cua observat en les altres esquaramides en el qual les unitats esquaramídiques s'uneixen a través d'enllaç d'hidrogen en direccions antiparal·leles. També s'observen interaccions secundàries CH- π similars a les descrites per la forma I del compost **2**. Els anells piridínics adopten una conformació de zig-zag i les interaccions dels grups CH_{aril} \cdots N_{piridina} també s'observen.

3,4-bis-(2-dimethylamino-ethylamino)-1,2-dioxo-3- cyclobutene, (4)

L'*screening* polimòrfic del compost **4** va resultar en diversos polimorfs, no tots en forma pura (Fig. D.15). Vàries indexacions dels difractogrames de la forma I no

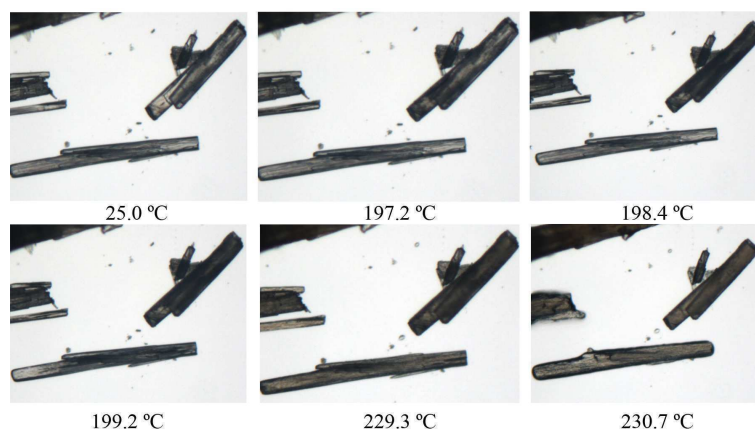


Fig. D.13: Fotogrames de termomicroscopia del compost **3**, mostrant la transició de fase sòlida de la forma I a la II i la subsequent fusió durant l'escalfament a 10 °C/min

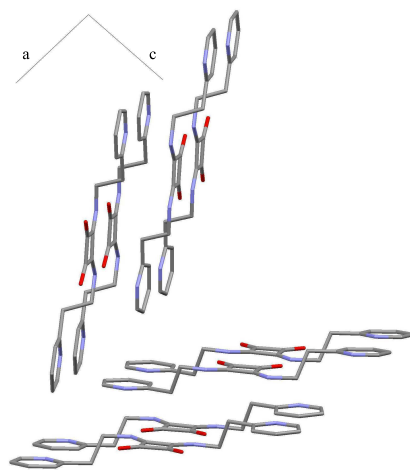


Fig. D.14: Estructura cristal·lina de la forma I del compost **3** (hidrogens no presents)

van tenir èxit, suggerint una contaminació d'una altra fase o una resolució pobre del difractograma.

L'anàlisi per DSC de la forma I (+ α , hipotètica), presenta una transició endotèrmica a 45 °C cap a la forma IV (p.f.=227 °C) durant l'escalfament (confirmat per DRXP de temperatura variable). Diversos anàlisis d'escalfament i refredament amb DSC presenten una transició a la mateixa temperatura amb menor entalpia en el refredament, suggerint una transició de reversibilitat incompleta (Fig. D.17) i confirmada per termomicroscopia. La forma II presenta una transició sòlid-sòlid endotèrmica cap a la forma IV a 150°C (confirmada per DRXP de temperatura variable). Finalment, l'anàlisi de DSC de la forma III presenta una transició sòlid-sòlid a 44 °C cap a la forma d'alta temperatura.

En termes de relació termodinàmica entre les formes d'aquest sistema multi-

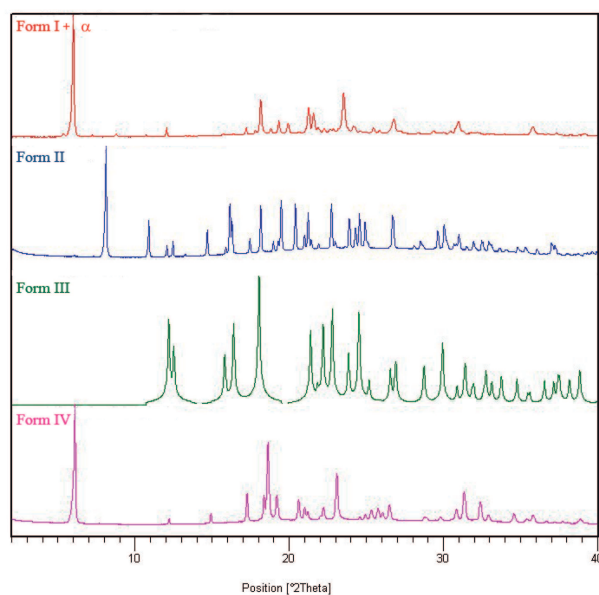


Fig. D.15: DRXP experimentals de les formes I + α , II i IV i el DRXP calculat de la forma III del compost 4

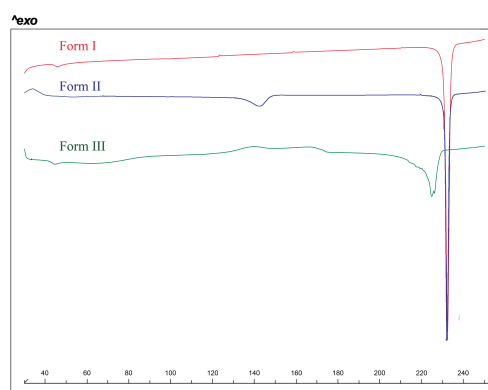


Fig. D.16: Termogrames de DSC de les formes I (+ α), II i III

polimòrfic es pot concloure que la forma I (+ α) seria enantiotròpica amb la forma IV, així com també la forma II amb la forma IV. Mostres de forma III mantingudes a t.a. van transformar irreversiblement cap a la forma I (+ α). Un esquema de la relació termodinàmica entre les diferents formes es pot observar a la figura D.18.

Les dues estructures cristal·lines obtingudes de les formes II i III (Fig. D.19) presenten el típic motiu cap i cua d'enllaç d'hidrogen entre unitats esquaramídiques amb orientacions paral·leles i antiparal·leles.

Després d'estudiar quatre compostos model d'esquaramides secundàries en estat sòlid, l'existència d'un sintó supramolecular robust auto-associatiu s'observa en vuit estructures cristal·lines resoltes de les tretze formes polimòrfiques obtingudes. Presenten un mateix motiu estructural imperturbable en forma de cadena en el qual

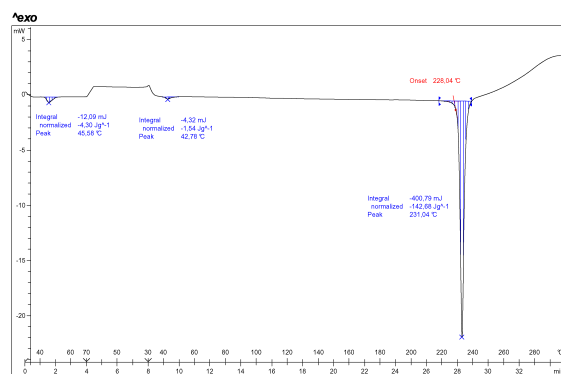


Fig. D.17: DSC de la forma I mostrant una transició reversible cap a la forma IV durant un experiment d'escalfament-refredament

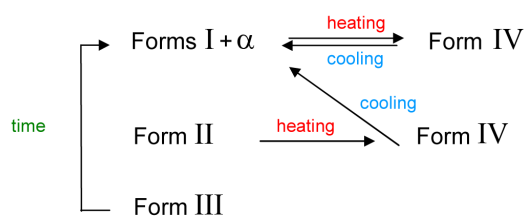


Fig. D.18: Transformacions polimòrfiques del compost 4

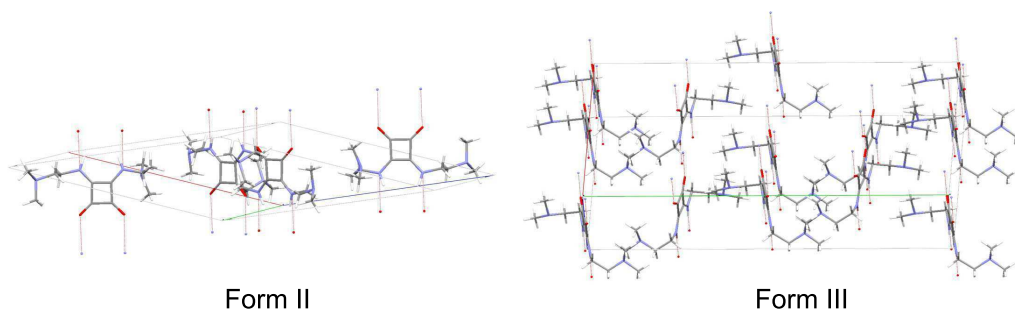


Fig. D.19: Estructures cristal·lines de les formes II i III del compost 4

agregats d'esquaramida interaccionen a través d'enllaços d'hidrogen. El següent esquema resumeix les característiques polimòrfiques principals dels quatre compostos model estudiats (Fig. D.20).

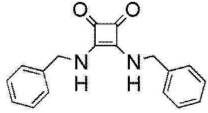
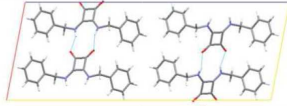

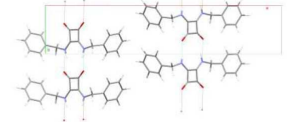

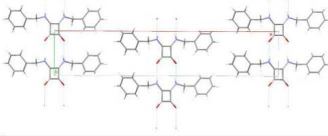

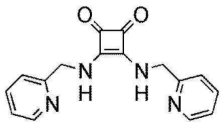
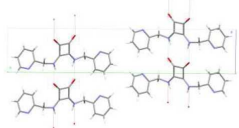

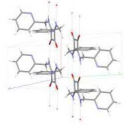
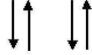
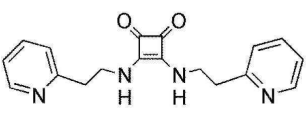
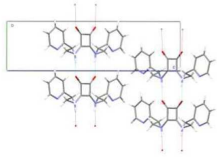
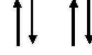
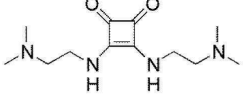
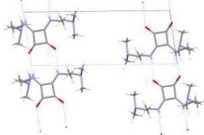
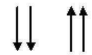
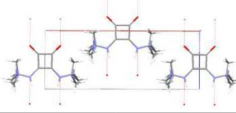

Compound (n° of forms)	Forms	Space group	Z (Z')	Crystal Structure	Catemic head-to-tail
1 (3) 	I	C2	4 (1)		 Unparallel
	II	Pc	4 (2)		 Antiparallel
	III	C2/c	4 (1)		 Antiparallel
2 (2) 	I	Pc	2 (1)		 Parallel
	II	P-1	2 (1)		 Antiparallel
3 (4) 	I	Pna21	4 (1)		 Antiparallel
4 (4 or 5) 	II	P21/a	4 (1)		 Antiparallel
	III	Fdd2	8 (1)		 Parallel

Fig. D.20: Resum dels sistemes polimòrfics estudiats

De la solució al cristall

En aquesta secció, les preferències estructurals d'un model d'esquaramida concret (**2**) són analitzades per tal d'entendre la relació entre l'estructura dels agregats en solució i l'estat sòlid.

Estudis previs en solució demostren que les esquaramides secundàries presenten dues conformacions en solució: anti/anti i anti/sin. Ambdues poden produir un sinó $R_2^2(n)$ amb grups acceptors i donadors d'enllaç d'hidrogen apropiats (Fig. D.21).

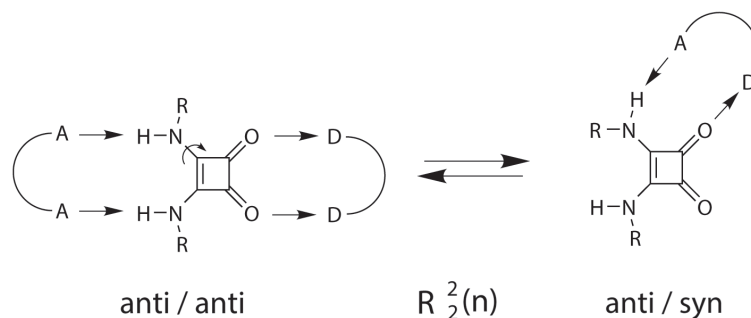


Fig. D.21: Dues conformacions diferents de les esquaramides secundàries

Inicialment, **2** es va analitzar per ^1H -RMN i el seu espectre en CDCl_3 a baixa temperatura presenta tres conjunts de senyals N-H, suggerint que **2** està present com a mescla de dues conformacions diferents, una simètrica i una asimètrica (anti/anti (Fig. D.24, **2c**) i anti/sin (Fig. D.24, **2a** or **2b**)) gràcies a la rotació de l'enllaç C-N_{amida} que es congela a baixa temperatura (Fig. D.22).

El desplaçament químic observat en experiments de dilució en base a 2D ^1H -RMN COSY fa concloure que, dels conformers asimètrics, el dimèric **2b** és preferit (Fig. D.23). Totes les formes conformacionals possibles es relacionen a través de la següent proposta esquemàtica (Fig. D.24).

Els resultats indiquen que a mesura que s'augmenta la concentració a 240 K, la forma auto-associativa preferida és la **2b**. Per aquest motiu, en circumstàncies en les quals el mode d'agregat és similar al de l'estructura cristal·lina es dedueix que els cristalls haurien de presentar el conformer **2b** (contràriament als resultats obtinguts de l'*screening* polimòrfic, que es basen en el **2c**). Aquestes observacions sugereixen que la formació dels agregats en cadena cap i cua estan afavorits gràcies a la cooperativitat dels enllaços d'hidrogen.

Tenint en compte aquests resultats en solució, es va estudiar el fenomen de la cooperativitat i la seva relació amb la preferència d'aquests compostos per la conformació en cadena anti/anti en estat sòlid dissenyant un nou compost model senzill: la dimetilesquaramida (**5**). Per fer-ho es va aplicar la teoria desenvolupada per

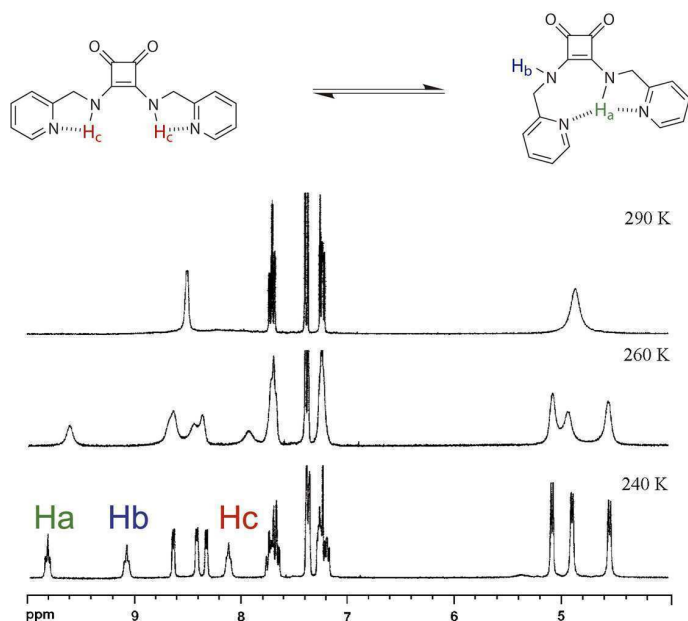


Fig. D.22: Equilibri conformacional i espectre de ^1H -RMN del compost **2** en CDCl_3 a 240 K, 260 K i 290 K

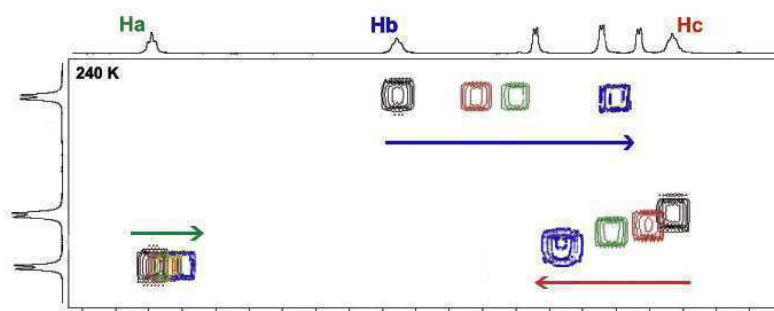


Fig. D.23: 2D ^1H -RMN COSY a 240 K del compost **2** durant la dilució

Chris Hunter, la qual es basa en l'ús d'uns paràmetres que quantifiquen el caràcter donador o acceptor d'enllaç d'hidrogen d'un grup funcional. Aquests paràmetres es calculen a partir de la superfície de potencial electrostàtic (MEPS) de la molècula, obtenint una energia màxima i mínima que es tradueix en els paràmetres α i β (Fig. D.25).

Amb aquest estudi es va observar que l'energia d'interacció de l'agregat en conformació anti/anti de **5** disminuïa dramàticament per efecte de la cooperativitat i, en canvi, l'energia del sin/sin es mantenia constant (Fig. D.26), suggerint una explicació per la qual les diesquaramides, en absència de grups funcionals addicionals, presenten només el sintó supramolecular anti/anti en estat sòlid.

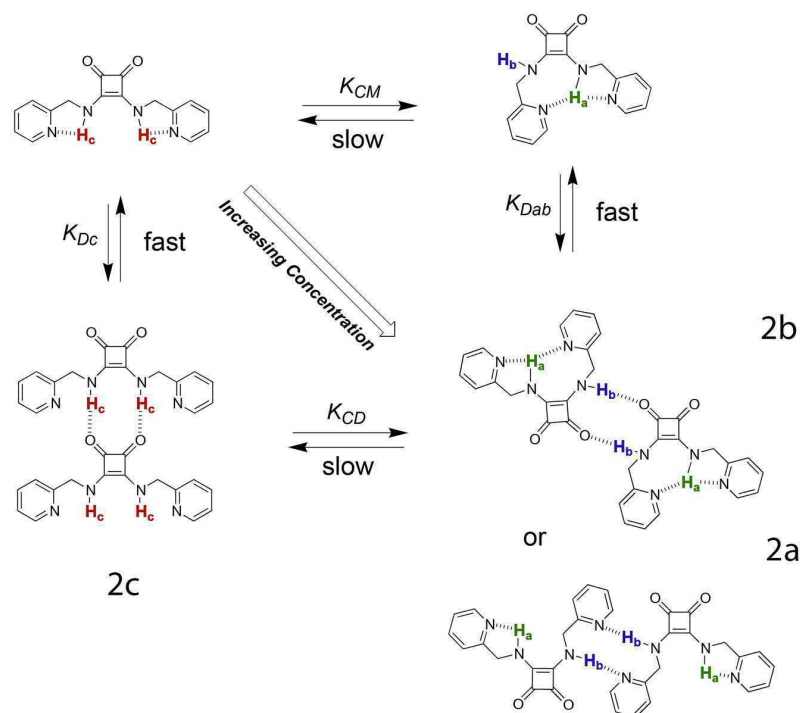


Fig. D.24: Cycle termodinàmic proposat per a la dimerització del compost **2**

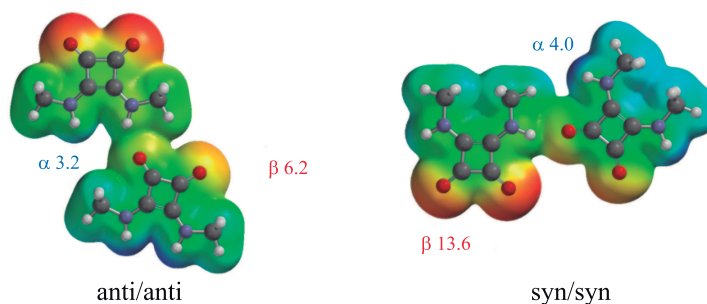


Fig. D.25: Superfícies MEP i paràmetres d'enllaç d'hidrogen després de la primera interacció dels conformers anti/anti i sin/sin.

El resultat d'aquest estudi teòric es va contrastar amb un *screening* polimòrfic experimental de **5** a través del qual només es va obtenir una forma polimòrfica que presenta el sintó predit anti/anti en cadena (Fig. D.27). La teoria dels paràmetres d'enllaç d'hidrogen també es va aplicar al sistema del compost **2** (estudiat en dissolució) i es van confirmar les observacions experimentals.

Com que la conformació sin/sin no es va observar en cap dels compostos estudiats, es va dissenyar una nova diesquaramida cíclica covalentment forçada (**6**) per tal d'estudiar les seves característiques estructurals (Fig. D.28, (a)). La seva estructura cristal·lina presenta la formació d'enllaços d'hidrogen esperada entre els

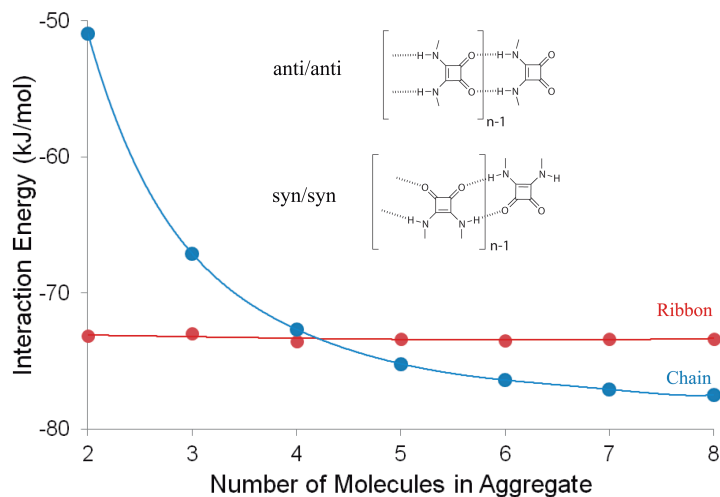


Fig. D.26: Energies d'interacció del monòmer terminal (anti/anti: blau; sin/sin: vermell) calculat amb DFT B3LYP 6-31+G* nivell de teoria utilitzant Spartan'10

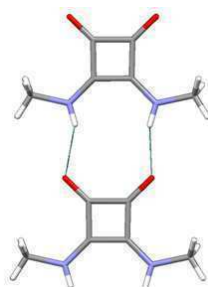


Fig. D.27: Estructura cristal·lina del compost **5**

NH...OC establerts entre dues molècules adjacents formant cadenes pràcticament al mateix pla (Fig. D.28, (b)).

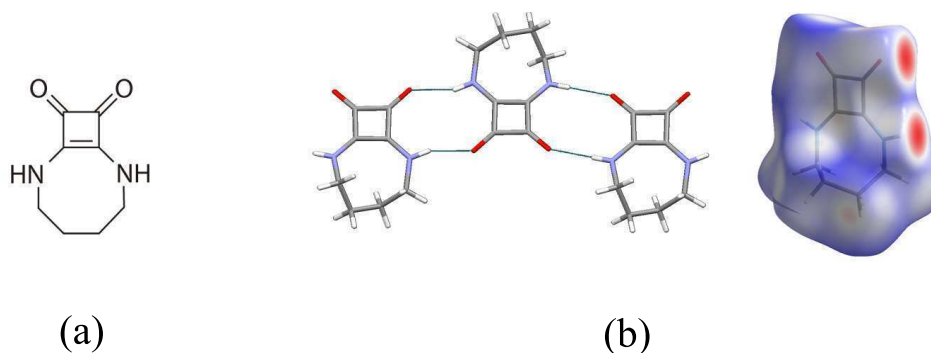


Fig. D.28: (a) Esquema del compost **6** (b) Estructura cristal·lina i superfície de Hirshfeld del compost **6** en les quals es mostren les interaccions laterals en vermell

En el primer estudi de les esquaramides **1**, **2** i **3** es va observar que les interaccions competitives com el $\pi - \pi$ stacking no afectaven la conformació anti/anti. Per tal d'estudiar el seu efecte en la conformació sin/sin, a *priori* menys estable, es va dissenyar una altra esquaramida macrocíclica contenint grups aromàtics (**7**, Fig. D.29, (a)). La seva estructura cristal·lina presenta la formació d'enllaços d'hidrogen entre grups $\text{NH} \cdots \text{OC}$ distorsionada en el pla en forma de zig-zag i interaccions addicionals entre $\text{CO} \cdots \text{H}_{\text{aromatic}}$ i $\pi - \pi$ stacking (Fig. D.29, (b)). Aquest fenomen, observat per primera vegada, suggereix que la cooperativitat estabilitza els agregats anti/anti superant l'efecte de les interaccions secundàries mentres que la conformació no cooperativa sin/sin és menys resistent a la seva presència.

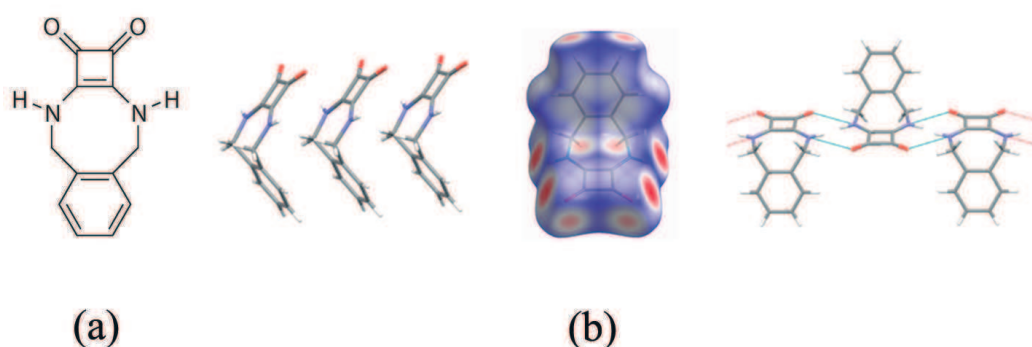


Fig. D.29: (a) Esquema del compost **7** (b) Estructura cristal·lina i superfície de Hirshfeld del compost **7** en la qual es mostren les interaccions laterals en vermell

Una vegada es va observar la conformació sin/sin en diesquaramides, ens vam qüestionar si les monoesquaramides, les quals estan més impedides en termes de cooperativitat, podrien presentar la conformació sin/sin en estat sòlid. Per aquest motiu es va dissenyar una monoesquaramida-ester senzilla (**8**) (Fig. D.30) i es va realitzar un *screening* polimòrfic experimental. Només es va obtenir una forma i la seva estructura cristal·lina presenta dímers esquaramida/esquaramida fortament auto-associats interaccionant a través d'enllaços d'hidrogen en conformació sin/sin, com també interaccions secundàries $\text{CO} \cdots \text{H}_{\text{ethyl}}$ (Fig. D.31).

Aquest resultat suggereix que, en absència de grups donadors/acceptors competitiu, els dímers són més estables que les cadenes probablement degut al fet que la cooperativitat es troba impedida per alinear les unitats esquaramídiques en cadena. En aquest sentit, un altre compost model es va dissenyar (**9**) contenint un grup piridínic addicional i se'n van calcular els paràmetres α and β per contrastar-los amb els resultats experimentals de l'*screening* (Fig.D.32, (a)). L'estructura cristal·lina confirma la predicció que grups competitiu alteren el sintó supramolecular (Fig. D.32, (b)).

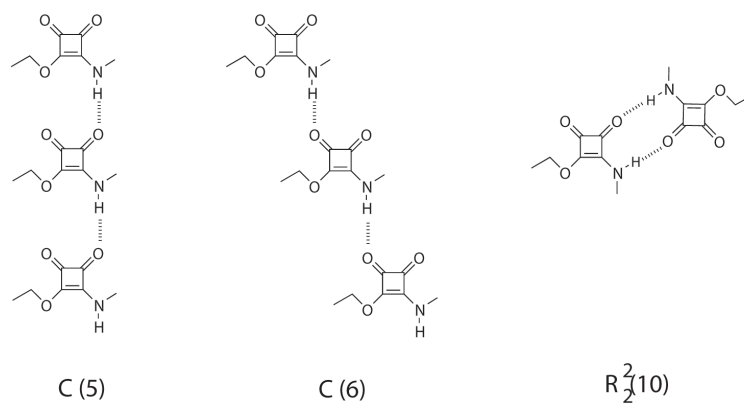


Fig. D.30: Sintons supramoleculars possibles pel compost 8

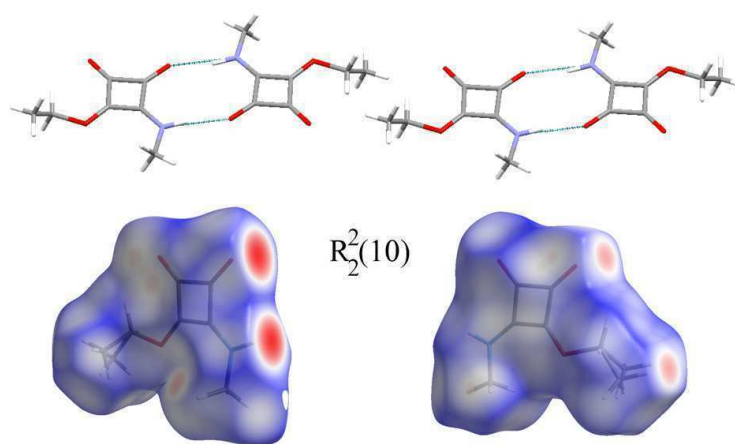
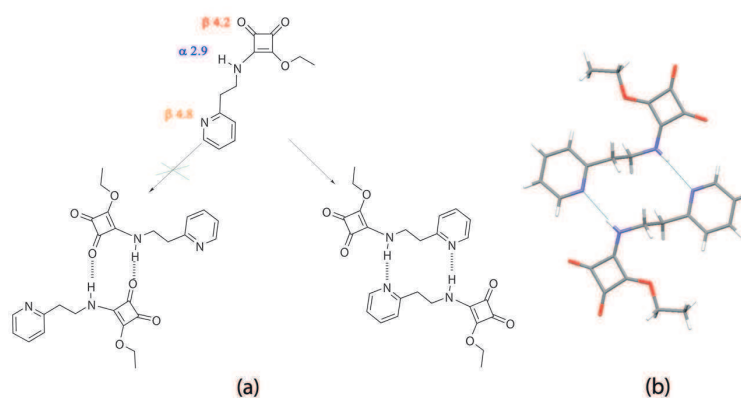


Fig. D.31: Agregats dimèrics observats en l'estructura cristal·lina del compost 8 juntament amb la superfície de Hirshfeld

Fig. D.32: (a) Paràmetres α i β pel compost 9 (b) Dímers en l'estructura cristal·lina del compost 9

Enginyeria cristal·lina: disseny de cocristalls

En la següent fase d'aquesta tesi es van dissenyar nous materials en base als coneixements adquirits sobre l'estat sòlid dels derivats d'àcid esquàric. Com s'ha mostrat

en les seccions anteriors, tots els intents de cristal·lització de les diferents formes de les esquaramides van resultar en l'existència d'una sola conformació anti/anti cap i cua, a no ser que la molècula es forçés covalentment. Per aquest motiu, una primera idea va ser dissenyar cocristalls amb coformers donadors/acceptors complementaris com els fenols i els àcids carboxílics apropiats per una conformació anti/anti i sin/sin respectivament (Fig. D.33).

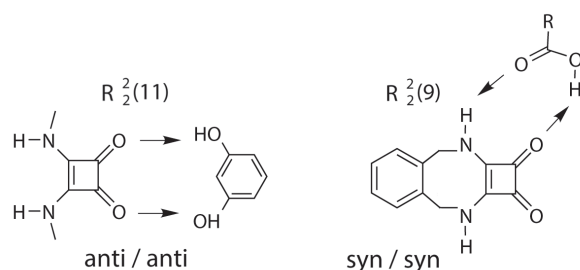


Fig. D.33: Esquema dels possibles sintons supramoleculars amb coformers acceptors i donadors d'enllaços d'hidrogen

Encara que el resorcinol i els àcids carboxílics semblessin òptims des d'un punt de vista geomètric, els càlculs suggerien que no s'obtidrien cocristalls amb les diesquaramides **5** i **7**, degut al fet que les energies d'interacció d'aquests heterosintons era menor a la dels homosintons (Fig. D.34).

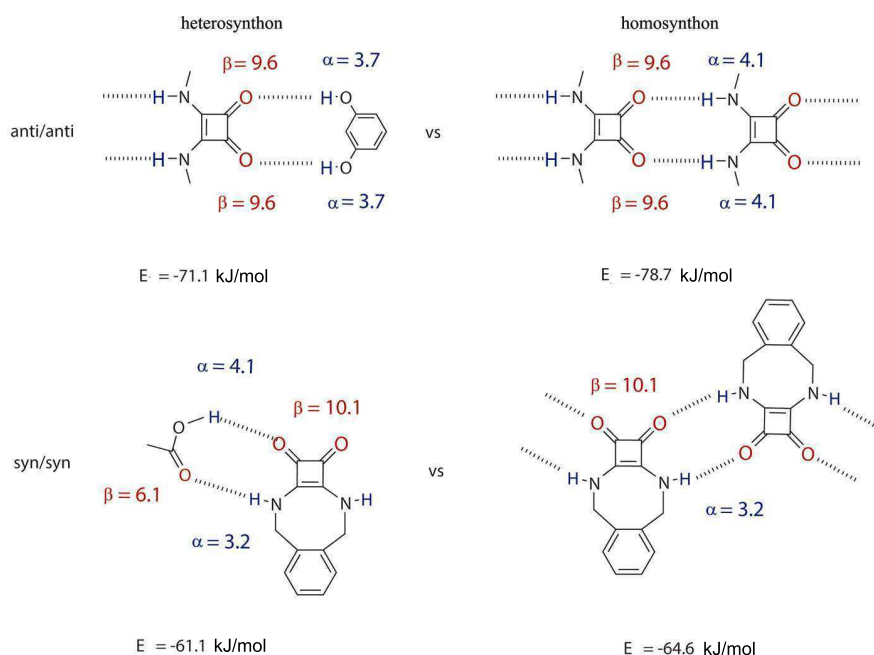


Fig. D.34: Energies d'interacció estimades dels heterosintons i els homosintons per a les conformacions anti/anti i sin/sin dels compostos **5** i **7**, respectivament.

Per a corroborar aquesta predicció, es va portar a terme un *screening* experimental (extensiu a altres bons grups donadors/acceptors d'enllaç d'hidrogen) amb

els compostos **5** i **7** i no va produir cap cocristall.¹ Aquests resultats reforcen la teoria que l'autoagregació dels anells esquaramídics en conformació anti/anti en estat sòlid és robusta i difícil de ser perturbada per altres grups competitius.

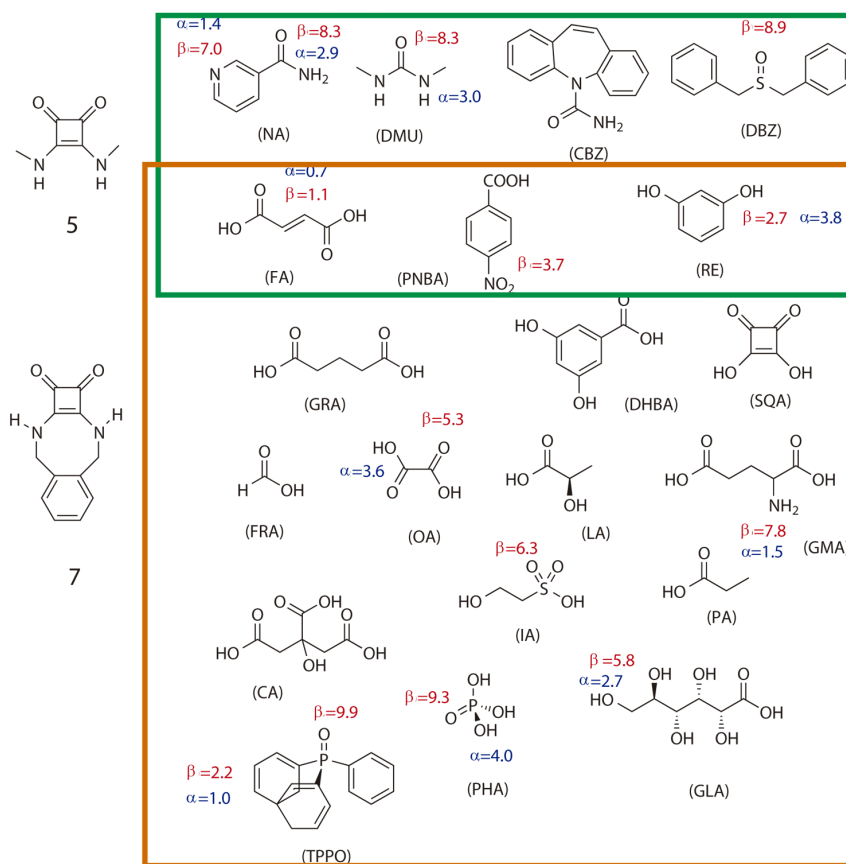


Fig. D.35: Coformers utilitzats en l'*screening* de cocristalls dels compostos **5** i **7**

Per aquesta raó, vam dissenyar dues noves estratègies d'enginyeria cristal·lina: la primera basada en impedir la conformació anti/anti en cap i cua a través d'enllaços intramoleculars (Fig. D.36 (a)) i la segona, que consisteix en aprofitar la conformació anti/anti i escollir coformers complementaris que interaccionin amb les cadenes secundàries perifèriques funcionalitzades de les esquaramides (Fig. D.36 (b) i (c)).

Primera estratègia: preorganització

En aquesta estratègia es va estudiar l'efecte d'introduir un acceptor d'enllaç d'hidrogen extra a l'esquaramida amb l'objectiu de modificar la preferència pel model auto-associatiu cooperatiu observat en les esquaramides estudiades fins el moment i

¹En el cas del compost **7** es van identificar indicis d'una fase nova que no es va poder caracteritzar suficientment com per afirmar la presència d'un cocristall

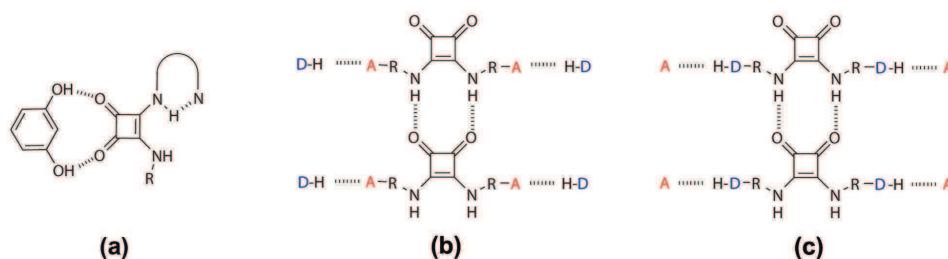


Fig. D.36: Esquema del disseny de cocrystals: (a) via enllaços d'hidrogen intramoleculars i (b, c) via interaccions perifèriques

generar nous sintons supramoleculars. Es van dissenyar els compostos **10** i **11** (Fig. D.37).

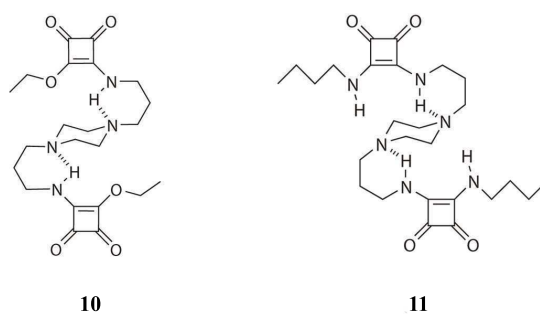


Fig. D.37: Esquema dels compostos **10** i **11**

Es va realitzar un *screening* polimòrfic no exhaustiu pel compost **11** però desafortunadament no es va poder obtenir l'estructura cristal·lina de l'única forma obtinguda.

Encara que les esquamides són bons donadors/acceptors d'enllaç d'hidrogen, les mono-esquamides poden presentar diversos sintons supramoleculars i per aquest motiu es va seguir l'estratègia amb el compost **10**. Quatre sintons diferents es podien esperar: la configuració en anti/anti podia produir dos sintons, el polímer cap i cua i el monomer intramolecular (Fig. D.38 (a) and (b)), mentre que la configuració en sin/sin podia produir la cadena i el monòmer intramolecular (Fig. D.38 (d) and (c)).

Es va portar a terme un *screening* polimòrfic obtenint tres formes: dues anhidres i un hidrat, de les quals se'n va poder resoldre la seva estructura cristal·lina a partir del difractograma de pols, exceptuant l'hidrat (Fig. D.39 i Fig. D.40).

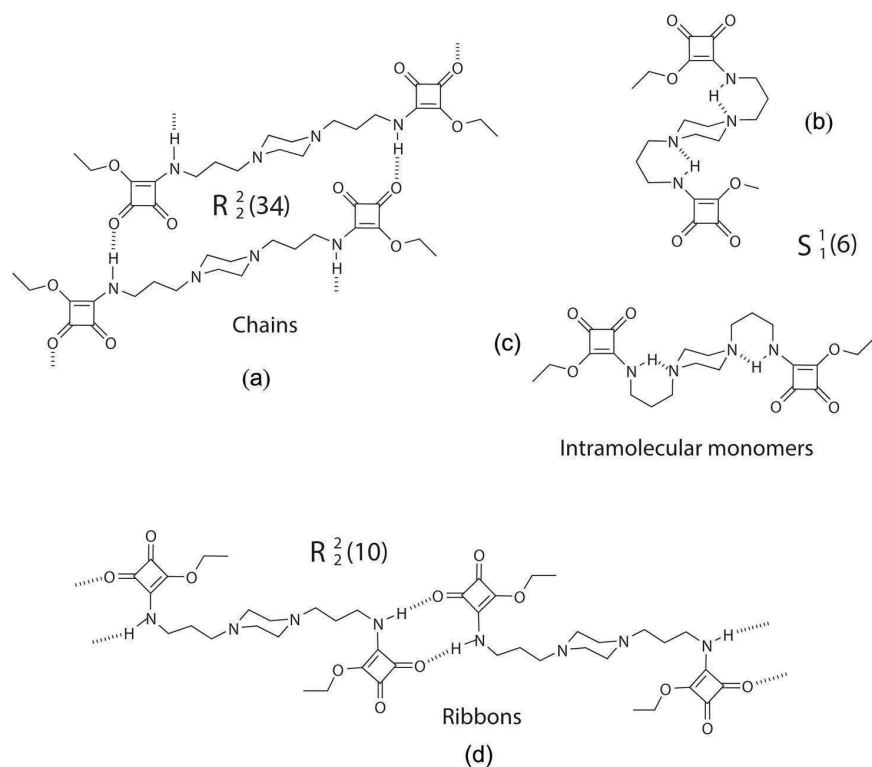


Fig. D.38: Sintons supramolulars esperats pel compost **10** amb les seves corresponents descripcions gràfiques

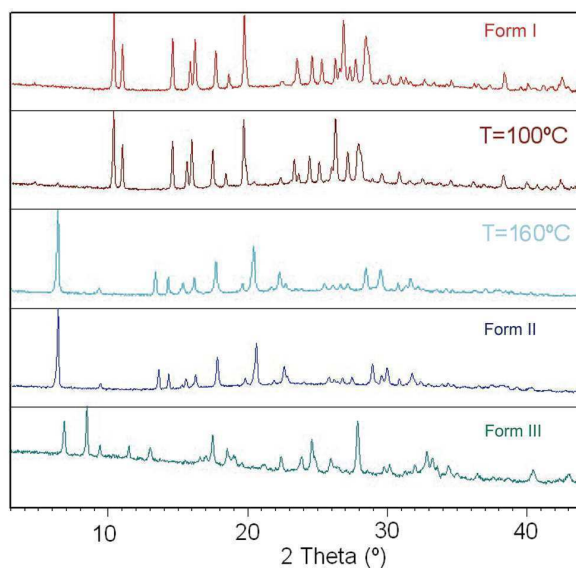


Fig. D.39: Diagrames de DRXP de les formes I, II i III. La forma II es va obtenir amb un experiment de DRXP de temperatura variable a partir de la forma I (també present en la figura)

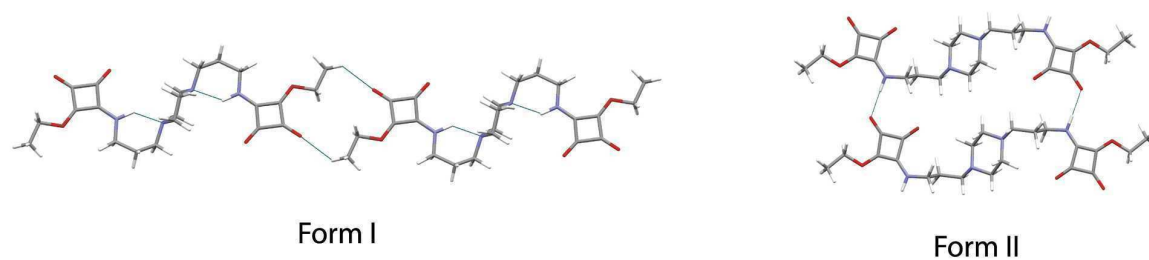


Fig. D.40: Estructures cristal·lines de les formes I i II mostrant interaccions d'enllaç d'hidrogen inter i intramoleculars

La forma I presenta un anell de sis membres a través d'enllaços d'hidrogen intramoleculars, quasi perpendiculars al pla definit per l'anell de piperazina. Capes paral·leles de molècules s'estabilitzen a través d'interaccions $\pi - \pi$ stacking entre els anells de ciclobutè i interaccions febles d'enllaç d'hidrogen entre els oxígens carbonílics i els hidrògens de la piperazina. La forma II, en canvi, presenta una configuració cap i cua a través d'enllaços d'hidrogen intermoleculars i els anells de ciclobutè interaccionen via $\pi - \pi$ stacking. En ambdós casos l'anell de piperazina adopta una conformació de cadira.

Una vegada confirmada la conformació intramolecular, vam decidir utilitzar la preorganització per a dirigir la formació de cocristalls amb coformers doblement donadors d'enllaç d'hidrogen i es va portar a terme un *screening* de cocristalls entre el compost **10** i el resorcinol esperant una estructura similar a la proposada en la figura D.41.

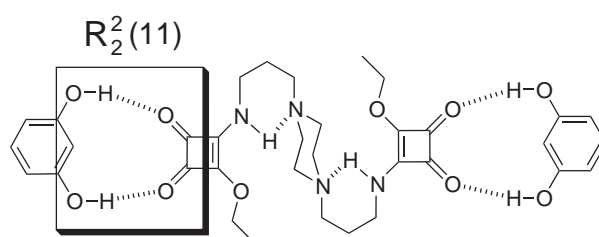


Fig. D.41: Complementarietat acceptor-donador entre el cocristall esperat pel compost **10** i el resorcinol

Es van obtenir dos cocristalls: un anhidre i un hidrat, amb estequiometries 1:2 (**10**:resorcinol) i 1:2:2 (**10**:resorcinol:water), l'estructura dels quals no corresponia a l'esperada (Fig. D.42). No obstant això, es van obtenir evidències de polimorfisme durant l'*screening* de cocristalls que no descarten el sintó supramolecular esperat $R_2^2(10)$.

En resum, vam estudiar com la formació d'un enllaç d'hidrogen intramolecular afecta el polimorfisme d'una monoessquaramida-ester. No obstant això, la preor-

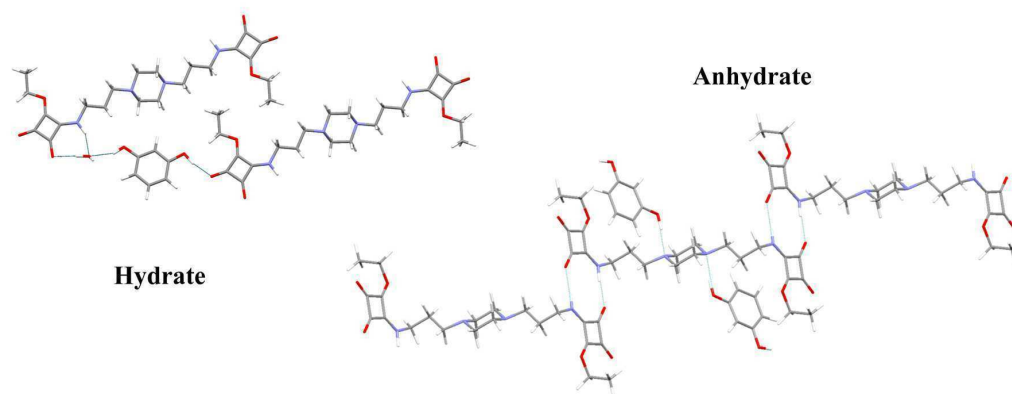


Fig. D.42: Estructura cristal·lina dels cocristalls amb resorcinol

ganització no ha sigut suficient com per dirigir la formació d'un cocristall entre un doble do-nador i un doble acceptor que havíem esperat. Per altra banda, s'han pogut observar tres dels quatre sintons supramoleculars proposats a *priori* pel compost **10**.

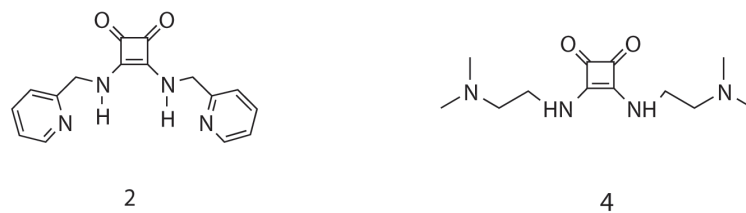
Segona estratègia: cocrystal·lització amb cofomers complementaris via interaccions perifèriques

Totes les dificultats en impedir el sintó cap i cua en anti/anti de les esquaramides secundàries revela que aquests compostos poden ser molt atractius per ser explotats com a plantilla estructural en el disseny de noves estructures multicomponents. Amb una funcionalització adequada dels substituents de les cadenes secundàries, els cofomers complementaris hi poden establir fortes interaccions perifèriques.

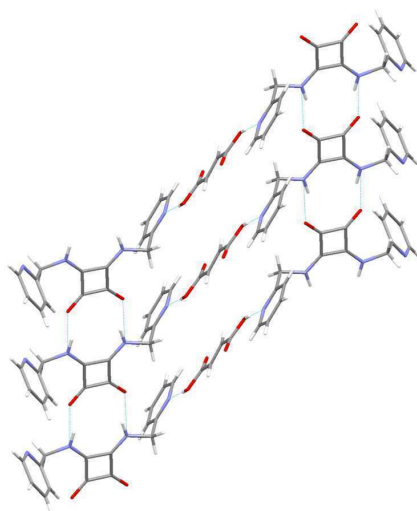
Cocristalls amb cofomers donadors d'enllaç d'hidrogen

Es va realitzar un *screening* de cocristalls entre dos models esquaramídics (**2** i **4**, Fig. D.43) que contenen grups piridil i dimetilamino, i un conjunt de cofomers donadors d'enllaç d'hidrogen (taula D.1) i el resultat va ser la identificació de tres i sis formes sòlides multicomponents, respectivament, com també indicis de l'existència d'altres fases. Seguidament es presenten les estructures cristal·lines obtingudes.

- Cocristall **2** : àcid fumàric : ACN

Fig. D.43: Esquema dels compostos **2** i **4**.Tab. D.1: Experiments de cocristal·lització dels compostos **2** i **4**. -: cap sòlid obtingut, 0: cap cocristall, 1: indicis de fases noves, 2: cocristall confirmat per DRXS o DRXP i ¹H-RMN

Coformer	Compost 2	Compost 4
Àcid fumàric	2	2
Àcid <i>p</i> -nitrobenzoic	2	1
Àcid glutàric	0	1
Àcid glutàmic	0	1
Àcid oxàlic	1	1
Àcid cítric	0	1
Àcid esquàric	1	2
Resorcinol	0	2
Urea	-	1
Nicotinamida	0	1

Fig. D.44: Estructura cristal·lina del cocristall solvat amb ACN entre el compost **2** i l'àcid fumàric, 1:1:2 (molècules d'ACN no presents)

- Sal 4 : àcid fumàric : MeOH : aigua

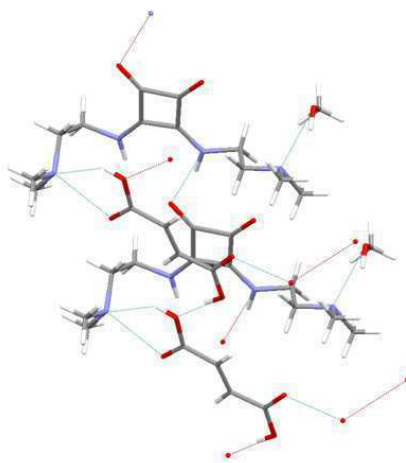


Fig. D.45: Estructura cristal·lina del cocrystal solvat amb MeOH/aigua entre el compost **4** i l'àcid fumàric, 2:2:1:3 (molècules d'aigua no presents)

Les estructures cristal·lines de **2** i **4** amb àcid fumàric presenten un tipus de conformació cap i cua diferent. Les dues són cadenes, però el cocrystal de **2** presenta un motiu tipus anell $R_2^2(10)$ format per deu àtoms en el qual hi participen els dos donadors i acceptors d'enllaç d'hidrogen. Per altra banda, el cocrystal de **4** cristal·litza mitjançant una estructura cap i cua desplaçada, possiblement a causa de les interaccions de l'àcid fumàric, formant una cadena (C(6)), en la qual participen només un donador i un acceptor d'enllaç d'hidrogen (Fig. D.46).

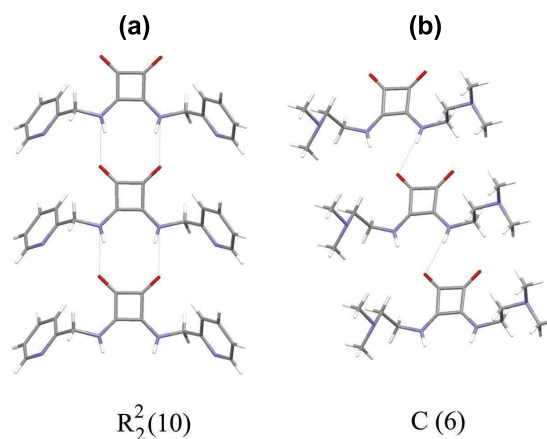


Fig. D.46: Motius estructurals en cap i cua de les formes multicomponents de (a) **2** i (b) **4** amb àcid fumàric (Coformers no presents)

- Cocrystal 4 : resorcinol

En aquest cas s'han identificat dues formes polimòrfiques anhidres de cocristall (Fig. D.47) de les quals només s'ha pogut resoldre una estructura cristal·lina a partir del difractograma de pols (Fig. D.48).

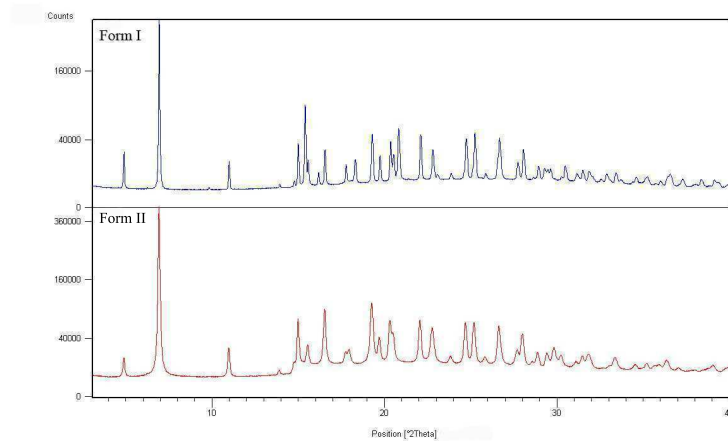


Fig. D.47: Diagrames de DRXP de les dues formes polimòrfiques del cocristall entre **4** i resorcinol (1:1)

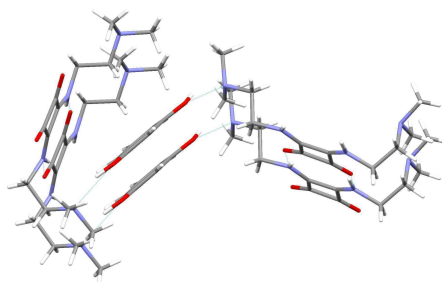


Fig. D.48: Estructura cristal·lina del cocristall entre **4** i resorcinol, forma I

- Sal 4 : àcid esquàric : aigua

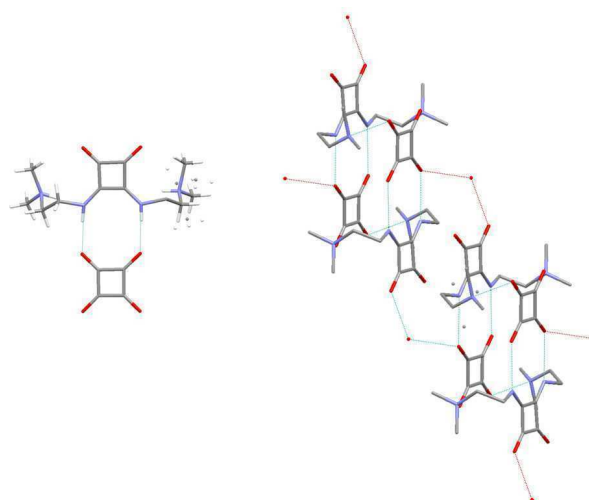


Fig. D.49: Sal hidratada entre 4 i àcid esquàric

Cocristalls amb coformers acceptors d'enllaç d'hidrogen

En aquest cas es va decidir expandir l'estratègia anterior funcionalitzant els substituents de les cadenes secundàries de les esquamides amb donadors d'enllaç d'hidrogen (Fig. D.50) i es va dissenyar el compost **12**.

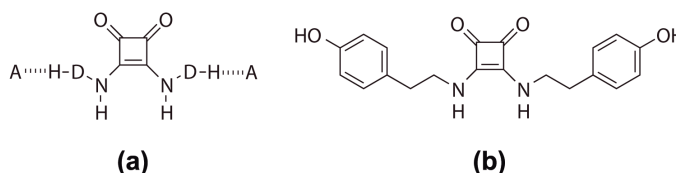


Fig. D.50: Esquema de (a) una diesquaramida general amb grups donadors d'enllaç d'hidrogen perifèrics i (b) compost **12**

El resultat de l'*screening* de cocristalls realitzat amb un conjunt de coformers acceptors d'enllaç d'hidrogen es resumeix a la següent taula D.2.

De tots els indicis observats, només es van poder obtenir dues estructures cristal·lines de solvats del compost **12**: en etanol i en DMSO/aigua (Fig. D.51).

Encara que els solvents no es van emprar com a coformers, les dues estructures cristal·lines posen de manifest que l'estratègia proposada per a la formació de cocristalls amb acceptors d'enllaç d'hidrogen via interaccions d'enllaç d'hidrogen perifèriques podria funcionar.

Tab. D.2: Experiments de cocrystal·lització del compost **12**. -: cap sòlid obtingut, 0: cap cocrystal·l, 1: indicis de fase nova, 2: cocrystal·l confirmat per DRXS o DRXP i ¹H-RMN

Coformer	Compost 12
àcid oxàlic	1
resorcinol	0
nicotinamida	1
isonicotinamida	1
bipiridina	1
piridina	1

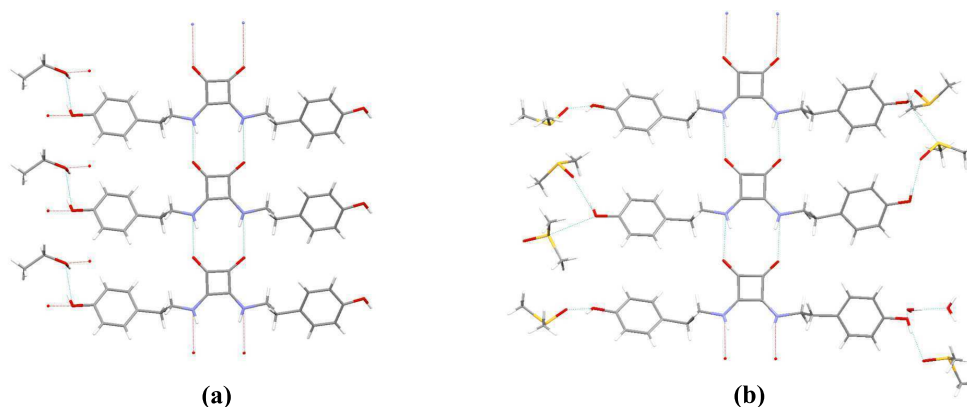


Fig. D.51: Estructures cristal·lines dels solvats de **12** amb (a) etanol i (b) DMSO/aigua

Autoensamblatge i efecte plantilla: arquitectures helicoidals

Considerant que el motiu estructural cap i cua es pot utilitzar com a plantilla, vam dissenyar una nova esquaramida asimètrica (**13**) funcionalitzada amb grups acceptor i donador d'enllaç d'hidrogen al mateix esquelet amb l'objectiu de produir noves topologies autoensamblades. En un primer moment, es van suggerir dos tipus d'estructura: (a) cíclica i (b) polimèrica, que podrien donar lloc a estructures helicoidals (Fig. D.52).

L'estructura cristal·lina del compost **13** revela una cadena d'agregats formant una hèlix (seguint el model (a) de la figura D.52), i les unitats es connecten entre elles mitjançant interaccions febles de CH- π (Fig. D.54). És una estructura sense precedent en les esquaramides.

Aquesta estructura és racèmica, una combinació d'una hèlix en rotació horària i una hèlix en rotació antihorària (Fig. D.55).

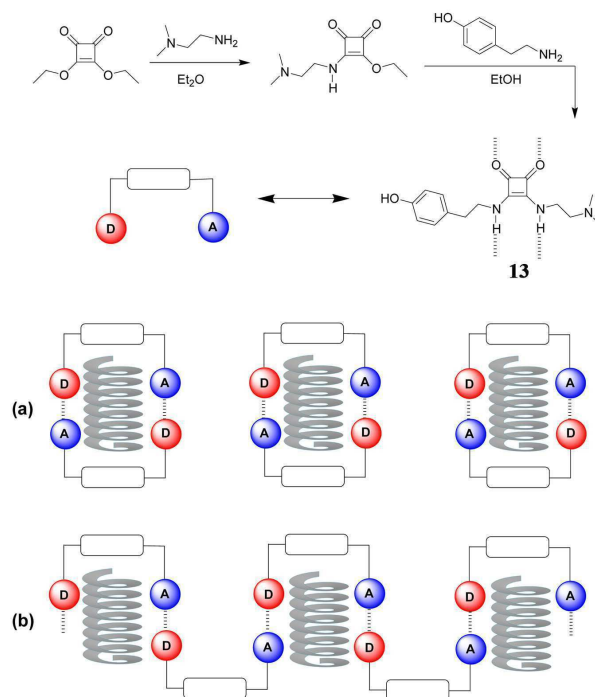


Fig. D.52: Possibles agregats de **13** (a) Cíclic i (b) Polimèric

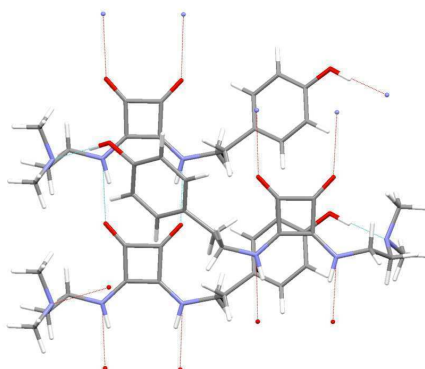


Fig. D.53: Estructura cristal·lina del compost **13**

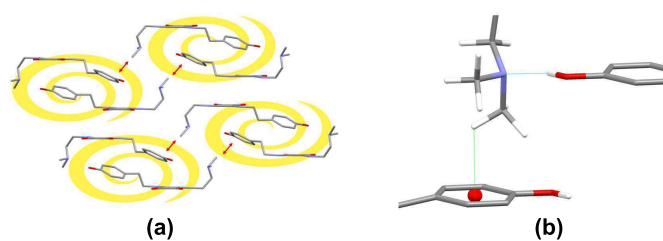


Fig. D.54: (a) Empaquetament helicoidal via interaccions $\text{CH} \cdots \pi$ i (b) interaccions $\text{CH} \cdots \pi$ entre el grup metilamino i l'anell aromàtic en el compost **13**

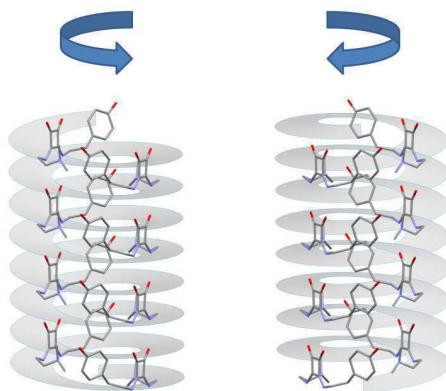


Fig. D.55: Rotació horària i antihorària de les dues hèlix diferents en el cristall racèmic del compost **13**

Derivats d'àcid esquàric amb càrrega: compressió electrostàtica

Finalment en aquesta tesi, es van estudiar altres derivats d'àcid esquàric tenint en compte efectes com la compressió electrostàtica, ja descrita en sals d'àcid esquàric a la bibliografia, i interaccions d'enllaç d'hidrogen de càrrega assistida.

Amb l'objectiu de combinar les interaccions esmentades es va explorar uns nous derivats zwitteriònics de l'àcid esquàric per tal de dissenyar noves estructures supramoleculares en l'estat sòlid. El compost **17** va ser l'objecte d'estudi (Fig. D.56).

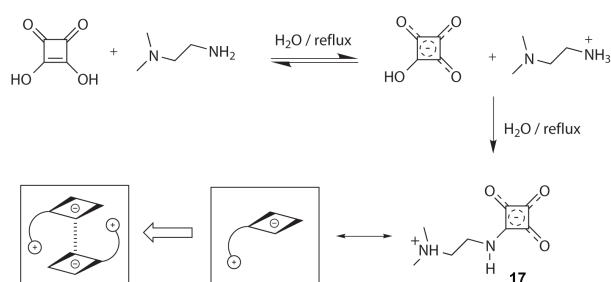


Fig. D.56: Síntesis de l'esquaramida zwitteriònica **17** i esquema de l'autoensamblatge a través de la compressió electrostàtica

En principi, dos sintons supramoleculares són geomètricament possibles: un anell $R_2^2(10)$ (Fig. D.57 (a)) i una cadena C(5) or C(6) (Fig. D.57 (b)).

Per tal d'estudiar aquesta hipòtesi, es va realitzar un *screening* polimòrfic del qual se'n van obtenir dues formes anhidres i un hidrat. Les tres formes presenten dímers electrostàticament comprimits i enllaçats entre ells via interaccions de N-H...O (Fig. D.58).

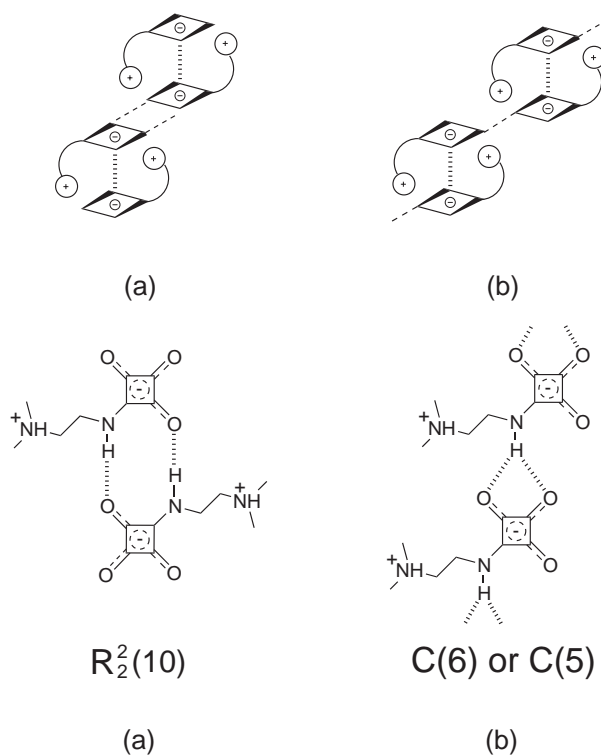


Fig. D.57: Motius estructurals d'ensamblatge diferents pel compost **17**

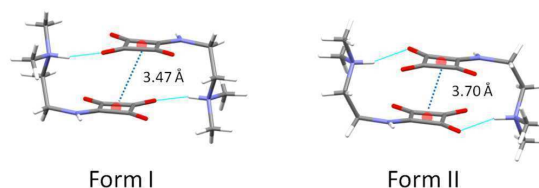


Fig. D.58: Dímers en *stacking* ($d_{centroïdes}$) per a les formes anhidres I i II del compost **17**

La particularitat de cada anhidre és la connexió dels dímers, produint sintons supramoleculars diferents pels dos polimorfs: anells $R_2^2(10)$ en la forma I i una cadena C(5) en la forma II (Fig. D.59).

En el cas de l'hidrat (forma III), s'observa un sintó supramolecular diferent: una cadena C(6) estabilitzada per molècules d'aigua a través d'enllaços d'hidrogen (Fig. D.60).

Per altra banda, durant l'*screening* polimòrfic es va obtenir una forma multicomponent degut a l'existència de traces d'àcid esquàric: una sal monosquarat/**17**. De la mateixa manera, l'estructura presenta els dímers electrostàticament comprimits ja observats en les altres formes descrites per aquest compost (Fig. D.61). Una característica important d'aquesta estructura és que els enllaços d'hidrogen entre els anells d'àcid esquàric s'estableixen en forma d'anells $R_2^2(10)$ prèviament observada en l'àcid esquàric.

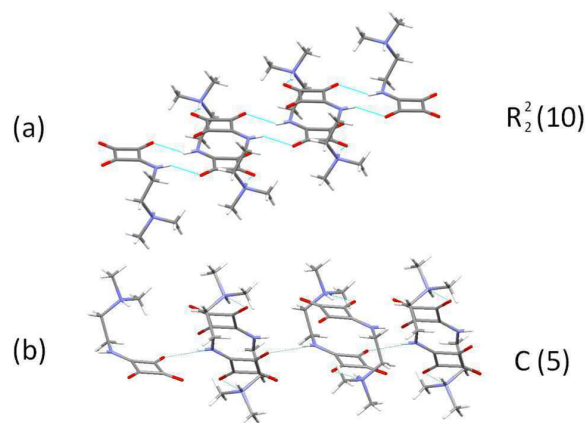


Fig. D.59: Sintons supramoleculars observats en la forma I (a) i la forma II (b) connectant els dímers electrostàticament comprimits en el cristall

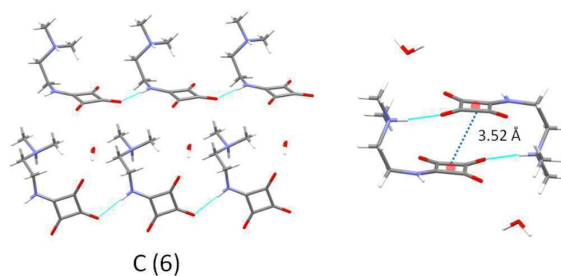


Fig. D.60: Sintó supramolecular observat juntament amb els dímers en *stacking* de la forma hidratada (forma III)

Aquests resultats suggereixen l'ús potencial d'estructures zwitteriòniques autoensamblades com a coformers eficients en la cerca de nous cocristalls amb una varietat d'acceptors/donadors d'enllaç d'hidrogen com àcids carboxílics, urees, amides, etc.

Aquesta tesi és un estudi multidisciplinar de l'estat sòlid de derivats de l'àcid es-

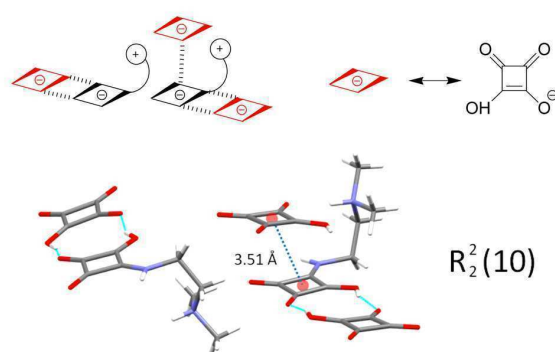


Fig. D.61: Estructura cristal·lina de la sal monosulfat/17

quàric, en el qual es combinen àrees com l'enginyeria cristal·lina, la síntesi orgànica, la química supramolecular i la cristal·lografia. A més a més, s'han utilitzat metodologies experimentals d'*screening* tant polimòrfic com de cocristalls, com també varies tècniques d'anàlisi. Finalment, el fet que els compostos model són difícils de cristal·litzar en qualitat de monocristalls, ha permès optimitzar un mètode de resolució d'estructures cristal·lines a partir del difractograma de pols.